Modeling of inclusion evolution in Ladle Metallurgy Furnace

Modeling of inclusion evolution in Ladle Metallurgy Furnace

By

Yousef Tabatabaei, B.Sc., M.Sc.

A Thesis

Submitted to the School of Graduate Studies
In Partial Fulfilment of the Requirements

For the Degree

Doctor of Philosophy

McMaster University

Title: Modeling of inclusion evolution in Ladle Metallurgy Furnace

Author: Yousef Tabatabaei, M.Sc. (Amirkabir University of Technology)

Supervisors: Dr. Kenneth S. Coley, Dr. Gordon A. Irons and Dr. Stanley Sun

Pages: xvi-227

Abstract

The Ladle Metallurgy Furnace (LMF) in secondary steelmaking processing allows (1) the adjustment of the chemical composition by ferroalloy addition, (2) temperature control by electrical reheating (3) homogenization of chemical composition by argon stirring (4) desulphurization and (5) control of inclusions produced during steel deoxidation. The solid oxide inclusions not only cause nozzle clogging during the continuous casting process and reduce production efficiency, but they are also harmful to the properties of the steel product. In the case of aluminum killed steel, calcium treatment of steel is typically employed to modify the solid alumina inclusions or magnesium aluminate inclusions to liquid or partially liquid calcium aluminates. Injected calcium in form of calcium wire creates calcium bubbles. A portion of calcium dissolves into the steel and diffuses into the steel bulk. However, during the dissolution process some of the injected calcium reacts, close to the injection plume, with dissolved sulfur and oxygen in the steel to form calcium sulfide and calcium oxide inclusions [1].

During ladle treatment of aluminum killed steel the inclusions which form initially are typically alumina. As the dissolved oxygen content of the steel is reduced to very low levels magnesium may be reduced from the slag and subsequently react with the inclusions resulting in a shift towards higher contents of MgO and formation of magnesium aluminate spinel. Magnesium may originate from the top slag, ferro alloys or refractories. Therefore, magnesium aluminate spinels are almost always present before calcium injection and any consideration of calcium treatment should also consider the modification of spinel in addition to alumina. The current work develops a fundamental kinetic model to describe

the evolution of the inclusion population during ladle treatment of aluminum killed steels. The model builds on previous work in the author's laboratory predicting the kinetics of slag metal reactions during ladle treatment and the transformation of alumina to magnesium aluminate spinel. The model addresses the modification of alumina inclusions by calcium and considers mass transfer of species to the inclusion-steel interface and diffusion within the calcium aluminate phases formed on the inclusion. The dissolution of calcium from calcium bubbles into the steel and formation of oxide and sulfide inclusions at the plume is coupled with the kinetic model for inclusion modification. It is found that rate of supply of calcium to the inclusions controls the overall rate of transformation. The inclusion-steel kinetic model is then coupled with the previously developed steel-slag kinetic model. The coupled inclusion-steel-slag kinetic model is applied to the chemical composition changes in molten steel, slag, and evolution of inclusions in the ladle. The result of calculations is found to agree well with industrial heats for species in the steel as well as inclusions during Ca treatment. The kinetic model is further extended to model the modification of spinel inclusions by calcium treatment.

Coupling the model for inclusions modification to a multi component kinetic model for the slag-steel reactions in the ladle furnace allowed prediction of the change of average composition of inclusions which was subsequently verified using plant data from ArcelorMittal Dofasco operations. Good agreement between the experimental and calculated average composition of inclusions was obtained for most of the industrial heats. Finally, a sensitivity analysis of the coupled kinetic model was performed to compare the

effect of the different processing conditions including sulphur content, stirring, total oxygen, slag composition and reoxidation, on the evolution path of inclusions.

Table of content

List of Figures

List of Tables

Nomenclature

a_i: activity of component i

d: diameter of inclusion particle (μm)

C_{v_m}: molar density of the steel $\left(\frac{mol}{m^3}\right)$

C_v: molar density of the liquid product layer $\left(\frac{kmol}{m^3}\right)$

D_i: Diffusion constant of component i ($\frac{m^2}{s}$)

ε: effective stirring power (W/t)

f_i : activity coefficient of species i with respect to 1 wt. % standard state

$J_{A,i}$: fluxes of A in layers i ($\frac{mol}{m^2.S}$)

k_{CA_6}, k_{CA_2}: rate constants of growth of CA_6 and CA_2 ($\frac{mol}{m.s}$)

$k_{m,i}$: mass transfer coefficient of component i in the metal phase through the boundary layer ($\frac{m}{s}$)

k_m^M: mass transfer coefficient of component M in the steel phase ($\frac{m}{s}$)

$k_{sl}^{M_xO_y}$: mass transfer coefficient of oxide M_xO_y in the slag phase ($\frac{m}{s}$)

$K_{M_xO_y}$: Equilibrium constant of $xM + yO = M_xO_y$

MW: molecular weight ($\frac{kg}{mol}$)

$Q_{A,i}$: mass rate of A flowing in phase i ($\frac{mol}{s}$)

ϕ_i: mass rate accounting for counter diffusion of two components for phase i ($\frac{mol}{s}$)

n_T: total number of moles of steel (mol)

N_i : mass transfer rate of component i $\left(\frac{\text{mol}}{\text{s}}\right)$

Sh: Sherwood number

u_i: stoichiometric coefficient

V_i: molar volume of phase i

ν: stoichiometric coefficient

Chapter 1

Introduction

1.1 Overview

Modern steelmaking processes include two major steps (see Figure 1-1): primary and secondary steelmaking. Primary steelmaking involves converting of hot metal from a blast furnace and steel scrap into liquid crude steel via the basic oxygen process or melting scrap steel and/or direct reduced iron (DRI) in an electric arc furnace. In secondary steelmaking, refining of the steel to achieve desired chemistry, temperature and cleanliness before casting is carried out in ladles via several operations, namely: adding alloying elements, lowering dissolved gases in the steel and removal or modification of inclusions. The ladle furnace is primarily used for deoxidation and desulphurization as well as for refining and modifying inclusions.

In the ladle furnace, reactions occur between the synthetic slag, the steel and the alloy additions; agitation of the steel for homogenization is obtained by argon stirring or electromagnetic stirring. Electrical arcing may also be employed for temperature control.

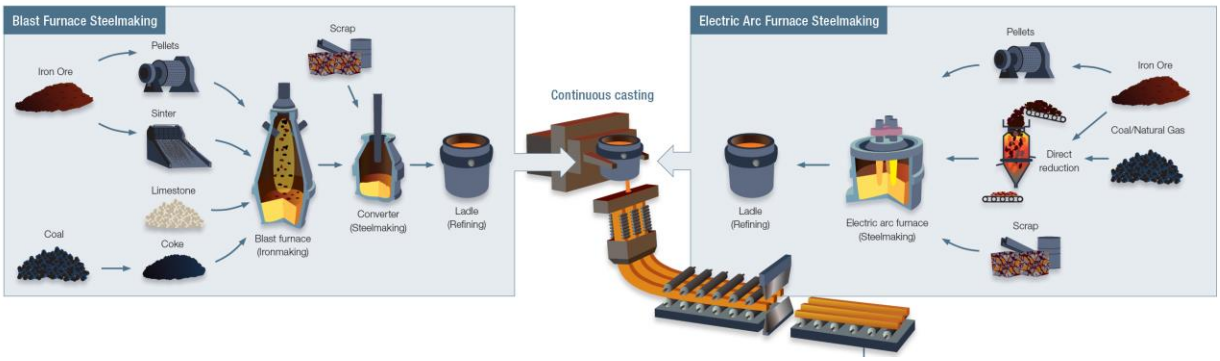

Figure 1-1. Schematic of integrated steel making process- reproduced with permission from ref [2]

Liquid steel obtained either from an oxygen converter or an electric arc furnace contains high concentrations of dissolved oxygen, ranging between 200 to 800 ppm. It is well known that the carbon in the steel can react with oxygen content at the end of heat in steelmaking furnaces via the reaction [3]

$$[\boldsymbol{C}] + [\boldsymbol{O}] = \boldsymbol{CO}(\boldsymbol{g}) \qquad \textbf{(1-1)}$$

Production of CO gas can create voids and defects in the steel when the continuous casting process is used. Therefore, the dissolved oxygen needs to be removed by adding a deoxidizer. The main purpose of deoxidation is to prevent the formation of carbon monoxide gas (blowholes) and FeO during solidification of the steel [4]. In addition, deoxidization is necessary for the removal of the dissolved Sulphur and prevent oxidation of alloy elements (Mn, Si, Ti…).

In the case of the production of Low Carbon Aluminum Killed steel (LCAK steel), deoxidation is carried out by adding aluminum which is an economical and effective method to remove dissolved oxygen according to the reaction:

$$2[Al] + 3[O] = (Al_2O_3)_{inclusion} \qquad \textbf{(1-2)}$$

Where [] denotes dissolved elements in liquid metal. As a result, non-metallic oxide inclusions of solid alumina with different morphologies and sizes are produced [5]. Presence of solid non-metallic inclusions during secondary processing of steel is detrimental to steel castability. Large clusters of aluminum oxide form layers on the inner surface of the continuous casting nozzle which causes nozzle clogging and leads to reduced process efficiency [6]. In addition, alumina particles in the steel give rise to poor mechanical properties of end product [7,8]. Thus, these inclusions need to be eliminated from the molten steel or modified to the desired morphology and composition. Inclusion control in ladle process include number of practices: (a) proper choice of deoxidants to avoid formation of undesired nonmetallic inclusions, (b) controlling blowing by argon gas to maximize flotation of inclusion to the steel-slag interface, (c) top slag control in secondary metallurgy to absorb inclusions floated to the slag-steel interface and (d) calcium treatment to modify solid inclusion to spherical liquid inclusions. The latter is used to modify solid alumina inclusions by transforming them to liquid or partially liquid spherical calcium aluminates.

1.2 The Objectives of This Study

In general, there are four types of interaction in the steel that are important in the current work: slag-steel, steel-inclusions and slag-inclusions, steel-calcium (Figure 1-2). Interaction between steel and slag has been already studied and modeled in the McMaster Steel Research Center. Graham [9] developed a multi-component kinetic model, combining slag and steel thermodynamic solution models and consideration of the stirring, arcing and alloying addition in the ladle, to describ quantitatively the kinetics of slag-metal

reactions. The kinetic model is based on a model proposed by Robertson et al. [10] and the cell model [11,12] is used to describe the thermodynamics of the slag.

The purpose of the current study is as follows:

- To develop quantitative sub-models for alumina and spinel modification by calcium treatment by considering all possible rate controlling steps to determine the rate controlling step for inclusion modification.
- To couple the proposed kinetic models with the multi-component kinetic slag-steel model to create a comprehensive model of the ladle furnace process
- Verify the application of the model with steelmaking plant trial data under a range of conditions.
- To conduct a sensitivity analysis of the coupled kinetic model in order to examine the influence of the different conditions and factors involved in the evolution of oxide inclusions to provide a direction for process improvement to steelmaking operations.

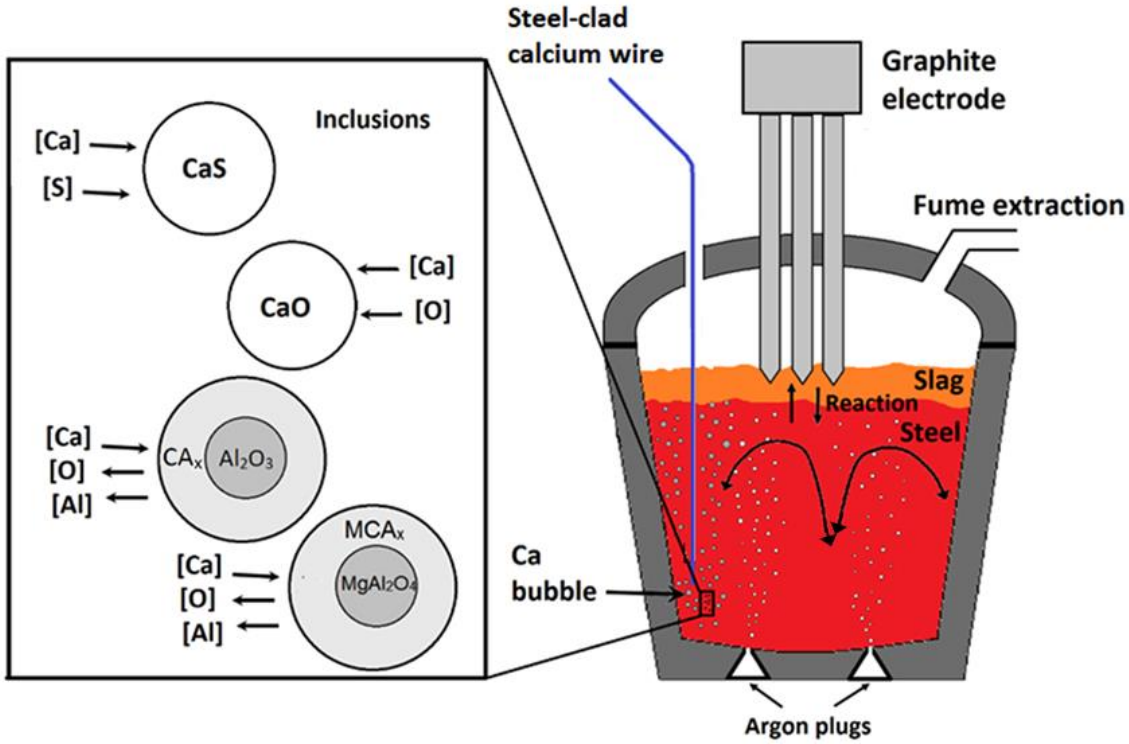

Figure 1-2.Schematic of ladle furnace and the occurring reactions

1.3 Thesis Outline

This thesis comprises, seven chapters: an introduction, a literature review, four modelling chapters and a concluding chapter. Chapters 3, 4 and 5 have been published or accepted for publication in Metallurgical and Materials Transactions B and Chapter six will be submitted for publication shortly, most likely as a two part series. The content and the role of each chapter in the thesis as a whole, is described briefly below.

Chapter 1: "Introduction". This chapter provides a general introduction to the research; describing the motivation for this study, defining detailed research objectives and presenting an outline of this thesis.

Chapter 2: "Literature Review". This chapter reviews relevant literature including: thermodynamics of calcium treatment, kinetics of calcium treatment, previous models proposed for alumina inclusions transformation and modification of spinel inclusions. Also, models developed for the kinetics of ladle processing are reviewed.

Chapter 3: "A multi-layer model for alumina inclusion transformation by calcium in the ladle furnace". The purpose of this chapter was to develop a sub-model describing the details of inclusion modification. A multi-layer growth model is proposed for modification of alumina inclusions. Diffusion through a multi-phase product layer and mass transfer of solute through the boundary layer to the inclusion are taken into account in this model. The model is then run for different steel compositions, showing that the transformation of an individual inclusion is controlled by mass transport from the liquid steel to the surface of the inclusion, and because the calcium is so rapidly consumed by the inclusions, the rate of the overall calcium treatment process is controlled by the rate at which calcium is supplied to the steel by the calcium bubbles. These two conclusions enabled significant simplification to the modelling treatment presented in subsequent chapters.

Chapter 4: "Model of inclusion evolution during calcium treatment in the ladle furnace". This chapter aims to couple the sub model developed in Chapter 3 with multi-component steel slag model to provide a kinetic model for the evolution of oxide and sulfide inclusions during ladle treatment as well as change of composition of steel and slag. The model combines sub models considering the kinetics of: dissolution of the calcium from the calcium bubbles into the steel, slag metal reactions, and steel inclusion reactions. The coupled inclusion-steel-slag kinetic model is applied in predicting the chemical

composition changes in molten steel and slag, and the evolution of inclusions in the ladle. The predictions steel, slag and inclusion composition agree well with data obtained from an industrial heat. This paper showed that inclusions consume the injected calcium so fast that the dissolved calcium remains as low as 0.1-0.2 ppm during calcium treatment. Also, it was found that most sulphide inclusions form at the reaction plane close to the injection plume.

Chapter 5: "A kinetic model for modification of $MgAl_2O_4$ spinel inclusions during calcium treatment in the ladle furnace". In this chapter an overall model of oxide inclusion evolution is proposed based on a fundamental kinetic model for modification of spinel inclusions combined with the building blocks developed in Chapters 3 and 4. The kinetic model for spinel modification considers mass transfer of solute through the boundary layer to the inclusion and diffusion within the product layer. The resulting overall model predicts inclusion development with time in excellent agreement with plant data for industrial heats. Sensitivity analysis has been also carried out to determine rate controlling step for spinel modification. It was found that rate of spinel modification is mixed between the rate of transfer of solutes through inclusion-steel boundary layer and rate of supply of solutes to the bulk steel. It was also showed that composition of liquid magnesium calcium aluminate is affected by concentration of dissolved Al, Ca, Mg and O in the melt.

Chapter 6: "Tracking inclusions during ladle refining using a kinetic model for the compositions of metal, slag and inclusions". In this chapter overall model was used to predict inclusion development during the ladle process for several industrial heats. The developed comprehensive kinetic model was also examined under a range of ladle

conditions examining the effect of sulphur, total oxygen contents, stirring intensity, and slag composition. Sensitivity analysis was performed to investigate effect of these factors on the composition of the inclusions during ladle refining. It was shown that sulphur content of the steel delays modification. Also with change of slag composition, stirring intensity and total oxygen the trajectory of inclusion composition changes.

Chapter 7: "Concluding Remarks". This chapter draws together the important findings from each of the previous chapters illustrating how each one contributes to the overall picture. Finally some general conclusions are offered.

Chapter 2

Literature review

2.1 Introduction

2.1.1 Non-metallic inclusions

Non-metallic inclusions are particles present in the molten steel. Inclusions could be consequence of reactions occurring during steelmaking processing or solidification (indigenous inclusions) or from external sources such as erosion of the refractories or slag entrapment (exogenous inclusions) [13]. Desired properties of the steel including mechanical properties, ductility, machinability, surface quality and corrosion resistance can be achieved by controlling the composition, size, shape and distribution of the inclusions [14].

Non-metallic inclusions in secondary steelmaking originates from [15] (a) the deoxidation process for example alumina inclusions (b) reoxidation of steel which causes reaction of dissolved aluminum with oxygen (c) slag entrapment during addition of fluxes or other operations (d) exogenous inclusions from other sources such as broken refractory and ceramic lining (e) chemical reactions of preexisting inclusions in the melt but modified during process, e.g reaction of alumina with dissolved species to form complex oxide inclusions.

The concept of "clean steel" is closely associated with size, shape, distribution and the amount of non-metallic inclusions in the steel. "Clean steel" implies that the amount and characteristics of the inclusions existing in the steel do not adversely affect the properties

required for a given steel product. A recent review by Kaushik et al. [16] summarizes the available online and offline techniques for cleanliness examination for use in research and industrial plant studies in order to diagnose the root cause of industrial problems.

In aluminum killed steel alumina particles, which results from the deoxidation process carried out after primary steelmaking, form the majority of indigenous inclusions. The size of these alumina inclusions can vary from sub-micron to a few hundred microns. The larger inclusions float up to the steel-slag interface or refractory surface aided by stirring through argon bubbling, but the smaller inclusions (< 10 micron) remain in the steel. These solid alumina inclusions have a high interfacial energy with steel which leads to a large tendency toward agglomeration and clustering [8] in the submerged entry nozzle (SEN) during continuous casting. Thus, these inclusions can cause nozzle clogging and decreased productivity [17]. Clogging is detrimental to steel castability and can give rise to surface defects such as blisters and silvers [18]. Remaining alumina inclusions may result in elongated strings of fragmented particles during rolling and lead to poor mechanical properties of the cast steel [7,19].

An effective approach to modify inclusions to a globular shape offering more desirable properties, is introduction of calcium to the molten steel. During the last 30 years calcium treatment has become an established method to control the composition, morphology, and distribution of inclusions in aluminum-killed steels. Calcium can be injected into the liquid steel as Ca-Si powder, Ca-Si wire or solid Ca wire. Calcium reacts with solid Al_20_3 inclusions to form lower melting points calcium aluminates, or with sulfur to form solid CaS [20]. Also, it modifies the morphology of inclusions, making inclusions less prone to

agglomeration, thus reducing nozzle blockage. Figure 2-1 represents the influence of Ca addition on the flow of an aluminum-killed steel melt through a tundish nozzle. Alumina inclusions can also react with dissolved magnesium in the melt and form magnesium aluminate spinel inclusions during the ladle process. It is shown that calcium treatment is effective in modification of spinel inclusions to liquid magnesium calcium aluminate [21,22]. Kinetics of calcium modification of spinel inclusions is reviewed in 2.3.4.

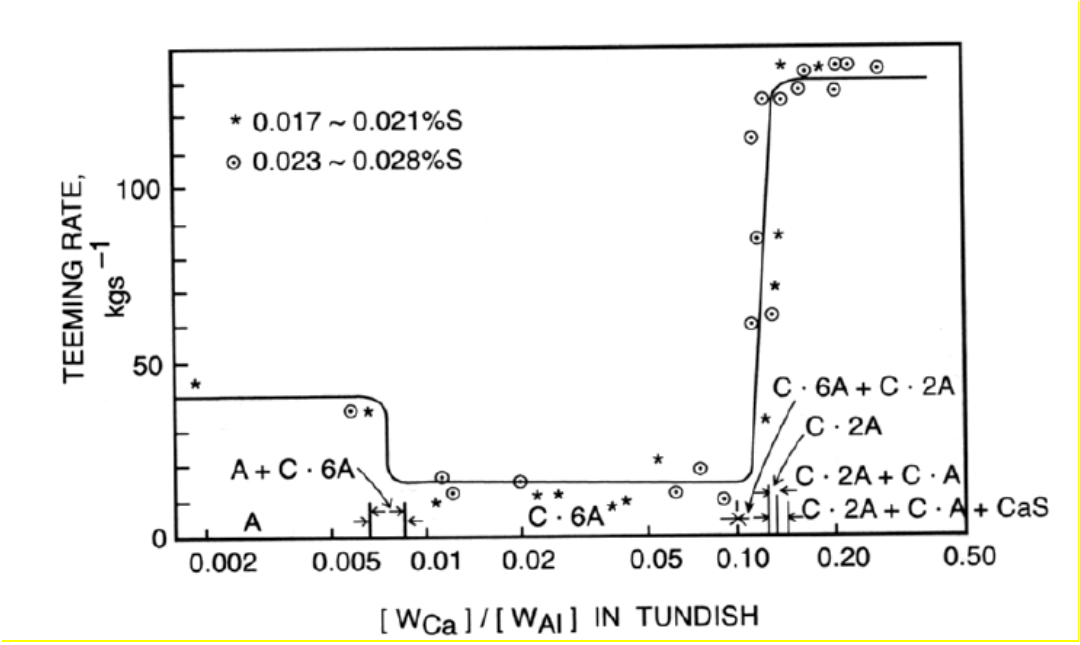

Figure 2-1. Effect of calcium addition on the flow of an aluminum-killed steel melt through the tundish nozzle- reprinted with permission from ref [6]

Ca treatment can also reduce the negative effect of sulfides [14]. Calcium acts as a sulfide shape control agent by transformation manganese sulfides during solidification into $(Ca, Mn)S$ inclusions, which do not deform to elongated stringers. Figure 2-2(a) represents a sample which was taken from a heat without Ca treatment showing MnS "stripes" inside

the dendrite arms whilst Figure 2-2(b) demonstrates spherical sulphides in Ca treated steel. These two mechanisms together have a strong influence on through-thickness ductility and toughness [23]

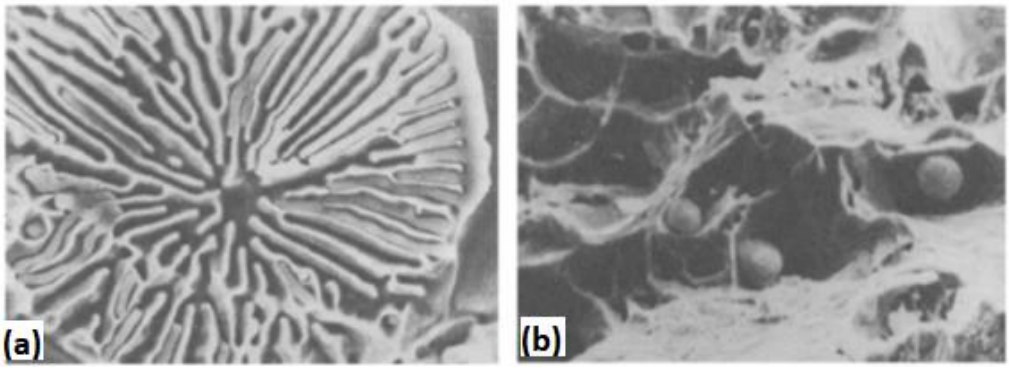

Figure 2-2. Sulfides in as-cast low Al steel with 0.01%S. (a) MnS stripes in Ca-free steel (b) globular sulfides in Ca treated steel- reprinted with permission from ref [14]

2.1.2 Calcium treatment

When calcium is added to liquid steel, the following reactions take place in the bath [24]:

$$Ca(s) \rightarrow Ca(l) \quad \textbf{(2-1)}$$

$$Ca(l) \rightarrow Ca(g) \quad \textbf{(2-2)}$$

$$Ca(g) \rightarrow [Ca] \quad \textbf{(2-3)}$$

Since the boiling point of calcium (1480℃) is less than the steelmaking temperature (1600℃) reaction (2-2***)*** occurs and calcium evaporates and forms bubbles, at the same time part of it will dissolve into the steel by reaction (2-3***)***. Actually, this dissolved calcium will react with the dissolved species and inclusions by the following reactions:

$$[Ca] + [O] \rightarrow CaO \quad \textbf{(2-4)}$$

$$[Ca] + [S] \rightarrow CaS \quad \textbf{(2-5)}$$

$$[Ca] + \left(x + \frac{1}{3}\right) Al_2O_3 \rightarrow (CaO.xAl_2O_3) + \frac{2}{3}[Al] \quad \textbf{(2-6)}$$

$$(CaO) + \frac{2}{3}[Al] + [S] \rightarrow (CaS) + \frac{1}{3}(Al_2O_3) \quad \textbf{(2-7)}$$

As oxygen content of the steel is extremely low for deoxidized steel, the extent to which reaction (2-4) takes place is negligible. If the sulphur content of steel is sufficiently low, reaction (2-6) will occur first, followed by reaction (2-7). The important question is sulfur content above which reaction (2-5) predominates so that there is insufficient calcium available to modify the alumina inclusions according to reaction (2-6). Kor [24] used the equilibrium constant for reaction (2-7) to conduct simple calculation of the critical sulfur content for the formation of liquid calcium aluminates as shown in Figure 2-3.

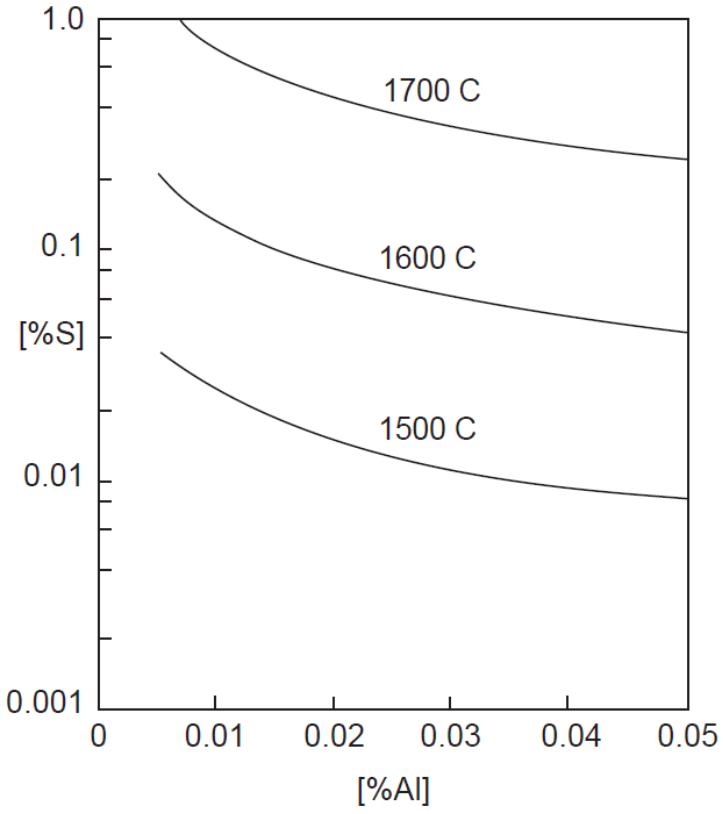

Figure 2-3. Critical steel sulfur and aluminum contents below which liquid alumina-saturated calcium aluminate is formed- reprinted with permission from ref [24]

Correlation between sulfur content and formation of liquid calcium aluminate is discussed more in detail in next section.

2.2 Thermodynamics of calcium treatment

Some researchers have tried to determine thermodynamically the circumstances under which inclusions will form. Larsen and Fruehan [25] carried out a theoretical thermodynamic analysis in order to determine the type of inclusions that form in steel during calcium injection as a function of aluminum and sulfur contents. Considering the following reaction, they stated that if the Al and S contents is less than those for the equilibrium of reaction (2-8), liquid inclusions will form.

$$15CaS + 33(CaO.Al_2O_3) = 4(12CaO.7Al_2O_3) + 10[Al] + 15[S] \qquad \textbf{(2-8)}$$

They also compared the results with inclusions found in number of samples from laboratory and industrial heats treated with calcium. The results from this study are summarized in Figure 2-4.

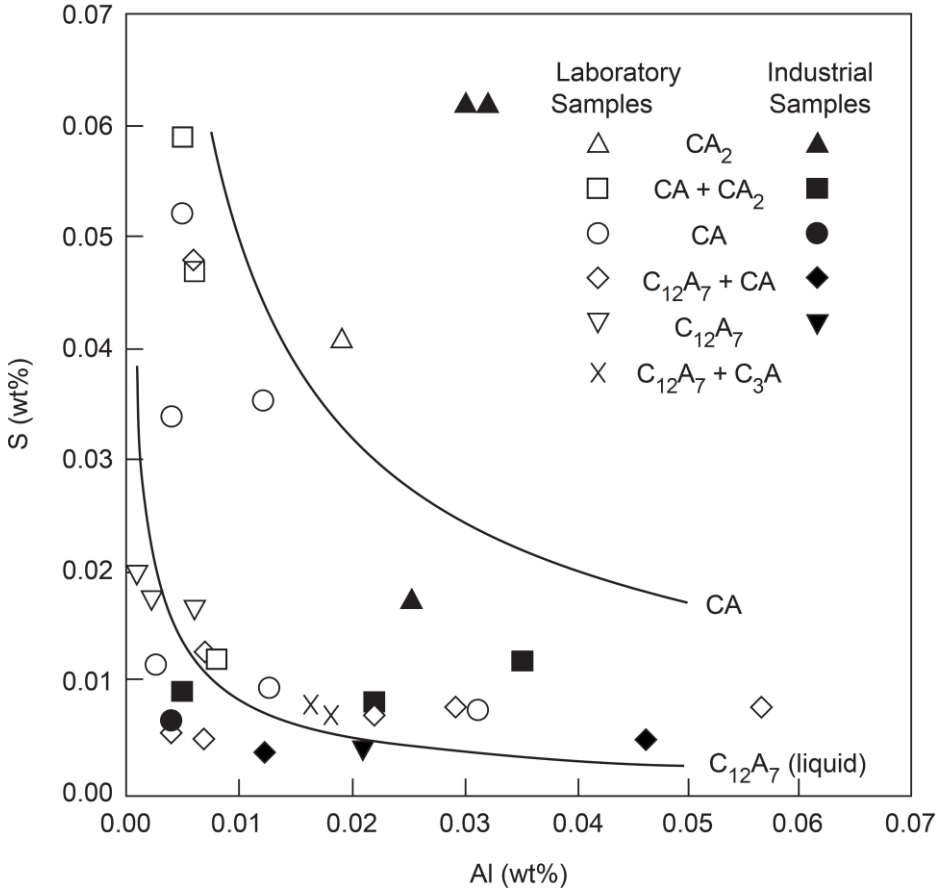

Figure 2-4. Composition of inclusions found in laboratory and plant samples compared with theoretical predictions- reprinted with permission from ref [25]

The curves given by Larsen and Fruehan are based on Gibbs free energy of formation of the different intermediate phases in the $CaO - Al_2O_3$ system assuming that a_i (liquid slag) $=a_i$ (in the solid $C_{12}A_7$ phase, where i=CaO, Al_2O_3) for the activity calculations. Later Ye et al. [26] used ThermoCalc to calculate the activities of CaO and Al_2O_3 and created similar Al-S equilibrium diagrams. The calculated activities and curves are shown in Figure 2-5.

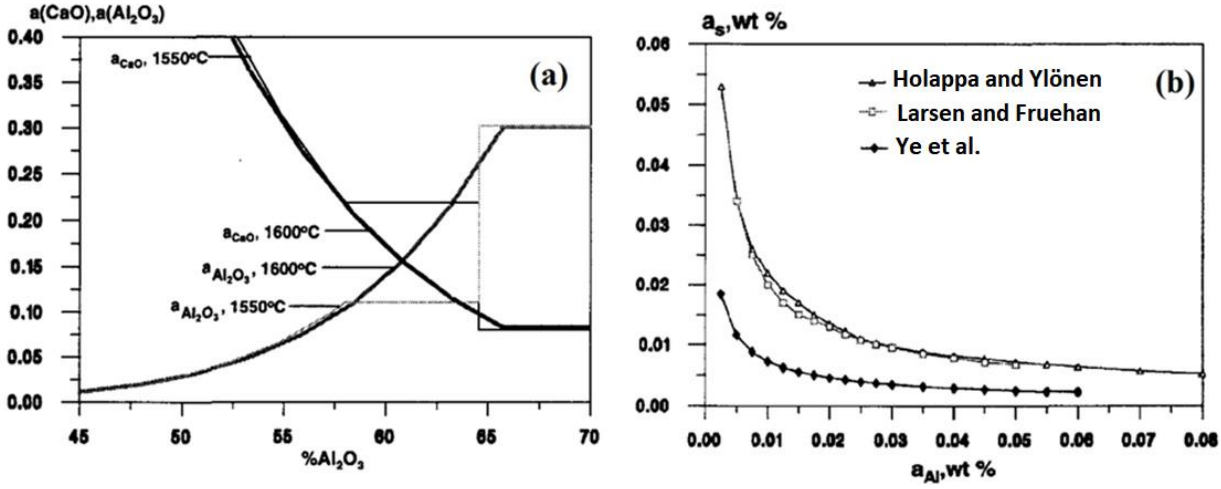

Figure 2-5. (a)The calculated activities of CaO and Al_2O_3 in the molten range of the CaO-Al_2O_3 system and (b) comparison of equilibrium diagram between a steel melt and a molten inclusion calculated by Holappa and Ylönen [27], *Larsen and Fruehan* [25] *and Ye et al.* [26]- *reprinted with permission from ref* [26]

Holappa et al. [28] performed thermodynamic calculations to study modification and the equilibrium state of liquid and solid inclusions containing oxidic and sulphidic components by applying a quasichemical slag model. They conducted basic equilibrium calculations of inclusion compositions and amounts in liquid steel corresponding to ladle treatment conditions as well as casting using the ChemSage program and database with a quasichemical slag model from GTT Technologies developed by Eriksson and Hack [29]. A "liquid window" was defined based on total aluminum and total calcium content of the steel inside which liquid calcium aluminate formed and CaS was unstable. The results of these calculations are presented in Figure 2-6. Below the liquid window solid calcium aluminates exist and above liquid window solid CaS forms. The limits of the liquid area were determined under different conditions by calculating the saturation lines for calcium aluminates and CaS, respectively. Figure 2-6 shows the effect of sulphur on the liquid

window at two different temperatures. At a typical ladle condition, 300 ppm Al and 50 ppm S, the liquid window is quite large and saturation of CaS does not occur up to addition of approximately 25 ppm Ca. Figure 2-6 shows that with increasing sulphur content less Ca is required to reach the saturation line for CaS i.e the stability of CaS increases and thus the liquid area shrinks. Although, as mentioned earlier sulphur content of the steel is usually less than 100 ppm in ladle processing, some of examined conditions are unrealistic. Also, Figure 2-6 demonstrates that at lower temperature the window becomes narrower.

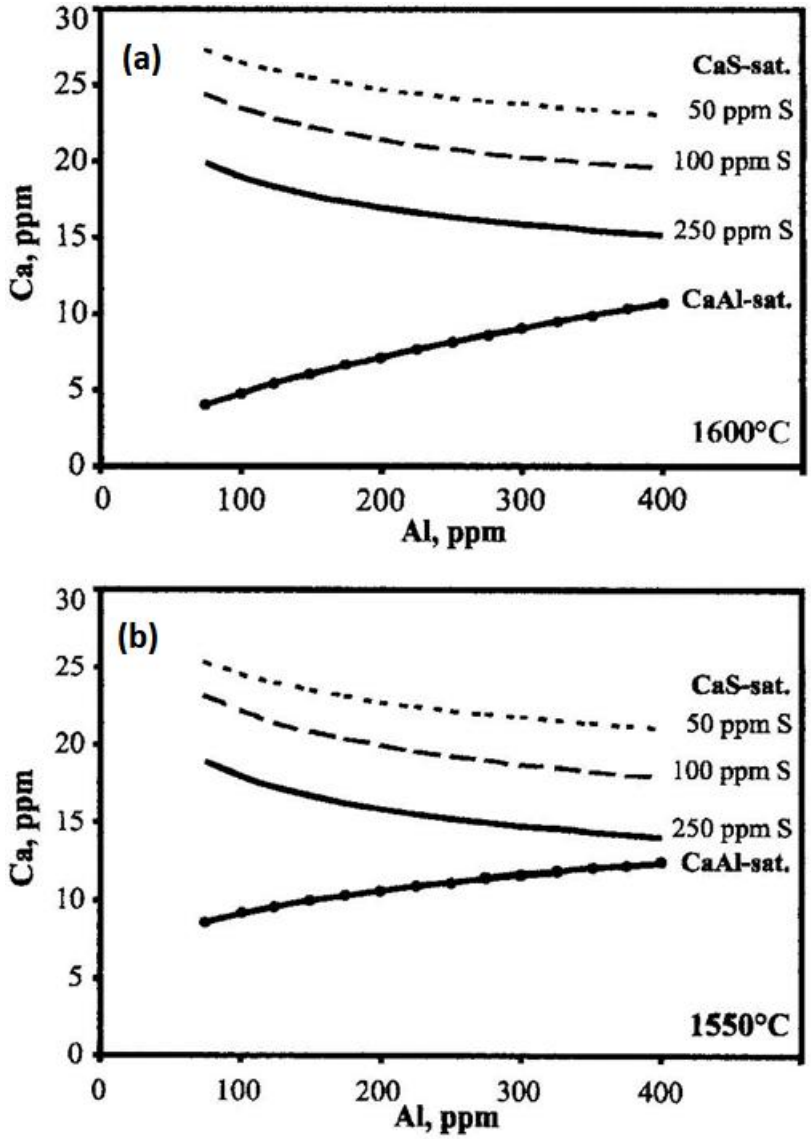

Figure 2-6. Effect of sulphur content of steel on liquid window at (a) 1600 ºC and (b) 1550 ºC- reprinted with permission from [28]

The change of the liquid window with total oxygen at constant sulphur content is shown in Figure 2-7. At lower oxygen content, with a smaller amount of calcium liquid calcium aluminate can form and the liquid window is obtained. When the oxygen content is increased, the calcium additions required to reach the liquid area increases and the window

becomes wider. Again, as it is seen in Figure 2-7(b) with increasing sulphur concentration the liquid window become narrower.

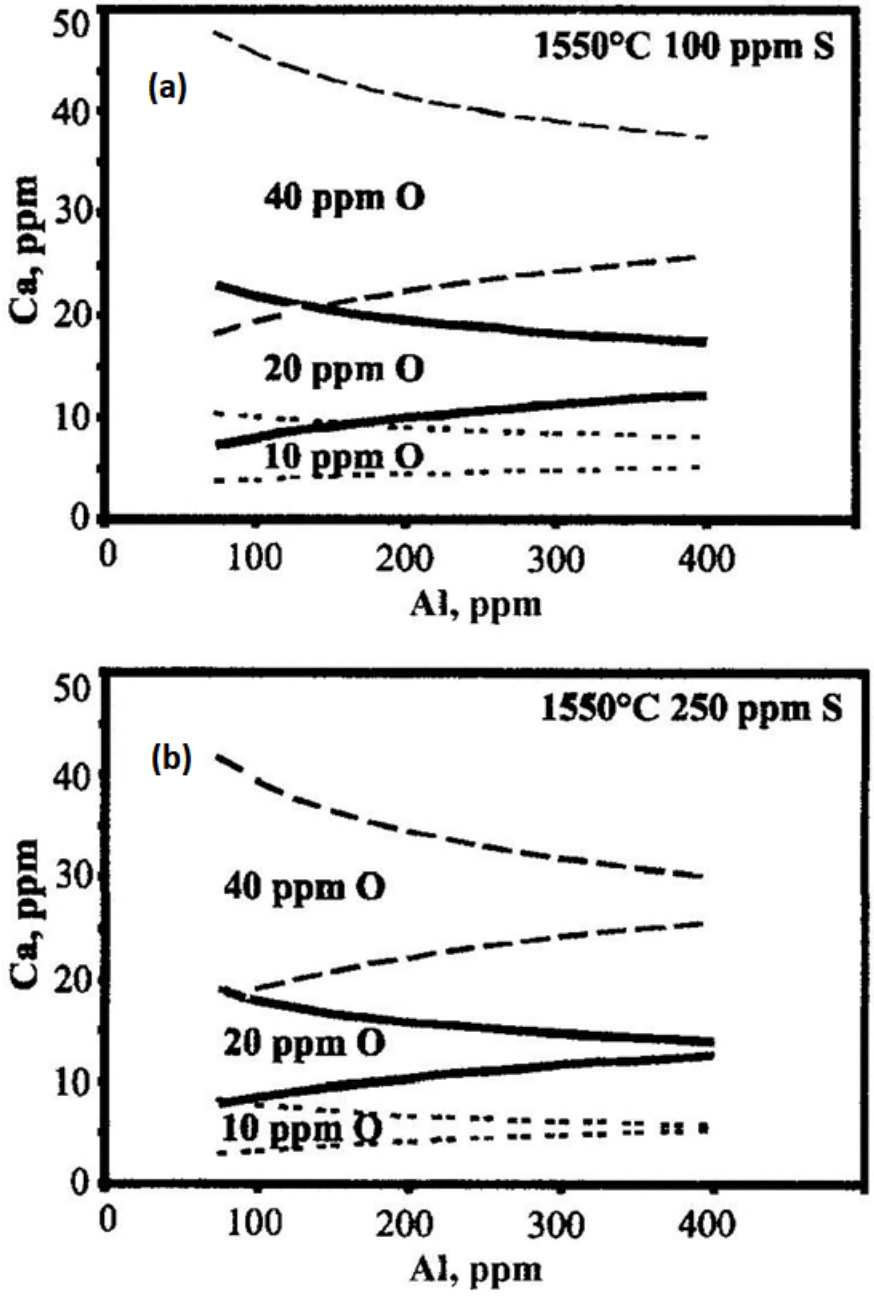

Figure 2-7. Effect of total oxygen on liquid window with two different sulphur content (a) 100 ppm (b) 250 ppm- reprinted with permission from [28]

Holappa et al. [28] also used thermodynamic calculations to predict which inclusions would form during solidification as shown in Figure 2-8. With decreasing temperature, solidification continues and the oxide inclusions formed alter from $CaO.2Al_2O_3$ to $CaO.6Al_2O_3$ and finally to Al_2O_3.

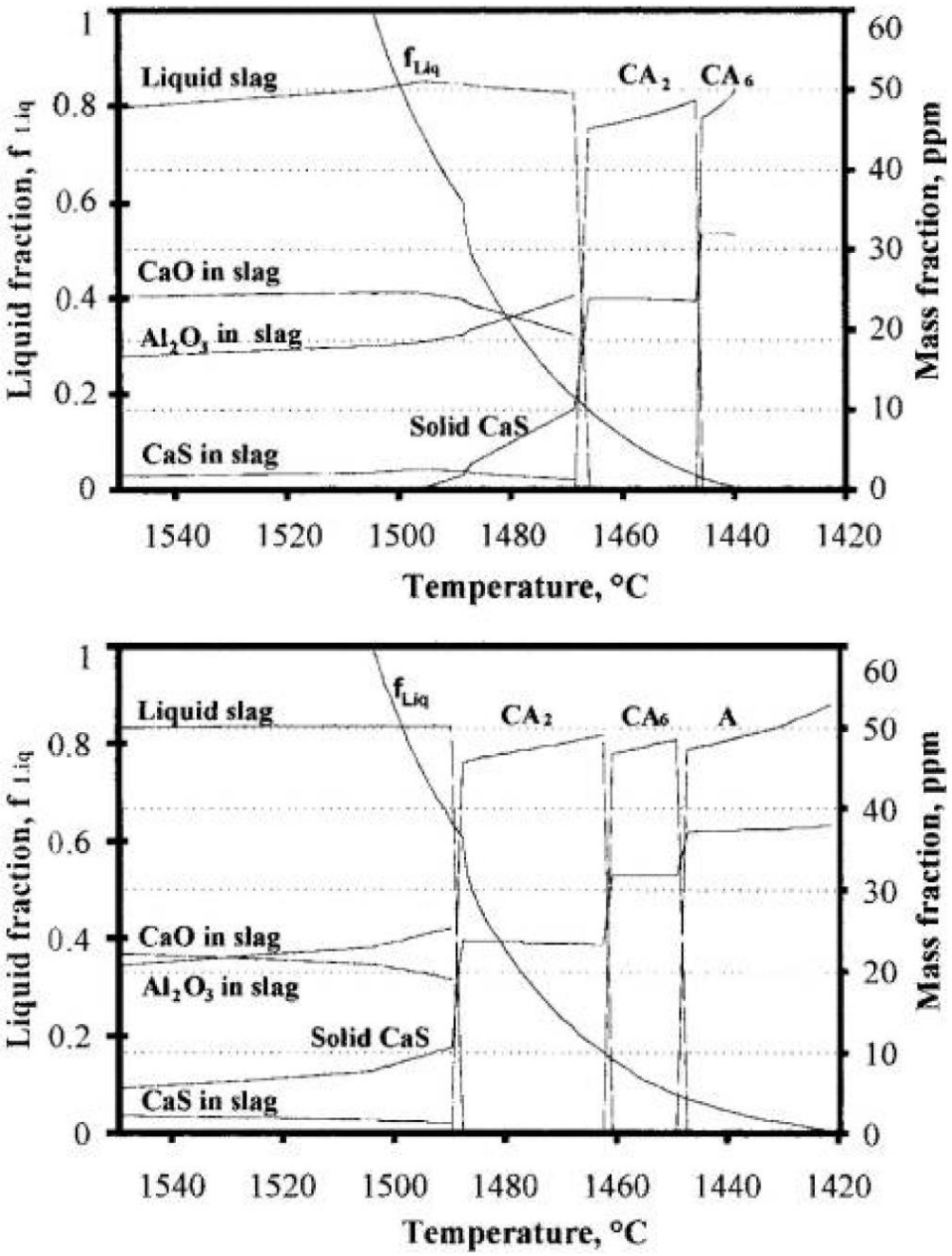

Figure 2-8. Inclusions during solidification- reprinted with permission from ref [28]

2.3 Kinetics of calcium treatment

The overall rate of a specific reaction, at any time, depends upon the properties of the phases and the kinetic steps involved in the reaction from the initial to the final state. In

general, a reaction which involves more than two phases requires a combination of number of separate reactions involving different phases at a time.

For example, for a simple reaction: A(I)+ B(I)= AB(II)

Which involves two immiscible phases I and II where A and B are soluble in phase (I), AB is soluble in phase (II). The kinetic steps in the above reaction taking place at the interface of phases (I) and (II) are as follows:

- The mass transfer of A and B from the bulk of phase (I) to the interface of phases (I) and (II).
- The chemical reaction of A and B at the interface to produce AB
- The mass transfer of the product AB away from the interface into the bulk of phase (II).

At any given moment the slowest kinetic step would control the rate of the reaction and is termed the "rate-controlling step" or the "rate-limiting step". In a real system, with several phases and interfaces the reactions at some interfaces may be controlled only by mass transfer, while at the other interfaces they may be controlled by chemical reaction, or by a combination of more than one step. Figure 2-9 shows five different possible rate controlling mechanism in two phase reaction.

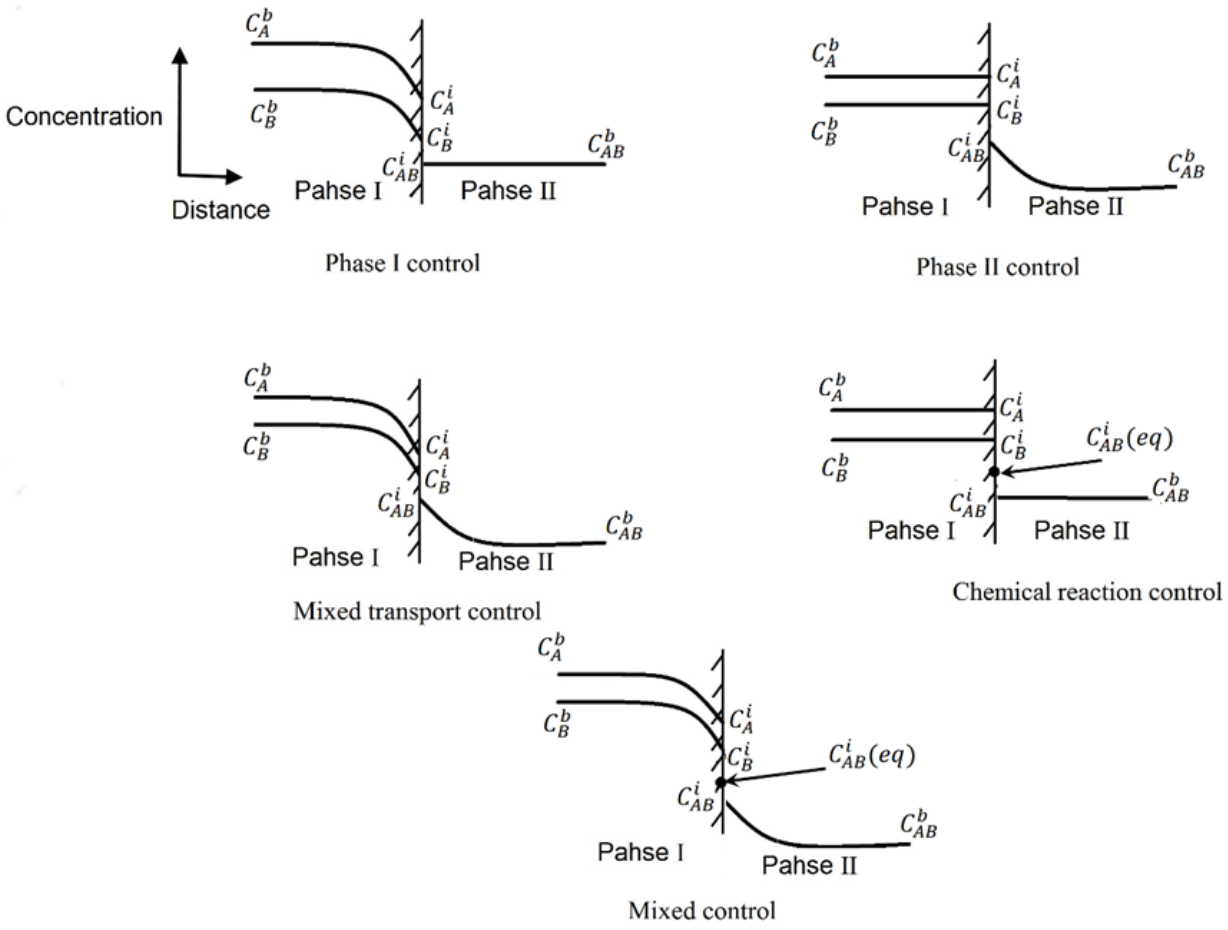

Figure 2-9 .Possible rate-controlling mechanisms in the two phase reaction- redrawn from ref [13]

The interfacial and bulk concentrations are indicated by superscripts i and b, respectively.

Case 1: Mass transfer in the phase I is rate controlling. Equilibrium exists at the interface.

Case 2: Mass transfer in the phase II is rate controlling. Equilibrium exists at the interface.

Case 3: Mixed mass transfer control in phase I and II . Equilibrium exists at the interface.

Case 4: Chemical reaction at the interface is rate controlling. These are no concentration gradients in either phase. Equilibrium does not exist at the interface

Case 5: Mixed control (chemical reaction and mass transfer) in phase I and II. Equilibrium does not exist at the interface.

In the case of modification of alumina inclusions by calcium, the reaction can be divided into the following kinetic steps:

- Dissolution of calcium from the gas bubbles-steel interface to the bulk of steel
- Transfer of the dissolved calcium from the bulk steel to the steel-inclusion interface
- Diffusion of calcium from the steel-inclusion interface through the product layer to the alumina core
- Chemical reaction of the calcium with alumina
- Transfer of the dissolved aluminum or oxygen from the steel-inclusion interface to the bulk steel

Different authors proposed different models assuming different rate controlling steps for inclusion modification. In next sections these models including their assumptions and mechanisms are summarized.

2.3.1 Mass transfer in the steel as the rate controlling step

Efforts on modeling of kinetics of calcium treatment started in the 1990's. Lu et al. [1] investigated dissolution of calcium and formation of oxide and sulphide inclusions when feeding calcium into 40 kg heats with various sulphur and aluminum contents under an argon atmosphere. They found that the calcium absorption rate increased with both sulphur and oxygen contents. So, it was proposed that calcium dissolves through the gas/liquid boundary layer and is met by oxygen and sulphur diffusing towards the gas/liquid interface where reactions of calcium with oxygen and sulphur drive the concentration to very low levels (Figure 2-10).

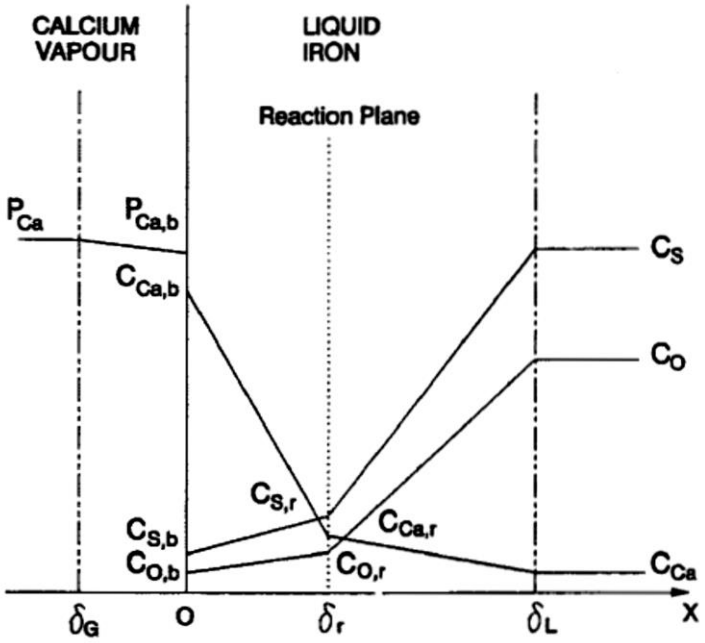

Figure 2-10. Schematic representation of concentration profiles within calcium vapour/melt boundary- reprinted with permission from ref [1]

Assuming chemical equilibrium at the interfaces and quasisteady state diffusion of species, using Fick's first law, balance of the calcium flux against fluxes of oxygen and sulphur can be written as:

$$\frac{D_O(C_O-C_{O,r})}{\delta_L-\delta_r}+\frac{D_S(C_S-C_{S,r})}{\delta_L-\delta_r}=\frac{D_{Ca}(C_{Ca,b}-C_{Ca,r})}{\delta_r} \quad \textbf{(2-9)}$$

Very large equilibrium constants for both desulphurization and deoxidation leads to very low equilibrium concentrations at the reaction plane in comparison with the other concentration terms in equation (2-9).Therefore:

$$\delta_r=\left(\frac{D_{Ca}C_{Ca,b}}{D_OC_O+D_SC_S+D_{Ca}C_{Ca,b}}\right)\delta_L \quad \textbf{(2-10)}$$

Based on the foregoing considerations, Lu et al. defined an "enhancement factor", as the rate of calcium dissolution in the presence of Sulphur and oxygen relative to that of simple dissolution:

$$E=\frac{D_{Ca}/\delta_r}{D_{Ca}/\delta_L}=1+\frac{D_OC_O+D_SC_S}{D_{Ca}C_{Ca,b}} \quad \textbf{(2-11)}$$

After substituting equation (2-10) in (2-9):

$$C_{Ca,r}=\left[\left(\frac{D_O\,K_{CaO}+D_SK_{CaS}}{D_OC_O+D_SC_S}\right)C_{Ca,b}\right]^{\frac{1}{2}} \quad \textbf{(2-12)}$$

With the knowledge of concentration at the reaction plane, and inclusion interface, the concentration of dissolved species can be calculated.

The basis for their model is shown schematically in Figure 2-11.

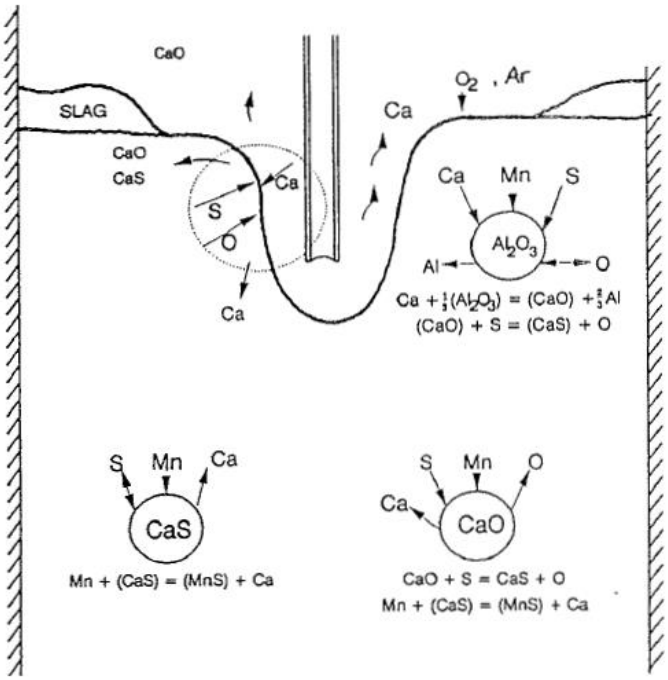

Figure 2-11.Schematic representation of overall model- reprinted with permission from ref [1]

They made the following assumptions to develop the model:

1. The inclusions are so small that diffusion within them is rapid and they have homogeneous composition.
2. Due to rapid chemical reactions, equilibrium is obtained at all interfaces.
3. The inclusion interfacial area was taken from quantitative image analysis of samples.

With knowledge of the rates of diffusion of the dissolved species to and from inclusions the resulting changes of inclusion composition can be calculated from mass balance considerations. The results of the model compared with experimental data is shown in Figure 2-12.

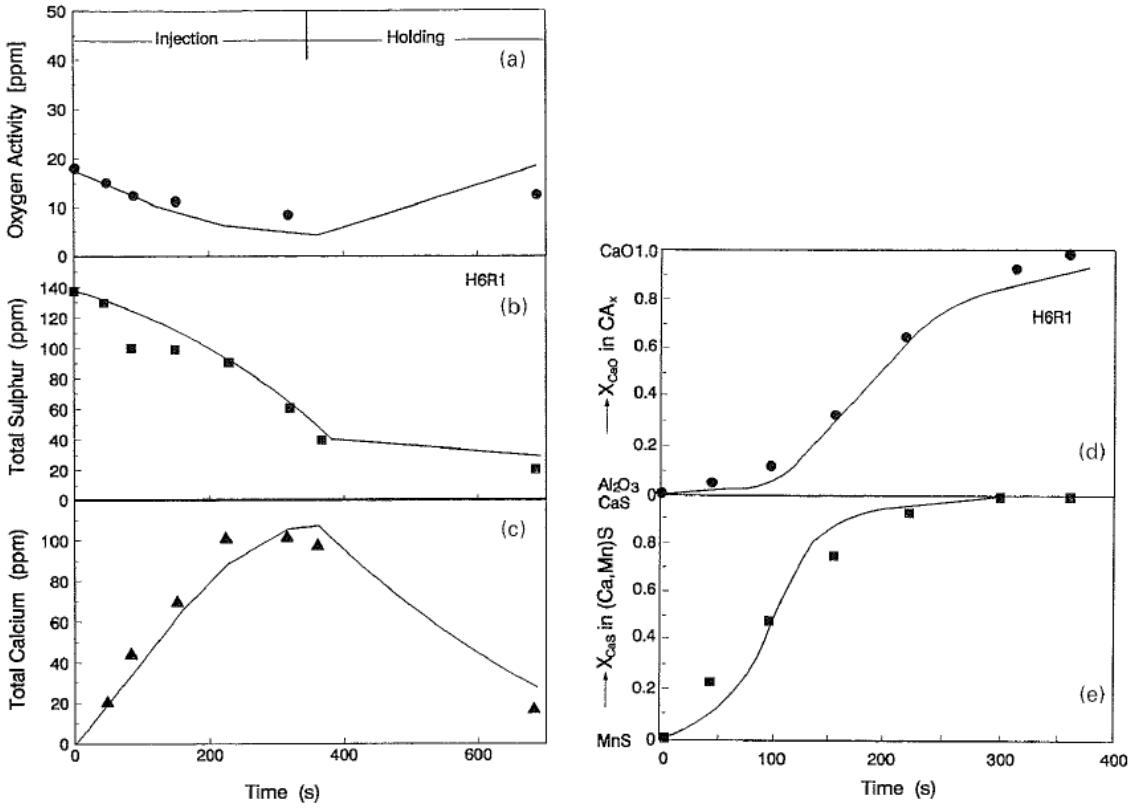

Figure 2-12. Change of steel and inclusions composition according model by Lu et al.- reprinted with permission from ref [1]

Visser et al. [30] developed a model based on results from microscopic analysis, flow field calculations, as well as thermodynamic and kinetic considerations to describe the change of the concentration, composition and size of the inclusions in the liquid steel during calcium treatment. In their model it is assumed that dissolved calcium and oxygen react with Al_2O_3 to form CA with gradually increasing CaO fraction. If oxygen activity is sufficiently low and Sulphur sufficiently high, dissolved calcium and sulphur react at the surface of the particle to form CaS.

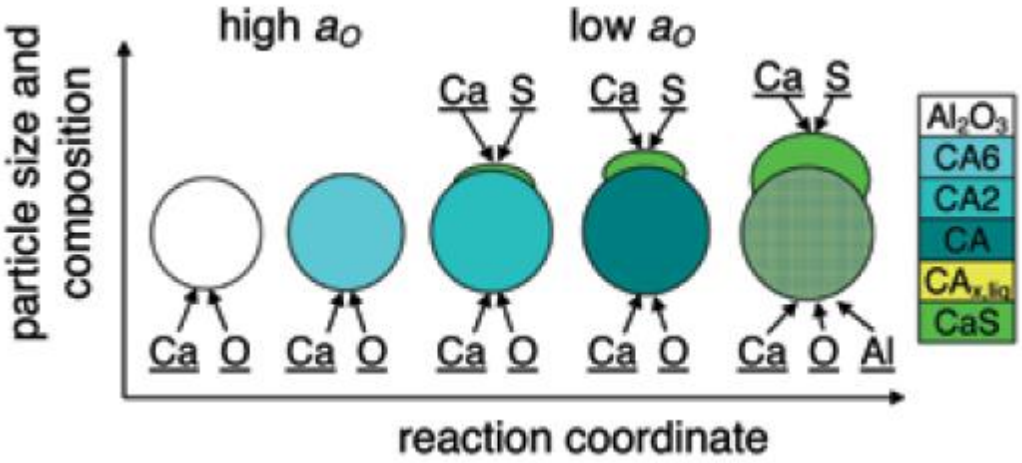

Figure 2-13. Mechanism of the conversion of an Al_2O_3 particle to an $nCaO.Al_2O_3$/CaS particle proposed by Visser et al.- reprinted with permission from ref [30]

They divided steel bath into two reaction zones: one representing the volume of steel where the calcium wire breaks up and the calcium droplets and bubbles float up (plume zone- high calcium/low oxygen), the other representing the rest of the liquid steel volume, (bulk- low calcium and somewhat higher oxygen).

In addition, these authors assumed that the formation reactions of CaO, CaS and Al_2O_3 are rate limited by mass transfer of the solutes to the particle surface where equilibrium between the solutes and the solid phases is assumed.

Mass fluxes of solutes i to and from the inclusion surface can be expressed as follows:

$$J_i = \frac{k_{m,i}\rho_{steel}}{100M_i}([\%i] - [\%i]^*) \qquad \textbf{(2-13)}$$

Where j_i, $k_{m,I}$ and M_i are molar flux, mass transfer and molecular weight of *i*, respectively.

According to mass balance:

$$J_{Ca} + \frac{3}{2}J_{Al} = J_O + J_S \quad (2\text{-}14)$$

By considering equations (2-13), (2-14) and equilibrium at the inclusion surface, evolution of inclusions can be described. Some of the results are illustrated in Figure 2-14. Figure 2-14(a) shows the result of the model compared with the measured values for total calcium content in the bulk region for assuming two different values of saturated calcium in the Ca plume. Figure 2-14(b) presents the predicted value and measurement results of average CaS over total calcium content for two values of Ca_{sat}. As it is seen in Figure 2-14 by assuming concentration of 1 ppm Ca at the plume, the model shows much better fit for total calcium and relative amount of CaS in inclusions. Slag-steel reaction was ignored in this work

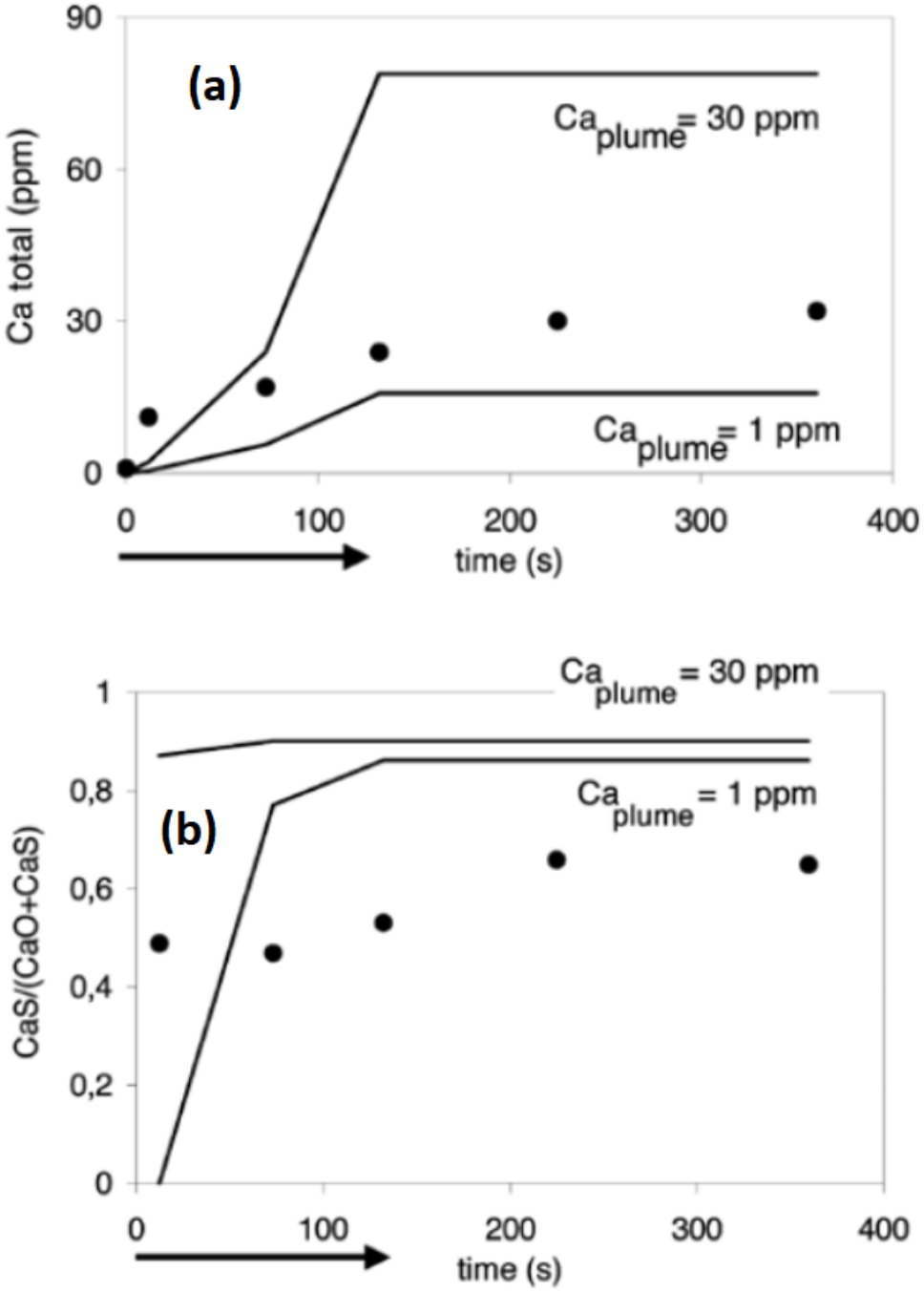

Figure 2-14. Predicted and measured average value of (a) Ca_{total} and (b) CaS of the particles in the bulk zone- reprinted with permission from ref [30]

2.3.2 Diffusion in the product layer as the rate controlling step

Ito et al. [31] investigated the rate of liquid calcium aluminate mofification with calcium for shape control in line pipe steel. They melted electrolytic iron (20 kg) in the crucible of an induction furnace. After chemical adjustment by addition of alloying elements, metallic aluminum and calcium-silicon wire (30% Ca-70% Si) were used as a deoxidizer and as an agent for inclusion shape control, respectively. Stirring was induced by argon gas flow from the bottom of the crucible. As they observed calcium aluminate only at the periphery of the particle, the unreacted core model as shown in Figure 2-15 was therefore adopted to study the shape control reaction of aluminum inclusions by calcium.

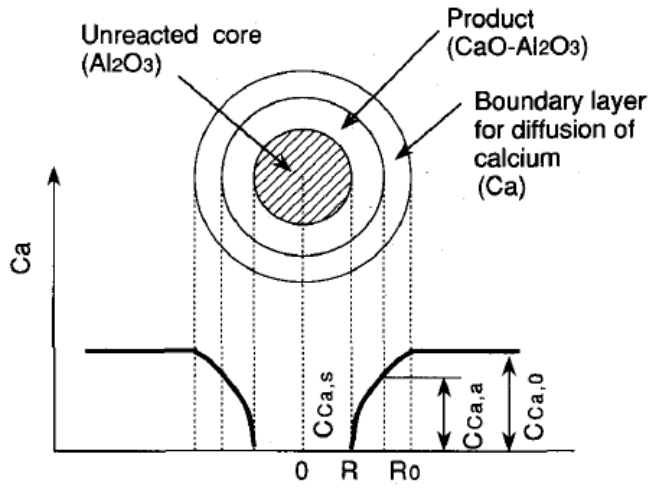

Figure 2-15.Schematic view of shape control of Al_2O_3 with Ca- reprinted with permission from ref [31]

The rate controlling steps in the unreacted core model are defined as:

1. Mass transfer control (calcium) in the molten steel.
2. Chemical reaction control at the interface between calcium-aluminate and unreacted alumina core.

3. Mass transfer control (calcium diffusion control) in the product layer of calcium-aluminate

They plotted the fraction of transformation with time assuming each of these steps as the rate controlling step (see Figure 2-16). By comparing the predicted results with experimental data they observed that results predicted by assuming mass transfer in the product layer offered the best fit with the experimental values. Therefore, it was concluded that diffusion through the product layer was the rate controlling step.

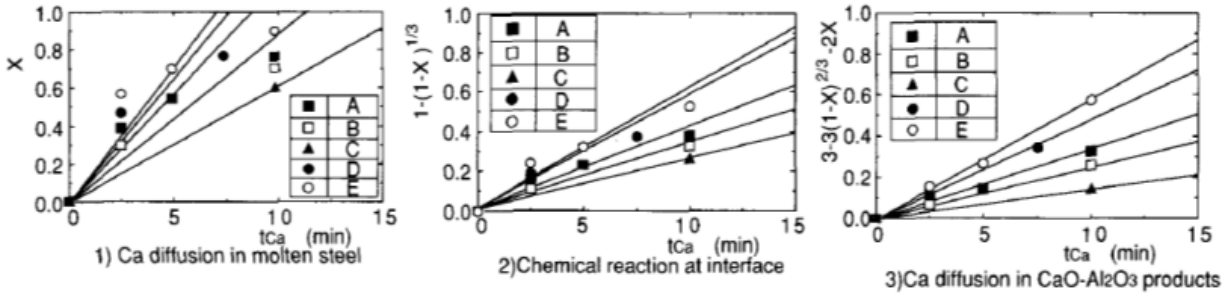

Figure 2-16. Determination of rate control step for shape control of Al_2O_3 inclusion with Ca- reprinted with permission from ref [31]

2.3.3 Chemical reaction as the rate controlling step

Higuchi et al. [32] also studied inclusion modification and developed a mathematical model for the kinetics of inclusion transformation. They melted 2 kg of electrolytic iron under a stream of purified argon gas, in an MgO crucible using a high frequency induction furnace. After chemical composition adjustment and flux addition, 30% Ca-70% Si steel-clad Ca-Si wire was used as the reagent for inclusion modification.

A schematic presentation of their proposed reaction sequence is illustrated in Figure 2-17.

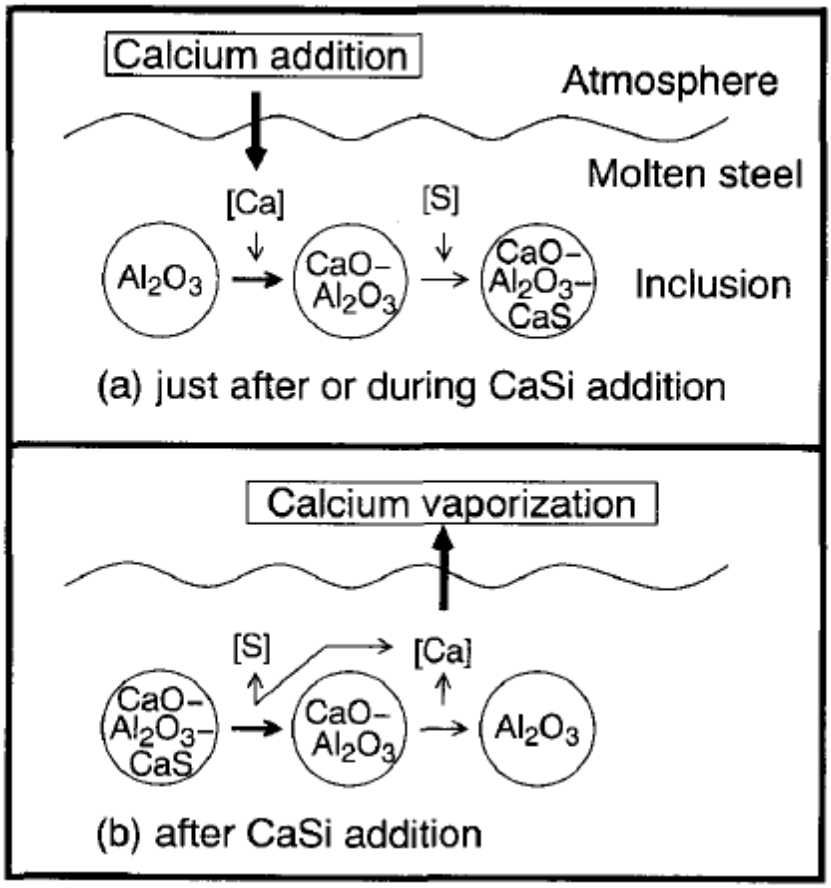

Figure 2-17. Mechanism of inclusion modification- reprinted with permission from ref [32]

According to their model calcium dissolved in the melt just after adding Ca-Si reacts rapidly with alumina inclusions to form calcium aluminate or calcium sulphide. The contents of CaO and CaS in the inclusions decreases gradually as the dissolved calcium evaporates over time.

To develop the model both the evaporation rate of calcium and the reaction rate between inclusions and the melt were considered. However, the diffusion term of calcium from the bulk to the surface within the melt was neglected.

The evaporation rate of calcium can be written as:

$$-\frac{dCa}{dt} = k_s A_s Ca \qquad \textbf{(2-15)}$$

Where Ca, K_S and A_s are concentration of calcium in the melt, mass transfer coefficient and interfacial area per melt volume between melt and atmosphere, respectively.

The rate of reaction between calcium in the melt and inclusions can be written:

$$-\frac{dCa,i}{dt} = K_i\,(Ca,i - Ca,e) \qquad \textbf{(2-16)}$$

Where $C_{a,i}$, $C_{a,e}$ and K_i are concentration of calcium in inclusions, equilibrium concentration of calcium in inclusions and apparent rate constant, respectively. And also:

$$a_{CaO} = f_{Ca}[Ca]a_O/K_{CaO} \qquad \textbf{(2-17)}$$

Where K_{CaO}, a_{CaO}, a_O and f_{Ca} represent the equilibrium constant for the reaction $Ca + O = CaO$, activity of CaO in inclusions, activity of oxygen and activity coefficient of Ca in the melt, respectively.

Similar equations can be written for CaS formation. Figure 2-18(a) shows total Ca and CaO content in the steel in which 2 g of Ca was added to 2 kg of the steel. As it is seen Figure 2-18(a) maximum values were obtained just after calcium addition and then decreased gradually. The calculated CaO fraction of inclusions presented Figure 2-18(b)

indicates good agreement with the measured ones in heat with 6g $CaSi$ addition. However, it should be noted that the parameters of K_i and K_s were determined by parameter fitting. Thus, since rate equations take similar form either mass transfer control or chemical reaction control, the calculated results do not confirm that chemical reaction is necessarily rate controlling step.

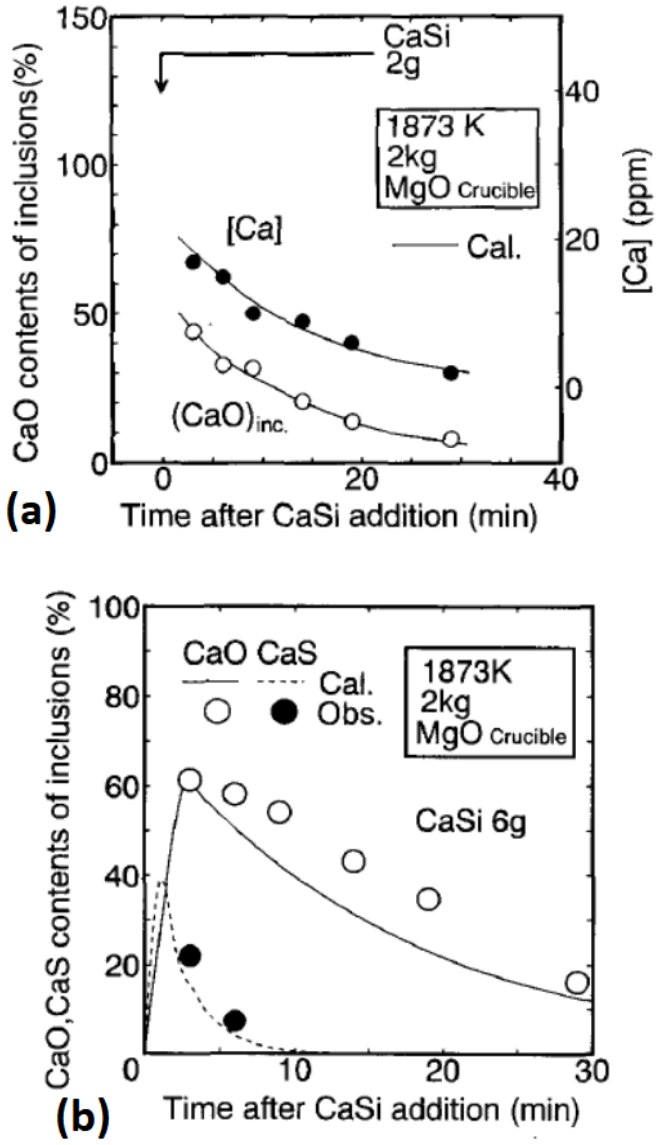

Figure 2-18. Comparison of observed values of [Ca] and CaO, CaS contents of inclusions and calculated values- reprinted with permission from ref [32].

Ye et al. [26] proposed that the reaction of inclusion modification occurs according to the following order:

$$Al_2O_3 => CA_6 => CA_2 => CA => CA_{x(liquid)}$$

They assumed that the process proceeds as follows:

1. Diffusion of dissolved Ca, O and S to the solid alumina surface,
2. Formation of a layer of CA_6 quickly on the alumina surface,
3. Creation of a layer of CA_2 quickly on the CA_6 surface,
4. Formation of a layer of CA on the CA_2 surface, and
5. Formation of a layer of liquid aluminate phase CA_x on the CA surface; dissolved Ca and O diffuse to the liquid CA_x surface which leads to increase in CaO content of the intermediate aluminates
6. Precipitation of a layer of solid CaS on CA_x due to the low activity of oxygen in equilibrium with CA_x which prevents further diffusion of the dissolved Ca and O to the aluminates. But diffusion of Ca and O continue from the CaO rich phases to the lower CaO-containing phase.

Thereafter, the inner core of aluminate inside the sulphide ring becomes homogeneous by increasing mole fraction of CaO in CA_x in the aluminate phase until reaching a homogeneous aluminate. Schematic diagram of the model is shown in Figure 2-19. Although the authors presented microscopic image of CaS ring surrounding calcium

aluminate, they did not provide any experimental evidence or microscopic observation for length of transformation of multi-layer structure to homogeneous aluminate.

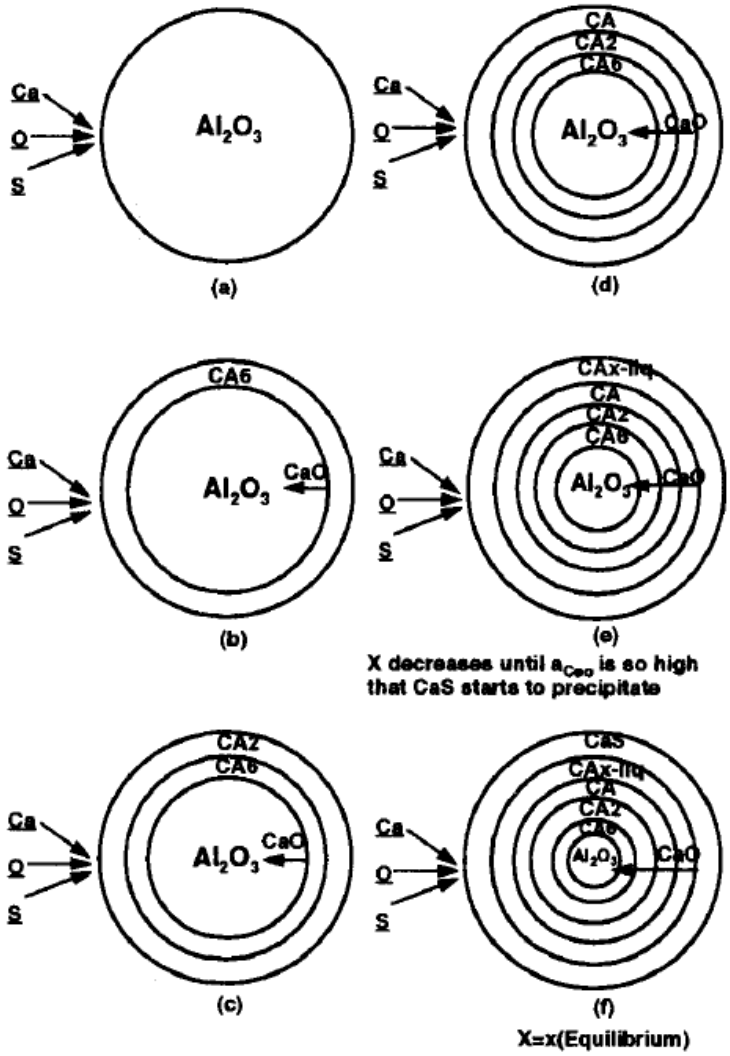

Figure 2-19. Mechanism of Al_2O_3 modification by calcium treatment- reprinted with permission from ref [26]

Han et al. [33] said that the mechanism of sequenced layers moving forward could not be detected in their experiment. They investigated reactions between Al_2O_3 and CaO in a resistance furnace. CaO and Al_2O_3 powder were pressed separately with a hydraulic

compressor to form cylinders. Then, samples, placed above each other, were pushed into the furnace and after certain amount of time, they were quenched and cooled. Finally, composition of the products were analyzed by SEM-EDS.

They assumed that the reaction between the liquid calcium aluminate and solid alumina can be divided into two steps:

a. calcium diffusion in the liquid calcium aluminate layer

b. chemical reaction at the alumina/calcium aluminate interface

They said that one of these two steps could be rate-controlling, but, since a significant calcium concentration gradient in the liquid product layer was not observed, they concluded the chemical reaction to be the rate controlling step. Besides, by analyzing the cross section of the reacted couple, they could not find any layer of CA_6, CA_2, or CA phases in the reaction product. This observation is confirmed by SEM analysis conducted by Visser et al. [30].

Han et al. [33] proposed a reaction model as shown in Figure 2-20.

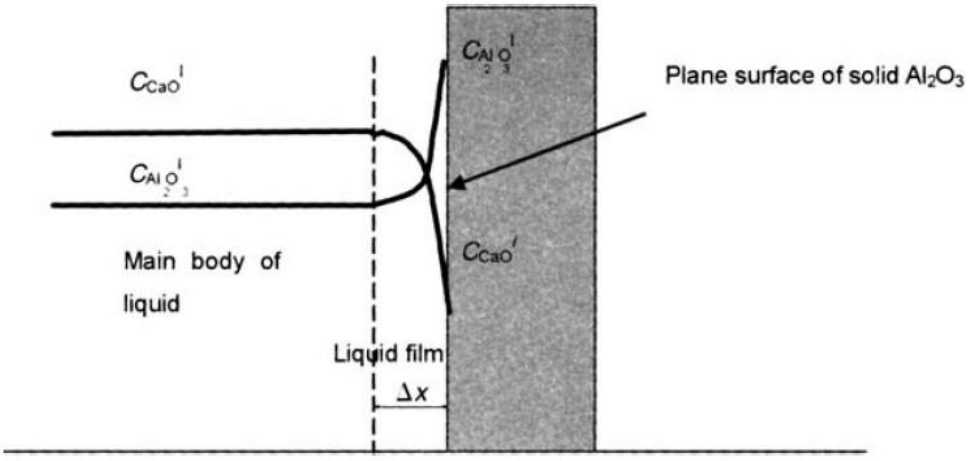

Figure 2-20. Schematic diagram of liquid calcium aluminate reaction with solid alumina- reprinted with permission from ref [33]

The flux of CaO in the liquid calcium aluminate transferred through the boundary layer to the surface of alumina by diffusion can be written as:

$$r_{CaO,1} = \frac{1}{S}\frac{dN_{CaO}}{dt} = \frac{D_{eff}}{\Delta x}\left(C_{CaO}^{1} - C_{CaO}^{i}\right) = k_D\left(C_{CaO}^{1} - C_{CaO}^{i}\right) \qquad \textbf{(2-18)}$$

Where C_{CaO}^{l} and C_{CaO}^{i} are the concentration of CaO in the liquid calcium aluminate at the interface between liquid calcium aluminate and alumina, respectively.

The dissolution rate of CaO at the alumina surface, assuming first order reaction:

$$r_{CaO,2} = \frac{1}{S}\frac{dN_{CaO}}{dt} = k_R C_{CaO}^{i} \qquad \textbf{(2-19)}$$

At steady state condition $r_{CaO,1}=r_{CaO,2}$, So by equating equations (2-18) and (2-19) after rearranging:

$$C_{CaO}^{i} = \frac{k_D}{k_D+k_R} C_{CaO}^{1} \qquad \textbf{(2-20)}$$

Substituting equation (2-19) in (2-20), one can write:

$$r = \frac{1}{\frac{1}{k_D}+\frac{1}{k_R}} C_{CaO}^{1} = k_{overall} C_{CaO}^{1} \qquad \textbf{(2-21)}$$

And $k_{overall}$ could be obtained by measuring the reaction area, reaction time, mass and composition of the liquid product.

They found that the reaction rate constant in this case could be represented by the Arrhenius law:

$$\ln k = -\frac{E}{RT} + \ln k_0 = -\frac{61631}{T} + 22.8 \qquad \textbf{(2-22)}$$

If the chemical reaction is the rate controlling step, the concentration profile will be the one shown in Figure 2-21

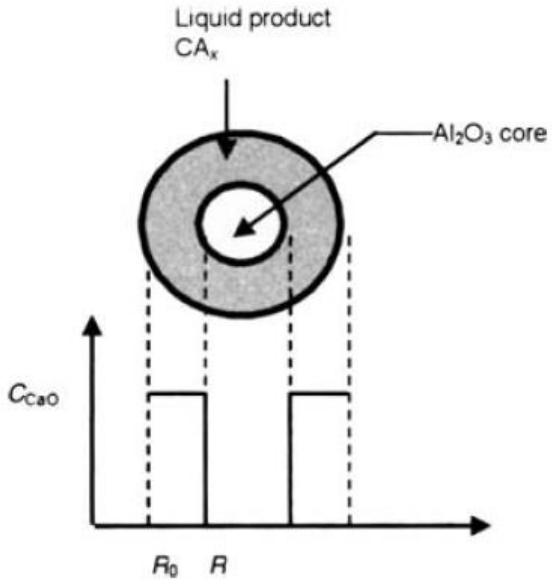

Figure 2-21. Schematic view of alumina inclusion modification- reprinted with permission from ref [33]

The rate of the reaction:

$$-\frac{x}{S}\frac{dN_{Al_2O_3}}{dt} = -\frac{x}{S}\,\rho_{Al_2O_3} S\frac{dR}{dt} = kC_{CaO}^{1} \qquad \textbf{(2-23)}$$

After rearrangement and integration, time of transformation:

$$t = \frac{x\,\rho_{Al_2O_3}}{kC_{CaO}^{1}}(R_0 - R) \qquad \textbf{(2-24)}$$

Time required for complete transformation is obtained by substituting R=0 in Eq (2-24).

However, it should be noted that fitting the rate equation to find the rate constant is not an appropriate method to determine the rate determining step since the rate equations for different rate controlling mechanism take have similar form. Assuming a shrinking coreLevenspiel [34] has carried analysis of rate equations for an unreacted core in which reaction of $(A(g) + bB(s) \rightarrow \text{solid product})$ occurs with different possible rate controlling step.

- Diffusion Through boundary layer Controls

Figure 2-22 shows the concentration gradient for an unreacted shrinking core particle in which diffusion through boundary is the rate controlling step.

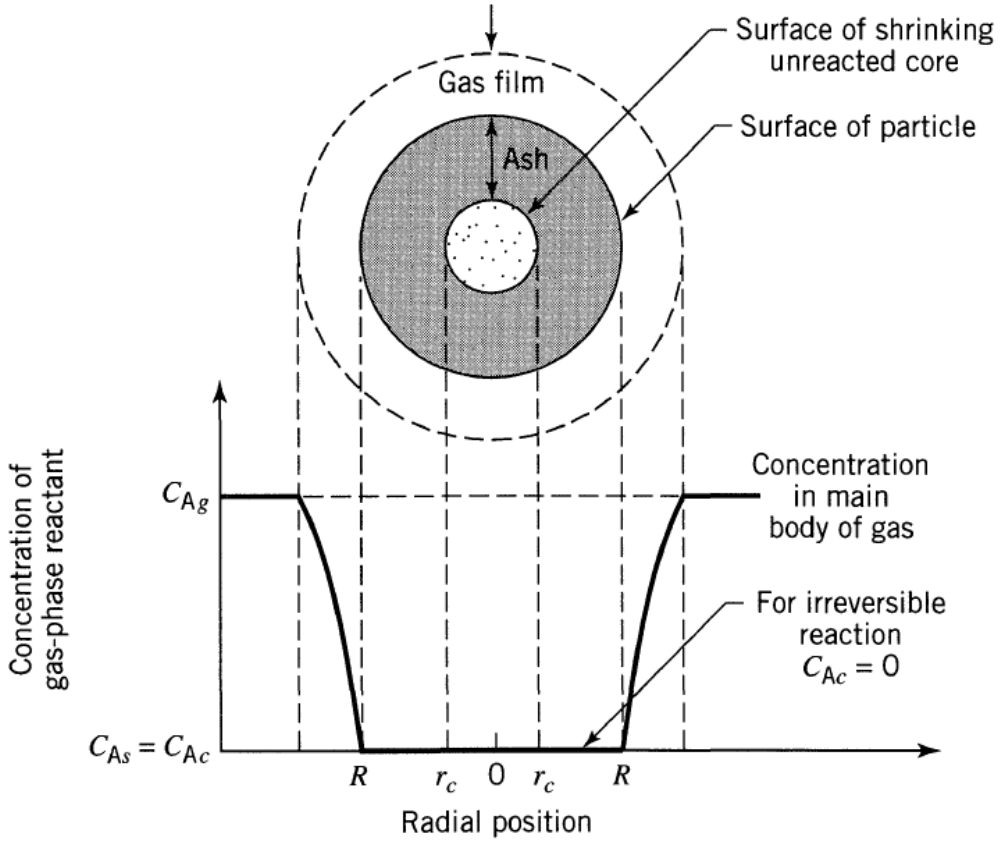

Figure 2-22. Schematic diagram of a reacting particle when diffusion through the boundary layer is the controlling resistance- reprinted with permission from ref [34].

Levenspiel [34] expressed that according to mass balance:

$$\frac{1}{S_{ex}}\frac{dN_B}{dt} = -\frac{1}{4\pi R^2}\frac{dN_B}{dt} = -\frac{b}{(4\pi R^2)}\frac{dN_A}{dt} = b\,k_g\left(C_{Ag} - C_{As}\right) = bk_gC_{Ag} = constant \qquad \textbf{(2-25)}$$

Where S_{ex} is exterior surface of the particle and K_g is the mass transfer coefficient in gas film.

- Diffusion through product (Ash) Layer Controls

Figure 2-23 presents the situation in which the resistance to diffusion through the product layer controls the rate of reaction.

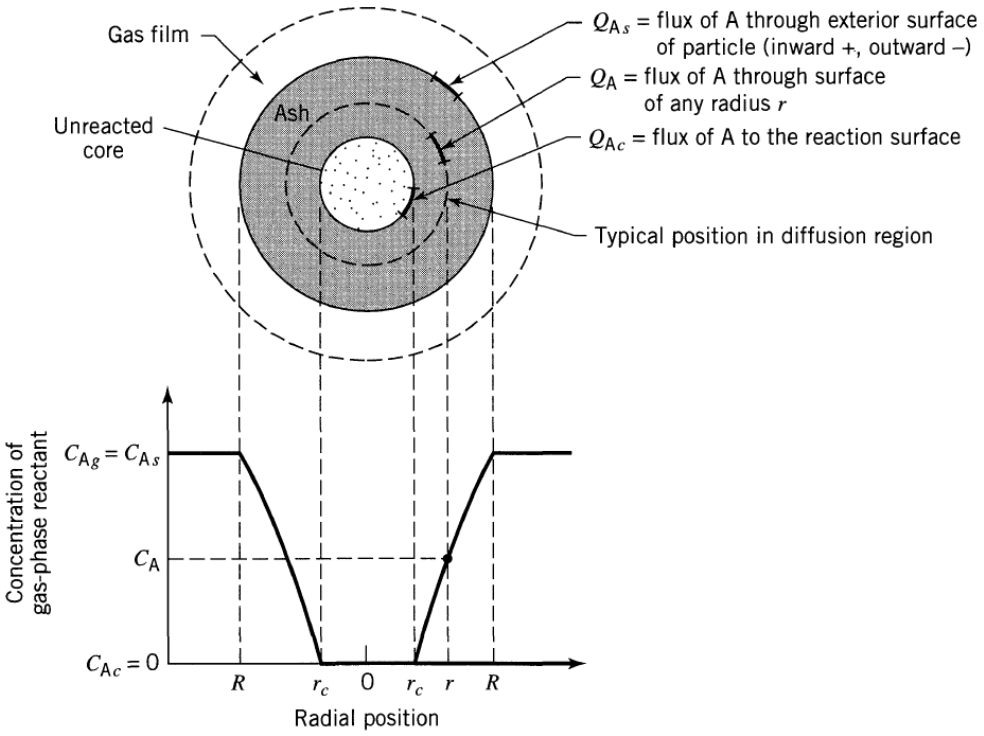

Figure 2-23. Schematic diagram of a reacting particle when diffusion through the ash is the controlling resistance- reprinted with permission from ref [34].

According to Levespiel's analysis the rate equation can be written as:

$$-\frac{dN_A}{dt} = 4\pi r^2 Q_A = 4\pi R^2 Q_{As} = 4\pi r_c^2 Q_{Ac} = constant \qquad \textbf{(2-26)}$$

Q is the flux and it is shown in Figure 2-23.

- Chemical Reaction Controls

Figure 2-24 illustrates concentration gradients within a particle when chemical reaction control

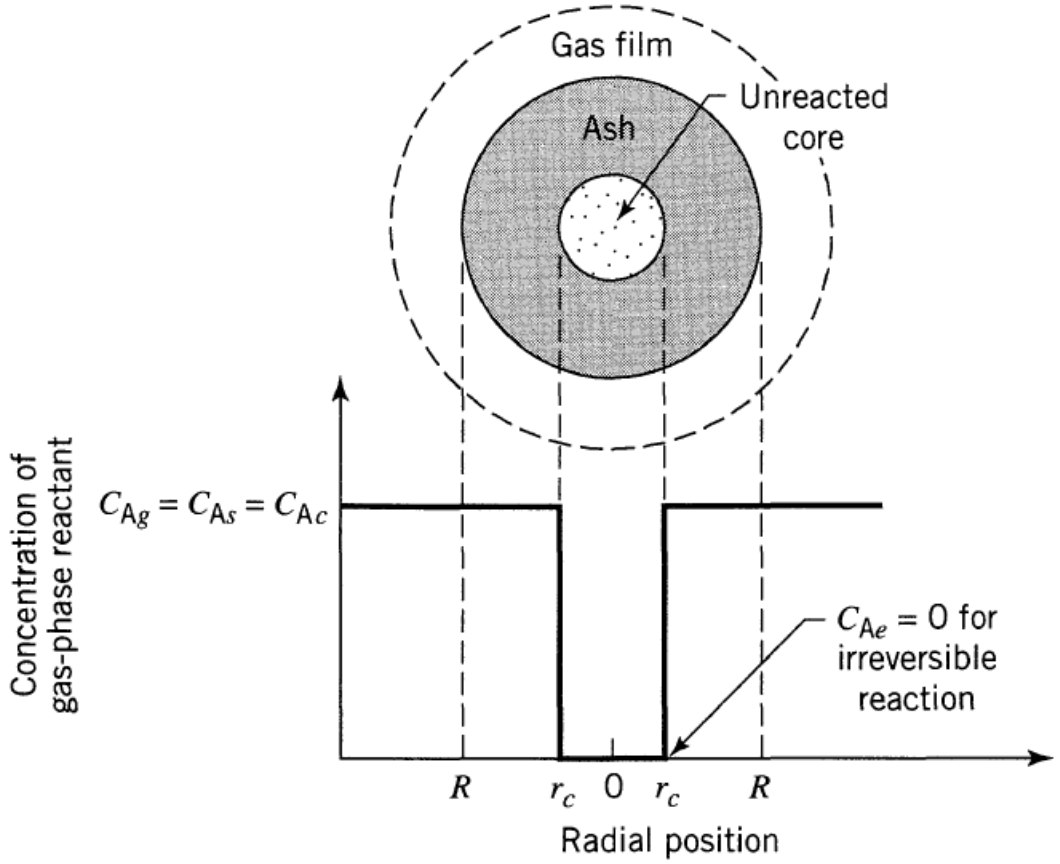

Figure 2-24. Schematic diagram of a reacting particle when chemical reaction is the controlling resistance- reprinted with permission from ref [34].

In this situation the rate equation takes the form:

$$-\frac{1}{4\pi r_c^2}\frac{dN_A}{dt} = -\frac{b}{4\pi r_c^2}\frac{dN_A}{dt} = bk''C_{Ag} \qquad \textbf{(2-27)}$$

Where k'' is the rate constant for chemical reaction.

As it is seen equations (2-25)-(2-27) have similar form except the fact that they consist of different constants.

2.3.4 Modification of spinel inclusions

During the process of metal deoxidation and desulphurization, the content of dissolved magnesium [Mg] in the steel will increase through reduction of MgO in the slag, leading to a transformation of the initial alumina inclusions to Magnesium Aluminate Spinel ($MgAl_2O_4$). The source of the magnesium which reacts to form spinel inclusions in liquid steel is substantially reaction between the liquid steel and the ladle slag with low FeO and MnO levels [35].

Verma et al. [36] stated that calcium modification of spinel inclusions is different from that of alumina in two ways:

a. Solid calcium aluminate is the first product to form when the calcium reacts with alumina, whereas liquid oxide forms as the first a product of reaction of calcium with spinel. Even a small fraction of MgO in the inclusion can promote liquid formation (Figure 2-25). This is also confirmed by Yang et al. [37] based on their industrial trial analysis and thermodynamic calculations.

b. The modification of spinels causes a decrease in the MgO content of the inclusions as show in Figure 2-26. They stated that the magnesium that was returned to the melt during calcium treatment would reform spinels during reoxidation.

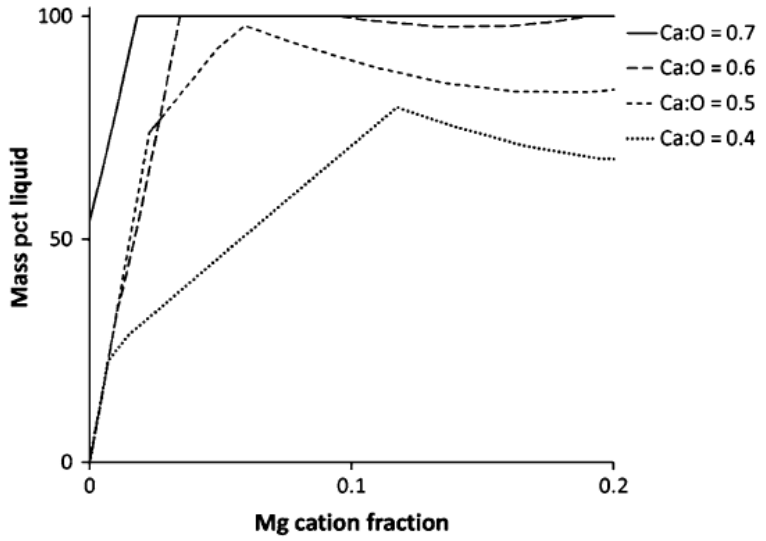

Figure 2-25. Effect of magnesium on liquidification of inclusions [36]

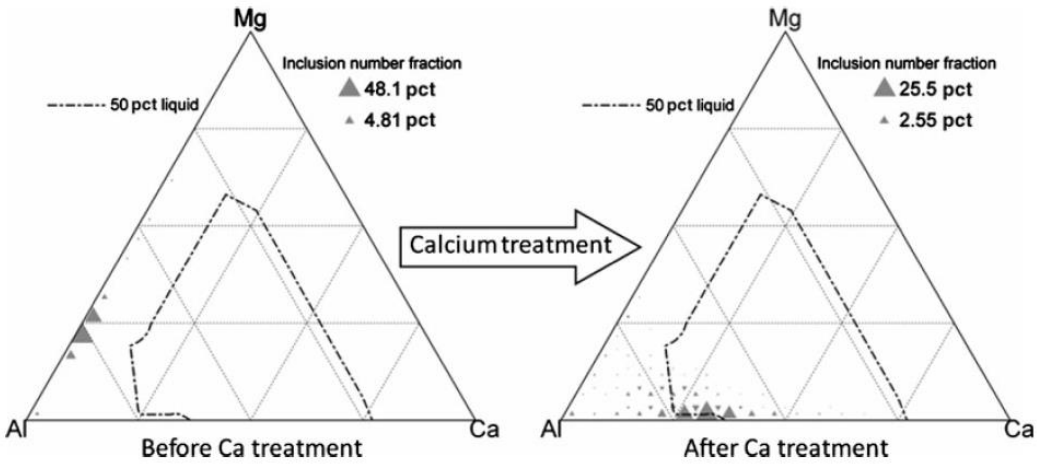

Figure 2-26. Change in inclusion composition after calcium treatment- reprinted with permission from ref [36]

They proposed the following mechanism for modification of spinel inclusions:

Injected calcium reacts with dissolved sulfur to form CaS and reduces MgO from the spinels

$$[Ca] + [S] \rightarrow CaS \quad \textbf{(2-28)}$$

$$[Ca] + (MgO) \rightarrow (CaO) + [Mg] \quad \textbf{(2-29)}$$

CaS reacts with the oxide (mainly Al_2O_3) inclusions, returning sulfur to the melt.

$$3CaS + Al_2O_3 \rightarrow (CaO) + (Al_2O_3) + 2[Al] + 3[S] \quad \textbf{(2-30)}$$

This mechanism is illustrated in Figure 2-27.

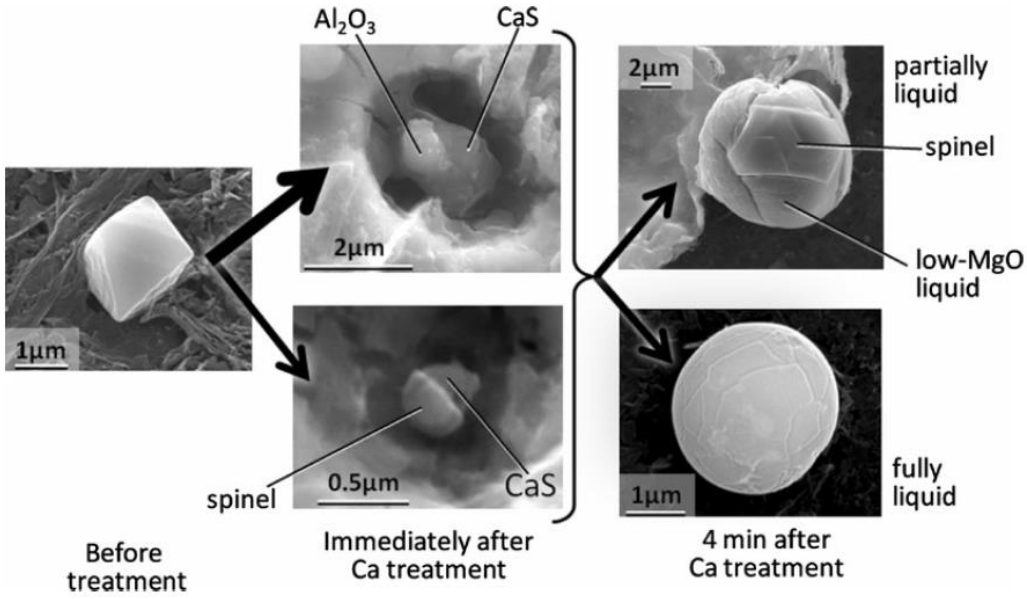

Figure 2-27. Inclusion morphologies after deoxidation and after calcium treatment- reprinted with permission from ref [36]

Yang et al. [38] studied the formation and modification of $MgO - Al_2O_3$ spinel inclusions in alloy steels by thermodynamic calculations, laboratory experiments, and industrial trials. They proposed a kinetic model for modification of spinel which involves the following steps: diffusion of [Ca] in the molten steel, diffusion of [Ca] in the resulting calcium aluminates, chemical reaction at the liquid steel–inclusion interface, diffusion of [Mg] in calcium aluminates, and diffusion of [Mg] in the molten steel. A schematic diagram of the model can be seen in Figure 2-28.

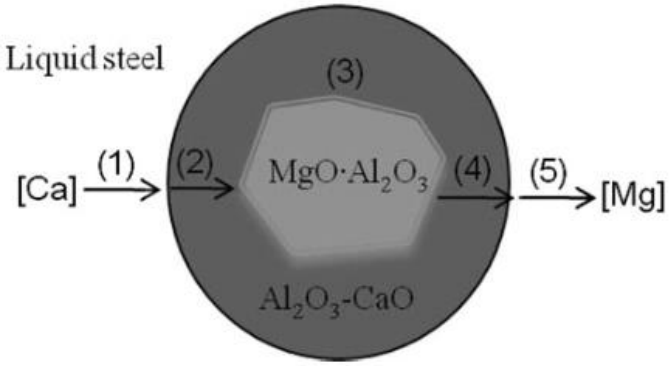

Figure 2-28. Schematic of the kinetic model proposed by Yang et al. [38] *on modification of MgO. Al_2O_3 inclusion by Ca treatment- reprinted with permission from ref* [38]

They argued that diffusion of calcium in the calcium aluminate is much faster than aluminum and due to similar properties between magnesium and aluminum, the diffusion coefficient of magnesium in the calcium aluminate should be smaller, so they concluded the diffusion of Mg in the calcium aluminate should be the rate controlling step for modification of spinel. This assumption does not seem entirely reasonable as the diffusivity of Mg^{2+} in the liquid is likely to be closer to that of Ca^{2+} than to a complex aluminate ion. In addition, it was said that the reduction reaction of (MgO) to [Mg] would occur, but as the reaction proceeds a calcium aluminate layer is produced around the inclusion and slows down the reducing reaction. Simultaneously, reaction of [Ca] and [O] with (Al_2O_3) takes place to produce calcium aluminate.

According to this model a mechanism was proposed for modification of spinel by calcium treatment which consists of following steps:

a. Reduction of a fraction of MgO in the inclusion by the dissolved calcium in the steel by the reaction:

$$y\ (MgO.Al_2O_3) + x[Ca] = (xCaO.yAl_2O_3) + y[Mg] \quad \textbf{(2-31)}$$

At this stage, the magnesium in the spinel is replaced by calcium; and then magnesium is dissolved in the steel and a thin layer of $xCaO.yAl_2O_3$ forms at surface of the spinel inclusion.

b. Formation of liquid $xCaO.yAl_2O_3$ layer at the outside of the spinel inclusion.

When the thin layer of calcium aluminate at the surface of the spinel inclusion becomes progressively thicker, the diffusion of Mg to the molten steel through this layer becomes very slow, then the following reactions dominate the modification process, precipitating a layer of ($xCaO.yAl_2O_3$) outside of the spinel inclusion.

$$[Ca] + [O] = (CaO) \quad \textbf{(2-32)}$$

$$[Al] + [O] = (Al_2O_3) \quad \textbf{(2-33)}$$

$$x[Ca] + 2y[Al] + (x + 3y)[O] = (xCaO.yAl_2O_3) \quad \textbf{(2-34)}$$

$$x(CaO) + y(Al_2O_3) = (xCaO.yAl_2O_3) \quad \textbf{(2-35)}$$

$$3(MgO) + 2[Al] = (Al_2O_3) + 3[Mg] \quad \textbf{(2-36)}$$

As the calcium is injected to the steel, there is a high concentration of Ca in the steel which can react to oxygen by reaction (2-32). Also, the high aluminum content of the steel can react with oxygen to form new precipitation of Al_2O_3. The dissolved aluminum or precipitated Al_2O_3 reacts with dissolved Ca to form calcium aluminate according to (2-34) and (2-35). Gibbs free energy for reaction (2-36) is much less negative than the other

proposed reactions which makes it least least-likely to occur. However, reaction (2-31) dominates the modification process at this stage.

c. Formation of a solid $CaS - CaO$ layer at the outer layer of the spinel inclusion

d. If the local sulfur concentration in the molten steel is high enough dissolved calcium and sulphur can react to form CaS. During cooling and solidification process the precipitated sulfur and the dissolved calcium can react to for CaS inclusions which precipitate at the surface of spinel inclusion.

Schematic plot of the proposed modification mechanism has been shown in Figure 2-29.

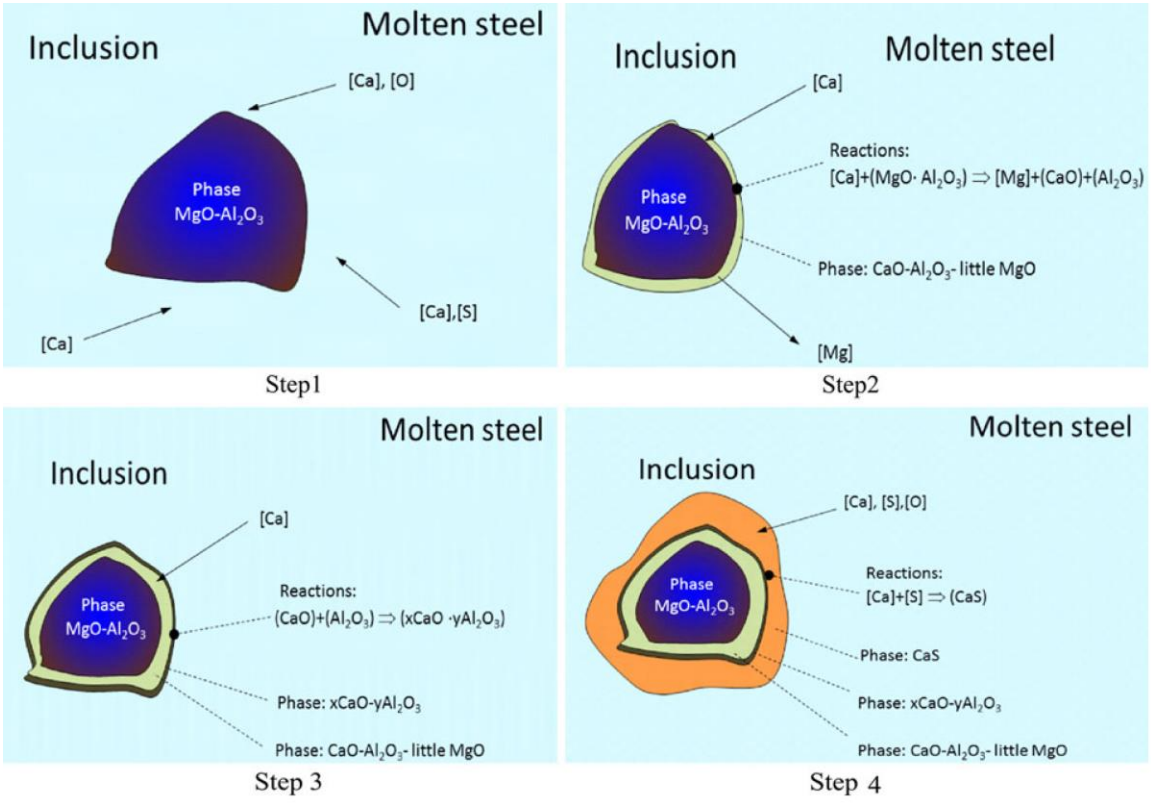

Figure 2-29. proposed Steps for the modification of $MgO\text{-}Al_2O_3$ by Yang et al.-reprinted with permission from ref [38]

Therefore, the inclusion will have a pure $MgO.Al_2O_3$ spinel core with or without calcium treatment since the core of the spinel inclusion does not participate in any of the reactions. However, under circumstances of long refining time or small inclusions that offer more opportunity for diffusion of magnesium, these inclusions can be fully modified. Then, the authors concluded that under the following situations the inclusions can be fully transformed: I. Condition which enhance dissolution of magnesium in the inclusions. II. Long modification time, or III. If the inclusions are sufficiently small.

Yang et al. [39] investigated calcium treatment of $MgO-Al_2O_3$ spinel inclusions by laboratory experiments and developed a kinetic model for the modification of $MgO-Al_2O_3$ inclusions. A total of 390 g of steel was melted in a crucible. Then, 0.3 g of aluminum wire was added to the melt for deoxidation and after about 5 min, 4 g of Mg was added for formation of spinel. Finally, Ca-treatment using 4 g Ca-Si addition in powder form was performed about 10 min later.

The mechanism of modification was described as following steps: (1) diffusion of the dissolved Ca in the boundary layer, (2) diffusion of Ca in the $CaO-Al_2O_3-MgO$ layer, (3) reaction between Ca and $MgO-Al_2O_3$ at the interface, (4) diffusion of the dissolved Mg in the inclusions, and (5) diffusion of the dissolved Mg in the boundary layer.

These workers stated that chemical reaction is much faster than diffusion, so they considered two cases to develop the kinetic model: first, that diffusion in the boundary layer is the rate controlling step and in the second case, the diffusion within inclusion product layer is rate controlling.

A. If diffusion of Ca or Mg in the inclusion product layer is rate-controlling, the schematic concentration profile would be similar to that shown in Figure 2-30.

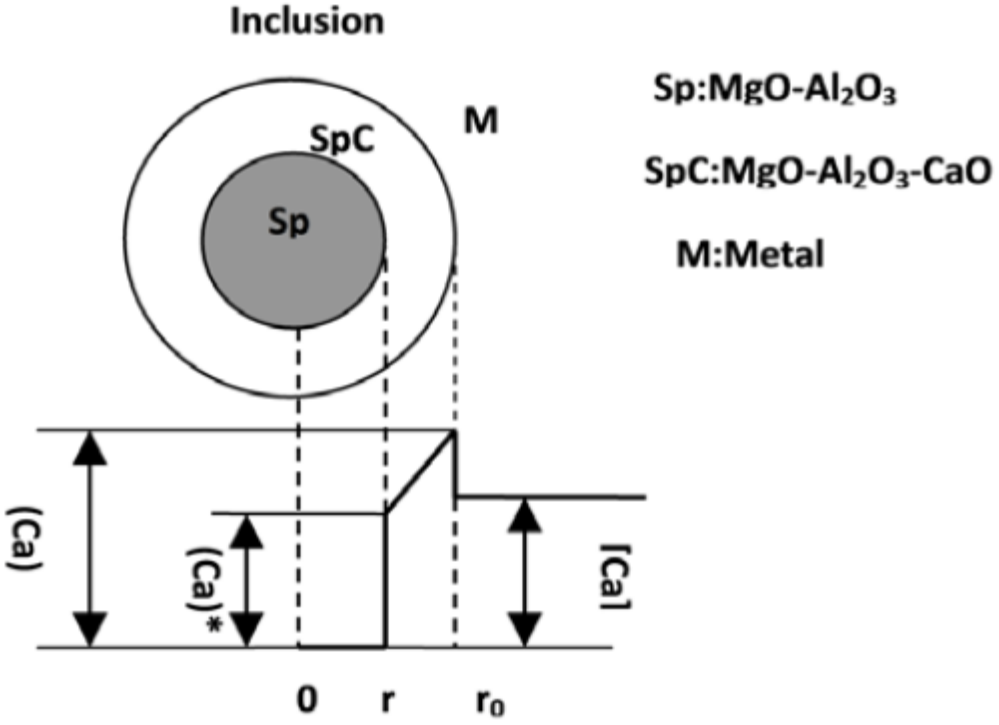

Figure 2-30. Ca concentration gradient when treating the diffusion of Ca in the inclusion layer as the rate-controlling step- reprinted with permission from ref [39]

As the change of the CaO in the inclusion is equal to the amount of diffused CaO per unit time:

$$\frac{d(CaO)}{dt} = \frac{D_S}{r^2}\frac{d}{dr}\left(r^2\frac{d(CaO)}{dr}\right) \qquad \textbf{(2-37)}$$

To solve this equation, it was assumed that the saturation CaO content of $MgO - CaO - Al_2O_3$ is 20% because during Ca treatment after reaching equilibrium in the experiments, the average weight percentage of CaO in the inclusion was close to 20%. For

diffusion of Mg, a similar equation can be written. The change of CaO content of inclusions with time for both cases are shown in Figure 2-31.

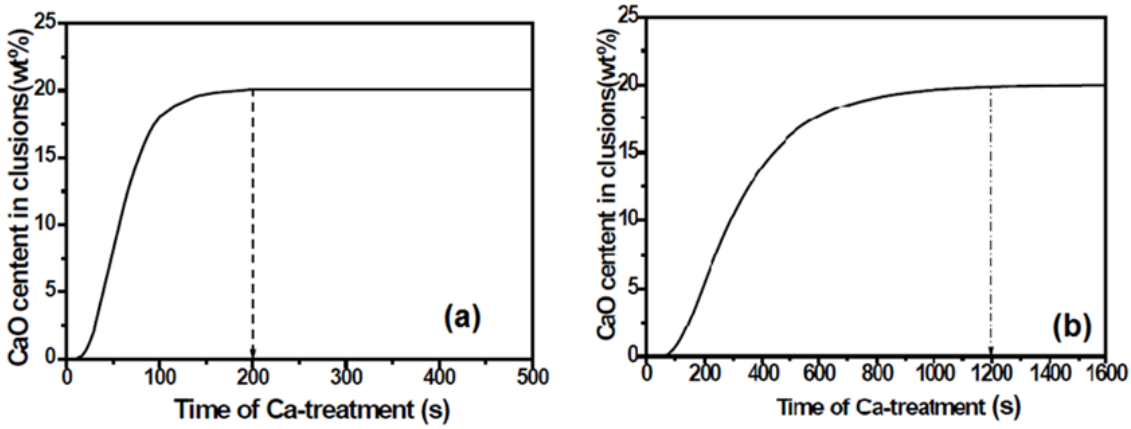

Figure 2-31. Calculated result for the CaO content in inclusions with respect to time of Ca-treatment when treating the diffusion of (a) Ca and (b) Mg in the inclusion layer as the rate-controlling step- reprinted with permission from ref [37]

But it should be noted that because they assumed a solid product layer, for the calculations they chose diffusivity of Mg^{2+} to be approximately 4 orders of magnitude lower than for Ca^{2+}. However, since these species have similar ionic radius, diffusion the coefficient could not be so different and since the mass transfer happens by counter diffusion of cations to maintain the charge balance, it does not make sense that the transport either Mg^{2+}or Ca^{2+} should be independently rate controlling. This issue is discussed in detail in Chapter 5.

B. If transport of Ca or Mg in the boundary layer is the rate-controlling step, concentration of Ca and Mg in the inclusion is assumed to be constant and the concentration profile is similar to that shown in Figure 2-32.

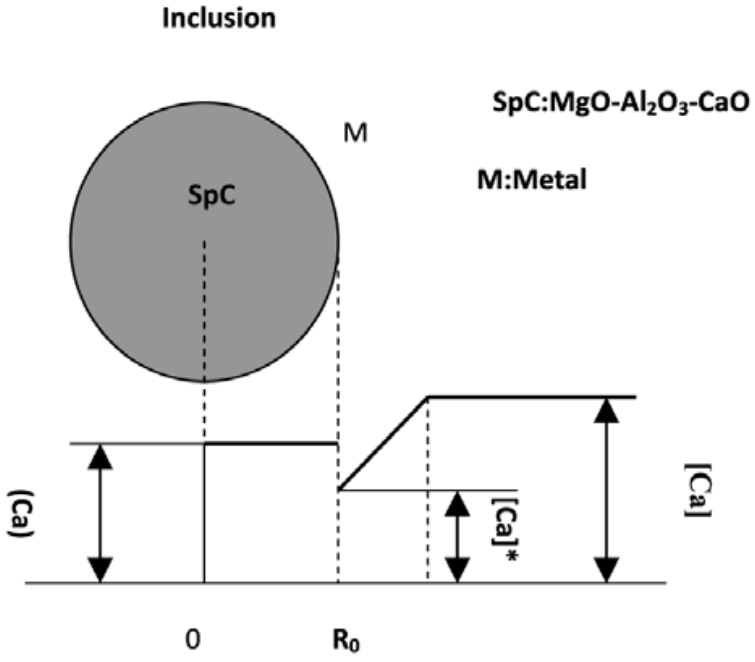

Figure 2-32. Distribution of Ca content when the diffusion of Ca in the steel boundary layer is the rate-controlling step- reprinted with permission from ref [39]

Based on the equilibrium state of [Ca] at the interface

$$\frac{d}{dt}\left\{\frac{4\pi}{3}\, r_0^3.(Ca).\rho_s\right\} = 4\pi.r_0^2\ \frac{D_m.\rho_m}{r_0}\{[Ca]-[Ca]^*\} \qquad \textbf{(2-38)}$$

$$[Ca]^* = \frac{(Ca)'}{L} \qquad \textbf{(2-39)}$$

$(Ca)'$ is the calcium concentration close to the inclusion side on the reaction interface, but because the inclusions are quite small, it is assumed that there is resistance to material transfer only in the liquid steel and thus (Ca)=(Ca)'.

From the above equations:

$$(Ca) = [Ca].L.\left\{1-\exp\left(-\frac{3D_m.\rho_m}{r_0^2.L.\rho_s}.t\right)\right\} \qquad \textbf{(2-40)}$$

Result of composition change for this case is seen in Figure 2-33.

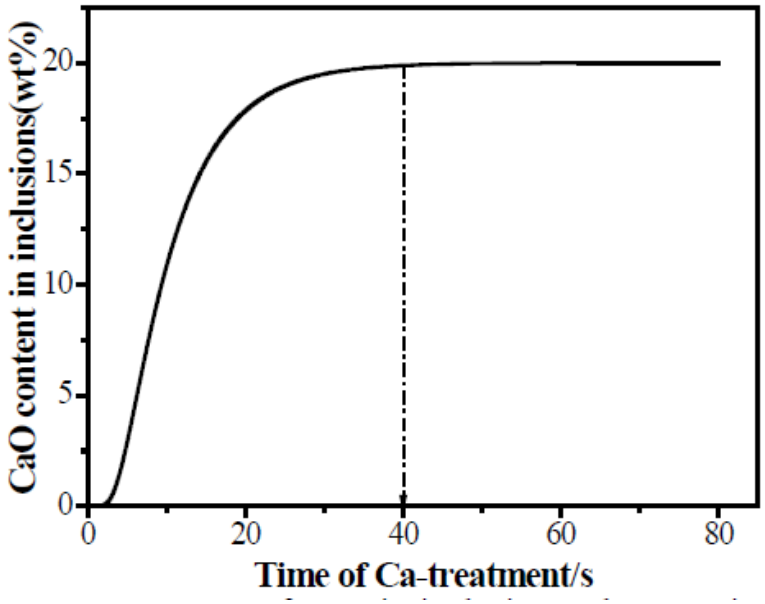

Figure 2-33. Content of CaO in inclusions when treating the diffusion of Ca and Mg in the boundary layer as the rate-controlling step- reprinted with permission from ref [39].

Comparing calculated results with experimental values as it is shown in Figure 2-34, Yang et al. *[39]* concluded that diffusion of magnesium through the inclusion product layer is the rate controlling step.

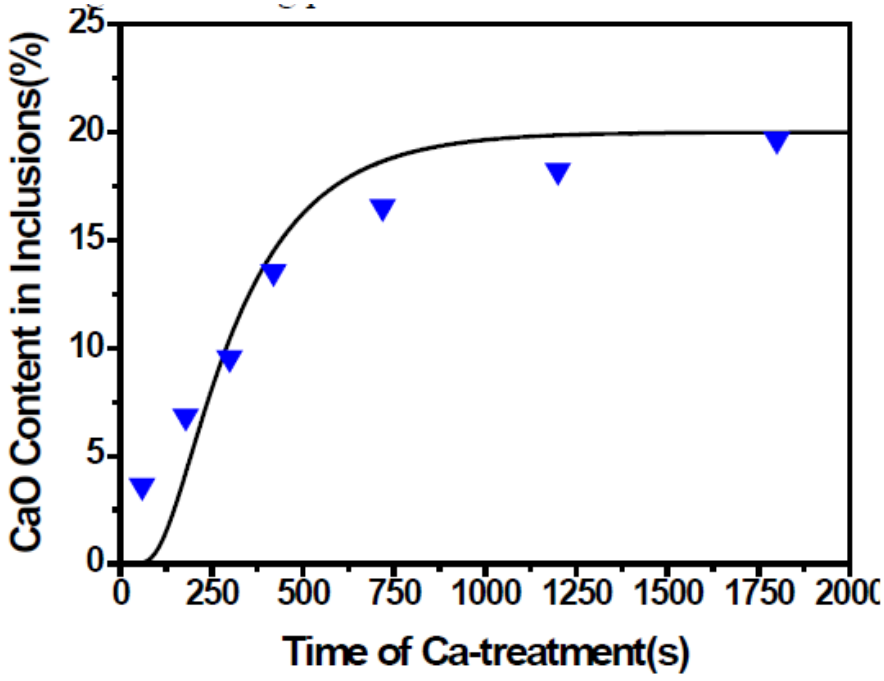

Figure 2-34. Comparison of the results of the model and experiment of the CaO content in inclusions with Ca-treatment time- reprinted with permission from ref [39]

2.4 Mathematical models for kinetics of steel-slag-inclusions in the ladle

Several attempts have been taken since the 1990s to mathematically model the kinetics of reactions occurring among steel, slag and inclusions in the ladle processes. Lu et al. [1] were the first researchers to model the kinetics of modification of oxide inclusions and formation of sulfide inclusions during calcium treatment based on their experiments in 40 kg steel heats. By assuming fast diffusion within the inclusions and fast reaction at the interfaces, they developed a mathematical model for inclusion evolution which offered very reasonable agreement with the experimental data.

In 2005 Peter et al. [40] developed a kinetic model by employing process simulation (Metsim) and thermodynamic (FactSage) models for simulation of the chemistry change of slag and metal. Correlation between overall mass transfer rate constants and stirring

powers were determined by analyses of 20 heats for real LMF practices. It was assumed that at a given time reaction, occurs between certain amount of slag and metal at the slag/liquid steel interface. The alloying addition, flux dissolution in slag, and even reoxidation of steel by open eye were considered in the model, although non-metallic inclusions were not taken into accounts in the simulation.

Visser et al. [30] simulated the change of the concentration, composition and size of the inclusions during calcium treatment in the ladle furnace by developing a reactor model. They divided the steel bath into two reaction zones: one including the plume zone saturated with calcium and low oxygen and the other the rest of the liquid steel which had low calcium and somewhat higher oxygen. Circulating current, flowing between these zones was estimated using CFD flow field calculations. In the plume zone CaO and CaS are deposited on the Al_2O_3 particles. In their model it was assumed that dissolved calcium and oxygen react with Al_2O_3 to form calcium aluminate with gradually increasing CaO fraction. In addition, it was assumed that mass transfer of the solutes to the particle surface was the rate controlling step for the formation reactions of CaO, CaS and Al_2O_3.

Graham and Irons [41] developed a multicomponent coupled slag–metal kinetic model for industrial operations in the ladle furnace which assumed rates were mixed transport controlled in the metal and slag phases. They investigated formation of spinel inclusions as a function of (MnO+FeO) content of the slag and also calcium aluminate according to calcium and oxygen content of the steel, but did not provide a mathematical model to describe change of composition of the inclusions. Later, this model was coupled to a

particle model for transformation of alumina inclusions to magnesium aluminate spinel by Galindo et al. [42]. Simultaneous deoxidation and solid state cation counter-diffusion within spinel inclusions were taken into account. The coupled model was verified with plant data from ArcelorMittal Dofasco. It was found that there was close correlation between reactions at the slag-metal interface and the transformation of inclusions in the steel.

Harada et al. [43] proposed a kinetic model to describe the ladle metallurgy process. The model considered interaction between steel, slag and inclusions originating from slag entrainment, as well as by deoxidation reactions, dissolution of the refractory into the slag and formation, flotation and agglomeration of inclusions. The activities of the individual components for a given oxide system of the inclusions were fixed and the composition change of inclusion was assumed to be controlled by mass transfer within the boundary layer. However, they did not consider formation of sulfide inclusions in their model and several model parameters were calculated by fitting the model results, these parameters would require to be modified if the operational conditions changed. In a further study by Harada et al. [44] their kinetic model was employed to clarify the mechanism by which inclusion composition was changed and the model was validated by laboratory experiments. They observed that the inclusion composition gradually changed from Al_2O_3 to $MgO \cdot Al_2O_3$ after the addition of Mg, and the inclusions originating from slag remained in the steel for the duration of the experiment (30 mins).

Some researchers have employed computational thermodynamic software combined with kinetics calculations to model reactions occurring in the ladle furnace. Recently,

Kumar [45] used the macro-processing feature in FactSage to predict the change of composition of slag, steel and inclusions. Model parameters were found using experiments and industrial trials. Inclusion removal by floatation was assumed to be first order with a fixed rate constant. The kinetic model was used to find the rate of magnesium pick-up in the steel and transfer to oxide inclusions in the steel considering steel-MgO crucible reaction, magnesium evaporation and inclusion removal. The model was also used by Kumar and Pistorius [46] to quantify the rate of calcium transfer from slag to steel to inclusions that may modify alumina inclusions in laboratory scale experiments. They assumed that the mass transfer coefficient in the steel, k_{steel} was 10 times larger than in the slag, k_{slag} and experimental data was used to determine $k_{steel} \times A_{Interface}$. Van Ende and Jung [47] employed the Effective Equilibrium Reaction Zone (EFRZ) model applied to the FactSage macro processing code to model kinetics of LMF process. The slag/metal interactions, flux and alloying additions, and arcing in the LMF process were also considered in the model. In the EERZ model, calculation is carried out in a finite number of reaction zones in which equilibrium is attained. Kinetics of reaction is taken into account by varying the reaction zone volumes according to physical descriptions of fluid dynamics. Their model could predict steel and slag composition, as well variation of the amounts of different types of inclusions and overall composition of inclusions. The model was validated against plant data taken from Graham and Irons [41,48].

Shin et al. [49] also employed the EERZ model to predict the evolution of inclusions during the secondary refining processes. In their model, the reaction zone mass per unit step was considered for describing the mass transfer in each phase. i.e a constant mass of

metal from the bulk metal and a constant mass of slag from the bulk slag enter the metal–slag reaction zone at a fixed time interval. The reaction zone mass was dependent on the ”effective reaction zone depth” in each phase. The effective reaction zone depth was fitted from the mass transfer coefficients in metal and slag phase which was determined experimentally.

A comprehensive model for variation of inclusion composition in gas stirred ladles was proposed by Scheller and Shu [50]. Slag-steel reaction, refractory dissolution into slag and liquid steel, inclusion formation, and removal due to gas stirring was considered in the model. The FactSage database was used to calculate the equilibrium composition at the slag/metal interface. Data from plant heats was used to determine fixed constant dissolution rate of refractory into slag and liquid steel. Various and arbitrary inclusion removal rates depending on the type of inclusion were also chosen to reproduce the inclusion population from the plant data.

2.5 Summary

As discussed above, modeling of ladle metallurgy furnace kinetics is a complicated task as many reactions occur simultaneously. On the other hand, these reactions happening at the steel - slag interface, steel-inclusion interface and steel-calcium bubble interface are closely linked. Thus, kinetics of each of these reactions needs to be understood to construct a comprehensive model of the LMF process. As presented earlier, there are some uncertainties in the literature regarding calcium modification of inclusions with respect to; (1) the assumptions (2) the rate constants and (3) the rate determining steps. Different

studies claim different rate controlling steps for modification of alumina inclusions. This arises from the following factors; (1) there are some assumptions that are unrealistic or (2) some researchers ignored some kinetic steps in their models or (3) the experimental or industrial conditions were different in terms of concentration of dissolved species or injection condition. Some of the proposed models in the literature found the kinetics parameters just by fitting the results of the model with measured data . In the current study, kinetics parameters of the sub-models for inclusion modification are taken from the literature and sensitivity analysis is carried out as discussed in Chapters 3-5 to investigate the importance of each step. Also, the model should take into account competition of different inclusions such as alumina, spinel and sulphide for calcium, which is ignored in previously proposed models. The model should be able to track the trajectory of slag, metal and inclusion composition during ladle processing. The following chapters will present the Author's attempt to address these issues.

Chapter 3

A Multi-Layer Model for Alumina Inclusion Transformation by Calcium in the Ladle Furnace

In Chapter 3, the original concept of the model was suggested to me by Dr. Kenneth S. Coley. The detailed model development was carried out entirely by me, based on advice from Drs Irons, Coley and Sun. The manuscript was initially drafted by me, proofread by Dr. Kenneth S. Coley and reviewed to the final version by Dr. Gordon A. Irons and Dr. Stanley Sun. This chapter has been published in *Metallurgical and Materials Transactions B.* 49: 375. https://doi.org/10.1007/s11663-017-1120-8. The following Chapter is a pre-publication version of the article.

Abstract

Calcium wire injection is widely used for modification of solid alumina inclusions to liquid or partially liquid calcium aluminate. In the present work a multi-layer growth model is proposed for modification of alumina inclusions. Diffusion through a multi-phase product layer and mass transfer of solute through the boundary layer to the inclusion are taken into account in this model. It is assumed that outer surface of the inclusion is thermodynamically in equilibrium with the steel. The results show the mass transfer of calcium through the boundary layer and within the inclusion is complete in a matter of seconds; furthermore, once the liquid calcium aluminate forms it quickly consumes the other solid calcium aluminate phases. Because the calcium is so rapidly consumed by the

inclusions, the rate of transformation in a calcium treatment process is controlled by the rate that calcium is supplied to the steel by the calcium bubbles.

3.1 Introduction

Inclusion control in steelmaking practice relies upon the choice of deoxidants and the top slag, stirring by argon gas and calcium treatment. The latter modifies solid alumina inclusions to liquid spherical calcium aluminates. This process has been widely used in low-carbon aluminum-killed (LCAK) steels to alleviate submerged entry nozzle (SEN) clogging by solid alumina inclusions during continuous casting. The presence of alumina inclusions has unfavorable effects not only on the production efficiency [1], but also steel mechanical properties [2].

Calcium treatment is one of the most difficult practices in steelmaking because (a) calcium boils and has low solubility in the steel, forming bubbles which are not completely dissolved in the steel, (b) calcium also reacts strongly with oxygen and sulphur [3] so these elements in the steel must be well-controlled and (c) there is a very narrow window of liquid calcium aluminate composition at steelmaking temperatures (see Figure 3-1). Since the early days of calcium treatment in the 1990s great improvements have been made in the practical aspects so most plants can control calcium treatment on a day-to-day basis, but it is a very sensitive process [4]. Nevertheless, our fundamental understanding of the mechanism and kinetics of the transformation is not established and discrepancies exist in the literature in terms of mechanism and rate controlling step [5-9].

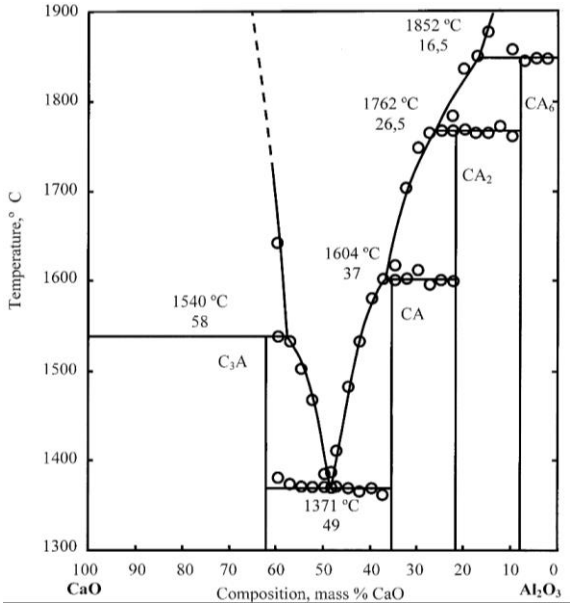

Figure 3-1. $CaO - Al_2O_3$ phase diagram reprinted with permission from [51]

Lu et al. [5] were the first to model the kinetics of formation of oxide and sulfide inclusions during and after calcium injection based on their experiments in 40 kg steel heats. They assumed fast diffusion within the inclusions and fast reaction at the interfaces and developed a mathematical model for inclusion evolution which offered very reasonable agreement with the experimental data. Later, Ito et al. [7] employed an unreacted shrinking core model for alumina transformation. They assumed three different possible rate-determining steps: (a) mass transfer in the melt, (b) mass transfer in the product layer, and (c) chemical reaction at the interface. By comparing the calculated results against experimental data they concluded that diffusion through the product layer was the rate controlling step. However, they did not include the dissolution rate of calcium in their analysis. Higuchi et al. [8] also developed a mathematical model of the kinetics of inclusion transformation similar to that developed by Lu et al. [5] with the additional consideration

of the chemical reaction rate between inclusions and the melt. In their case, mass transport of calcium from the bulk to the surface of particles in the melt was ignored.

Ye et al. [9] proposed that the reactions for inclusion modification occur according to the following sequence: Al_2O_3 => CA_6 => CA_2 => CA => CA_x where C: CaO and A: Al_2O_3 and CA_x refers to liquid calcium aluminate which can have a range of composition according to the phase diagram in Figure 3-1. However, Han et al. [6] did not observe multiple layers in their experiments with a $CaO - Al_2O_3$ couple and concluded that chemical reaction between alumina and liquid calcium aluminate was the rate determining step. Visser et al. [11] developed a model based on results from inclusion analysis, in addition to thermodynamic, kinetic and fluid flow considerations to describe the change of concentration, compositio and size of the inclusions in the liquid steel were considered. Their model assumed that dissolved calcium and oxygen react with Al_2O_3 to form calcium aluminate with gradually increasing CaO fraction and that the formation of CaO, CaS and Al_2O_3 are rate limited by mass transfer of the solutes to the particle surface where local equilibrium was assumed. Since the dissolved calcium concentration in the steel was unknown, their simulations employed two values for calcium concentration, 1 ppm and 30 ppm Ca. They found that the simulations with 1 ppm Ca resulted in better agreement with measured values for dissolved oxygen, CaS proportion of total calcium and total calcium.

To summarize, there are considerable uncertainties in literature regarding the kinetic control of the modification of alumina inclusions by calcium. The objective of the present work is to develop a comprehensive mathematical model. In this paper the parts of the

model concerning diffusion in the melt and within the inclusions are presented. The aspects relating to mass transfer from the calcium bubbles will be addressed in a subsequent paper because it requires the modelling of specific injection practices.

The current work is part of a larger program to develop a model describing inclusion modification during ladle treatment. This model, described in detail in a publication to be submitted shortly, is based on real process conditions and considers the change in slag and metal composition with time, in addition to the change in inclusions induced by calcium injection. The steel/slag reaction component of the larger model has been developed and validated by other workers in the authors' laboratory [12], as has the sub-model for calcium injection [5]. The current work presents a new sub-model developed to describe the behavior of a single inclusion as a function of conditions in the steel. This has been used to define the requirements of the inclusion modification component of the larger model. The paper, presenting the larger model, reports excellent agreement between model predictions and plant data. Unfortunately, the plant data could not be used directly, to support the current findings because the assumptions, used to restrict the model to the behavior of a single inclusion, represent constraints that do not exist in a real ladle. We would suggest that the excellent agreement between the overall model and the plant data, offers strong justification for the current work. We also note that every aspect of the current model is justified by well-established knowledge of the $CaO - Al_2O_3$ system and the conditions assumed represent realistic conditions for ladle metallurgy.

3.2 Mathematical model

3.2.1 Outline of the Model System

The objective of this model is to describe the mass transport steps to and within alumina inclusions during calcium treatment of aluminum-killed low-carbon steel. In the typical industrial practice aluminum is added to the steel during tapping from the furnace into the ladle. Further aluminum additions may be made after the ladle arrives at the ladle metallurgy station. Typically, the steel is stirred by argon injected through bottom plugs in the ladle. The stirring serves to float out the larger inclusions and to homogenize the melt which may have alloys added to it. The stirring is usually carried out for several minutes which is well beyond the mixing time for the ladle [13], so the dissolved elements and inclusions are homogenously distributed.

Automated inclusion analysis of steel samples reveals that most of the alumina inclusions are in the range of 1 to 10 microns; the larger ones have floated out and the smaller ones are not detectable by the technique. At this time the total oxygen content in the steel may be between 10 and 50 ppm, depending on specific practices. The total oxygen content is the sum of dissolved oxygen and oxygen in inclusions. If one assumes that the total oxygen and dissolved oxygen contents are 30 and 5 ppm, respectively, and that the inclusions are 5 micron alumina inclusions, it is a simple matter to calculate that there are 1.8×10^{12} inclusions per m^3 of steel with an interfacial area of 141 m^2/m^3. This is a huge amount of interfacial area so the overall rate of reaction of oxygen and aluminum at alumina inclusions is very rapid. This is the reason that the dissolved oxygen and

aluminum contents in the steel shortly after aluminum addition are found to be very close to thermodynamic equilibrium with alumina [14].

Once the sulphur and oxygen levels have been adjusted in the steel, calcium is injected. The most common technique is to inject steel-clad calcium wire deeply into the melt. The objective is to give the calcium bubbles the maximum residence time to dissolve during their rise in the steel. Nevertheless, 60 to 80% of the calcium may be lost because the boiling is a turbulent process that creates large bubbles and considerable splashing of steel. Figure 3-2 shows a schematic representation of the transport processes and expected concentration gradients in the melt and inclusion. It must be appreciated that the one calcium bubble stands for a plume of calcium bubbles rising in the melt that are at least centimeter size, and that the one inclusion represents the huge number of micron-size inclusions in the melt. The inclusions are assumed to be all the same size and are all experiencing the same rate of reaction because the melt is so well homogenized by the stirring. In the present paper the transport processes and concentration gradients around the inclusion are modelled in detail. As mentioned earlier, the details of the calcium dissolution will be left to a subsequent paper. All that is required for the present paper are the bulk calcium, aluminum and oxygen contents. The bulk aluminum and oxygen contents are assumed to be held constant at levels close to equilibrium with alumina. The calcium content is also assumed to be at a constant level in the bulk of the steel. Maintaining constant bulk values is mainly for convenience to simplify the explanation of the model for the inclusion transport. Moreover, the bulk values around each inclusion will be essentially

the same because the steel is well-stirred. In actual practice and in the subsequent paper the bulk concentrations will be transient, depending on the specific practice.

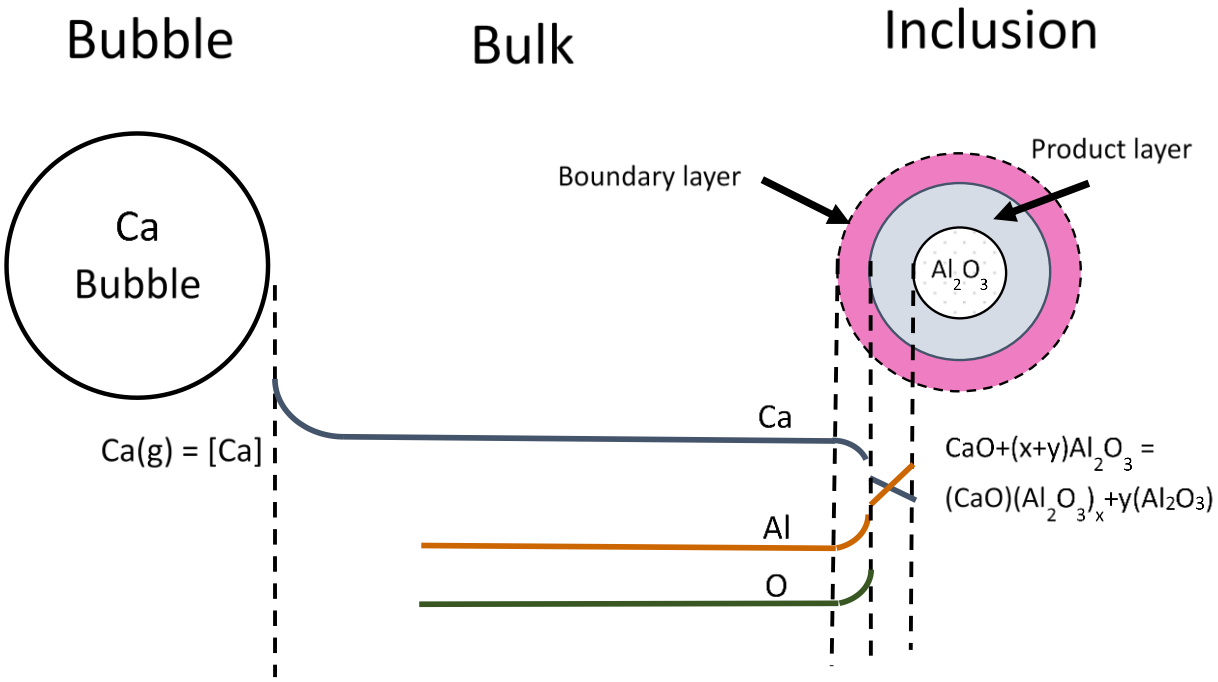

Figure 3-2. Schematic diagram of reactions and transfer of calcium

3.2.2 Alumina transformation

As explained above, the initial conditions are an alumina inclusion in steel containing a constant bulk content of calcium, aluminum and oxygen. To describe the transformation of alumina inclusions into calcium aluminate, an unreacted shrinking core model [15] is used in which the reaction starts at the outer surface of the particle. The product layer boundary moves into the solid, leaving behind converted material. According to this model, conversion of the alumina particle includes the following kinetic steps: (a) Transport of calcium from the bulk through the boundary layer to the surface of particle (b) Diffusion

of calcium oxide through the product layer(s) to the surface of the unreacted core (c) Chemical reaction at the alumina surface (d) Diffusion of alumina through the product layer(s) to the outer surface of the particle (e) Mass transport of aluminum and oxygen to the bulk of the steel.

To develop the model, one must consider $CaO - Al_2O_3$ phase diagram to examine the thermodynamic equilibria and each of the possible layers in the product layer (Figure 3-1). At 1600 °C, it is expected that the following equilibria exist: Al_2O_3 with CA_6, CA_6 with CA_2 and CA_2 with liquid CA_x. Therefore a multi-layer shrinking core model is assumed for the modification of alumina particles. A schematic diagram of the model is shown in Figure 3-3. The concentrations of the diffusing species are also shown schematically, respecting the phase equilibria at the phase boundaries.

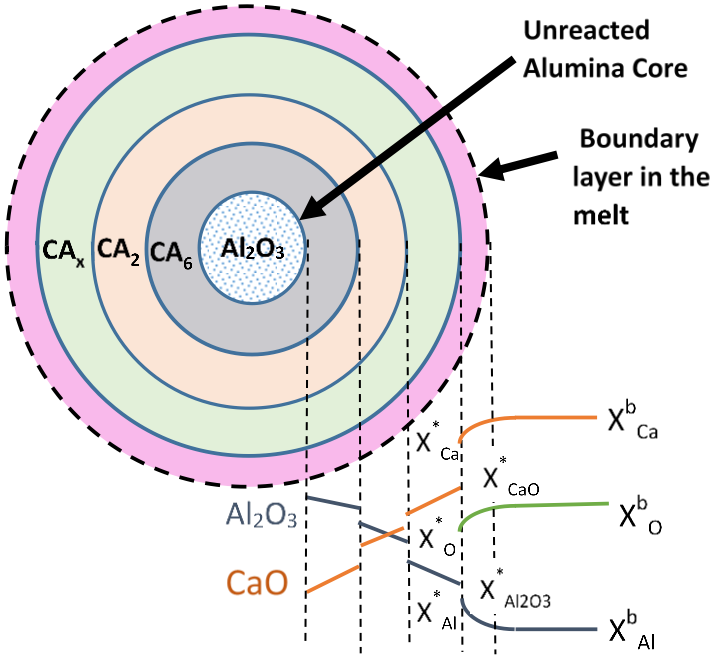

Figure 3-3. Schematic diagram of the multi-layer kinetic model and the concentration gradients

Buscaglia and Milanese [16] developed a general model for diffusion-controlled solid-state reactions of spherical particles in multiphase binary systems. In this study, their model is employed with some modifications for the calcium aluminate system. The assumptions of the model are as follows:

- Reactions occurring at a constant temperature of 1600°C lead to the formation of three intermediate phases as shown in Figure 3-3: CA_6, and CA_2 and liquid calcium aluminate.
- At the start of the process there is a very thin layer of all phases.
- Simultaneous growth of all phases, not necessarily at the same rate, occurs according to the governing equations.
- Since the temperature is high, chemical reactions are fast relative to mass transport processes, so equilibrium is attained at all interfaces.
- Ideal contact at the phase boundaries is considered, forming compact layers without pores or cracks.
- Mass transfer is mathematically described by quasi steady-state counter molecular diffusion of CaO and Al_2O_3 through the product layers. Whilst this is a legitimate phenomenological treatment, the authors recognize that the mechanism and actual diffusing species may be quite a bit more complex. Movement of each phase boundary is caused by consumption and formation of the adjacent phases which is related to the rates of diffusing species. This process is illustrated below for the case of CA_2 , recognizing that similar equations can be written for the other phases in the product layer.

A schematic diagram of the concentration profile and adjacent phases for CA_2 is depicted in Figure 3-4. The possible reactions at the interfaces are as follows:

(a) $Al_2O_3 + \frac{1}{4} CA_2 \rightarrow \frac{1}{4} CA_6$
(b) $CaO + \frac{1}{2} CA_6 \rightarrow \frac{3}{2} CA_2$
(c) $CaO + \frac{\vartheta'}{(2-\vartheta')} CA_2 \rightarrow \frac{2}{2-\vartheta'} CA_{\vartheta'}$
(d) $Al_2O_3 + \frac{1}{2-\vartheta'} CA_{\vartheta} \rightarrow \frac{1}{(2-\vartheta')} CA_2$

Where ϑ'defines the composition of the liquid calcium aluminate in thermodynamic equilibrium with CA_2 at 1600 °C according to phase diagram in Figure 3-1.

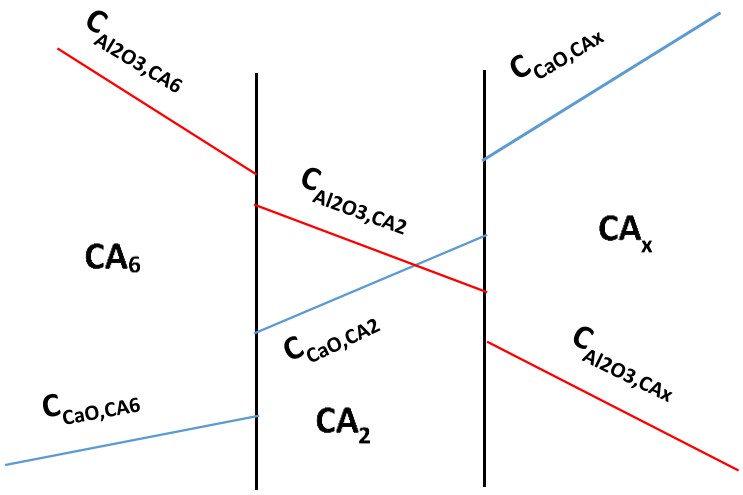

Figure 3-4. Concentration profile within CA_2 and adjacent phases

In general, if $J_{A,i}$ and $J_{A,i+1}$ are the fluxes of Al_2O_3 in adjacent layers i and $i+1$ respectively, if $J_{A.i} > J_{A,i+1}$ the phase i will grow at the expense of phase $i+1$ (e.g. reaction a and d). Similarly, for CaO diffusion, $J_{C,i+1} > J_{C,i}$, will contribute to the growth

of phase $i+1$ at the expense of phase i (e.g. reaction b and c). Therefore, the flux balance for the specific case of CA_2 can be written:

$$\frac{dn_{CA_2}}{dt} = -\frac{1}{4}\left(J_{Al_2O_3,CA_6} - J_{Al_2O_3,CA_2}\right) + \frac{3}{2}\left(J_{CaO,CA_2} - J_{Al_2O_3,CA_6}\right) - \frac{2}{(2-\upsilon')}\left(J_{CaO,CA_x} - J_{CaO,CA_2}\right) + \frac{1}{(2-\upsilon')}\left(J_{Al_2O_3,CA_2} - J_{Al_2O_3,CA_x}\right) \quad \textbf{(3-1)}$$

After rearrangement:

$$\frac{dn_{CA_2}}{dt} = -\frac{1}{4}\left(J_{Al_2O_3,CA_6} + 6J_{CaO,CA_6}\right) + \frac{6-\upsilon'}{4\,(2-\upsilon')}\left(J_{Al_2O_3,CA_2} + 2\,J_{CaO,CA_2}\right) - \frac{1}{(2-\upsilon')}\left(J_{Al_2O_3,CA_x} + \upsilon'\,J_{CaO,CA_x}\right) \quad \textbf{(3-2)}$$

Similar expressions could be written for CA_6 and CA_x. The only difference is that the first term and last term does not apply for the CA_6 and CA_x, respectively. Replacing mass flux by mass rate:

$$\frac{dV^T_{CA_2}}{dt} = -\frac{V_{CA_2}}{4}\left(Q_{Al_2O_3,CA_6} + 6\,Q_{CaO,CA_6}\right) + \frac{V_{CA_2}(6-\upsilon')}{4\,(2-\upsilon')}\left(Q_{Al_2O_3,CA_2} + 2\,Q_{CaO,CA_2}\right) - \frac{V_{CA_2}}{(2-\upsilon')}\left(Q_{Al_2O_3,CA_x} + \upsilon'\,Q_{CaO,CA_x}\right) \quad \textbf{(3-3)}$$

Where $V^T_{CA_2}$ and V_{CA_2} are total volume and molar volume of CA_2 respectively. $Q_{A,i}$ and $Q_{C,i}$ are amount of materials flowing per unit time for Al_2O_3 and CaO respectively and are defined by Eq (3-4)[17]:

$$Q = 4\pi D\,\frac{r_{i-1}r_i}{r_i - r_{i-1}}\left(C_i - C_{i-1}\right) \quad \textbf{(3-4)}$$

Considering spherical geometry, the mass rate accounting for counter diffusion of two components for phase i at steady state is [16]:

$$\Phi_i = \left(Q_{A,i} + \upsilon_i Q_{C,i}\right) = 4\pi k_i \frac{r_{i-1} r_i}{r_i - r_{i-1}} \quad \textbf{(3-5)}$$

Where k_i having the units mol s^{-1} cm^{-1} is the rate constant which is related to the diffusivity via the concentration gradient. When two counter diffusing components A and C are mobile, matter transport is described by two distinct terms, $Q_{A,i}$ and $Q_{C,i}$. Where υ_i, r_{i-1} and r_i are the stoichiometric coefficient, interior radius and exterior radius, respectively.

The relation between initial volume of the Al_2O_3 sphere and the volumes of the transformed or partially transformed sphere can be obtained considering the mass balance:

$$V^0_{Al_2O_3} = \frac{4}{3}\pi {r_0}^3 = V^t_{Al_2O_3} + \sum \frac{V_i^t}{z_i} \quad \textbf{(3-6)}$$

Where $V^0_{Al_2O_3}$, $V^t_{Al_2O_3}$ and V_i^t are respectively the volume of the Al_2O_3 core at t=0, the volume of Al_2O_3 core and the volume of phase i at time t, and z_i is the volume of phase i formed per unit volume of Al_2O_3 core transformed. Bearing in mind that the final term in Eq (3-6) represents the volume of alumina that has been transformed in terms of the sum of the volumes of the product phases, z_i is:

$$z_i = \frac{V_i}{\nu_i V_{Al_2O_3}} \quad \textbf{(3-7)}$$

Where ν_i, $V_{Al_2O_3}$ and V_i are stoichiometric coefficient of phase i, molar volume of Al_2O_3 core and molar volume of phase i, respectively. Substituting Eq (3-5) into (3-3) and after rearrangement one can write:

$$4\pi\left(r^2_{CA_2}\frac{dr_{CA_2}}{dt} - r_{CA_6}\frac{dr_{CA_6}}{dt}\right) = -\frac{V_{CA_2}}{4}\Phi_{CA_6} + \frac{V_{CA_2}(6-\nu')}{4(2-\nu')}\Phi_{CA_2} - \frac{V_{CA_2}}{(2-\nu')}\Phi_{CA_6} \quad \textbf{(3-8)}$$

Similarly for other phases:

$$4\pi\left(r_{CA_6}^2\frac{dr_{CA_6}}{dt}-r_{Al_2O_3}^2\frac{dr_{Al_2O_3}}{dt}\right)=\frac{V_{CA_6}}{(6-\nu')}\Phi_{CA_6}-\frac{V_{CA_6}}{4}\Phi_{CA_2} \quad \textbf{(3-9)}$$

$$4\pi\left(r_{CA_x}^2\frac{dr_{CA_x}}{dt}-r_{CA_2}^2\frac{dr_{CA_2}}{dt}\right)=-\frac{V_{CA_x}}{(2-\nu')}\Phi_{CA_2}+\frac{2V_{CA_x}}{(2-\nu')\nu'}\Phi_{CA_x} \quad \textbf{(3-10)}$$

Using Eq (3-6) for the Al_2O_3 Core:

$$4\pi r_{Al_2O_3}^2\frac{dr_{Al_2O_3}}{dt}=-\frac{1}{z_{CA_6}}\left(\frac{V_{CA_6}}{(6-\nu')}\Phi_{CA_6}-\frac{V_{CA_6}}{4}\Phi_{CA_2}\right)-\frac{1}{z_{CA_2}}\left(-\frac{V_{CA_2}}{4}\Phi_{CA_6}+\frac{V_{CA_2}(6-\nu')}{4(2-\nu')}\Phi_{CA_2}-\frac{V_{CA_2}}{(2-\nu')}\Phi_{CA_x}\right)-\frac{1}{z_{CA_x}}\left(-\frac{V_{CA_x}}{(2-\nu')}\Phi_{CA_2}+\frac{2V_{CA_x}}{(2-\nu')\nu'}\Phi_{CA_x}\right) \quad \textbf{(3-11)}$$

Where ν' is the stoichiometric coefficient of liquid calcium aluminate in equilibrium with CA_2 and V_i is molar volume of phase i. Replacing Φ using Eq (3-5) relates the radii of phases to the rate constants.

These four differential equations (3-8)-(3-11), for the growth of each phase were solved with the Runge-Kutta method [18]. When the alumina core is completely consumed, the transformation continues by reaction of CA_6 with CaO to produce CA_2.

The remaining issue is the estimation of the rate constants. The rate constant k_i can be obtained from the diffusion flux equation by combining Eqs (3-4) and (3-5)

$$k_i=D_A\left(C_{A,i}-C_{A,i-1}\right)+\upsilon_i D_B(C_{B,i}-C_{B,i-1}) \quad \textbf{(3-12)}$$

considering the Nernst-Einstein equation in a chemical potential gradient [19]:

$$k_i=\frac{1}{V_i}\int_{a_C^I}^{a_C^{II}}\left(\frac{D_{A,i}}{\nu_i}+D_{C,i}\right)d\ln a_C \quad \textbf{(3-13)}$$

For compounds with narrow homogeneity range, rate constant takes the form of [19]:

$$k_i = \frac{u_i(u_{i-1}-u_{i+1})}{(u_{i-1}-u_i)(u_i-u_{i+1})}\left(D_{A,i} + u_i D_{C,i}\right)\frac{|\Delta G_i^0|}{V_i RT} = D_{eff}\frac{u_i(u_{i-1}-u_{i+1})}{(u_{i-1}-u_i)(u_i-u_{i+1})}\frac{|\Delta G_i^0|}{V_i RT} \qquad \textbf{(3-14)}$$

Where $D_{A,i}$ and $D_{C,i}$ are the self-diffusion coefficients of counter diffusing species, Al_2O_3 and CaO, respectively. u_i is stoichiometric coefficient of phase i. $|\Delta G_i^0|$ is the standard Gibbs free energy for the formation of one mole of CA_{u_i} from the adjacent phases, T is the temperature, and R is the gas constant. Values for the diffusivity in CA_6 were not found in the literature. There were only two papers which measured diffusivity values of calcium aluminates but in low temperatures. So the diffusion coefficients in higher temperatures have to be extrapolated using Arrhenius equation. These values along with diffusivity coefficients of similar mixed oxide systems are listed in Table 3-1.

Table 3-1. Diffusivity coefficients for different mixed oxide systems

Phase	Explanation	Experiment temperature	Estimated value of D $\left(\frac{m^2}{s}\right)$ at 1600 °C		Ref
CA_2	Coefficient of interdiffusion for the formation of CA_2 in the molar mix of CA and A	1350-1450 °C	2.4×10^{-12}	Extrapolated at 1600 °C	[34]
$CaAl_2O_4$ and $BaAl_2O_4$	Interdiffusion coefficient for formation of $CaAl_2O_4$ and $BaAl_2O_4$ in 1:1 molar mix of CaO - Al_2O_3 and BaO - Al_2O_3	1200-1380 °C	$D_{CA} = 2.23 \times 10^{-12}$ $D_{BA} = 1.22 \times 10^{-10}$	Extrapolated at 1600 °C	[35]
Spinel $MgO - Al_2O_3$	Mg self diffusion in spinel and coexisting melt at bulk chemical equilibrium using an isotopic tracer	1261-1553 °C	$D_{Mg} = 1.4 \times 10^{-13}$		[36]
aluminous Spinel	The diffusion coefficients of Fe^{2+}	950 to 1325°C	$D_{Fe} = 5.4 \times 10^{-15}$	Extrapolated at 1600 °C	[37]

and Mg in aluminous spinel	$D_{Mg} = 4.4 \times 10^{-15}$

Comparing the estimated values of diffusivity coefficients of calcium aluminates with other oxides, it seems that they are too high probably because the activation energies are different at higher temperatures and the estimated values are not accurate. Although, the value $D = 1 \times 10^{-12}\ \frac{m^2}{s}$ is chosen for the calculations, the sensitivity of the model to these values will be discussed later. The free energy values were calculated using FactSage 6.4 software with FactPS database [20,21]. As shown in Table 3-2.

Table 3-2. Calclated values of rate constants

Reaction	$\Delta G^o\ (J/mol)$	$k\ (\frac{mol}{cm.\,s})$
$CA_6 + 4CA = 5CA_2$	-14058	$k_{CA_2} = 2.5 \times 10^{-10}$
$4A + CA_2 = CA_6$	-7988.3	$k_{CA_6} = 3.9 \times 10^{-11}$

The rate constant for the growth of the liquid calcium aluminate layer is calculated using Eq (3-13) which requires the species diffusivities and the activity of calcium oxide at the interfaces on either side of liquid calcium aluminate. The diffusivities are discussed below. The activity at the inner interface is in equilibrium with CA_2, whereas for the interface with steel the condition is more complicated. The boundary conditions for all species are calculated by coupling the mass balance at the interface with local thermodynamic equilibrium. Mass balances for calcium, aluminum and oxygen at the interface give:

$$N_{Ca} = N_{CaO} \qquad \textbf{(3-15)}$$

$$N_{Al} = 2N_{Al_2O_3} \quad \textbf{(3-16)}$$

$$N_O = N_{CaO} + 3N_{Al_2O_3} \quad \textbf{(3-17)}$$

Where N_i, the mass transfer through the boundary layer from the bulk of the steel to the surface of a spherical particle can be described by:

$$N_i = 4\pi r^2 . k_{m,i} C\ (X_i^b - X_i^*) \quad \textbf{(3-18)}$$

Where $k_{m,i}$ is the mass transfer coefficient across the boundary layer, r is the particle radius, C is the total molar concentration in the steel phase, X_i^b is the mole fraction of the species i in the bulk steel and X_i^* is the mole fraction of species i at the interface. It is well established that spherical particles smaller than 14 μm have little relative motion in steel, so the Sherwood number takes on its limiting value of 2 for radial diffusion [22,23]. The Sherwood number is:

$$Sh = \frac{k_{m,i} d}{D_i} \quad \textbf{(3-19)}$$

Where d is the particle diameter and D_i is the diffusion coefficient of the species in the steel. The values of diffusivity used for calculating $k_{m,i}$ are listed in Table 3-3.

Table 3-3. Diffusivity values for species in steel [5]

	Ca	Al	O
Diffusion Coefficient (m^2/s)	3×10^{-9}	3.5×10^{-9}	3.1×10^{-9}

Molar flow of species i in the liquid product layer can be described by the following equation [22]:

$$N_i = \left(\frac{4\pi r_{ex} r_{in}}{r_{ex} - r_{in}}\right)(CD_i)(X_i^{ex} - X_i^{in}) \quad \textbf{(3-20)}$$

Where r_{ex} and r_{in} are exterior and interior radius of the product layer, respectively. C is the molar concentration, D_i is the diffusivity of species i and X_i^{ex} and X_i^{in} are mole fraction of species i at exterior and interior radius respectively. Estimated diffusivity values at 1600 °C used in this work are $D_{CaO} = 3.01 \times 10^{-6} \frac{cm^2}{s}$ [24] and $D_{Al_2O_3} = 1.48 \times 10^{-6} \frac{cm^2}{s}$ [25].

Thermodynamic equilibrium at the inclusion-steel interface is based on the simultaneous deoxidation equilibria of Ca and Al in steel with the Al_2O_3 and CaO components in the calcium aluminate phase according to the following reactions.

[Ca]+[O]=(CaO)$_{inc}$

$$K_{CaO} = \frac{a_{CaO}}{\left(\frac{f_{Ca}X^*_{Ca}n_T MW_{Ca}100}{St_{mass}}\right)\ \left(\frac{f_O X^*_O n_T MW_O 100}{St_{mass}}\right)} \qquad \textbf{(3-21)}$$

2[Al]+3[O]=(Al$_2$O$_3$)$_{inc}$

$$K_{Al_2O_3} = \frac{a_{Al_2O_3}}{\left(\frac{f_{Al}X^*_{Al}n_T MW_{Al}100}{St_{mass}}\right)^2\ \left(\frac{f_O X^*_O n_T MW_O 100}{St_{mass}}\right)^3} \qquad \textbf{(3-22)}$$

Where f_i represents activity coefficient of species i, MW_i is the mole weight and n_T and St_{Mass} are total number of moles and mass of the steel. The values used for oxidation equilibrium constants are $K_{CaO} = 1.2 \times 10^9$ [26] and $K_{Al_2O_3} = 3.16 \times 10^{12}$ [27].

For simplicity in modeling the variation of the activities $a_{Al_2O_3}$ and a_{CaO} in the $Al_2O_3 - CaO$ system are fitted to a function using values calculated by FactSage 6.4

software (FToxid database) at 1873 K [20,21]. The activities and corresponding fitted functions are shown in Figure 3-5.

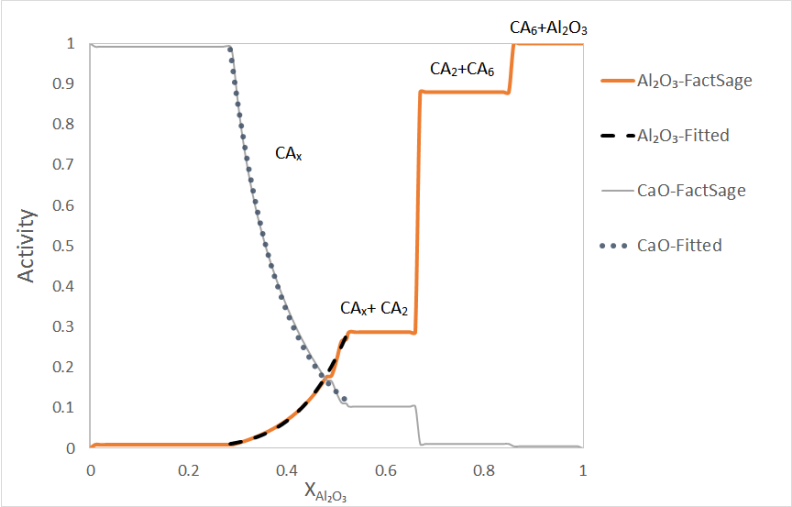

Figure 3-5. Calculated activities of the components in the Al_2O_3-CaO system and the respective fitted functions

The function for $a_{Al_2O_3}$ with the mole fraction $X_{Al_2O_3}$ is:

$$a_{Al_2O_3} = 9.40288 X_{Al_2O_3}^{5.38576} \quad \textbf{(3-23)}$$

And that for CaO is:

$$a_{CaO} = 15.34197 \exp\left(-\frac{X_{Al_2O_3}}{0.1031}\right) + 0.018 \quad \textbf{(3-24)}$$

In order to find the equilibrium activities and interfacial concentrations, equations (3-15)-(3-17) for the interfacial mass balances are solved in conjunction with the equilibrium conditions, equations (3-21) and (3-22). The non-linear system of equations is solved numerically for the unknowns $X_{Ca}^*, X_{Al}^*, X_O^*, X_{CaO}^*, X_{Al_2O_3}^*$ using the Newton-Raphson method [18] thereby allowing the calculation of the interfacial mass transfer rates.

3.3 Results

3.3.1 Multi-layer growth model

As noted earlier, the bulk dissolved concentrations of Ca, Al and O are boundary conditions for the model. Currently there is no way to measure directly the dissolved calcium content in steel. A value of 2 ppm Ca is assumed for the base case, but will be examined in the sensitivity analysis. The aluminum content is assumed to be 300 ppm, which is typical of LCAK steel. The dissolved oxygen content is assumed to be 5 ppm, close to equilibrium with the dissolved aluminum and pure alumina. An initial diameter for the alumina inclusion of 5 microns is assumed for all calculations. Diffusion coefficients and rate constants used for the calculations are summarized in Table 3-4.

Table 3-4. Summary of kinetic constants

Kinetic parameter	value
k_{CA_6} , k_{CA_2}	3.9×10^{-10} , $2.5 \times 10^{-11}\ mol\ cm^{-1}s^{-1}$
D_{CaO} , $D_{Al_2O_3}$	3.01×10^{-10} , $1.48 \times 10^{-10}\ m^2s^{-1}$
D_{Ca} , D_{Al} , D_O	3×10^{-5} , 3.5×10^{-5}, $3.1 \times 10^{-5}\ cm^2s^{-1}$

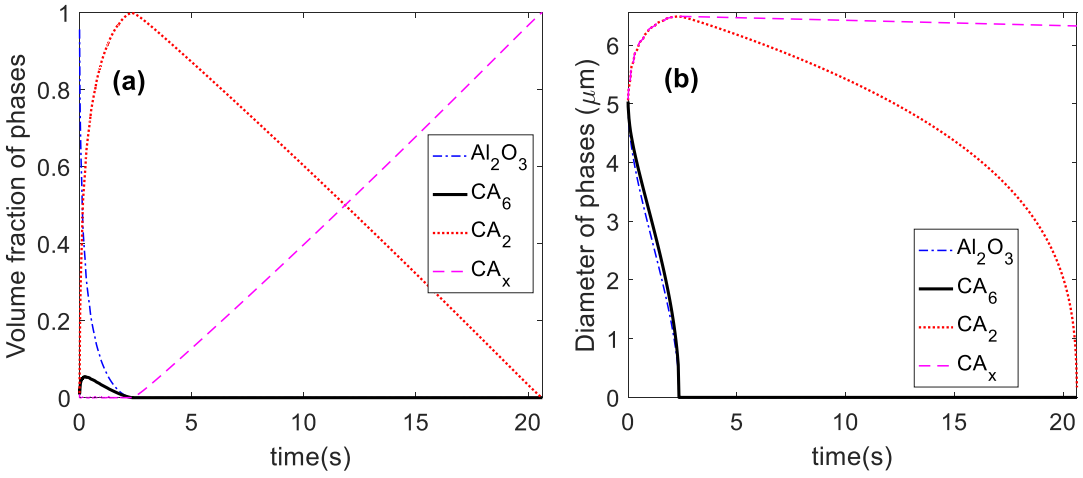

Figure 3-6. Change of (a) volume fraction and (b) diameter of different calcium aluminate phases as depicted in Figure 3-3 for [Ca] =2 ppm, [Al] =300 ppm and [O] =5 ppm

The results for each phase are reported as the calculated variation of volume fraction, Figure 3-6(a) and corresponding outer diameter, Figure 3-6(b). Initially CA_6 and CA_2 phases grow at the expense of the alumina core. The Al_2O_3 core is completely consumed in the early stages of the process, followed by CA_6 and then CA_2. The liquid calcium aluminate is the final phase of transformation. It should be noted that this modification process is quite fast which is consistent with observations of Han et al. [6]. In this calculation, it is assumed that the concentration of dissolved calcium is constant. Since the practical time scale for modification is in the range of minutes, one can conclude that the rate controlling step in the modification is more likely related to the mass transfer of calcium from the calcium bubbles to inclusions *i.e.* supply of calcium to the melt. Because there are several kinetic steps in the model, sensitivity analysis is performed to investigate effect of each step on the transformation time.

3.3.2 Sensitivity analysis

To check the sensitivity of the model to the estimated values and the effect of each kinetic step, additional calculations are performed with one order of magnitude higher and lower values for the parameters listed in Table 3-4. For the following calculations dissolved $[Ca]$, $[Al]$ and $[O]$ contents are assumed to be 2, 300 and 5 ppm, respectively, unless otherwise specified.

A. Rate constants for CA_6 and CA_2

Figure 3-7 shows that by decreasing rate constants for CA_6 and CA_2 by a factor of 10, the total time of transformation increases, from 20.6 to 29.1 seconds, only a factor of 1.41. This factor is much less than 10, suggesting that diffusion through these phases has a minor role in this mixed control. Moreover, these are transient phases, another reason for a minor role in control of the rate. The liquid calcium aluminate is the only phase that is growing continuously.

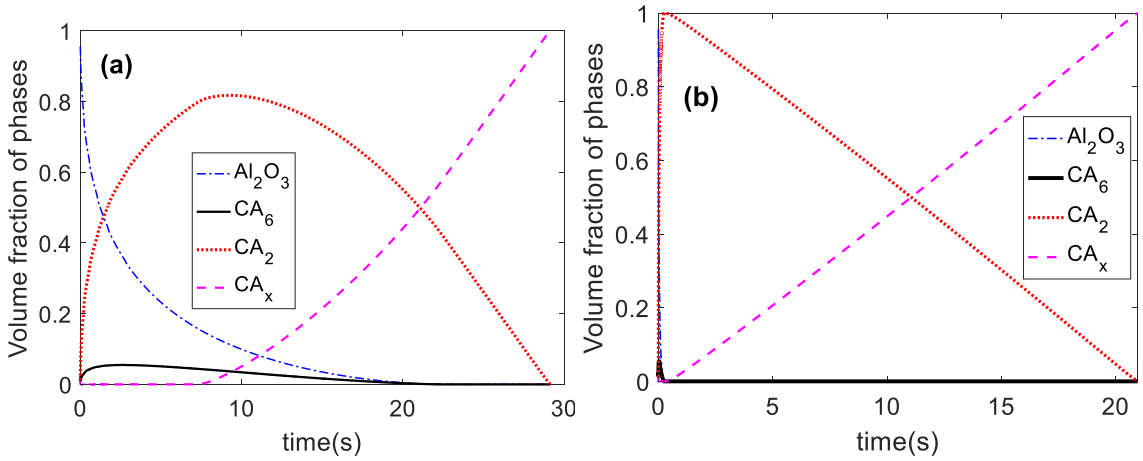

Figure 3-7. Change of volume fraction of different calcium aluminate phases for (a) $0.1k_{CA_6,CA_2}$ *(b)*$=10k_{CA_6,CA_2}$

Diffusivity of CaO and Al_2O_3 in the liquid CA_x

The effect of variation of diffusivity in the liquid CA_x by a factor of 10 on the modification of alumina to liquid calcium aluminate is presented in Figure 3-8. Decreasing the diffusivity by 10-fold increases the transformation time to 21.3 s, a 1.03-fold increase. On the other hand, increasing the diffusivity by 10, does not change the transformation time. The result shows that sensitivity of the process to diffusivity in liquid calcium aluminate is similar to that in the solid phases.

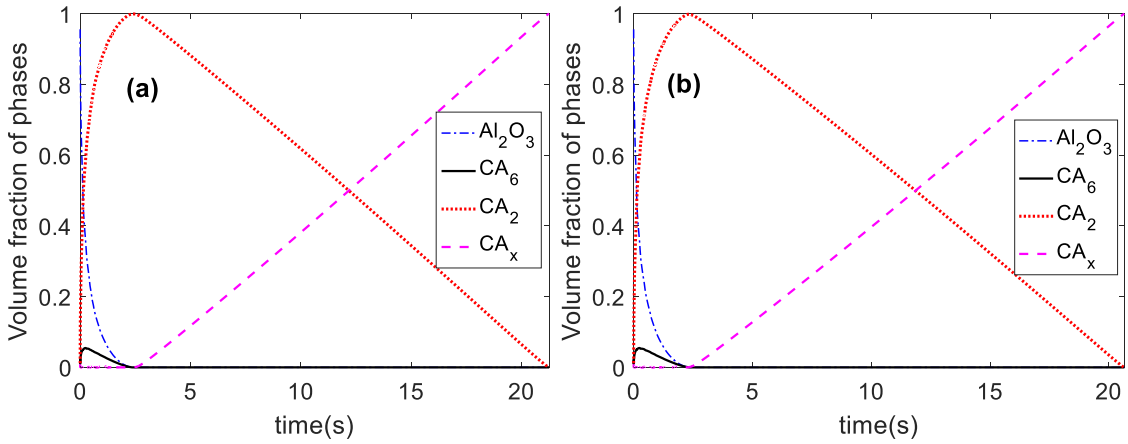

Figure 3-8. Change of volume fraction of different calcium aluminate phases for (a) $0.1D_{CA_x}$ *(b)* $10D_{CA_x}$

B. Diffusivity of solutes in the steel

Figure 3-9 shows the effect of changing the diffusivity of solutes in the melt by an order of magnitude. Decreasing the mass transfer coefficient from the melt increases the transformation time to 161 seconds, a 7.8 fold increase; conversely increasing the mass transfer coefficient causes a decrease to 3.2 seconds, a 6.43 fold decrease. While these changes are less than the order of magnitude change expected if mass transport to the inclusion surface completely controlled the rate, more control lies in the liquid boundary layer around the inclusion.

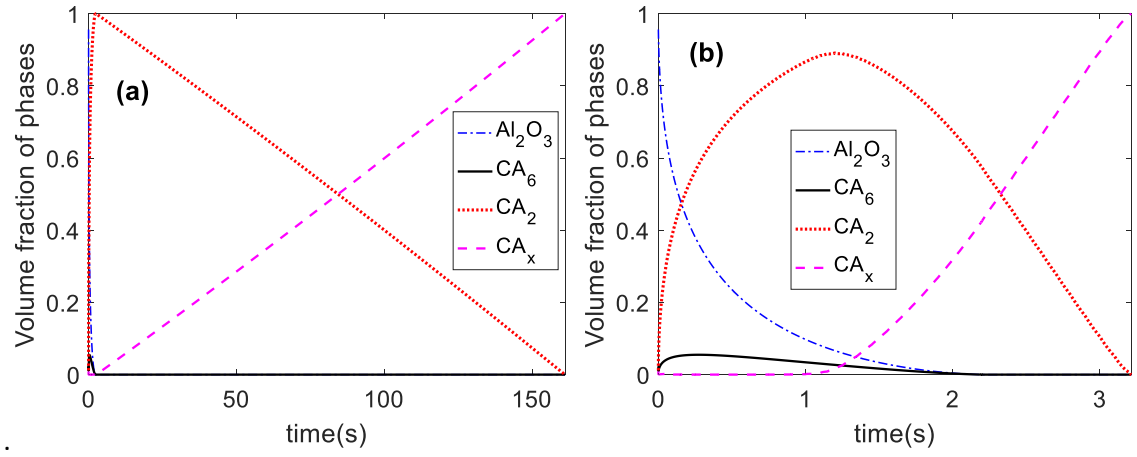

Figure 3-9. Change of volume fraction of different calcium aluminate phases for (a) $0.1D_{Steel}$*(b)* $10D_{Steel}$

In summary, changing the diffusivities in any of the phases results in a change in the overall rate, and shows that control is mixed between each of the phases in fairly fine balance, with most control in the liquid boundary layer. The dependence on liquid calcium aluminate diffusion is the most complex because this phase grows at the expense of the solid phases. From a practical sense the more important observation may be that the predicted transformation times are much shorter than expected from industrial practice. This suggests that the rate determining step for calcium treatment is likely to be calcium supply to the melt; transport around and in the inclusion only affects the phase distribution during the transformation. The authors are currently working on adding a calcium dissolution step to the model.

C. Concentration of solutes

While the rate of calcium transfer from the bubbles to the melt is not included in the model, we can evaluate the effect to some extent by changing the concentration of dissolved species, $[Ca]$, $[Al]$ and $[O]$. This also illustrates the controlling steps in the liquid

boundary layer. In the model calcium is transferred from the bulk to the surface of the inclusion and oxygen is transferred from surface to the bulk, therefore, decreasing $[Ca]$ or increasing $[O]$ decreases the driving force for the process. As mentioned earlier, the oxygen content in the steel is very close to equilibrium with the inclusions, so it is unrealistic to change it by a factor of 10. Figure 3-10 shows the influence of increasing dissolved oxygen from 2 to 6 ppm, a factor of 3 for which the rate of transformation decreases by a factor of 2. Thus, the oxygen content has significant control on the rate. This result is due to the non-linear equilibrium relationships between [Ca], [Al] and [O] contents at the inclusion interface.

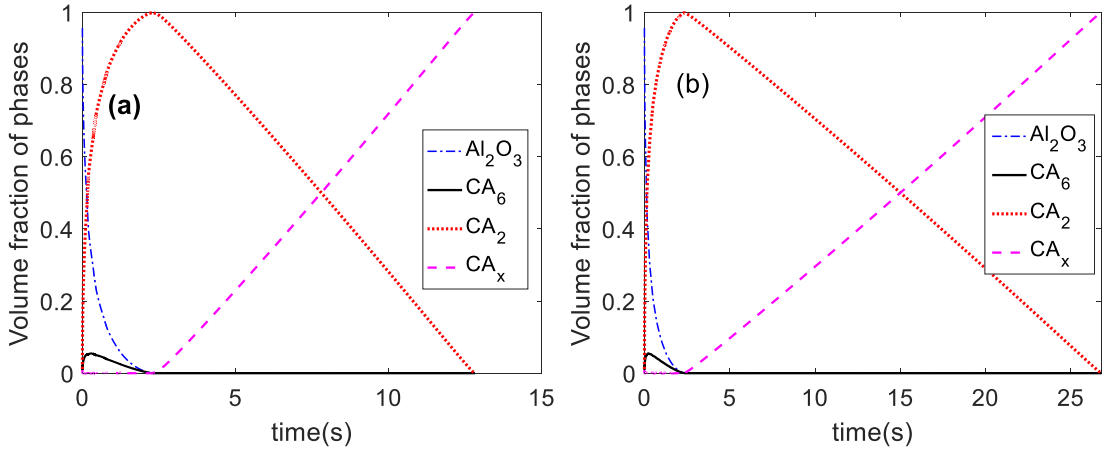

Figure 3-10. Change of volume fraction of different calcium aluminate phases for (a) [Ca] = 2 ppm, [Al] = 300 ppm and [O] = 2 ppm (b) [Ca] = 2 ppm, [Al] = 300 ppm and [O] = 6 ppm

Effect of calcium content of the steel on modification is depicted in Figure 3-11; in this case the calcium content is reduced from 2 to 0.2 ppm, a factor of 10, resulting in a 5.8 fold decrease in the transformation rate. One would expect the rate to be first-order with respect

to the calcium content, but there is mixed control with oxygen diffusion at the interface because of the imposed interface equilibria, as also seen in Figure 3-10.

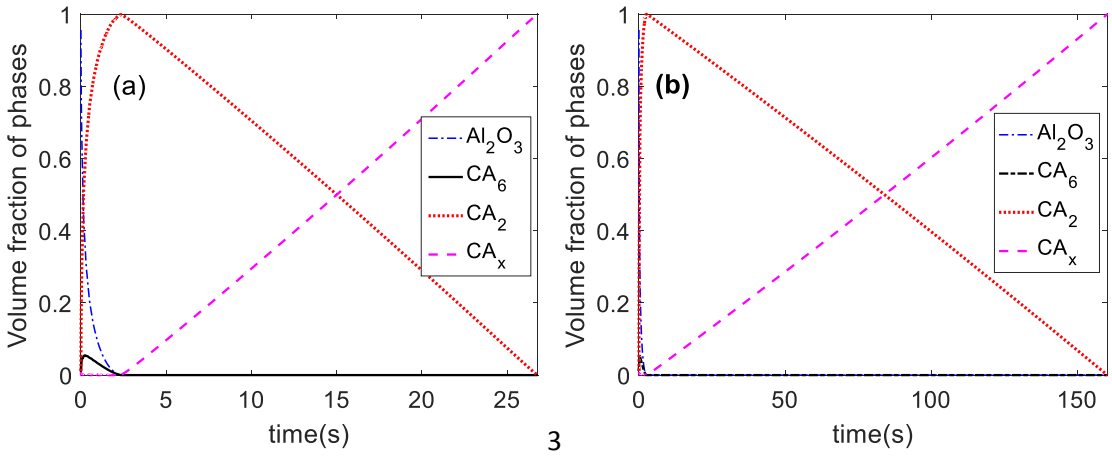

Figure 3-11. Change of volume fraction of different calcium aluminate phases for (a) [Ca] = 2 ppm, [Al] = 300 ppm and [O] = 6 ppm (b) [Ca] = 0.2 ppm, [Al] = 300 ppm and [O] = 6 ppm

Aluminum has a similar effect to oxygen because aluminum also transfers from the inclusion to the steel. By comparing Figure 3-12 with Figure 3-6 it is seen that by changing dissolved aluminum from 300 ppm to 150 ppm, a factor of 2, the time decreased from 20.6 second to 13.8 second, by a factor of 1.5.

These sensitivity analyses show that the transformation rate is in a regime of mixed control among all the possible rate-controlling steps. The most controlling ones are diffusion of Ca, O and Al through the liquid boundary layer; these steps are coupled by a mass balance and equilibrium at the inclusion interface, resulting in non-linear dependencies of the rate on these solute concentrations. Within the inclusion the diffusion through the solid and liquid phases are similar in their degree of control. It should also be

noted that the solid phases disappear, leaving the liquid calcium aluminate as the predominate phase.

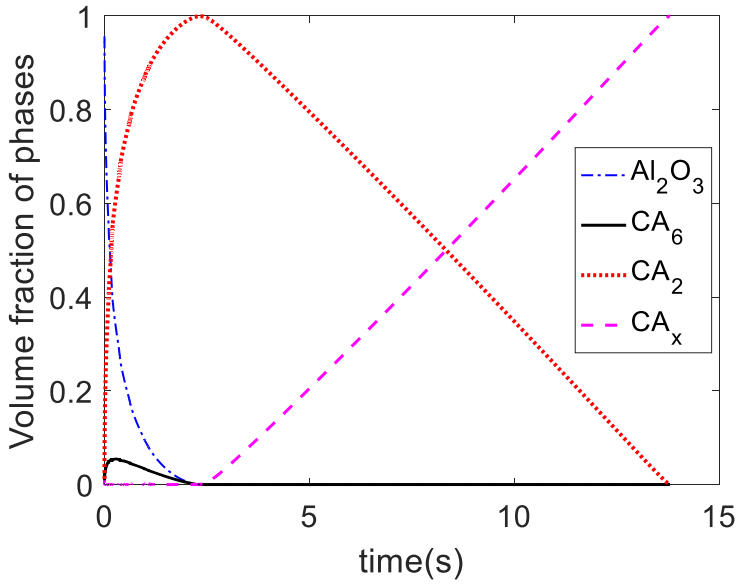

Figure 3-12. Change of volume fraction of different calcium aluminate phases for [Ca] = 2 ppm, [Al] = 150 ppm and [O] = 5 ppm

3.3.3 One-Layer Model

The model results suggest that the multi-layer model could be replaced by simply modelling the growth of the liquid calcium aluminate. A schematic diagram of the one-layer model of alumina modification and the corresponding transformation rate is illustrated in Figure 3-13(a). It should be noted that interfacial concentrations are calculated in a similar way to the multi-layer model, *i.e.* diffusion through the boundary layer is included in the model. Figure 3-13(b) shows that the transformation time is 22.4 s, close to 20.6 s in Figure 3-6(a). There are two reasons for the similarity in the model solutions: first, the solid layers are transient phases, so their effects are short-lived; second, the

diffusivities in the solid phases and the liquid phase are similar, exerting similar control over the rate.

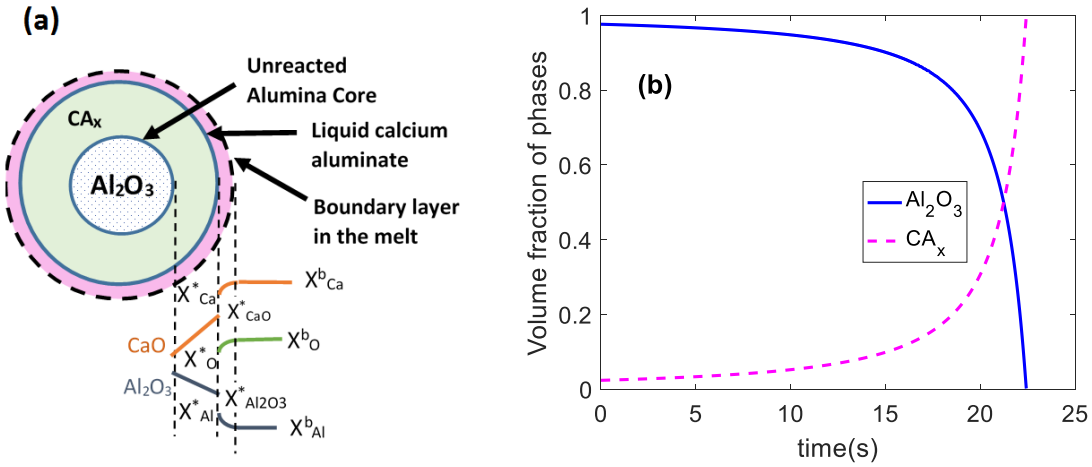

Figure 3-13. (a)Schematic diagram one-layer model and (b) the corresponding change of volume fraction of liquid CA_x and alumina, [Ca] =2 ppm, [Al] =300 ppm and [O] =5

3.4 Discussion

In the literature, discrepancies exist concerning the rate controlling step of alumina inclusion transformation by calcium. Some researchers proposed that diffusion in the product layer is the rate controlling step [8], whereas others suggest that mass transfer in the melt [11] or chemical reaction at the interface [6] determines the kinetics of the process. The present model is the first to provide a comprehensive model of coupled diffusion for the inclusion which makes it possible to properly assess the controlling steps.

As would be expected for a micron-size particle at high temperature, diffusion-controlled reactions are very rapid, being complete in a matter of seconds. The same conclusion was reached in a study by Galindo et al. [28] on the transformation of single particles of alumina inclusions to magnesium aluminate spinel. That work went on to

couple the particle model to a slag-metal reaction model because the slag was the source of magnesium for the spinel. It was found that once the conditions at the slag-metal interface became reducing to the MgO in the slag, the released dissolved magnesium quickly reacted with the alumina. The transformation rate was found to be controlled at the slag-metal interface, as the reaction with the large number of inclusions was much faster. The number of inclusions in the steel was similar to the number described in this paper. Thus, it would be expected that the rate of alumina transformation would be controlled by the rate of supply of calcium to the melt. The coupling of a calcium bubble model with the present inclusion model will be left to a subsequent paper.

Similar arguments were made in the section 3.2.1 'the outline of the model system', regarding alumina formation. Aluminum is readily dissolved in steel, aside from the problem that aluminum floats out rapidly. Once there are sufficient alumina particles in the melt, further aluminum additions result in rapid attainment of equilibrium of dissolved oxygen and aluminum with alumina, controlled by the rate of aluminum supply to the melt.

Another very important aspect of calcium treatment that is beyond the scope of this paper is the transformation of sulphide inclusions. This will be addressed in the subsequent paper. In reality, part of the dissolved calcium is consumed by these sulfide inclusions which delays the transformation of alumina inclusions.

Desulphurization of hot metal (carbon-saturated iron from the blast furnace) by magnesium injection is another comparable system because magnesium boils and forms bubbles that react with sulphur dissolved in the iron. Irons and Guthrie [29] developed a

model for the process based on small-scale experiments. They found that sulphur reacts with the magnesium bubbles, and that some of the magnesium sulphide that is formed is stripped from the bubbles, and forms inclusions in the melt. These inclusions act as sites for further reaction between dissolved magnesium and sulphur in the melt. These authors developed a model in which they were able to calculate the rates of desulphurization and magnesium dissolution as a function of the following ratio:

$$\frac{\beta}{\propto} = \frac{k_p A_p + k_b A_b}{k_b A_b H P_{Mg}} \qquad \textbf{(3-25)}$$

which is the ratio of the rate of desulphurization at particles and at bubbles to the rate of magnesium dissolution. They found that for a very low ratio (large number of bubbles to particles) that most magnesium dissolved and there was little desulphurization, thus there was a high dissolved magnesium content in the iron. On the other land, a very high ratio resulted in any dissolved magnesium immediately reacting to form magnesium sulphide at the inclusions, and little resulting dissolved magnesium. Industrial dissolved magnesium contents were found to be between these two extremes which, of course, depend on the ratio of bubbles to inclusion particles. In Galindo's work [28] in steel there was a high ratio of inclusions to slag interface, so there was little dissolved magnesium. In the previous studies of calcium treatment of steel [5,8,11] a wide range of dissolved calcium contents are used to rationalize experimental findings, which on initial inspection suggest widespread disagreement. Kobiyashi et al. [30] proposed that the dissolved calcium, in a steady state system of calcium/argon bubbling and liquid iron, is less than 30 ppm. The analysis of Lu et al. [5] demonstrated that the effective dissolved calcium content is less

than 1 ppm. This content corresponds to the calcium activity in equilibrium between the sulphur content in the steel and CaS activity in the sulphide inclusions and between the oxygen content in the steel and CaO activity in the oxide inclusions; thus, this analysis is consistent with the present arguments that the inclusions closely approach equilibrium with the melt. In the work of Visser et al. [11] a presumed value of slightly more than 1 ppm for dissolved calcium showed the best agreement of model predictions with measurements. Harada et al. [31] calculated the dissolved calcium to be less than 1 ppm. However, when one considers that the observed dissolved calcium is not an equilibrium solubility value, but represents the instantaneous balance between the rates of dissolution and consumption, the wide range of observed calcium concentrations may be due to a wide range of bubble to particle ratios. The current work shows that even a small amount of dissolved calcium less than 1 ppm is enough to modify inclusions within a few minutes which is in agreement with the literature [6,7,32] This hypothesis will be explored in detail in a subsequent publication by the authors.

The present model was structured so that each product phase would grow according to its governing diffusion equation, but it is clear from all the results that the liquid calcium aluminate phase rapidly consumes the other phases. As shown by the results in Figure 3-13, diffusion in the other phases can be ignored and the overall results in terms of calcium transformation are virtually the same. The nonlinear response of the transformation rate to factors such as diffusion coefficients within the inclusion and mass transfer coefficient in the liquid can be explained as follows: Because the transformation is under mixed control involving a number of steps, the response of the rate to changes

affecting any individual step will be "damped" by the other steps. For this reason, the response to changing the diffusivities in the solid layers is non-linear. The response to changing factors with more controlling influence such as the concentration of calcium in the melt, is more linear.

This finding has very interesting implications for modeling of the overall process. First of all, it means that the model can be simplified with little loss in accuracy to consider only the formation of the liquid calcium aluminate. More significantly, it shows that the kinetics of the transformation within the inclusion strongly favor the formation of the desired liquid calcium aluminate. These findings are in keeping with the reported inclusion morphologies in the literature [11,33], i.e. inclusions with an alumina core and a single liquid aluminate shell, or based on the rapid transformation entirely transformed inclusions. As described in the Introduction, the formation of liquid calcium aluminates is difficult to accomplish in practice for a number of reasons. The volatility of calcium means that it tends to escape the steel; it does not dissolve readily, and also tends to react with sulphur and oxygen. Therefore, it is remarkable that one can form liquid calcium aluminates at all. The present work strongly suggests that if calcium is dissolved in the steel, and avoids dissolved sulphur and oxygen, it will react with alumina to form as much liquid calcium aluminate as possible. If the liquid phase were not strongly favored, then it is unlikely that the process would work at all.

3.5 Conclusions

The kinetics of calcium treatment of inclusion in the ladle furnace is modeled mathematically. This is the first model which considers multi-component diffusion of Ca,

Al and O through the boundary layer and within multi-layer product layer constrained by thermodynamic equilibrium at the interfaces.

1. For a single inclusion in a steel of fixed calcium content the rate control for the aluminate transformation is mixed between all steps, however, mass transport through the steel inclusion boundary layer is more important as changing the mass transfer in the boundary layer by a factor of 10 will change transformation time by a factor of approximately 7. Whereas changes to the other kinetic parameters has a much smaller effect for example changing the diffusivities within the inclusion by a factor of 10 change the transformation time by a factor of maximum 1.4.

2. The control through the boundary layer is mixed between oxygen, aluminum and calcium diffusion, and complicated by the imposed equilibria amongst CaO and Al_20_3 in the phase at the surface and dissolved Ca, Al and O.

3. The reactions at the inclusion are extremely fast, for example, using the accepted literature values for the transport properties the modification to liquid calcium aluminate is complete within 22 seconds. Decreasing the mass transfer coefficient in the liquid steel by an order of magnitude results in a transformation time of 160 seconds. Even the latter is fast relative to typical times observed in ladle treatment which has important practical implications for ladle metallurgy where calcium is injected into the steel:

(a) There are generally a large number of inclusions with enormous interfacial area in the steel reacting rapidly, so the bulk steel composition will closely follow the equilibria with the phases at the inclusion surface.

(b) The rate of calcium transformation must be controlled by the rate of calcium dissolution from the calcium bubbles.

(c) The present model suggests that if calcium is dissolved in the steel, and avoids oxygen and sulphur in the melt, any calcium that reaches an aluminate inclusion will transform rapidly to make as much liquid calcium aluminate as possible which is fortunate for the desired outcome in the industrial process.

3.6 Acknowledgement

The Authors are grateful for the support of the members of the McMaster Steel Research Centre, the Natural Sciences and Engineering Research Council of Canada and ArcelorMittal Dofasco.

3.7 References

[1] J. Lamut, J. Falkus, B. Jurjevec, and M. Knap: Arch. Metall. Mater., 2012, vol. 57, pp. 319–24.

[2] S. W. Robinson, I. W. Martin, and F. B. Pickering: Met. Technol., 1979, vol. 6, pp. 157–69.

[3] Neerav Verma, Petrus C Pistorius, Richard J Fruehan, Michael Potter, Minna Lind, and Scott Story: Metall. Mater. Trans. B, 2011, vol. 42, pp. 711–19.

[4] Robert B Tuttle, Jeffrey D Smith, and Kent D Peaslee: Metall. Mater. Trans. B, 2005, vol. 36, pp. 885–92.

[5] D Lu, G. A Irons, and W Lu: Ironmak. Steelmak., 1994, vol. 21, pp. 362–72.

[6] Z Han, L. Liua, M. Lind, and L. Holappa: Acta Metall. Sin., 2006, vol. 19, pp. 1–8.

[7] Yo-ichi Ito, Mamoru Suda, Yoshiei Kato, Hakaru Nakato, and Ken-ichi Sorimachi: ISIJ Int., 1996, vol. 36, pp. S148–50.

[8] Yoshihiko Higuchi, Mitsuhiro Numata, Shin Fukagawa, and Kaoru Shinme: ISIJ Int., 1996, vol. 36, pp. 151–54.

[9] Guozhu Ye, Par Jonsson, and Thore Lund: ISIJ Int., 1996, vol. 36, pp. S105–8.

[10] D. A. Jerebtsov and G. G. Mikhailov: Ceram. Int., 2001, vol. 27, pp. 25–28.

[11] H Visser, R Boom, and M Biglari: ATS Int. Steelmak. Conf., 2008, pp. 172–80.

[12] K. J. Graham and G. A. Irons: in Int. Symp. Highly Innov. Nov. Oper. "Future Steelmak. Metall., 2010, pp. 65–74.

[13] Juergen Mietz and Franz Oeters: Can. Metall. Q., 1989, vol. 28, pp. 19–27.

[14] K Beskow and L Jonsson: Metall. Mater. Trans. B, 2001, vol. 32, pp. 319–28.

[15] O Levenspiel: Chemical Reaction Engineering, 2nd ed, John Wiley & Sons, New York, 1999.

[16] Vincenzo Buscaglia and Chiara Milanese: J. Phys. Chem. B, 2005, vol. 109, pp. 18475–82.

[17] J. Crank: The Mathematics of Diffusion, 2nd ed, Clarenden press, Oxford, 1975.

[18] Amos Gilat and Vish Sabramaniam: Numerical Methods for Engineers and Scientists, 3rd Editio, Wiley, 2013.

[19] V Buscaglia and U Anselmi-Tamburini: Acta Mater., 2002, vol. 50, pp. 525–35.

[20] C.W. Bale, P. Chartrand, S.A. Degterov, G. Eriksson, and K. Hack: Calphad, 2002, vol. 26, pp. 189–228.

[21] C.W. Bale, E. Bélisle, P. Chartrand, S.a. Decterov, G. Eriksson, K. Hack, I.-H. Jung, Y.-B. Kang, J. Melançon, A.D. Pelton, C. Robelin, and S. Petersen: Calphad, 2009, vol. 33, pp. 295–311.

[22] Julian Szekely and Nickolas J. Themelis: Rate Phenomena in Process Metallurgy, Wiley-Interscience, New York, 1971.

[23] Franz. Oeters: Metallurgy of Steelmaking, Düsseldorf : Verlag Stahleisen, 1994.

[24] Tunezo Saito and Kazua Maruya: Diffusion of Calcium in Liquid Slags, 1958.

[25] Y Oishi, M Namba, and Joseph A Pask: J. Am. Ceram. Soc., 1982, vol. 65, p. 247−253.

[26] Mitsutaka Hino and Kimihisa Ito: in Thermodyn. Data Steelmak., Mtsukata Hino and Kimihisa Ito, eds., Tohoku University Press, Tokyo, 2010, pp. 16–17.

[27] Hiroyasu Fujiwara, Atsushi Hattori, and Eiji Ichise: Tetsu-To-Hagane/Journal Iron Steel Inst. Japan, 1999, vol. 85, pp. 201–7.

[28] Alan Galindo, Gordon A. Irons, Ken Coley, and Stanley Sun: in Challenges Transform. Solut. to Sustain. Steelmak. Cast. Environ. Metall. Innov. CTSSC-EMI Symp. 2015, Tokyo, Japan, 2015.

[29] G. A. Irons and R. I. L. Guthrie: Ironmak. Sleelmaking, 1981, pp. 114–22.

[30] S. Kobayashi, Y. Omori, and K. Sabong: Trans. ISIJ, 1971, vol. 11, pp. 260–69.

[31] Akifumi Harada, Nobuhiro Maruoka, Hiroyuki Shibata, and Shin-ya Kitamura: ISIJ Int., 2013, vol. 53, pp. 2110–17.

[32] Dennis (D-Z.) Lu: McMaster University, 1992.

[33] Dongwei Zhao, Haibo Li, Chunlin Bao, and Jian Yang: ISIJ Int., 2015, vol. 55, pp. 2115–24.

[34] M M Ali and S J Raina: Cem. Concr. Res., 1989, vol. 19, pp. 47–52.

[35] M.M. Ali, S.K. Agarwal, and S.K. Handoo: Cem. Concr. Res., 1997, vol. 27, pp. 979–82.

[36] Y. J. Sheng, G. J. Wasserburg, and I. D. Hutcheon: Geochim. Cosmochim. Acta, 1992, vol. 56, pp. 2535–46.

[37] Hanns Peter Liermann and Jibamitra Ganguly: Geochim. Cosmochim. Acta, 2002, vol. 66, pp. 2903–13.

Chapter 4

Model of Inclusion Evolution During Calcium Treatment in the Ladle Furnace

In Chapter 4 model development was carried out by me. Dr. Kenneth S. Coley provided extensive discussion during model development and Dr. Stanley Sun kindly provided inclusions analysis data and gave very useful guidance for data analysis. Data analysis was performed by me. The manuscript was initially drafted by me and reviewed and edited to the final version by Dr. Kenneth S.Coley, Dr. Gordon A. Irons and Dr. Stanley Sun. This chapter has been published in *Metallurgical and Materials Transactions B*. 49: 2022. https://doi.org/10.1007/s11663-018-1266-z. The following Chapter is the pre-publication version of the article.

Abstract

Calcium treatment of steel is typically employed to modify alumina inclusions to liquid calcium aluminates. However, injected calcium also reacts with the dissolved sulfur to form calcium sulfide. The current work aims to develop a kinetic model for the evolution of oxide and sulfide inclusions in Al-killed alloyed steel during Ca-treatment in the ladle refining process. The model considers dissolution of the calcium from the calcium bubbles into the steel and reduction of calcium oxide in the slag to dissolved calcium. A steel-inclusion kinetic model is used for mass transfer to the inclusion interface and diffusion

within the calcium aluminate phases formed on the inclusion. The inclusion-steel kinetic model is then coupled with a previously developed steel-slag kinetic model. The coupled inclusion-steel-slag kinetic model is applied to the chemical composition changes in molten steel, slag, and evolution of inclusions in the ladle. The result of calculations are found to agree well with an industrial heat for species in the steel as well as inclusions during Ca treatment.

4.1 Introduction

The requirements for the production of superior-quality steel for specific applications have led to the development of various secondary steelmaking processes. Refining of the steel before casting is carried out in ladles via several operations, namely: deoxidation, desulphurization, alloy addition, removal of inclusions, and control of inclusion shape, size, number and composition. Ineffective elimination and/or modification of non-metallic inclusions during secondary treatment of steel can cause nozzle blockage during continuous casting [1] and quality issues in the cast product [2,3]. Calcium treatment is the most common approach to modify nonmetallic inclusions. Ca additions modify solid alumina to globular liquid $CaO - Al_2O_3$ (CA_x) inclusions and magnesium aluminate spinel inclusions to calcium-magnesium aluminates. This results in not only improved castability, but also minimization of inclusion-related surface defects, enhancing the machinability of the final product at high cutting speeds and decreasing of the susceptibility of high-strength low-alloy (HSLA) and pipeline steels to hydrogen-induced cracking [4]. Ca treatment can also be utilized for desulphurization to very low levels [5], but it may also result in the formation of deleterious CaS inclusions. In summary, calcium treatment

is effective in alleviating nozzle clogging caused by alumina inclusions, but the treatment should be done cautiously.

Calcium is usually introduced to the steel by steel-clad Ca wire injection. The boiling point of calcium (1480 °C) is lower than steelmaking temperature (~1600 °C), thus when calcium is added to liquid steel, calcium bubbles form, from which some calcium dissolves into the steel. Actually, most of the injected calcium escapes to the atmosphere and the recovery in industry is usually less than 30% [6]. The dissolved calcium reacts with dissolved oxygen, sulphur and alumina inclusions by the following reactions:

$$[Ca] + [O] \rightarrow CaO \quad \textbf{(4-1)}$$

$$[Ca] + [S] \rightarrow CaS \quad \textbf{(4-2)}$$

$$[Ca] + [O] + \left(x + \frac{1}{3}\right) Al_2O_3 \rightarrow CaO.(Al_2O_3)_x + \frac{2}{3}[Al] \quad \textbf{(4-3)}$$

In spite of the fact that since the 1990's, many studies have been conducted to understand the mechanism and kinetics of alumina inclusion modification by calcium [7-11], some uncertainties remain in the literature. Previous work by the authors developed a fundamental multi-layer growth model [12] and concluded that, for the case of a fixed calcium content in the steel, the rate of supply of calcium to the alumina inclusion is the rate controlling step for modification. This work also showed that changing the fixed concentration of dissolved calcium had a profound effect on the rate of transformation. The latter result suggested that the rate of supply of calcium to the steel relative to the abundance of inclusions, will also have a significant effect on transformation rate.

There has been a number of attempts to model reaction kinetics of steelmaking processes. Lu et al. [7] were the first researchers to model the kinetics of evolution of oxide and sulfide inclusions during calcium treatment based on their experiments in 40 kg steel heats. They assumed fast diffusion within the inclusions and fast reaction at the interfaces and developed a mathematical model for inclusion evolution which offered very reasonable agreement with the experimental data. Visser et al. [10] developed a model to describe the change of the concentration, composition and size of the inclusions in the liquid steel during calcium treatment. They divided the steel bath into two reaction zones: one including the plume zone with high calcium and low oxygen and the other representing the rest of the liquid steel which had low calcium and somewhat higher oxygen. In their model it was assumed that dissolved calcium and oxygen react with Al_2O_3 to form calcium aluminate with gradually increasing CaO fraction. If oxygen activity was sufficiently low, dissolved calcium and sulphur reacted at the surface of the particle to form CaS. In addition, it was assumed that mass transfer of the solutes to the particle surface was the rate controlling step for the formation reactions of CaO, CaS and Al_2O_3.

Graham and Irons [13] simulated the ladle metallurgy process using a multicomponent coupled slag–metal kinetic model which assumed rates were mixed transport controlled in the metal and slag phases. They investigated formation of spinel inclusions as a function of (MnO+FeO) content of the slag and also calcium aluminate according to calcium and oxygen content of the steel, but did not provide a mathematical model to describe change of composition of the inclusions. Nevertheless, it was clear that there was close coupling between reactions at the slag-metal interface and the transformation of inclusions. Later

on, this model was coupled to the particle model for transformation of alumina to magnesium aluminate spinel inclusions by Galindo et al. [14] and a similar conclusion was found.

A coupled kinetic model to describe industrial operations in the ladle furnace was proposed by Harada et al. [15]. The model considered interaction between steel, slag and inclusions originating from slag entrainment, as well as by deoxidation reactions, dissolution of the refractory into the slag and formation, flotation and agglomeration of inclusions. The activities of the individual components for a given oxide system of the inclusions were fixed and the composition change of inclusion was assumed to be controlled by mass transfer within the boundary layer. However, they did not consider formation of sulfide inclusions in their model and determined several model parameters to fit the model results with plant data or experimental results which should be modified if the operational conditions are different.

In a further study, Harada et al. [16] employed the same kinetic model to that in [15] to simulate the reactions during the ladle refining process and to clarify the mechanism of compositional changes in inclusions. Experiments were also conducted to validate the model. They observed that the inclusion composition gradually changed from Al_2O_3 to $MgO \cdot Al_2O_3$ after the addition of Mg, and the inclusions originating from slag remained in the steel for the duration of the experiment (30 mins).

Recently, Kumar and Pistorius [17] used FactSage macros to simulate steel–slag and steel–inclusion reaction kinetics and quantify rate of calcium transfer from slag to steel to

inclusions that may modify alumina inclusions in laboratory scale experiments. They assumed that the mass transfer coefficient in the steel, k_{steel} was 10 times larger than in the slag, k_{slag} and experimental data was used to determine $k_{steel} \times A_{Interface}$.

More recently Shin et al. [18] employed the Effective Equilibrium Reaction Zone (EERZ) model to calculate the evolution of inclusions during the secondary refining processes. In their model, the reaction zone volume is defined per unit step for metal and slag phase which is dependent on the ”effective reaction zone depth” in each phase. The effective reaction zone depth was fitted from the mass transfer coefficients in metal and slag phase which was determined experimentally.

Because of the close coupling between the slag-metal reactions and inclusion transformation, a model is required that considers steel-slag reaction and steel-inclusion reactions as well as the reactions involved in adding reagents to the steel. The present work proposes a kinetic model for modification of inclusions which considers all possible rate controlling steps including reduction of calcium from the slag and calcium bubble dissolution, mass transfer through the boundary layer and diffusion within the product layer. The model also takes into account simultaneous formation and competition for the calcium from alumina and sulfide inclusions. Coupling the inclusion model with a multi-component steel-slag model [19] allows tracking of the trajectory of slag, metal and inclusion composition during ladle treatment.

4.2 Description of the model

To develop a model for the ladle furnace, including calcium treatment, the transfer of species between slag, metal and inclusions as well as the reaction of additions such as calcium must be considered. Therefore the following interactions are included in the model: (a) the kinetics and mechanism of calcium supply to the steel, (b) mechanism and kinetics of inclusion modification and competition for calcium between inclusions, namely calcium sulfide, calcium oxide and calcium aluminate and (c) slag-metal reactions that will modify the steel composition and alter the balance of competition between different reactions. A schematic diagram of the ladle furnace and the ongoing reactions between slag, steel and inclusions during calcium treatment is shown in Figure 4-1.

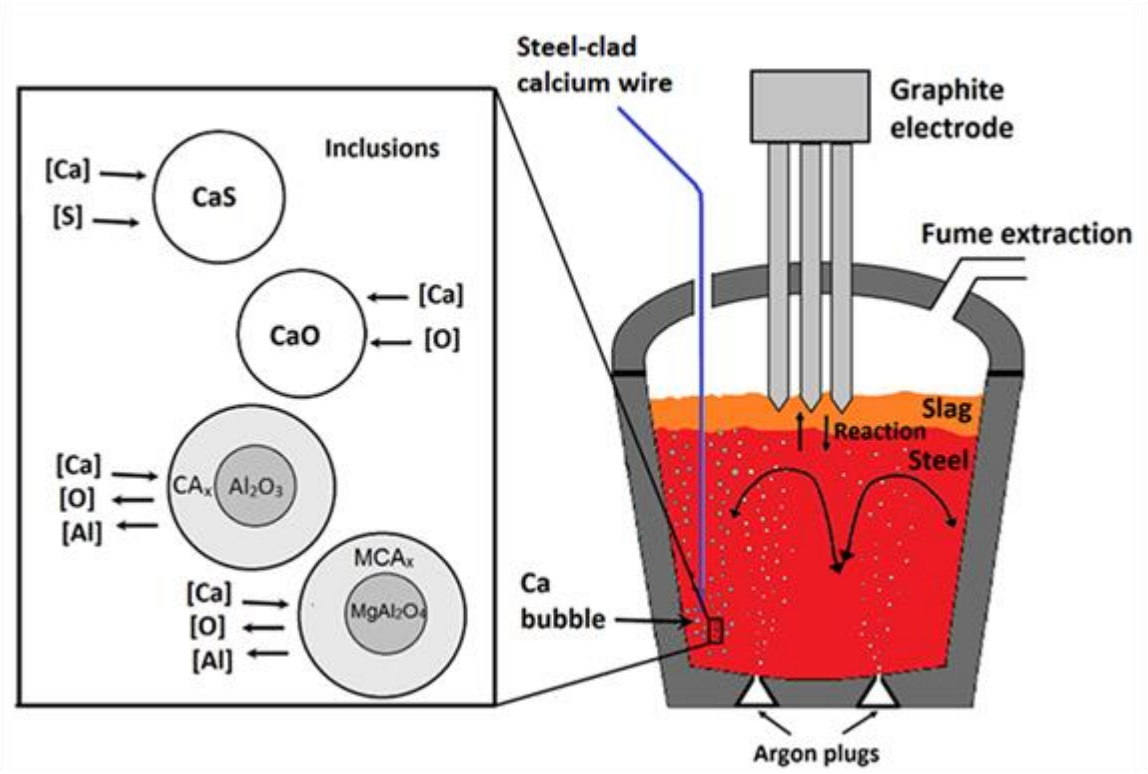

Figure 4-1. Schematic diagram of a ladle furnace and the reactions between slag, metal and inclusions

4.2.1 Calcium injection

To include the injection and dissolution rate of calcium into the steel, a model developed by Lu et al. [7] was adopted in the present work. These workers found that when calcium dissolves by diffusion through the boundary layer surrounding a calcium bubble, it reacts with diffusing oxygen and sulfur at the reaction plane to form CaO and CaS, causing the calcium concentrations to drop to a very low level as shown in Figure 4-2.

The steep concentration gradient accelerates the mass transfer of calcium, hence an enhancement factor E is incorporated into the dissolution equation (4-4). It is worth noting that while the presence of dissolved sulphur and oxygen significantly enhances the rate of pickup of total calcium in the steel, it actually slows the rate of calcium dissolution. This is apparent in Figure 4-2 if one considers the very low calcium concentration gradient between the reaction plane and the bulk steel.

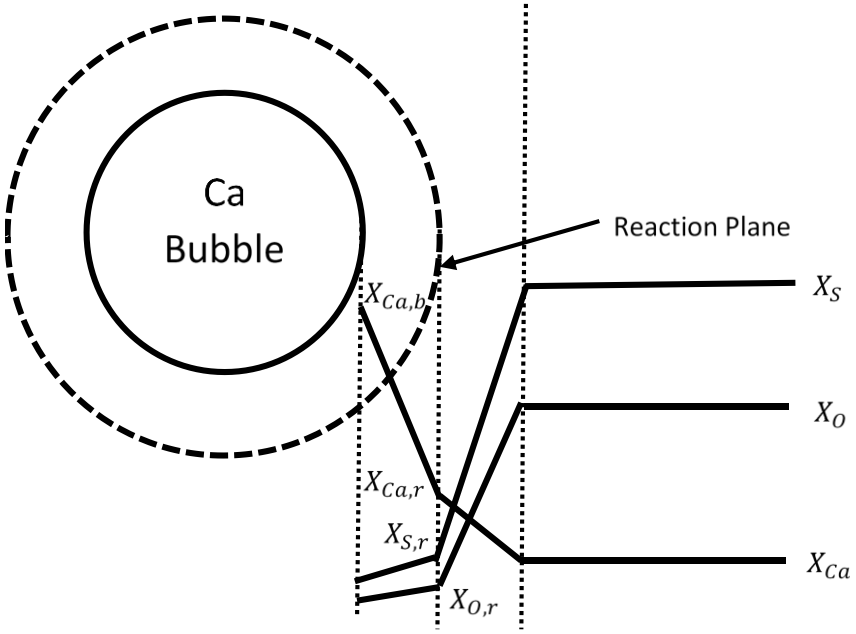

Figure 4-2. Schematic diagram of the calcium dissolution, redrawn based on ref [52]

Therefore, the enhanced dissolution rate of calcium is:

$$\frac{dX_{Ca}}{dt} = k_{Ca,L} A_{B,L} \frac{E}{E-1} \left(X_{Ca,r} - X_{Ca}\right) \quad \textbf{(4-4)}$$

Where X_{Ca} is the mole fraction of dissolved calcium, $k_{Ca,L}$ is the mass transfer coefficient of calcium through boundary layer to the steel, $A_{B,L}$ is the interfacial area of calcium bubbles per unit volume of steel, $X_{Ca,r}$ is the mole fraction of calcium at the reaction plane. and E is the enhancement factor defined by the Eq (4-5)

$$E = 1 + \frac{D_O X_O + D_S X_S}{D_{Ca} X_{Ca,b}} \quad \textbf{(4-5)}$$

Where D_O, D_S and D_{Ca}represent the diffusivities in steel, of O,S and Ca respectively, $X_O$and X_S are the mole fractions of dissolved O and S in bulk steel and $X_{Ca,b}$ is the mole fraction of calcium at the bubble-steel interface at saturation. By reaction of oxygen and sulfur with calcium, oxide and sulfide inclusions form in the injection zone.

4.2.2 Steel-Inclusion reactions

When calcium is injected into the steel, alumina particles transform to calcium aluminate and CaO and CaS form. All of these inclusions compete for the available calcium. To calculate the rate of inclusion evolution it is necessary to consider all the kinetic steps. Figure 4-3 shows a schematic diagram of expected concentration gradient of Ca, Al, O and S among bubble, steel and inclusions. The dissolving calcium reacts with diffusing oxygen and sulfur to form calcium oxide and calcium sulfide inclusions. The dissolved calcium transforms alumina inclusions to calcium aluminate. The authors recently developed a multi-layer model to describe the inclusion transformation which

included all the possible solid phases that could form in the $Al_2O_3 - CaO$ system [12]. This model demonstrated that the overall transformation was controlled by a combination of transport of calcium to the bulk steel and transport of calcium from the steel to and within the inclusions. Therefore, in the current work, a shrinking core model [21] based on liquid calcium aluminate forming directly from alumina, is assumed for the transformation. The dissolved calcium can also react with dissolved oxygen and sulfur to form secondary calcium oxide and calcium sulfide inclusions depending on the O, S and Ca content of the steel. The assumptions of the model are as follows:

- At the start of the process a very thin layer of liquid CA_x is assumed to exist at the surface of alumina inclusions.
- Chemical reactions are fast relative to mass transport processes, due to the high temperature, so equilibrium is attained at all interfaces.
- Mass transfer within liquid CA_x is mathematically described by quasi steady-state counter molecular diffusion of CaO and Al_2O_3 through the product layers. While this is a legitimate phenomenological treatment, the authors recognize that the mechanism and actual diffusing species may be more complex.
- The molten steel is well mixed, so there is a uniform concentration of dissolved species and inclusions in the steel.
- An initial and constant number of alumina inclusions are assumed at the beginning of injection. The number is taken from the SEM (Scanning Electron Microscopy) analysis of the steel. The size of alumina inclusions is chosen to match that found by SEM.

Hence, the model includes the following steps:

- Dissolution of calcium from the gas bubble-steel interface into the bulk steel
- Transfer of the dissolved calcium or other solutes through the boundary layer between the bulk steel and inclusion interface
- Diffusion of calcium from the steel-inclusion interface through the product layer to the alumina core
- Chemical reaction of the calcium with alumina

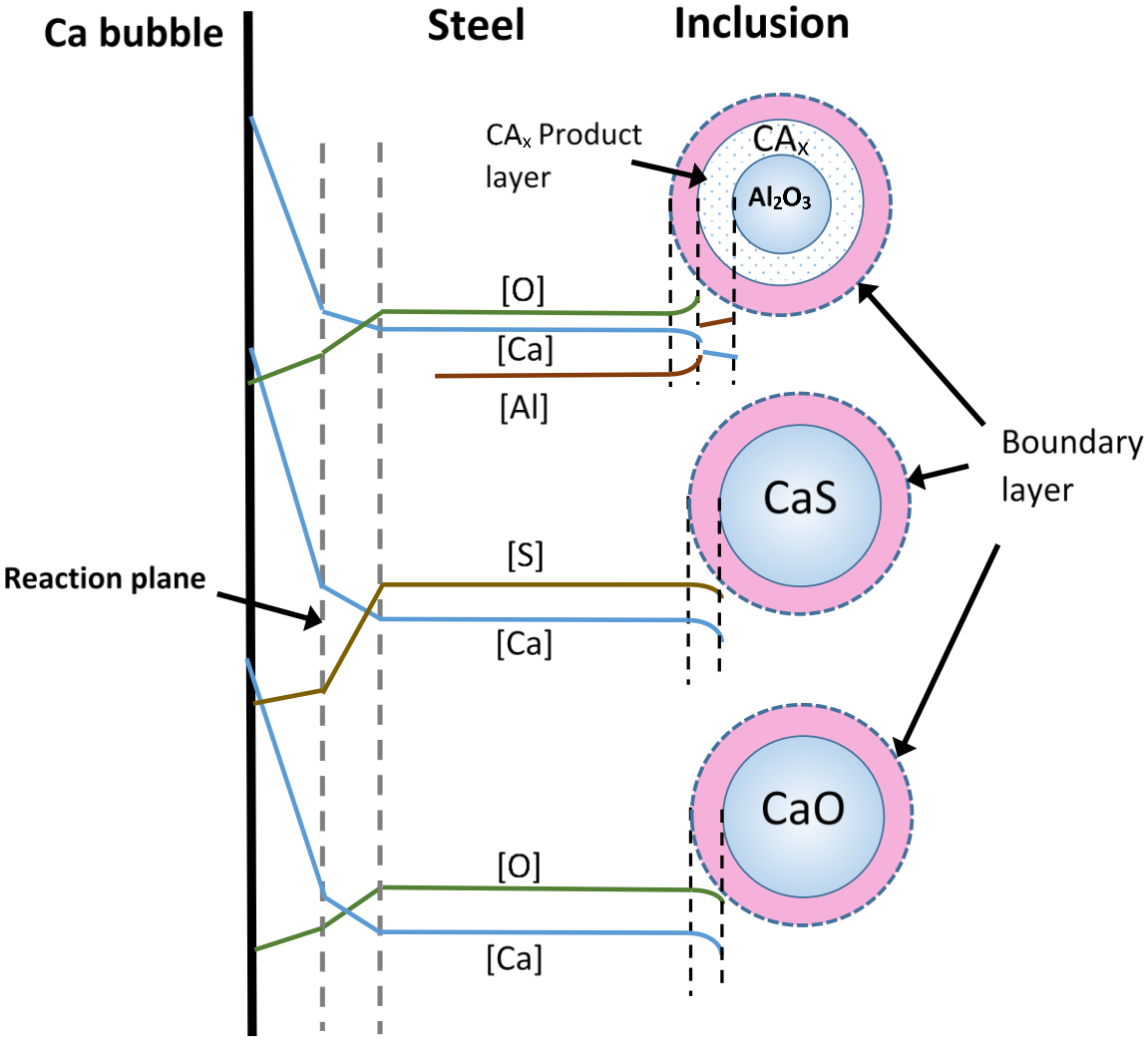

Figure 4-3. Schematic diagram of reactions and transfer of species in the steel and inclusions

It is worth mentioning that magnesium-aluminum spinel inclusions are also modified by calcium to calcium-magnesium aluminate inclusions. There has been number of studies on the modification of spinel inclusions [22-24], but modification of spinel inclusion is not considered in the present work. The authors are currently working to include modeling of spinel transformation by calcium treatment with the current model.

4.2.2.1 **Interfacial concentrations**

The rate of alumina inclusion evolution is calculated by coupling mass balance at the inclusion-steel interface with local thermodynamic equilibrium. In the case of modification of alumina inclusions by calcium, the mass balance for calcium, aluminum and oxygen leads to the following equations:

$$N_{Ca} = N_{CaO} \quad \textbf{(4-6)}$$

$$N_{Al} = 2N_{Al_2O_3} \quad \textbf{(4-7)}$$

$$N_O = N_{CaO} + 3N_{Al_2O_3} \quad \textbf{(4-8)}$$

Where N_i, the mass transfer rate of species i through the boundary layer from the bulk steel to the surface of a spherical particle can be described by the following equation:

$$N_i = 4\pi r^2 . k_{m,i} \mathrm{C_{v_m}} \, (X_i^b - X_i^*) \quad \textbf{(4-9)}$$

Where $k_{m,i}$ is the mass transfer coefficient across the boundary layer, r is the particle radius, $\mathrm{C_{v_m}}$ is the molar density of the steel, X_i^b is the mole fraction of species i in the bulk steel and X_i^* is the mole fraction of species i at the interface. From dimensionless analysis, $k_{m,i}$ is obtained using the Sherwood number defined as:

$$Sh = \frac{k_{m,i} d}{D_i} \quad \textbf{(4-10)}$$

Where Sh is the Sherwood number, d is the particle diameter and D_i is the diffusion coefficient of the species i in the steel. For small spherical particles, the Sherwood number may be assumed to be equal to 2 [25,26].

Mass transfer within the alumina inclusion is assumed to occur by quasi steady-state, counter molecular diffusion of CaO and Al_2O_3 , through the liquid calcium aluminate. The mass transfer rates of CaO and Al_2O_3 are driven by the concentration gradient. Molar flow of species i in the liquid product layer can be described by the following equation [25]:

$$N_i = \left(\frac{4\pi r_{ex} r_{in}}{r_{ex} - r_{in}}\right)(\mathrm{C_v} D_i)(X_i^{ex} - X_i^{in}) \qquad \textbf{(4-11)}$$

Where r_{ex} and r_{in} are exterior and interior radius of the product layer, respectively. $\mathrm{C_v}$ is the molar density of the liquid layer, D_i is the diffusivity of species i and X_i^{ex} and $X_i^{in}$are mole fraction of species i at exterior and interior radius respectively.

Thermodynamic equilibrium at the inclusion-steel interface is obtained considering simultaneous deoxidation equilibria of Ca and Al in steel with the Al_2O_3 and CaO components in the calcium aluminate phase according to the following reactions.

[Ca]+[O]=(CaO)$_{inc}$

$$K_{CaO} = \frac{a_{CaO}}{\left(\frac{f_{Ca} X^*_{Ca} n_T MW_{Ca} 100}{St_{mass}}\right)\left(\frac{f_O X^*_O n_T MW_O 100}{St_{mass}}\right)} \qquad \textbf{(4-12)}$$

2[Al]+3[O]=(Al$_2$O$_3$)$_{inc}$

$$K_{Al_2O_3} = \frac{a_{Al_2O_3}}{\left(\frac{f_{Al} X^*_{Al} n_T MW_{Al} 100}{St_{mass}}\right)^2\left(\frac{f_O X^*_O n_T MW_O 100}{St_{mass}}\right)^3} \qquad \textbf{(4-13)}$$

Where f_i represents activity coefficient of species i with respect to 1 wt% standard state, MW_i is the molar weight, n_T is total number of moles of steel and St_{Mass} is total mass of the steel.

For the sake of simplicity in modeling the activities $a_{Al_2O_3}$ and a_{CaO} in the $Al_2O_3 - CaO$ system are fitted to a sigmoidal function using values calculated by FactSage 6.4 software (FT Oxide database) at 1873 K [27,28]. The values used for oxidation equilibrium constants are $K_{CaO} = 1.2 \times 10^9$ [29], $K_{Al_2O_3} = 3.16 \times 10^{12}$[30] and $K_{CaS} = 1.7 \times 10^7$[31].

4.2.2.2 Inclusion evolution

Modification of alumina inclusions according to the phase diagram is shown in Figure 4-4. First a layer of calcium aluminate forms on the surface of the alumina core. The modification continues with shrinkage of alumina core and growth of the product layer. At this stage, the composition of calcium aluminate produced is close to that in equilibrium with alumina. As the core is consumed, if calcium injection continues, the modification proceeds by increasing the mole fraction of CaO in the calcium aluminate inclusion. When the composition of liquid calcium aluminate reaches the CaO saturation composition, it is assumed that a layer of CaO precipitates on the outer surface of the inclusion hindering further modification (see Figure 4-4). After this stage more calcium injection results in increasing thickness of the CaO layer.

The change of the radius of the alumina core can be calculated by considering the relation between molar flux and volume:

$$\frac{dV}{dt} = \frac{dV}{dn} \times \frac{dn}{dt} \quad \textbf{(4-14)}$$

By substituting:

$$4\pi r^2 \frac{dr_{Al_2O_3}}{dt} = \frac{MW_{Al_2O_3}}{\rho} \times N_{Al_2O_3} \quad \textbf{(4-15)}$$

Where $N_{Al_2O_3}$ is number of mole of Al_2O_3 leaving the alumina core per unit time which is sum of the alumina reacting with CaO to form CA_x and alumina transferred through the product layer to dissolve in the steel in the form of aluminum. After substitution and rearrangement one can obtain:

$$4\pi r^2 \frac{dr_{Al_2O_3}}{dt} = \frac{MW_{Al_2O_3}}{\rho} \times (\vartheta' N_{Ca} + \frac{1}{2} N_{Al}) \quad \textbf{(4-16)}$$

Where ϑ'defines the composition of the liquid calcium aluminate in thermodynamic equilibrium with alumina at 1600 °C according to phase equilibria. N_{Ca} and N_{Al} are calculated using Eq (4-9). The inclusion composition is calculated from the calcium aluminate and alumina core diameters.

After the core is consumed, modification can continue by further dissolution of calcium in calcium aluminate inclusions and thereby increasing the CaO fraction. Change of composition can be calculated as follows:

$$X_{Al_2O_3} = \frac{n_{Al_2O_3}}{n_{Al_2O_3} + n_{CaO}} \text{ and } X_{CaO} = 1 - X_{Al_2O_3} \quad \textbf{(4-17)}$$

Where

$$\frac{d_{n_{Al_2O_3}}}{dt} = \frac{1}{2} N_{Al} \text{ and } \frac{d_{n_{CaO}}}{dt} = N_{Ca} \quad \textbf{(4-18)}$$

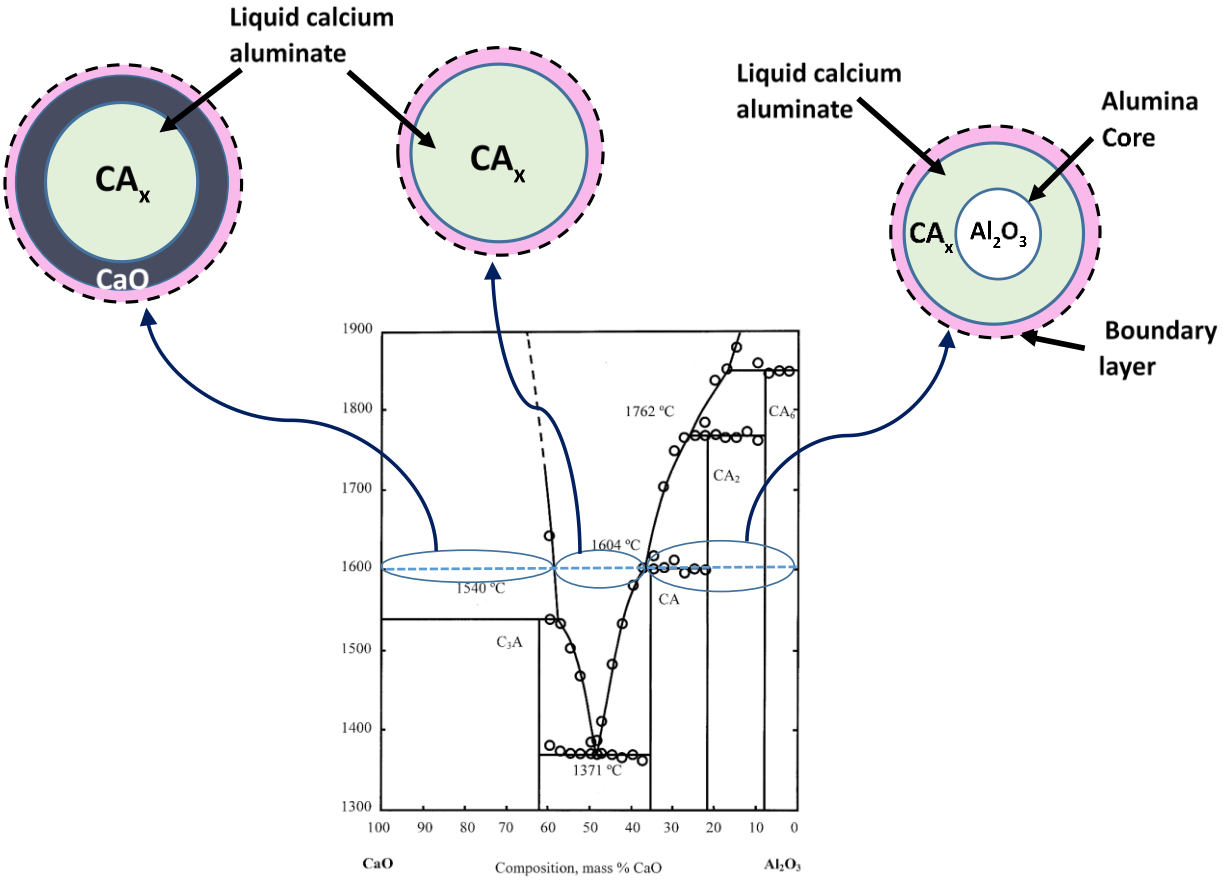

Figure 4-4. Modification of alumina inclusion and corresponding phases

4.2.2.3 **Dissolved species**

Change of the dissolved species due to the injected calcium and steel-inclusion reaction can be calculated by considering mass balance. For calcium

$$\frac{dX_{Ca}}{dt} = k_{Ca,L}A_{B,L}\frac{E}{E-1}\left(X_{Ca,r} - X_{Ca}\right) - k_{Ca,CA_x}A_{CA_x}\left(X_{Ca} - X^i_{CAx}\right) - k_eA_e(X_{Ca} - 0)$$

(4-19)

Where the first term on the R.H.S shows the calcium dissolution flux through the bubble/steel interface to the steel, including the enhancement factor. The second terms

describe transfer of calcium to the CA_x inclusions and the last term represents evaporation of calcium from the surface of the steel melt. Mass transfer coefficients for inclusions are calculated using Eq (4-10) assuming the Sherwood number equals 2. The evaporation rate constant k_e is obtained from the work of Lu et al. [7]. Similar equations can be written for Al, S and O as follows.

$$\frac{dX_{Al}}{dt} = -k_{Al,CA_x} A_{CA_x} \left(X_{Al} - X^{\,i}_{Al,CA_x}\right) \quad \textbf{(4-20)}$$

$$\frac{dX_O}{dt} = -k_{O,L} A_{B,L} \frac{E}{E-1} \left(X_O - X_{O,r}\right) - \left(k_{O,CA_x} A_{CA_x}\right)\left(X_O - X^{i}_{O,CA_x}\right) \quad \textbf{(4-21)}$$

$$\frac{dX_S}{dt} = -k_{S,L} A_{B,L} \frac{E}{E-1} \left(X_S - X_{S.r}\right) \quad \textbf{(4-22)}$$

By solving these four differential equations, change of concentration of dissolved species due to interaction with inclusions can be calculated. Inspection of Figure 4-2 shows that the first term in Eqs (4-21) and (4-22)***(4-22)(4-22)*** respectively represent the oxygen and sulphur consumed in forming oxides and sulphides inclusions.

4.2.3 Slag-metal reaction

In the present work the multicomponent kinetic model of Graham and Irons [13] described in greater detail in ref [19] was used to calculate the effect of steel - slag reactions during ladle processing. The model is based on the mixed coupled reaction model proposed by Robertson et al. [32] and developed to describe dephosphorization and deoxidation.

The model proposed by Robertson [32] assumed that the rates are controlled by multicomponent transport in both metal and slag. Moreover, it was assumed that chemical

reactions are sufficiently fast such that there exists local equilibrium at the slag-metal interface between elements and their oxides and sulphides.

A general reaction between the oxide in the slag and the respective species in the steel is:

$$x[M] + y[O] = (M_x O_y) \quad \textbf{(4-23)}$$

The equilibrium constant for the reaction at the interface is:

$$\mathrm{K_{M_xO_y}} = \frac{\mathrm{a_{M_xO_y}}}{\left[\frac{f_M X_M^* n_T MW_M 100}{St_{mass}}\right]\left[\frac{f_O X_O^* n_T MW_O 100}{St_{mass}}\right]} \quad \textbf{(4-24)}$$

Where f_i are the activity coefficients for species i in the steel with respect to 1 wt% standard state at the slag-steel interface, and X_i^* are the molar fractions of the respective species at the slag-steel interface. The activities of the components in the slag are calculated using the cell model formalism [33,34].

Considering transport of species from the bulk phases to the interface, the mass balance at the interface takes the form:

$$k_m^M C_{v_m}(X_M^b - X_M^*) = k_{sl}^{M_xO_y} C_{v_{sl}} (X_{M_xO_y}^* - X_{M_xO_y}^b) \quad \textbf{(4-25)}$$

$C_{v_m}$and $C_{v_{sl}}$ are the molar density of the metal and slag phase respectively; k_m^M and k_{sl}^{MxOy}, are the mass transfer coefficients in the metal and slag phase respectively. By coupling all the mass transport equations with the overall balance of oxygen and equilibria at the interface then solving the system of nonlinear equations, the interfacial concentrations are calculated.

$$k_m^O \; C_{v_m}(X_O^b - X_O^*) = \sum_{i=1}^{n} y_i k_{sl}^{M_xO_y} C_{v_{sl}} (X_{M_xO_y}^* - X_{M_xO_y}^b) \quad \textbf{(4-26)}$$

The change of concentration in the bulk steel and slag due to steel-slag reaction are calculated using the following equations:

$$\frac{dX_{M_xO_y}}{dt} = -k_{sl} M_x O_y \left(\frac{A}{V_{St}}\right)\left(X^b_{M_xO_y} - X^*_{M_xO_y}\right) \quad \textbf{(4-27)}$$

$$\frac{dX_M}{dt} = -k^M_m \left(\frac{A}{V_{St}}\right)\left(X^b_M - X^*_M\right) \quad \textbf{(4-28)}$$

The kinetics of desulphurization in the ladle are modeled similarly to oxidation. The only difference is that the interfacial concentrations are related by means of an equilibrium partition coefficient for desulphurization, L_S.

The model also takes into account the stirring effect, the effect of ladle furnace power on temperature, change of composition due to alloying addition.

4.2.4 Flow chart of the calculation program

The MATLAB^{TM} software was used to develop a computer code for solving the equations in this work. The algorithm employed is illustrated in Figure 4-5. First, composition of the molten steel and slag in addition to the number and size of inclusions are initialized. It is worth mentioning that there are two time loops for calculations. The outer loop for calculating change of composition due to the steel-slag reaction is shown by Δt and the inner loop for steel-inclusions reaction (dt). Since the processing conditions for the ladle are provided every 0.1 min and also slag-steel reactions occur more slowly than steel-inclusions reactions, $\Delta t = 60\ s$ and $dt = 1\ s$ are chosen for calculations in this work.

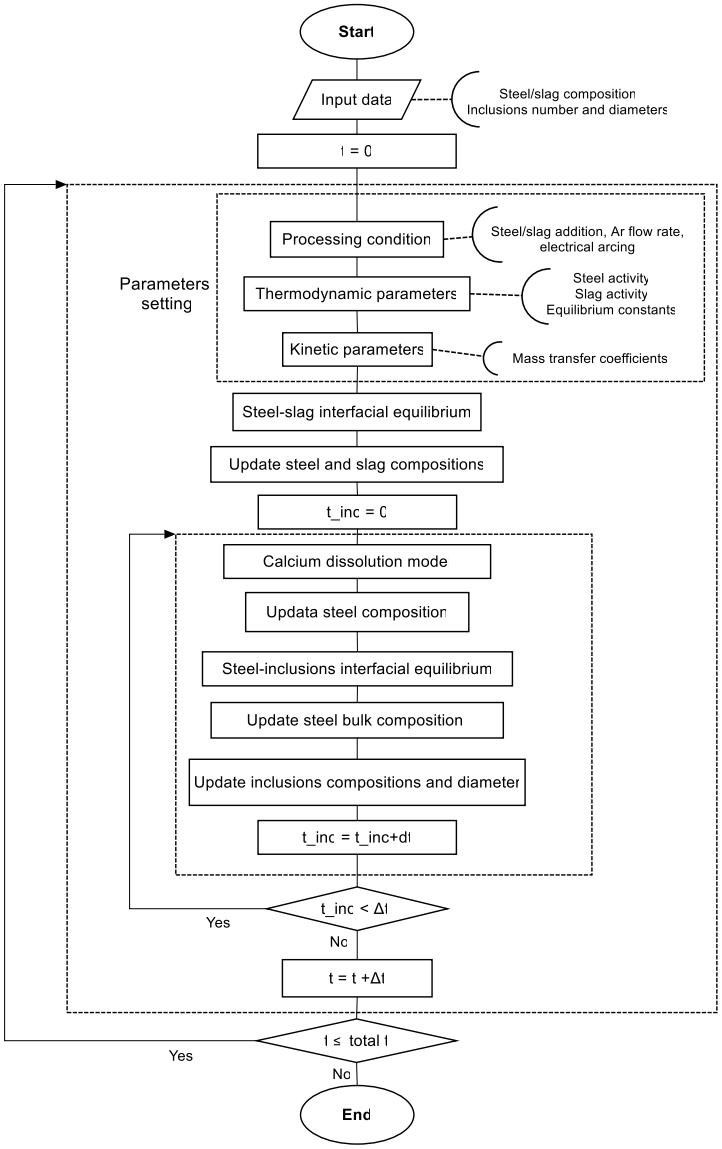

Figure 4-5. Flow chart of the coupled steel-slag-inclusion kinetic model

To calculate steel-slag interfacial concentrations, thermodynamic and kinetic parameters such as activities, thermodynamic equilibrium constants and mass transfer coefficients should be determined. Temperature is also updated at this stage according to arcing or stirring conditions. Mass transfer coefficient of all the components in the molten

steel is assumed to be equal and is determined by the empirical correlation with effective stirring power developed by Graham and Irons [13]:

$$k_m = (0.06 \pm 0.002)\varepsilon^{1.4\pm0.09} \quad \textbf{(4-29)}$$

Where k_m is the volumetric mass transfer coefficient of the molten steel which includes the mass transfer coefficient, interfacial area between the metal and slag phase and volume of steel and ε is the effective stirring power (W/t).

The mass transfer coefficients of the components in the slag phase $k_{sl}^{M_xO_y}$ are calculated from individual ratios with the mass transfer coefficient of the species in steel $k_{sl}^{M_xO_y}/k_m^M$ which are the same as developed by Graham and Irons [13] for this system.

After calculation of interfacial concentrations, the flux of each element in the steel and slag phase is calculated in each time step Δt. Then, the composition change of steel and slag is calculated. In the inner loop, first the calcium content of the steel is determined using the enhanced dissolution model described in section 4.2.1. To calculate the calcium dissolution rate it is necessary to know the mass transfer coefficient at the calcium bubbles boundary layer and the bubbles interfacial area. These parameters are very difficult to measure, so in this study they are estimated based on work of Lu et al. [20] and fitting to the industrial heat. Steel-inclusion interfacial concentrations are calculated by considering mass balance and local thermodynamic equilibrium as explained in section 4.2.2.1. By knowing the interfacial concentrations the flux of each component to the inclusions is calculated and hence the change of the composition of bulk steel and inclusions is calculated. Also the amount of sulfide and oxide inclusions produced is calculated.

4.3 Results

In this section the kinetic model is validated by comparison with data from an industrial heat of steel. The model can specifically calculate the following changes: (a) composition of components in the steel and the slag (b) composition of component in the inclusions (c) the ratio of the oxide to sulfide inclusions.

4.3.1 Ladle conditions

The initial chemical compositions of the steel and the slag at the beginning of ladle process used in the calculations are listed in Table 4-1 and Table 4-2 and the operational conditions are shown in Table 4-3, which were obtained from the processing of a low-carbon aluminum-killed heat at ArcelorMittal Dofasco. In this heat the Ca injection process was stopped every minute and the sample was taken for chemistry and inclusion analysis to have inclusion analysis during injection. To the authors' knowledge such results have never been reported in the literature.

Table 4-1. Initial steel composition (Wt %)

C	Mn	P	S	Si	Al	N	Ca	O
0.0501	1.03	<0.016	0.0123	0.063	0.0268	0.0045	0.00019	<0.001

Table 4-2. Initial slag composition (Wt %)

P_2O_5	TiO_2	CaS	FeO	CaO	MnO	SiO_2	MgO	Al_2O_3
0.09	0.44	0.425	1.15	42.4	0.56	13.56	12.86	28.34

Table 4-3. Ladle processing conditions for calculations

Initial steel temperature (K)	1867
Steel mass (tonne)	164.5
Slag mass (tonne)	2.58
Ladle diameter (m)	3.2
Steel height (m)	3.35
Slag height (m)	0.127
Ar flow rate (Nm^3/h/plug)	4 at low stirring regime and 25 at high stirring regime

4.3.2 Inclusion analysis

4.3.2.1 Number and size of inclusions

In this section data from automated SEM analysis [35] (ASPEX® Personal SEM Explorer with Metals Quality Analyzer) is used to determine the inclusion size and number for the model. The system classifies inclusions into different classes according to their compositions. The number of the various inclusions per unit volume of steel was calculated from automated SEM data using the Schwartz-Saltykov method [36] as discussed in the Appendix. It was ensured that inclusions were not entrained slag based on their chemistry, size (<5 microns) and morphology. All the inclusions used in this study were checked and entrained slag (if any) was removed from the data set for the analysis.

As mentioned earlier, an average size and number of alumina inclusions was chosen as the starting point for the model. As will be explained later, some calcium modification occurs before calcium injection, so the classes of inclusions which the initial alumina at any time are $CA_6, CA_2, CA, C_{12}A_7, C_3A$ and Al_2O_3. Table 4-4 shows the results for these classes. The resolution of the instrument is not fine enough to resolve the multi-layer structure, so that only the average composition is measured for individual inclusions. Typically 2000-3000 inclusions were counted in a 15 mm^2sample. It is apparent that there are some variations in the distributions and sizes, but the average size and number at the bottom of the Table 4-4 represents a reasonable estimate of the average number and size of inclusions which were originally alumina.

CaS was also found in the samples, as well as $CaMnS$ which forms from CaS during solidification. Inclusions containing Ca, S and other minor elements such as Al, Mg and Si were combined with $CaMnS$ inclusions as other CaS inclusions in Table 4-5. The total number of sulphide inclusions dramatically increases during the injection process which strongly supports the enhanced dissolution model. Therefore, for the model it was assumed that the primary CaS inclusions that were formed according to enhanced dissolution were 1 micron diameter. The number of CaS inclusions was calculated in the model and compared with the measured numbers of sulphide inclusion in the results as a validation of the model.

Table 4-5 shows the average diameter and number of sulphide and oxide inclusions during injection.

Primary CaO inclusions may also have formed at the reaction plume, however, during injection the oxygen content of the steel was less than 5ppm, and only very few very small CaO inclusions are likely to have formed., thus it is not surprising that none were detected by ASPEX., it is also likely that CaO inclusions were dissolved in the water used during sample preparation for the SEM. . The system found some unclassified inclusions with high Ca content. These results are labelled as "CaO" in Table 4-5, indicating that it is an assumed phase. Again, the numbers of "CaO" inclusions increases with injection time just as the the CaS inclusions did. The numbers are much smaller than the sulphides, as would be expected by the enhanced dissolution model because there is much less dissolved O than S in the steel.

Less than 5% of the inclusions are spinel so the calcium associated with the spinel is negligible in comparison to alumina and sulphides in this specific heat. The authors recognize that spinel formation is common in ladle treatment and are currently working on an extension of the current model to include the modelling of calcium treatment of spinel inclusions.

4.3.2.2 Distribution of calcium sulfide and calcium aluminate inclusions

By knowing the diameter and the number of inclusions per unit volume of sulphide and calcium aluminate inclusions as shown in Table 4-4 and Table 4-5, the amount of Ca in each type of inclusion and subsequently total Ca may be calculated. Figure 4-6 shows the distribution of Ca in the various inclusions during injection in comparison with the total

Ca content measured independently by Optical Emission Spectroscopy (OES). Total Ca by SEM is the total Ca in sulfide and calcium aluminate inclusions measured by SEM.

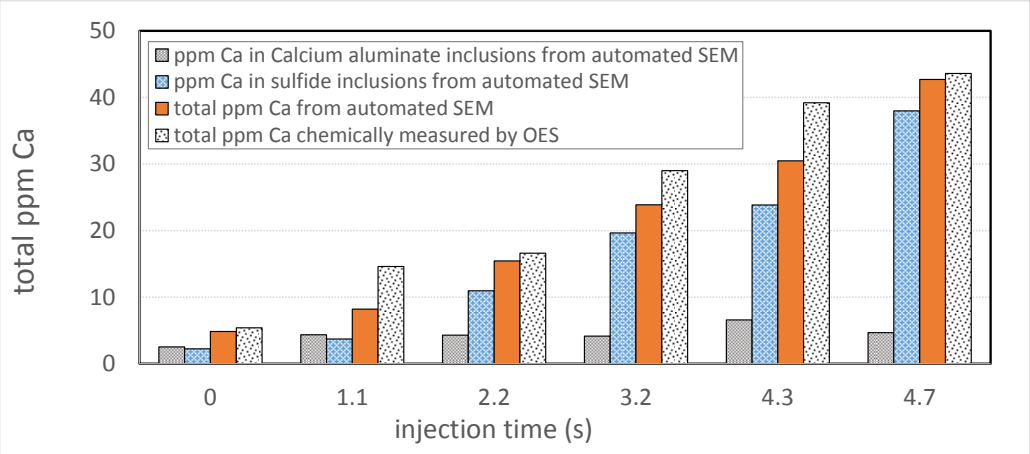

Figure 4-6. Calcium distribution in different inclusions based on inclusion analysis result

Table 4-4. Diameter and number of calcium aluminate inclusion during calcium injection

	C_3A		$C_{12}A_7$		CA		CA_2		CA_6		Al_2O_3		total number of calcium aluminate inclusions
time of injection	$d\ (\mu m)$	$No\left(\frac{\times 10^{-12}}{m^3}\right)$	$d\ (\mu m)$	$No\left(\frac{\times 10^{-12}}{m^3}\right)$	$d\ (\mu m)$	$No\left(\frac{\times 10^{-12}}{m^3}\right)$	$d\ (\mu m)$	$No\left(\frac{\times 10^{-12}}{m^3}\right)$	$d\ (\mu m)$	$No\left(\frac{\times 10^{-12}}{m^3}\right)$	$d\ (\mu m)$	$No\left(\frac{\times 10^{-12}}{m^3}\right)$	$\left(\frac{\times 10^{-12}}{m^3}\right)$
0	1.14	0.77	1.06	2.8	1.43	6.5	1.50	9.6	0.82	0.87	1.35	0.89	20
1.2	1.59	0.51	2.94	1.2	1.83	3.9	1.65	3.4	1.14	0.58	1.00	1.2	9.6
2.2	1.22	1.6	2.31	1.8	1.78	5.9	1.01	7.2	4.05	0.17	0.80	4.2	17
3.2	0.88	1.1	2.20	2.8	1.69	6.0	1.11	14.0	0.78	0.54	1.88	0.38	14
4.3	0.96	3.1	3.18	2.2	1.60	4.3	1.31	2.4	0.00	0	1.40	0.44	12
4.7	1.17	3.9	2.44	2.7	1.45	5.5	1.43	1.9	0.92	0.73	1.81	0.39	15
Average									diameter (μm)	1.5	number $\left(\frac{10^{-12}}{m^3}\right)$		15

Table 4-5. Diameter and number of sulphide and oxide inclusion during calcium injection

	CaS		$CaS\ other$		Total number of sulphide inclusions $\left(\frac{\times 10^{-12}}{m^3}\right)$	CaO	
Time of injection	$d\ (\mu m)$	$No\left(\frac{\times 10^{-12}}{m^3}\right)$	$d\ (\mu m)$	$No\left(\frac{\times 10^{-12}}{m^3}\right)$		$d\ (\mu m)$	$No\left(\frac{\times 10^{-12}}{m^3}\right)$
0	0.00	0	0.98	19	19	0.00	0
1.2	0.65	2.3	0.84	43	46	0.00	0
2.2	0.94	5.4	0.94	100	110	0.00	0
3.2	0.99	2.4	0.93	170	190	2.56	0.28
4.3	1.05	56	0.96	160	220	1.05	0.61
4.7	1.26	57	1.39	860	140	1.51	0.43
Average		diameter (μm)	1.5			number $\left(\frac{\times 10^{-12}}{m^3}\right)$	0.44

* CaO is not classified in ASPEX® analysis. However some unclassified inclusions of high Ca content assumed to be CaO

The total calcium content from automated SEM inclusion analysis is on average 21% below the total calcium content determined by OES, indicating that most of calcium is captured in the inclusion analysis. The major reason for the difference is thought to be the way inclusions are analyzed by automatic SEM. A size threshold is set that defines the smallest inclusion size that can be reliably counted, 0.5 microns in this case. Other researchers have also found that submicron inclusions are missed from SEM analysis [37-39]. Also, since the size of the sample is usually small, occurrence of inclusions of clean

steels is limited [40]. It also can be due to loss of calcium oxides and sulphides during sample preparation.

Figure 4-6 shows that most of the calcium reacts to form sulphide rather than calcium aluminates. It seems that calcium aluminate inclusions reach a saturated value and the rest of injected calcium contributes to form CaS inclusions.

For model calculations a constant number of alumina/calcium aluminate inclusions is assumed as is the initial diameter. The latter is based on the average diameter of calcium aluminates from Table 4-4. The effect of initial number and diameter of inclusions on transformation will be examined in detail in a future publication.

4.3.3 Species in the steel

Figure 4-7shows the results of the model calculations for dissolved elements in the steel. Time zero was taken as the beginning of the ladle process after tapping. At 11 minutes Al was added under strong stirring to deoxidize the steel (Figure 4-7c) to promote desulphurization, but it also resulted in reversion of Mn and Si to the steel from the slag (Figure 4-7a and b). There is very good agreement between the model and the measured Mn, Si and Al contents in the steel, just as there was in the original work used for the slag-metal model [13]. A second aluminum addition was made at 37 minutes, just before Ca wire injection. The very strong aluminum deoxidation drives the calculated dissolved oxygen to levels far below the limits of oxygen probes (Figure 4-7e). With the very strong deoxidation, CaO is also reduced from the slag. The calculated dissolved Ca content is remarkably low in spite of the fact that the dissolved Ca content at the slag-metal interface

during the high stirring rate is in the range of 0.003-0.005 ppm. Once the injection starts the dissolved Ca content remains low (Figure 4-7(e)). Both before and during injection the dissolved Ca reacts very quickly with the inclusions, so the level remains low. It only climbs once the inclusion reactions are complete, approximately 4 minutes in Figure 4-7(e). At this time the higher dissolved Ca drives the oxygen level very low, Figure 4-7f. The reactions with the inclusions are discussed in the next section.

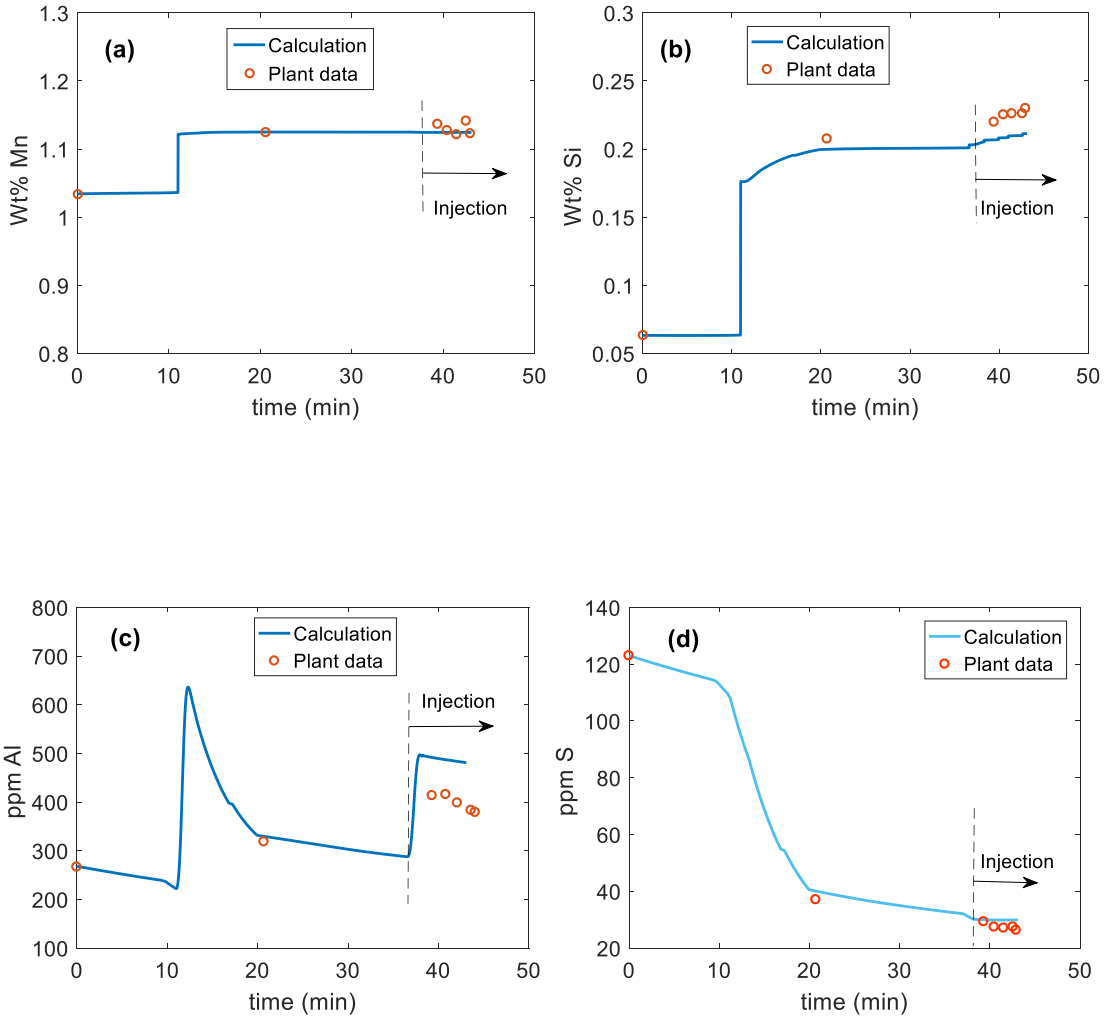

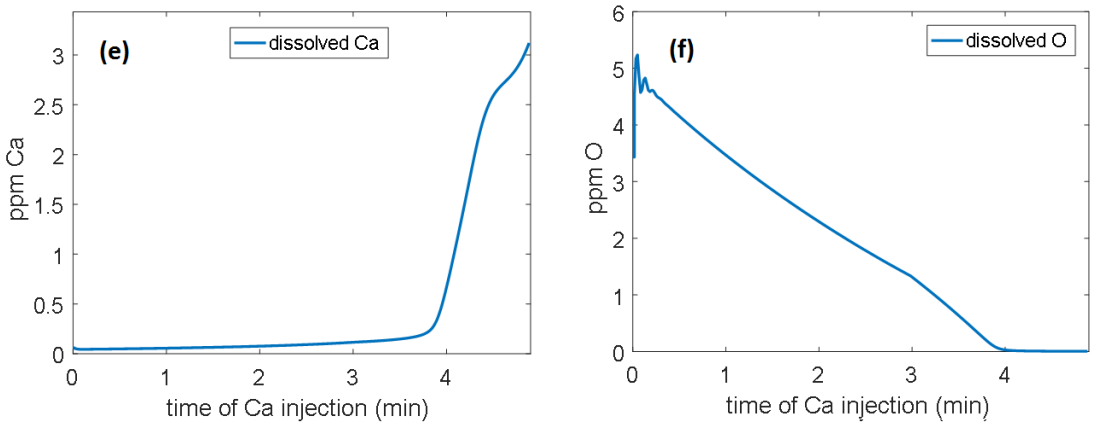

Figure 4-7. Change of species in the steel during ladle process (a) Mn (b) Si (c) Al (d) S (e) Ca and (f) O . Time zero for (a)-(d) is beginning of ladle processing after tapping and time zero for (e)and (f) is the start of Ca injection, 38.3 minutes in (a)-(d).

4.3.4 Inclusion evolution

The change of composition of the calcium aluminate inclusions is presented in Figure 4-8. According to plant measurements there is approximately 2 ppm Ca in the molten steel before injection. This is total calcium which is summation of calcium in inclusions and dissolved calcium in steel. However, the oxygen and sulfur content of the steel is high prior to aluminum addition, so the total calcium is likely present as some combination of calcium oxide and calcium sulphide, but evidently the CaO and CaS were too small to observe in the ASPEX. To test this analysis, the model was run assuming 2 ppm calcium was present in the steel prior to aluminum addition either CaS, CaO or dissolved calcium. The results were identical in all three cases. When the aluminum is added, introducing alumina inclusions, they react with the calcium from these very fine inclusions. Because the calcium bearing inclusions are very small, this can happen in a few seconds. That explains the sharp jump right at the beginning of aluminum addition seen in Figure 8(a). This result is consistent with the previous finding that if there is sufficient

calcium available in the melt, inclusions will react to absorb all that calcium very quickly [12]. The dissolved calcium from slag especially during the high stirring period is sufficient to partially modify alumina inclusions to calcium aluminate. Kumar and Pistorius [17] also reported modification of alumina and spinel inclusions by calcium transferred from slag in laboratory scale. In another study Shin and Park [41] observed that the spinel inclusion changed entirely into a liquid oxide inclusion via the transfer of calcium from slag to metal in their experiments. There is remarkable agreement between the model prediction and the plant data regarding the extent of modification by this mechanism. Figure 4-8(b) shows that it takes approximately three minutes to modify alumina inclusions completely. At the end of the process, the calcium aluminate inclusions reach saturation level with CaO, and further inclusion reaction stops.

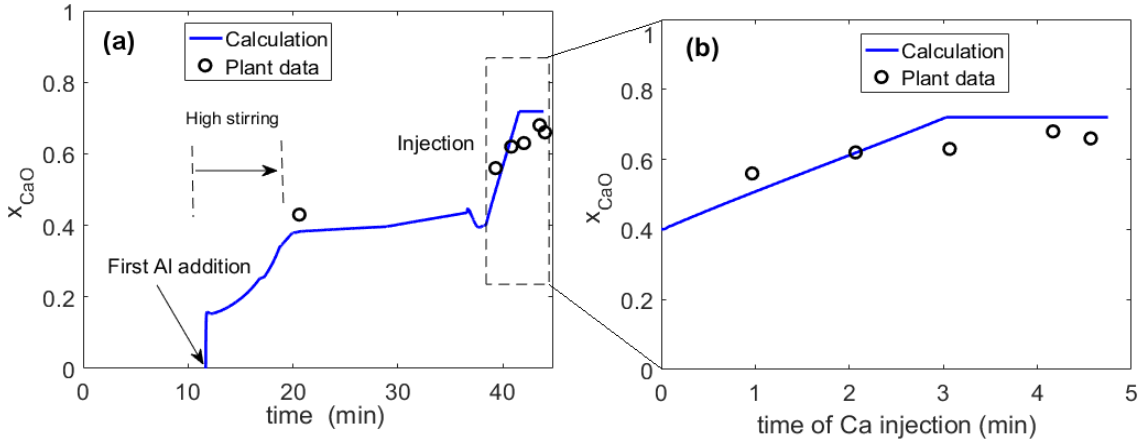

Figure 4-8. Evolution of inclusions (a) and (b) calcium aluminate modification Time zero for (b)-(d) is the start of Ca injection, 38.3 minutes in Figure 4-7 (a)-(d).

Figure 4-9 shows the relative abundance of sulphide and oxide inclusions, calcium aluminate inclusions and total calcium in the molten steel. As oxygen concentration in the

molten steel is much lower than sulfur, the amount of oxide inclusion produced at the injection zone is much lower than sulfide inclusions.

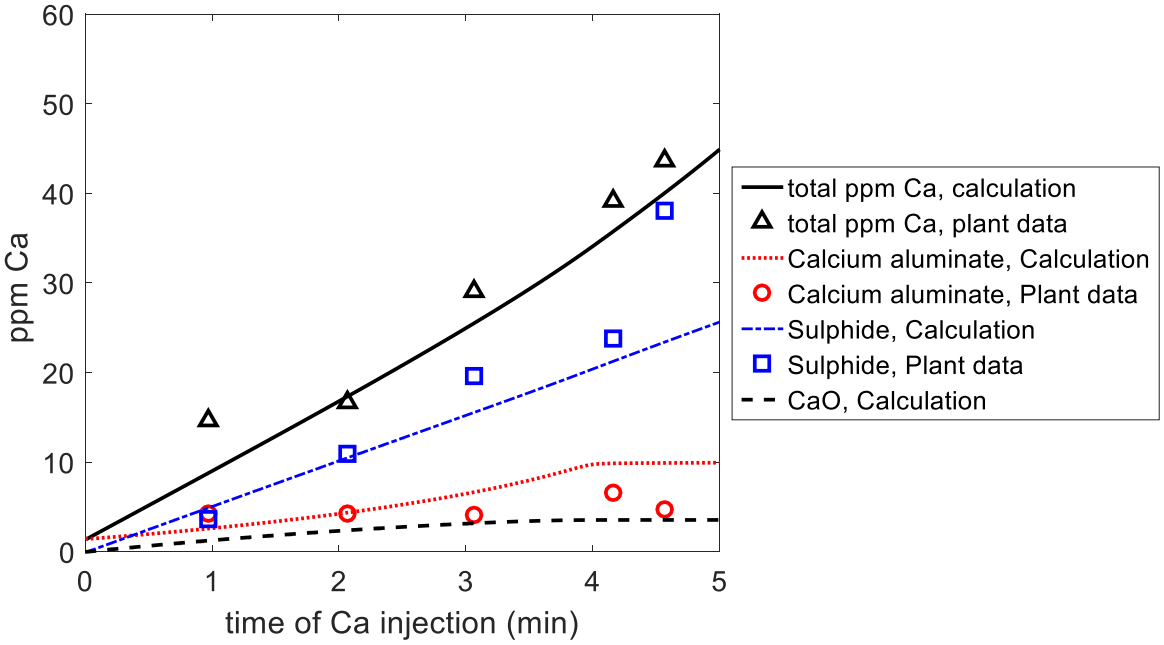

Figure 4-9. CaS and CaO, calcium aluminate inclusions and total calcium in the molten steel. Time zero is the start of Ca injection, 38.3 minutes in Figure 4-7 (a)-(d).

Total calcium is calculated by summation of the dissolved calcium and calcium in combination with sulfide, oxide and calcium aluminate inclusions.

As mentioned above, one problem is estimating the $k_{Ca,L} \times A_{B,L}$ parameter, since measuring the bubble interfacial area is impossible. The $k_{Ca,L} \times A_{B,L}$ parameter was found to be in the range of $(1 \times 10^{-3} - 10 \times 10^{-3})S^{-1}$in the work of Lu [20] in 40 kg steel heats by fitting the total calcium pickup to the enhanced dissolution model. According to the model, the total pickup rate is limited by availability of calcium, even though the recovery

is much less than 100%. The total calcium content increases linearly with time because the injection rate is constant. The same procedure is used here, yielding $3.7 \times 10^{-4}\ S^{-1}$. The calcium injection rate was much higher in the industrial case, but the ladle size was even greater in scale resulting in an overall smaller value. The authors are carrying out further investigations using industrial heats to understand how $k_{Ca,L} \times A_{B,L}$ changes with injection conditions.

4.4 Discussion

These model results present a remarkably self-consistent explanation for the observed behavior in the full-scale ladle treatment for the dissolved species and the evolution of the inclusion composition. The most important aspect to appreciate is that there are a huge number of inclusions in the steel, so that if reactions with the inclusions are possible, then the bulk composition will respond immediately to the conditions. Thus, when aluminum is added to the steel, the oxygen content will quickly reach a low equilibrium value with alumina inclusions. A low oxygen content in the steel also permits reduction of CaO in the slag at the slag-metal interface. The dissolved Ca reacts very quickly with alumina, resulting in some alumina transformation before Ca injection. There is very close-coupling between the slag and inclusions under these conditions. Once the Ca injection starts, there is a much faster supply of Ca resulting faster transformation. Thus, supply of Ca is rate-controlling for the inclusions transformations; diffusion in the inclusions is much faster. The model also provides a quantitative explanation for the timing and extent of the aluminate transformation, along with the CaS formation. The agreement of the model with the industrial data may be considered all the more remarkable when one considers that the

only parameter fitted to the current data, was the $k_{Ca,L} \times A_{B,L}$ for calcium in the bubble plume.

The previous model of transport for the inclusions [12] that was used in the present model showed that diffusion in the liquid boundary layer and in the shrinking core layers was fast, and that the reactions were complete in a matter of seconds for a fixed bulk calcium content in the steel. Thus, the transformation is controlled by calcium availability, either from injection or the slag. Since those steps are so fast, they could be eliminated in the model as long as the proper boundary conditions for Ca, O and Al are maintained at the inclusion interface.

There are some discrepancies between the model and the data (such as the dissolved Si and Al during injection) which could have been resolved by adjusting parameters, but that was not the objective of this work. The plant data presented in this paper represents the first heat that was studied using this model and more work is required to understand some of the details. In particular, the calcium injection provides strong stirring which should enhance the mass transfer rate, but it may also cause splashing and reduce the area of slag in contact with steel. These phenomena could result in reoxidation of steel.

As mentioned above and in a previous publication [12] the rate of supply of calcium to the melt is the rate controlling step for alumina transformation. It was argued [12] that the instantaneous Ca content in the melt is the balance point between supply and consumption of Ca. During the strong stirring before the Ca injection the rate of Ca supply via reduction of the slag was approximately 3.2×10^{-4} kg/s, which lead to an instantaneous Ca content

of about 0.003 ppm. During the injection the Ca supply rate was 2.1×10^{-2} kg/s, so the Ca content rose to approximately 0.1 ppm. Once the calcium aluminate inclusions reach saturation the rate of calcium consumption decreases towards the end of injection and after all the oxygen is consumed the dissolved Ca increases.

As explained in a previous publication [12], the finding in the previous paragraph explains the fact that previous workers fitted various dissolved Ca contents to explain their results [10,16]. Lu et al. [7] were able to explain it rationally on the basis of the attained activities of sulphides, oxides and dissolved sulphur and oxygen.

It should be noted that sulfide and oxide inclusions compete for the available calcium. First, as explained by the enhanced dissolution model, the diffusing Ca will react with S and O in the steel and the dissolved Ca can react with alumina inclusions for modification. So, the more S and O in the steel, the more CaO and CaS inclusions form at the reaction plane and less Ca is available for alumina inclusions which can delay modification process. This finding explains the fundamental difficulty in making free-machining steel by adding sulphur to calcium-treated steel; any free calcium will quickly react to make solid CaS promoting nozzle clogging during casting.

Assuming that CaS inclusions are of uniform diameter, the number of CaS inclusions produced at the reaction plane is calculated using the first term in Eq (4-22). Table 4-5 shows that average size of sulphide inclusions is about 1 μm. Figure 4-10 shows the change of number of CaS inclusions during injection. There is good agreement between calculated result and plant data except the discrepancy at the end.

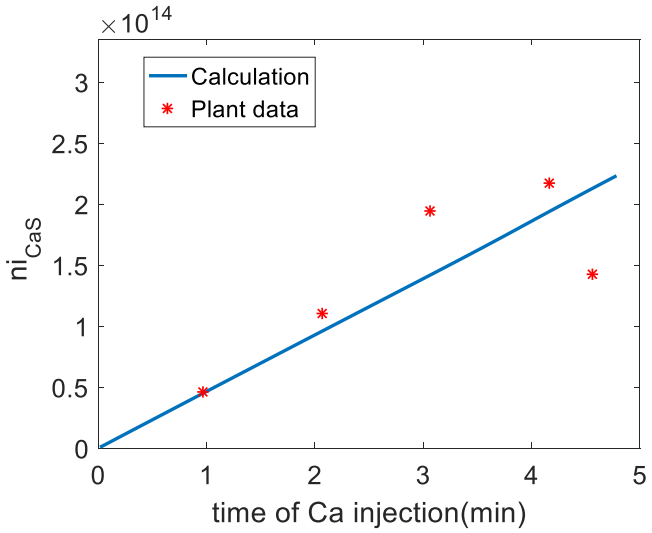

Figure 4-10. Change of number of CaS inclusions. Time zero is the start of Ca injection, 38.3 minutes in Figure 4-7 (a)-(d).

After steelmaking, Low Carbon Aluminum Killed (LCAK) steels are deoxidized (killed) with relatively large aluminum additions (0.01 – 0.06%Al). As mentioned earlier, the reaction between dissolved aluminum and oxygen is very rapid, resulting in dissolved oxygen contents in the range of 1 – 5 ppm and total oxygen contents in the range of 10 to 50 ppm in the form of alumina. In most results, as in the present work, the alumina inclusions are in the 1 – 10 micron range. The larger ones are eliminated rapidly by flotation and/or agglomeration. The smaller ones are below the limit of detection, but found to represent 10 to 20% of the total (see Figure 6). The present work provides a reasonable model for 80% of these inclusions. It appears that other phenomena such as inclusion agglomeration, flotation and reoxidation do not have a significant effect. In a study by Kang et al. [42] samples were taken at different stages of ladle treatment and investigated by SEM. Also, inclusions were examined using a Confocal Scanning Laser Microscopy (CSLM) and found that alumina particles attracted each other and

agglomerated. However, spinel inclusions and solid calcium aluminate inclusions did not show any sign of attraction or agglomeration. The other interesting finding of the present work is that the primary oxide and sulphide inclusions are also in the range of 1 to 10 microns, possibly for the same reasons. Further work is underway to gather more evidence.

Because of the similarity of worldwide operations for low carbon aluminum killed (LCAK) steel it is possible that the present model could be used very widely with only fine tuning to local conditions. In a parallel study, also at ArcelorMittal Dofasco, Sun et al. [43] found that the difference between the total aluminum content and soluble aluminum in the steel was a good indicator of how much calcium was required for each heat. These analyses are rapid enough for process control. The current model also runs fast enough for process control as well. This avenue is under development in the McMaster Steel Research Centre with its industrial partners.

4.5 Conclusions

The aim of this work was to develop a kinetic model for the transformation of inclusions during calcium treatment and implementation of the steel-inclusion kinetic model to a previously developed kinetic model for the slag-steel reactions in the Ladle Metallurgy Furnace. Combining a calcium dissolution model with a shrinking core model for inclusion transformation and a slag-steel reaction model results in a fundamental kinetic model which allows determination of the change of composition of the steel, slag and evolution of inclusions during Ca treatment. The coupled slag-steel –inclusion model shows that

1. Modification of alumina inclusions are controlled by the rate of supply of calcium because the inclusions consume the injected calcium so fast that the dissolved calcium reaches a fairly constant low value approximately 0.1-0.2 ppm during calcium treatment. This is highlighted by huge difference between dissolved calcium content of the steel compared to Ca reduced by the slag.

2. The steel slag reactions is increased due to the calcium injection contribution to stirring in addition to that of argon.

3. Calcium transferred from the slag especially during high stirring period can be sufficient to partially modify alumina inclusions to calcium aluminate.

4. By only considering CaS inclusions form at the injection plume, the model offers excellent prediction of sulfides formation suggesting that all CaS is formed at the plume.

4.6 Acknowledgement

The Authors are grateful for the support of the members of the McMaster Steel Research Centre, the Natural Sciences and Engineering Research Council of Canada. The strong support and collaboration with ArcelorMittal Dofasco in planning and executing the work was vital.

4.7 Appendix: Volumetric size distributions of inclusions

An automated inclusion analysis SEM technique, ASPEX, was used to obtain planar distribution of inclusion on the polished section. Particle sizes are divided into number of

size groups after they are measured on plane sections. The number and size of particles in the plane section is determined, but to obtain the size distribution on a volume basis, the analysis of the obtained data is required. It is assumed that the particles are spherical so that equivalent sphere diameters or equivalent circle diameters can be considered. ASPEX measures equivalent circle diameters of inclusions which can be presented in a particle size distribution histogram.

The number of circles per unit area N_A as a result of N_V spheres per unit volume of diameter D is

$$N_A = D.N_V \qquad \textbf{(4-A1)}$$

So, larger spheres are more likely to be intersected by the plane of the polished section. Moreover, a sphere may be sectioned anywhere in its diameter. But, only largest spheres can lead to largest circle diameter at the sectioning surface. Therefore, the probability of spotting circles in this largest size group could be calculated and the residual probability distributed to the smaller size groups of circles. Then, circles from the next smallest size group of spheres are calculated and so on. Using this approach, the size distribution of spheres in the volume could be derived from the measurement of the size distributions of circles on the sectioning plane. The details of the method can be found in [36]. Schwartz [43] and Saltykov [44] developed a matrix of coefficients $(\alpha(i,j))$ for the number of circles in size group (i) arising from spheres in size group (j) using probability distributions for sectioning randomly distributed spheres of sizes in k equal size groups. The number of spheres per unit volume in size group j from the numbers of circles in size groups i is:

$$N_V(j) = \frac{1}{\Delta}\{\alpha(j,j)\ N_A(j) + \alpha(j,j+1)\ N_A(J+1) + \cdots + \alpha(j,k)\ N_A(k)\} \qquad \textbf{(4-A2)}$$

where $j = 1\ to\ k$, Δ is the size interval used in the histograms and k is the number of size groups.

4.8 References

[1] K.G. Rackers and B.G. Thomas: in 78th Steelmak. Conf. Proc., Iron and Steel Society, Nashville, USA, 1995, pp. 723–34.

[2] S. W. Robinson, I. W. Martin, and F. B. Pickering: Met. Technol., 1979, vol. 6, pp. 157–69.

[3] L. Zhang and B. G. Thomas: in XXIV Natl. Steelmak. Symp., Morelia, Mich, Mexico, 2003, pp. 138–83.

[4] E.T. Turkdogan: Fundamentals of Steelmaking, 1st Ed., Maney, London, 2010, pp. 285–90.

[5] A. Ghosh: Secondary Steelmaking: Principles and Applications, 1st Ed., CRC Press, London, 2001, pp. 203–17.

[6] S. Basak, R. Kumar Dhal, and G. G. Roy: Ironmak. Steelmak., 2010, vol. 37, pp. 161–68.

[7] D. Lu, G. A. Irons, and W. Lu: Ironmak. Steelmak., 1994, vol. 21, pp. 362–72.

[8] Y. Higuchi, M. Numata, Sh. Fukagawa, and K. Shinme: ISIJ Int., 1996, vol. 36, pp. 151–54.

[9] Y. Ito, M. Suda, Y. Kato, H. Nakato, and K. Sorimachi: ISIJ Int., 1996, vol. 36, pp. S148–50.

[10] H. Visser, R. Boom, and M. Biglari: ATS Int. Steelmak. Conf., 2008, pp. 172–80.

[11] Z. Han, L. Liua, M. Lind, and L. Holappa: Acta Metall. Sin., 2006, vol. 19, pp. 1–8.

[12] Y. Tabatabaei, K. S. Coley, G. A. Irons, and S. Stanley: Metall. Mater. Trans. B, 2017, vol. 46, pp. 375–87.

[13] K. J. Graham and G. A. Irons: in Int. Symp. Highly Innov. Nov. Oper. "Future Steelmak. Metall., 2010, pp. 65–74.

[14] A. Galindo, G. A. Irons, K. S. Coley, and S. Sun: in Challenges Transform. Solut. to Sustain. Steelmak. Cast. Environ. Metall. Innov. CTSSC-EMI Symp. 2015, Tokyo, Japan, 2015.

[15] A. Harada, N. Maruoka, H. Shibata, and Sh. Kitamura: ISIJ Int., 2013, vol. 53, pp. 2110–17.

[16] A. Harada, N. Maruoka, H. Shibata, M. Zeze, and N. Asahara: ISIJ Int., 2014, vol. 54, pp. 2569–77.

[17] D. Kumar and P. C. Pistorius: in Proc. 10th Int. Conf. Molten Slags, Fluxes Salts, John Wiley & Sons, Hoboken, NJ, USA, 2016, pp. 145–53.

[18] J. H. Shin, Y. Chung, and J. H. Park: Metall. Mater. Trans. B, 2017, vol. 48, pp. 46–59.

[19] K. Graham: PhD thesis, McMaster University, 2008, pp. 172–81.

[20] D-Z. Lu: PhD thesis, McMaster University, 1992, pp. 206–29.

[21] O. Levenspiel: Chemical Reaction Engineering, 2nd Ed., John Wiley & Sons, New York, 1999, pp. 570–577.

[22] N. Verma, P. C. Pistorius, R.J. Fruehan, M.S. Potter, H.G. Oltmann, and E.B. Pretorius: Metall. Mater. Trans. B, 2012, vol. 43, pp. 830–40.

[23] N. Verma, P. C. Pistorius, R. J. Fruehan, and R. J. Lee: in Mater. Sci. Technol. Conf. Exhib. 2009, MS T'09, Pittsburgh, PA, 2009, pp. 1042–53.

[24] S. F. Yang, J. Sh. Li, Z. F. Wang, J. Li, and L. Lin: Int. J. Miner. Metall. Mater., 2011, vol. 18, pp. 18–23.

[25] J. Szekely and N. J. Themelis: Rate Phenomena in Process Metallurgy, 1st Ed., Wiley-Interscience, New York, 1971.

[26] F. Oeters: Metallurgy of Steelmaking, 1st Ed., Düsseldorf: Verlag Stahleisen, 1994.

[27] C.W. Bale, P. Chartrand, S.A. Degterov, G. Eriksson, and K. Hack: Calphad, 2002, vol. 26, pp. 189–228.

[28] C.W. Bale, E. Bélisle, P. Chartrand, S. A. Decterov, G. Eriksson, K. Hack, I.-H. Jung, Y.-B. Kang, J. Melançon, A.D. Pelton, C. Robelin, and S. Petersen: Calphad, 2009, vol. 33, pp. 295–311.

[29] M. Hino and K. Ito: Thermodynamic Data for Steelmaking, 1st Ed., Tohoku University Press, Tokyo, 2010, pp. 16–17.

[30] H. Fujiwara, A. Hattori, and E. Ichise: Tetsu-To-Hagane/Journal Iron Steel Inst. Japan, 1999, vol. 85, pp. 201–7.

[31] Q. Han, X. Zhang, D. Chen, and P. Wang: Metall. Mater. Trans. B, 1988, vol. 19B, pp. 617–22.

[32] D. G. C. Robertson, B. Deo, and S. Ohguchi: Ironmak. Steelmak., 1984, vol. 11, pp. 41–55.

[33] M. L. Kapoor and M. G. Frohberg: in Chem. Metall. Iron Steel, 1971, pp. 17–22.

[34] H. Gaye and J. Welfringer: in Second Int. Symp. Metall. Slags Fluxes, 1984, pp. 357–75.

[35] F. Schamber: Introduction to Automated Particle Analysis by Focused Electron Beam, 2009.

[36] R. Higginson and C.M. Sellars: Worked Examples in Quantitative Metallography, 1st Ed., Maney, London, 2003, pp. 68–76.

[37] P. Kaushik, H. Pielet, and H. Yin: Iron Steel Technol., 2009, vol. 6, pp. 82–99.

[38] N. Verma, P. C. Pistorius, R.J Fruehan, M. Potter, M. Lind, and S. Story: Metall. Mater. Trans. B, 2011, vol. 42, pp. 711–19.

[39] M. Nuspl, W. Wegscheider, J. Angeli, W. Posch, and M. Mayr: Anal. Bioanal. Chem., 2004, vol. 379, pp. 640–45.

[40] B. G. Bartosiaki, J. A. M. Pereira, W. V. Bielefeldt, and A. C. F. Vilela: J. Mater. Res. Technol., 2015, vol. 4, pp. 235–40.

[41] J. H. Shin and J. H. Park: Metall. Mater. Trans. B, 2017, vol. 48, pp. 2820–25.

[42] Y. Kang, B. Sahebkar, P. R. Scheller, K. Morita, and D. Sichen: *Metall. Mater. Trans. B Process Metall. Mater. Process. Sci.*, 2011, vol. 42, pp. 522–34.

[43] S. Sun, S. Waterfall, N. Strobl, D. Liao, and D. Holdridge: in *8th Int. Symp. High-Temperature Metall. Process.*, 2017, pp. 347–57.

[44] H.A. Schwartz: *Met. Alloy.*, 1934, vol. 5, pp. 139–40.

Chapter 5

A kinetic Model for Modification of $MgAl_2O_4$ Spinel Inclusions During Calcium Treatment in the Ladle Furnace

In Chapter 5 the model was proposed by Kenneth S. Coley. Developing detail of the model and coding in Matlab was carried out by me. Dr. Kenneth S. Coley and Dr. Gordon A. Irons provided very helpful discussion during model development. The first draft was prepared by me and reviewed to the final version by Dr. Kenneth S.Coley, Dr. Gordon A. Irons and Dr. Stanley Sun who also provided useful insights into industrial practice and interpretation of industrial data. This manuscript has been accepted for publication in *Metallurgical and Materials Transactions B(2018)* https://doi.org/*10.1007/s11663-018-1354-0.*

Abstract

A common approach in the processing of Al-killed steels is the modification of alumina inclusions by calcium treatment. A model for this process has already been developed by the authors and validated with plant data. Often, magnesium aluminate spinels are also present and transformed to magnesium calcium aluminate inclusions during calcium treatment. In the present work, a fundamental kinetic model is proposed for modification of spinel inclusions considering mass transfer of solute through the boundary layer to the inclusion and diffusion within the product layer. Sensitivity analysis has been carried out

to determine rate controlling step for spinel modification. The rate of transformation of spinel inclusions is compared with that of alumina inclusions with the authors' prior model.

5.1 Introduction

Aluminum deoxidized steel forms solid alumina inclusions in the ladle furnace. These solid inclusions are known to create challenges during casting. Various practices are used for elimination of inclusions, such as transporting them to slag phase by argon stirring [1]. However, some alumina inclusions remain in the steel melt. It is well known that these alumina inclusions can transform to magnesium aluminate spinel inclusions $MgAl_2O_4$ by reaction of alumina with dissolved magnesium from top slag or ladle refractories or from magnesium contamination of aluminum or ferroalloy additions [2,3]. Magnesium aluminate spinel inclusions have a tendency to adhere to the inner wall of the submerged entry nozzle which negatively affects productivity of the process [4]. They also adversely affect properties of the final steel [5].

There is some disagreement in the literature on effectiveness of spinel modification by calcium treatment. While earlier work proposed that the modification of spinel by calcium would be less effective than pure alumina [6], more recent work indicates that, under reducing conditions, spinel modification by Ca treatment is easier than for alumina inclusions [7,8].

Kang et al. [9] studied the formation of liquid calcium aluminate inclusions from $MgAl_2O_4$ spinel in ladle treatment by thermodynamic calculations and laboratory experiments. Using a stability diagram they showed that when the spinel phase was in

contact with the liquid steel containing calcium it would become thermodynamically unstable and liquid magnesium calcium aluminate forms. It was also found that an extremely low activity of calcium, less than 2 ppm, is sufficient for formation of liquid oxide although, concentration gradients of Ca were observed in the formed liquid phase [9].

Pretorius et al. [8] by evaluation of metal samples from industrial heats, proposed that effective modification of spinel inclusions is possible and the mechanism is the preferential reduction of the MgO in the spinel to dissolved Mg in the steel followed by reaction of the residual Al_2O_3 from the spinel and resultant CaO to form completely liquid inclusions. Verma et al. [7] also showed that addition of calcium is effective in spinel modification. Pretorius et al. [8] further suggested that calcium modification of spinel inclusions is somewhat easier for low carbon aluminum killed (LCAK) steels with very low oxygen content. However, Yang et al. [10] from thermodynamic analysis of industrial data, have concluded that spinel inclusions can be modified into liquid inclusions only if the dissolved calcium content in the steel is at least 1 ppm. They developed a kinetic model to predict the time for modification of $MgAl_2O_4$ inclusions and concluded that diffusion of Mg in the inclusions is the rate-controlling step. However, the values they used for diffusivity of Mg and Ca in the $MgO-Al_2O_3-CaO$ product layer are very different $D_{Ca} = 2.5 \times 10^{-9}\frac{m^2}{s}$ and $D_{Mg} = 3.2 \times 10^{-13}\frac{m^2}{s}$ since a solid product layer was assumed. The present authors believe that the diffusivities of these species are not very different in the product layer as it is an ionic liquid solution and the diffusivities should be very close as theses ions

have very similar radii (72 pm for $Mg^{2+}$and 100 pm for Ca^{2+} [11]). In addition, the mechanism will require countercurrent diffusion of these species and they will both contribute to the effective chemical diffusivity.

Although, studies to understand the mechanism of calcium modification of alumina inclusions dates back to the 1990s [12-14], it is just in the last decade [7,9] that some effort has been put forward to understand mechanism of modification of magnesium aluminate spinel inclusions. While these studies have thrown some light on the modification of magnesium aluminate spinel, the only investigation of the kinetics of transformation from magnesium-aluminate spinel to magnesium calcium aluminate, is that discussed above [10].

The aim of the current work is to develop a fundamental quantitative kinetic model which considers all possible kinetic steps involved in the process and investigates the importance of each step through sensitivity analysis, thereby determining the rate controlling step.

This work is part of a larger effort to develop comprehensive models of slag-steel-inclusion interaction during ladle treatment. A prior model was developed for the modification of a single alumina inclusion by dissolved calcium in the steel [15] using the same approach as the present work: it was assumed that the reactions at interfaces reached local equilibrium and were transport controlled. This prior model was coupled with another model including sources of calcium to the steel (from injected calcium wire and from reduction from the slag) [16]. This latter model was based on real process conditions

which considered the changes in slag, metal and inclusion composition with time before and during calcium injection. It successfully modelled the behavior of the entire system. The current work describes modification of a single $MgAl_2O_4$ spinel inclusion by dissolved calcium, in an analogous way to that for alumina [15]. The results clarify the controlling transport steps at the surface and within the inclusion. The model is validated by coupling with the slag-steel model and comparing with plant data. All the findings with the current model are built on established knowledge of the $CaO - Al_2O_3 - MgO$ system and the assumptions represent conditions relevant to ladle metallurgy. A future publication is currently in preparation in which results from the combined model in different conditions will be compared with plant data validating both the combined model and the current model.

5.2 Mathematical model

5.2.1 Outline of the model system

As discussed above, Al_2O_3 inclusions are generated after deoxidation by Al that will react with dissolved Mg existing in the melt to produce spinel. Thus, the inclusion change from Al_2O_3 to $MgAl_2O_4$. During calcium treatment in the ladle, spinel inclusions will transform to magnesium calcium aluminate. The objective of this model is to describe the mass transport steps to and within spinel inclusions during calcium treatment of LCAK steels. To describe the transformation of spinel inclusions into magnesium calcium aluminate, an unreacted shrinking core model [17] is used in which the reaction starts at the outer surface of the $MgAl_2O_4$ particle and the magnesium calcium aluminate product layer boundary moves into the solid particle.

The assumptions employed for sensitivity analysis of the current model are as follows:

- At the start of the process a very thin layer of liquid $MgO-Al_2O_3-CaO$ is assumed to exist at the surface of spinel inclusions.
- Chemical reactions are fast relative to mass transport processes due to the high temperature, so local equilibrium is attained at all interfaces.
- The bulk steel concentrations of Ca, Mg, Al and O are fixed to simplify the discussion of the model.
- Mass transfer within the liquid $MgO-Al_2O_3-CaO$ layer is mathematically described by quasi steady-state counter molecular diffusion of CaO, Al_2O_3 and MgO through the product layers. While this is a legitimate phenomenological treatment, the authors recognize that the mechanism and actual diffusing species will be more complex.
- Diffusion in the spinel is assumed to be sufficiently fast that this phase will not be rate controlling. This assumption is based on previous work in the authors' laboratory which showed that spinel formation from alumina is controlled by mass transport in the steel [42]. The consequence of this assumption is that any concertation gradient in the spinel will be negligible.

The model considers the following steps in modification:

1/ Transport of Ca, Mg, Al and O though the boundary layer between the metal and steel.

2/ Reaction of the relevant species at the interface between the steel and the liquid aluminate product layer

3/ Transport of CaO, MgO and Al_2O_3 through the liquid product layer

4/ Reaction between the liquid product later and the spinel

5/ transport within the spinel

The model does not constrain the direction of transport which is set by the composition gradients formed during the process. Steps 2 and 4 can be considered fast because of the high temperature and therefore the reactions between the relevant species are considered to be in equilibrium across these interfaces. Transport in the spinel, step 5, has been previously shown to be fast relative to the other steps and therefore concentration gradients in the spinel may be assumed to be negligible.

The transport processes and concentration gradients around the inclusion are modelled in detail and shown schematically in Figure 5-1.

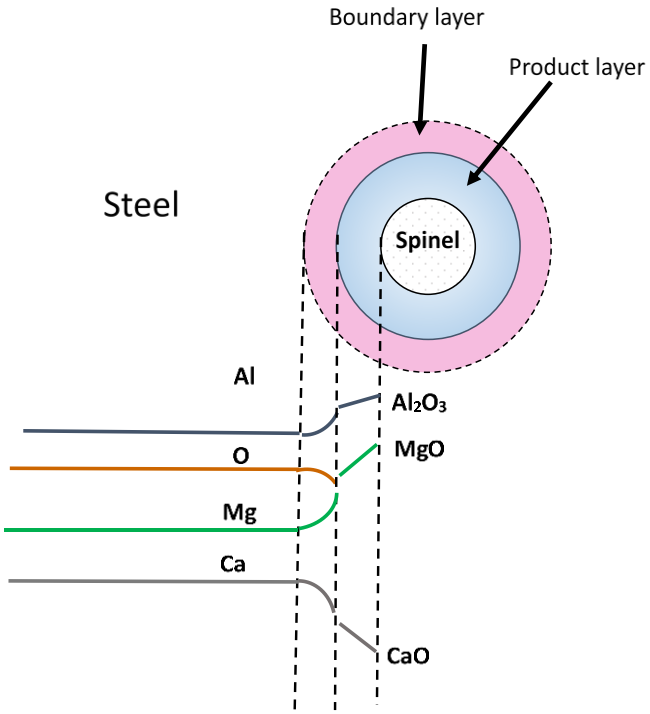

Figure 5-1. Schematic diagram of concentration gradient of species around and within the spinel inclusion

5.2.1.1 Interfacial concentrations

To calculate the rate of modification of a spinel inclusion, it is necessary to know the concentrations at the steel-inclusion interface which are calculated by coupling the mass balance at the steel-inclusion interface with local thermodynamic equilibrium. To develop the model, the $CaO - Al_2O_3 - MgO$ phase diagram is used to examine the thermodynamic equilibria. The diagram shown in Figure 5-2 was created using FactSage 7.0 (FToxide database) and agrees well with the literature [19].

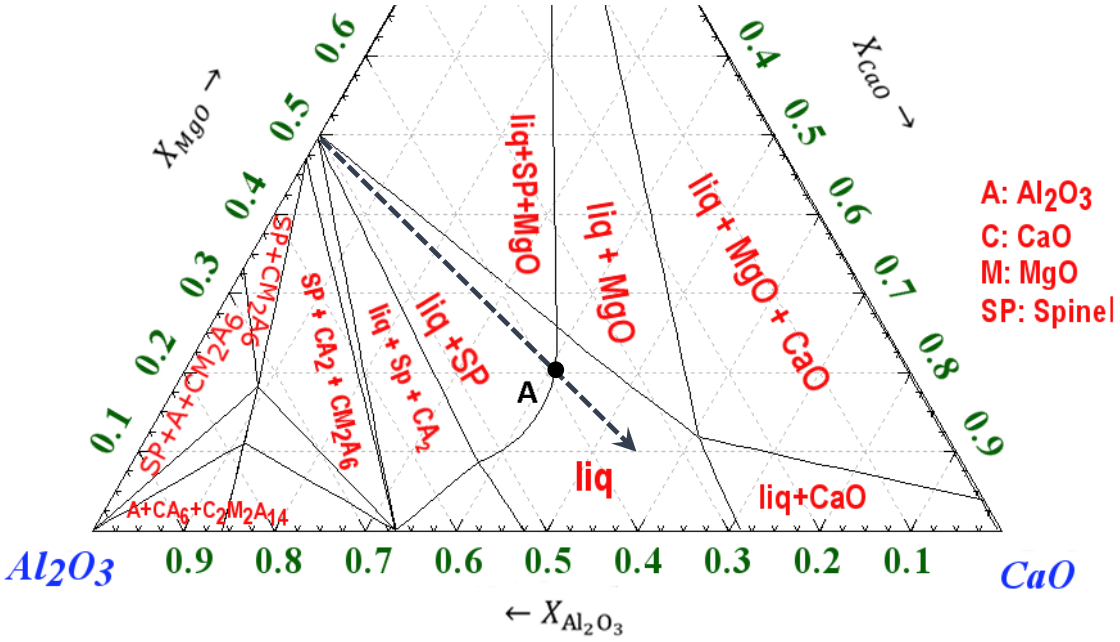

Figure 5-2. Section of isothermal ternary diagram of $CaO - Al_2O_3 - MgO$ at 1600 ºC (mole fraction)

It is assumed that the spinel inclusion follows the trajectory illustrated in Figure 5-2 to reach the liquid area. This path is observed in AM Dofasco plant data as delineated in Figure 5-3 where the composition of inclusions before and during Ca treatment for a LCAK heat is shown. This heat was stopped at different stages of Ca injection and samples were taken. Inclusions were analyzed using automated SEM (ASPEX) and the labels "calcium aluminate" and "spinel" are based on classification of inclusions by the ASPEX system; though some of inclusions in one class overlap with some of inclusions in the other class. This path for modification of stoichiometric spinels was also observed in microanalysis of industrial samples by Pretorius et al. [8]. Also in their experiments, Verma et al. [7] observed that MgO-rich and MgO-poor regions co-existed in partially modified spinel Inclusions which agrees with the delineated trajectory. It should also be noted that even before injection inclusions contain some calcium which can come from either alloying

elements or reduction of CaO in the slag by aluminum in the steel during high stirring periods as discussed in recent work by authors [16].

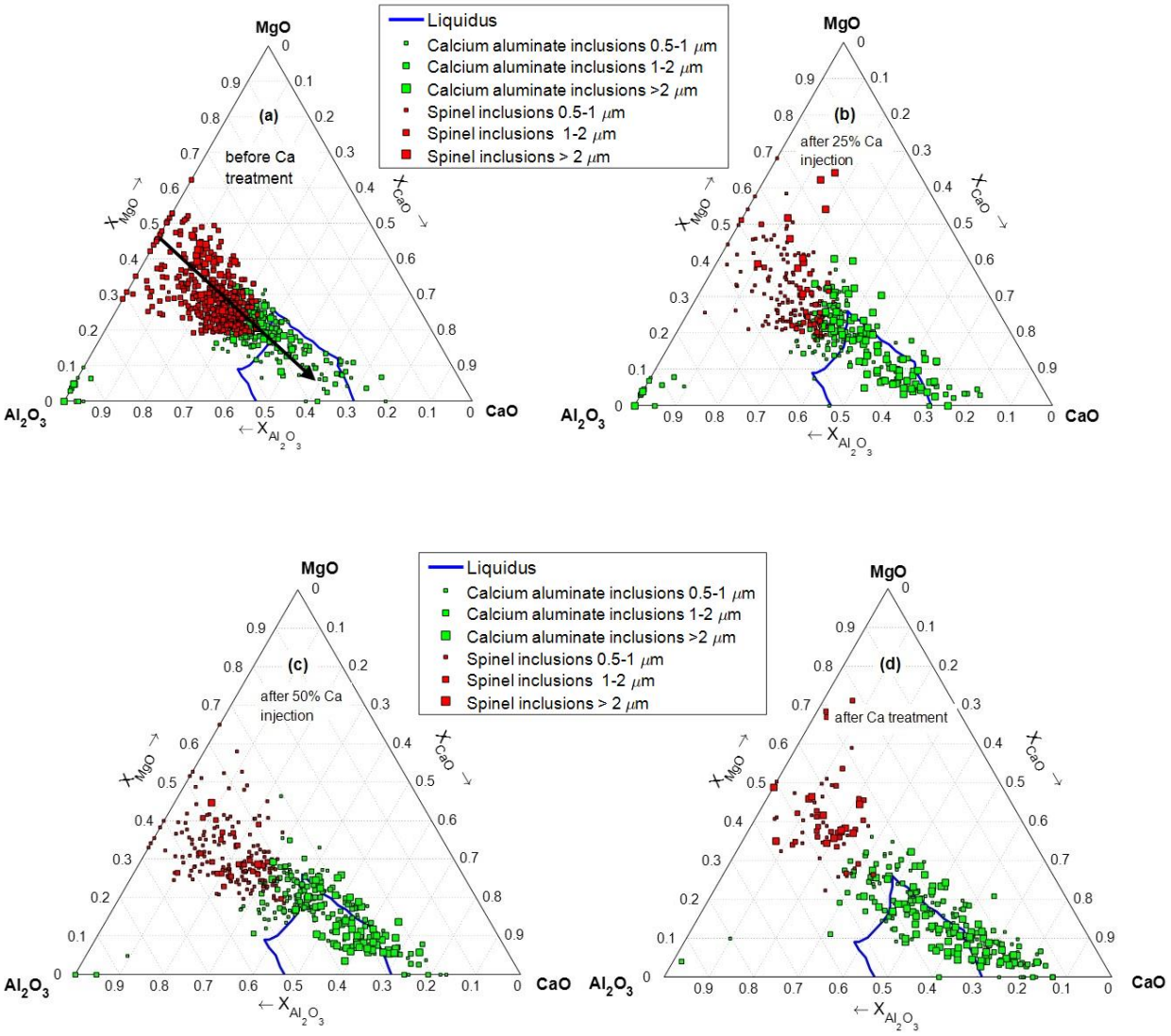

Figure 5-3. Distribution of oxide inclusions during Ca treatment of LKAC steel in the LMF. Samples were taken (a) before Ca injection (b) 25% of C a injection (c) 50% of Ca injection and (d) after Ca injection. The arrow in (a) shows the proposed path for the model.

Therefore the liquid magnesium calcium aluminate in equilibrium with the spinel will have the composition of point **A** $((MgO)_{1-\alpha-\beta}(CaO)_{\beta}(Al_2O_3)_{\alpha})$ shown in Figure 5-2.

Hence, the reaction occurring at the liquid product layer-spinel interface follows Equation (5-1) with stoichiometry defined by point A (α and β are determined to be 0.4 and 0.4, respectively according to Figure 5-3).

$$CaO + \frac{\beta}{\alpha}(MgAl_2O_4) = \frac{1}{\alpha}((MgO)_{1-\alpha-\beta}(CaO)_{\alpha}(Al_2O_3)_{\beta}) + \frac{2\beta+\alpha-1}{\alpha}MgO \qquad \textbf{(5-1)}$$

The mass balance for calcium, aluminum and magnesium at the steel inclusion interface leads to the following equations:

$$N_{Ca} = N_{CaO} \qquad \textbf{(5-2)}$$

$$N_{Al} = 2N_{Al_2O_3} \qquad \textbf{(5-3)}$$

$$N_{Mg} = N_{MgO} \qquad \textbf{(5-4)}$$

$$N_{MgO} = N_{Al_2O_3} - (\frac{2\beta+\alpha-1}{\alpha})N_{CaO} \qquad \textbf{(5-5)}$$

The equations (5-2)-(5-4) come from elemental mass balance for Ca, Al and Mg, respectively. Equation (5-5) is based on the reaction of stoichiometric spinel and CaO to produce liquid magnesium calcium aluminate according to Eq (5-1).

N_i, the mass transfer rate of species i through the boundary layer from the bulk steel to the surface of a spherical particle is described by Eq (5-6):

$$N_i = 4\pi r^2 . k_{m,i} \mathrm{C_{v_m}} (X_i^b - X_i^*) \qquad \textbf{(5-6)}$$

Where $k_{m,i}$ is the mass transfer coefficient across the boundary layer, r is the particle radius, $\mathrm{C_{v_m}}$ is the molar density of the steel, X_i^b is the mole fraction of species i in the bulk steel and X_i^* is the mole fraction of species i at the interface.

It is well established that spherical particles smaller than 14 μm have little relative motion in steel, so the Sherwood number takes on its limiting value of 2 for radial diffusion [20,21]. The Sherwood number is:

$$Sh = \frac{k_{m,i}d}{D_i} \qquad \textbf{(5-7)}$$

Where Sh is the Sherwood number, d is the particle diameter and D_i is the diffusion coefficient of the species i in the steel.

Mass transfer within the product layer is assumed to occur by quasi steady-state, counter molecular diffusion of CaO, Al_2O_3 and MgO through the liquid magnesium calcium aluminate product layer. The mass transfer rates of CaO, Al_2O_3 and MgO are driven by the concentration gradient. Molar flow of species i in the liquid product layer is described by the following equation [20]:

$$N_i = \left(\frac{4\pi r_{ex} r_{in}}{r_{ex} - r_{in}}\right)(\mathrm{C_v} D_i)(X_i^{ex} - X_i^{in}) \qquad \textbf{(5-8)}$$

Where r_{ex} and r_{in} are exterior and interior radius of the product layer, respectively. $\mathrm{C_v}$ is the molar density of the liquid layer, D_i is the diffusivity of species i and X_i^{ex} and X_i^{in} are mole fraction of species i at exterior and interior radius respectively.

Thermodynamic equilibrium at the inclusion-steel interface is obtained considering simultaneous deoxidation equilibria of Ca, Al and Mg in steel with the Al_2O_3, CaO and MgO components in the magnesium calcium aluminate liquid phase according to the following reactions.

[Ca]+[O]=(CaO)$_{inc}$

$$K_{CaO} = \frac{a_{CaO}}{\left(\frac{f_{Ca}X^*_{Ca}n_T MW_{Ca}100}{St_{mass}}\right)\left(\frac{f_O X^*_O n_T MW_O 100}{St_{mass}}\right)} \quad \textbf{(5-9)}$$

2[Al]+3[O]=(Al$_2$O$_3$)$_{inc}$

$$K_{Al_2O_3} = \frac{a_{Al_2O_3}}{\left(\frac{f_{Al}X^*_{Al}n_T MW_{Al}100}{St_{mass}}\right)^2\left(\frac{f_O X^*_O n_T MW_O 100}{St_{mass}}\right)^3} \quad \textbf{(5-10)}$$

[Mg]+[O]=(MgO)$_{inc}$

$$K_{MgO} = \frac{a_{MgO}}{\left(\frac{f_{Mg}X^*_{MG}n_T MW_{Mg}100}{St_{mass}}\right)\left(\frac{f_O X^*_O n_T MW_O 100}{St_{mass}}\right)} \quad \textbf{(5-11)}$$

Where f_i represents activity coefficient of species i with respect to 1 wt. % standard state, MW_i is the molar weight, n_T is total number of moles of steel and St_{Mass} is total mass of the steel.

$a_{Al_2O_3}$, a_{CaO} and a_{MgO} in the $Al_2O_3 - CaO - MgO$ system are obtained using the cell model formalism [22,23] as implemented by Graham and Irons [24]. The values used for oxidation equilibrium constants are $K_{CaO} = 1.2 \times 10^9$ [25], $K_{Al_2O_3} = 3.16 \times 10^{12}$[26] and $K_{MgO} = 1.62 \times 10^7$ [27]. The non-linear system of equations (5-2)-(5-4) and (5-9)-(5-11) is solved numerically for the unknowns $X^*_{Ca}, X^*_{Al}, X^*_{Mg}, X^*_O, X^*_{CaO}, X^*_{Al_2O_3}, X^*_{MgO}$ using the Newton-Raphson method [28] thereby allowing the calculation of the interfacial mass transfer rates.

5.2.1.2 Inclusion evolution

Modification of spinel inclusions according to the phase diagram is shown in Figure 5-4.

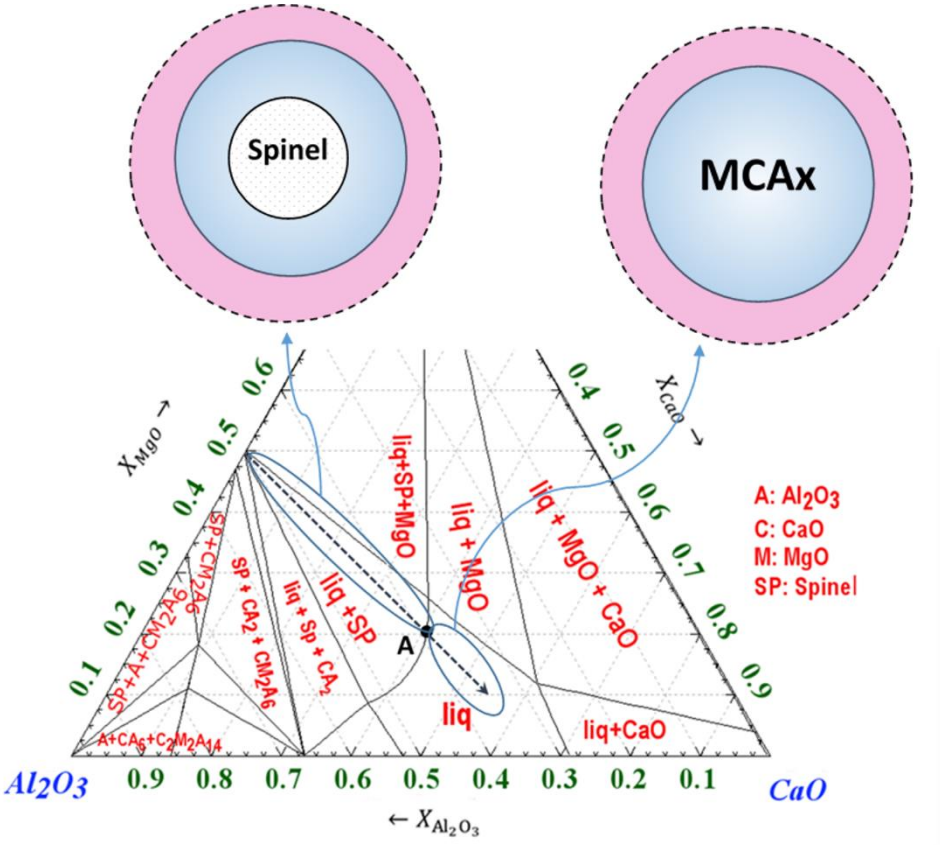

Figure 5-4. Modification of spinel inclusion and corresponding phases

First a layer of magnesium calcium aluminate (MCA) forms on the surface of the spinel core. The modification continues with shrinkage of spinel core and growth of the product layer. At this stage, the composition of magnesium calcium aluminate produced is close to that in equilibrium with spinel (Point A in Figure 5-2). As the core is consumed, if calcium injection continues, the modification proceeds by increasing the mole fraction of CaO and reduction of MgO or Al_2O_3 in the magnesium calcium aluminate inclusion.

The change of the radius of the spinel core can be calculated by considering the relation between molar flux and volume:

$$\frac{dV}{dt} = \frac{dV}{dn} \times \frac{dn}{dt} \quad \textbf{(5-12)}$$

By substituting:

$$4\pi r^2 \frac{dr_{Spinel}}{dt} = \frac{MW_{spinel}}{\rho} \times N_{Spinel} \quad \textbf{(5-13)}$$

Where N_{Spinel} is number of moles of spinel leaving the inclusion core per unit time which is sum of the spinel reacting with CaO in addition to Al_2O_3 and MgO transferred through the product layer to dissolve in the steel in the form of Al and Mg. After substitution and rearrangement one can obtain:

$$4\pi r^2 \frac{dr_{spinel}}{dt} = \frac{MW_{spinel}}{\rho} \times (\frac{\beta}{\alpha} N_{Ca} + \frac{1}{2} N_{Al}) \quad \textbf{(5-14)}$$

N_{Ca} and N_{Al} are calculated using Eq (5-6). The inclusion composition is calculated from the calcium aluminate and alumina core diameters.

After the core is consumed, modification can continue by further dissolution of calcium in magnesium calcium aluminate inclusions and thereby increasing the CaO fraction. The only difference is that in calculating interfacial concentration, instead of Eq (5-5), oxygen mass balance can be employed. Then, change of composition can be calculated as follows:

$$X_{Al_2O_3} = \frac{n_{Al_2O_3}}{n_{Al_2O_3}+n_{CaO}+n_{MgO}}, X_{CaO} = \frac{n_{CaO}}{n_{Al_2O_3}+n_{CaO}+n_{MgO}} \text{and } X_{MgO} = 1 - X_{Al_2O_3} - X_{CaO} \quad \textbf{(5-15)}$$

Where

$$\frac{d_{n_{Al_2O_3}}}{dt} = \frac{1}{2} N_{Al}, \frac{d_{n_{CaO}}}{dt} = N_{Ca} \text{ and } \frac{d_{n_{MgO}}}{dt} = N_{Mg} \quad \textbf{(5-16)}$$

5.3 Results

5.3.1 Spinel transformation

The bulk concentrations of dissolved Ca, Al, Mg and O are boundary conditions for the model. For the sake of simplicity the concentrations of the dissolved species are assumed constant with time, but their range will be examined in the sensitivity analysis. In addition, in section 5.3.4, when the model is coupled with the slag/metal model these values will be allowed to float and will be controlled by the balance of kinetics. The values are chosen to reflect typical conditions for LCAK steel. Our previous work [16] showed that during injection, the Ca content remains at a low value in the range 0.1 - 0.3 ppm. The dissolved oxygen content is assumed to be close to equilibrium with the dissolved aluminum and pure alumina. The Mg content is in the range of equilibrium with the spinel and oxygen in the steel. An initial diameter for the spinel inclusion of 5 microns is assumed for all calculations. Diffusion coefficients and rate constants used for the calculations are summarized in Table 5-1.

Table 5-1. Summary of kinetic constants

Kinetic parameter	value	Ref
D_{CaO} , $D_{Al_2O_3}$, D_{MgO}	3.01×10^{-10} , 1.48×10^{-10}, 1×10^{-9} $m^2 s^{-1}$	[32,33]
D_{Ca} , D_{Al} , D_{Mg}, D_O	3×10^{-9} , 3.5×10^{-9}, 3×10^{-9}, 3.1×10^{-9} $m^2 s^{-1}$	[12,34]

The MATLAB^{TM} software was used to develop a computer code for solving the equations in this work. Newton-Raphson method [28] was employed for calculation of the interfacial mass transfer rates.

The results for spinel modification are reported as the change in spinel core diameter with time as shown in Figure 5-5(a), varying of average composition of whole inclusion (the liquid product layer and the solid core) with time in Figure 5-5(b), and the corresponding path through which inclusion modification occurs across the ternary diagram in Figure 5-5(c).

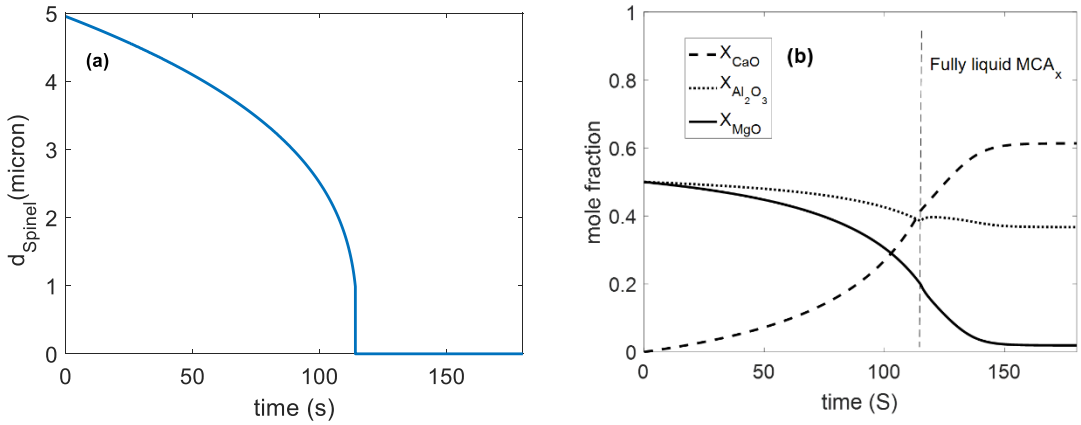

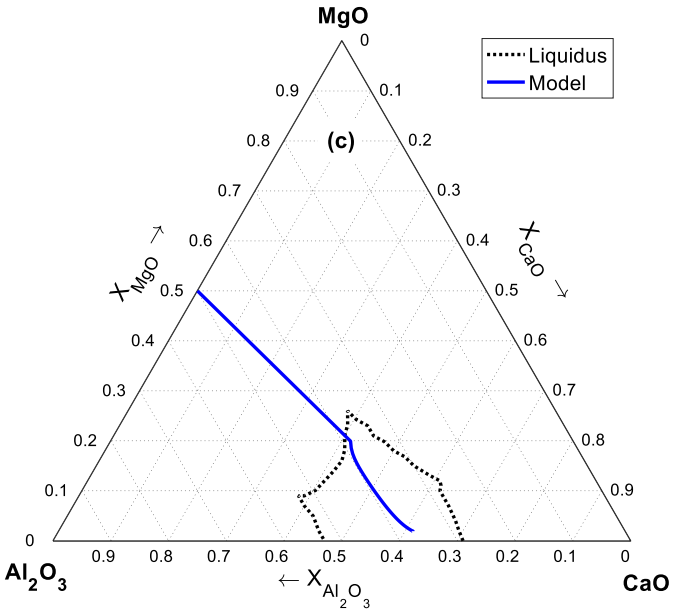

Figure 5-5. Change of (a) diameter (b) global composition of inclusions (c) path of modification in phase diagram [Ca] =0.2 ppm , [Mg] = 0.7 ppm, [Al] = 300 ppm, [O]=3 ppm,

The liquid magnesium calcium aluminate is the product of transformation of the spinel. It takes approximately 114 s to complete this transformation. If the modification continues the inclusion transforms to calcium aluminate.

Figure 5-5 (b) shows that as modification proceeds MgO is reduced from the inclusions and is replaced by CaO, but the mole fraction of Al_3O_3 remains almost constant. This result is consistent with the observation of Pretorius et al. [8] in the case of industrial samples.

5.3.2 Sensitivity analysis

Additional calculations were performed with one order of magnitude higher and lower values for the parameters listed in Table 5-1 to check the sensitivity of the model to each kinetic step and determine the rate controlling step.

5.3.2.1 Diffusivity of CaO, Al_2O_3 and MgO in the liquid product layer

The effect, on the modification of spinel, of varying the diffusivities in the liquid magnesium calcium aluminate product layer is shown in Figure 5-6; decreasing or increasing the diffusivity by a factor of 10 does not change the transformation time, so virtually all the control must lie in the boundary layer. The fact that the conversion rate is unchanged over a two order change in diffusivity even at approaching 100% conversion, shows that the product layer even at its thickest does not control the reaction rate. In theory with a very large inclusion, the thickness of the liquid product layer could become sufficiently large to control the rate. However, given the emphatic nature of the result presented in Figure 6, this could not happen with a realistically sized inclusion.

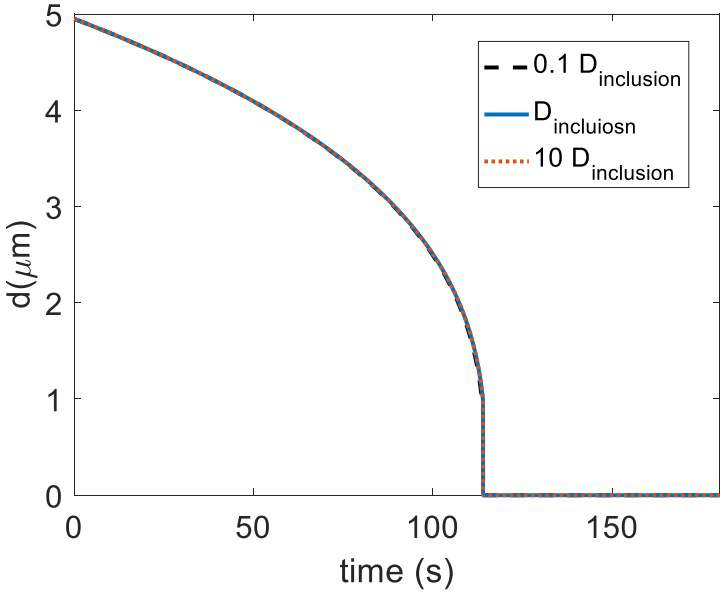

Figure 5-6. Effect of diffusivity within the product layer on transformation rate [Ca] =0.2 ppm , [Mg] = 0.7 ppm, [Al] = 300 ppm, [O]=3 ppm,

5.3.2.2 Diffusivity of solutes in the steel

Figure 5-7 shows the effect of changing the diffusivity or the mass transfer coefficient of all the solutes in the steel by an order of magnitude. Decreasing the value of the mass transfer coefficient from the melt increases the transformation time to 1100 seconds, a 10 fold increase; conversely increasing the value of the mass transfer coefficient causes a decrease to 11 seconds, a 10 fold decrease. As expected, these calculations show that control lies in mass transport to the inclusion surface through the liquid boundary layer.

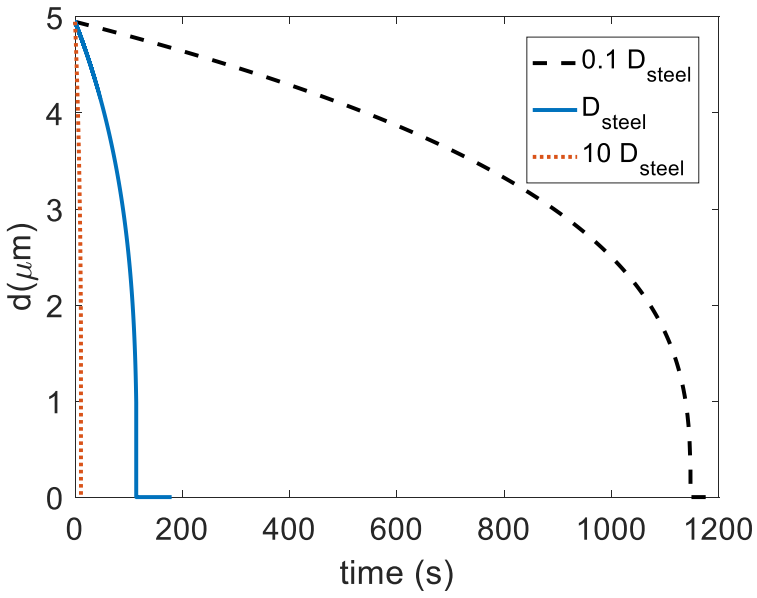

Figure 5-7. Effect of diffusivity in the steel on transformation rate. [Ca] =0.2 ppm , [Mg] = 0.7 ppm, [Al] = 300 ppm, [O]=3 ppm

5.3.2.3 Concentration of solutes

The fixing of composition of liquid magnesium calcium aluminate (point A in Figure 5-4) in equilibrium with spinel constrains the results of the model. However, considering the result of the previous section helps to simplify the model and release this constraint. According to the sensitivity analysis presented in section 5.3.2.1, the

diffusivities in the liquid aluminate product layer have no effect on the transformation rate, demonstrating that diffusion in the product layer is so fast that the product layer can be assumed to be homogeneous. Hence, the composition of the liquid magnesium calcium aluminate can be assumed to be in equilibrium with the spinel. If tie lines are depicted for two phase regions of $Spinel + MCA_x$ as shown in Figure 5-8, the equilibrium composition of liquid MCA_x as well as the amount of each phase can be calculated using lever rule. For example for a inclusion of composition P in Figure 5-8, the liquid MCA_x would have composition of M and mole fractions of spinel and liquid MCA_x are calculated by Eq (5-17).

$$X_{Sp} = \frac{MP}{MS} \quad , \quad X_{MCA_x} = \frac{SP}{MS} \tag{5-17}$$

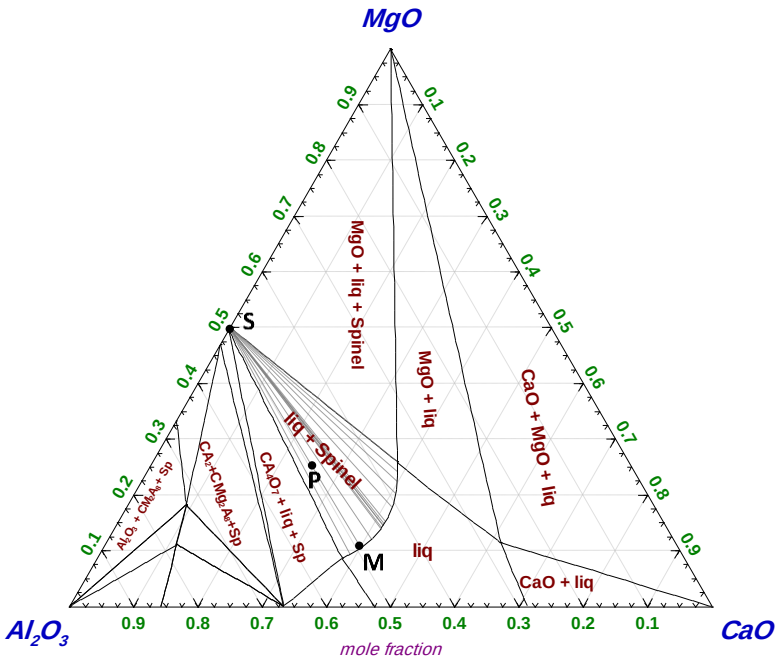

Figure 5-8. Tie lines in spinel +MCA_x two phase region of $CaO - Al_2O_3 - MgO$ phase diagram

The extent of control by the transport of the reactants and products in the boundary layer can be evaluated by changing the concentration of dissolved species $[Ca]$, $[Al]$, $[Mg]$, and $[O]$. This also clarifies the details of the controlling steps in the liquid boundary layer. In the model, calcium is transferred from the bulk steel to the surface of the inclusion and magnesium is transferred from the inclusion surface to the bulk steel as shown in Figure 5-1. Therefore, decreasing $[Ca]$ or increasing $[Mg]$ decreases the driving force for the modification process.

Figure 5-9 shows the influence of varying dissolved magnesium from 0.1 to 0.5 ppm. It is seen that on changing dissolved Mg from 0.1 to 0.5 ppm which is a change by a factor of 5, the rate of transformation increases by a factor of 1.5. Thus, the magnesium content controls the rate to some extent, but not entirely. Also, by increasing the magnesium content of the steel, the composition of liquid magnesium calcium aluminate in equilibrium with the spinel moves slightly toward higher MgO as it is seen in Figure 5-9(b).

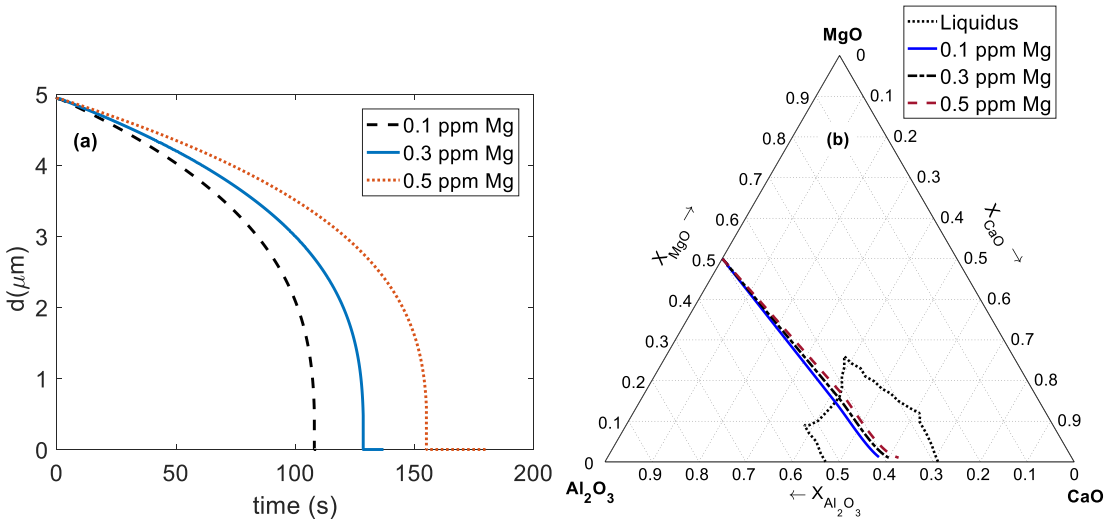

Figure 5-9. Effect of dissolved Mg on transformation rate [Ca] =0.2 ppm, [Al] = 300 ppm, [O] =3 ppm (a) Change of diameter with time and (b) path of modification in phase diagram

Figure 5-10 shows the influence of increasing dissolved calcium from 0.2 to 0.6 ppm, a factor of 3 for which the rate of transformation decreases by a factor of 1.5. Increasing calcium content of the steel has negligible effect on the composition of liquid MCA_x in equilibrium with spinel.

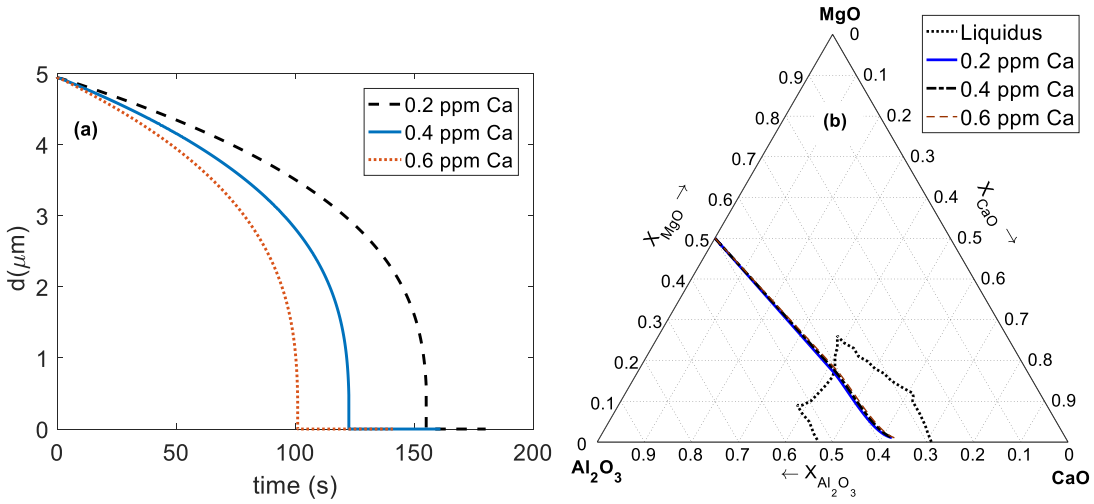

Figure 5-10. Effect of dissolved Ca on transformation rate [Mg] = 0.5 ppm, [Al] = 300 ppm, [O]=3 ppm (a) Change of diameter with time and (b) path of modification in phase diagram

The effects of dissolved oxygen and aluminum concentration on the rate of modification are shown in Figure 5-11 and Figure 5-12 respectively. Changing dissolved oxygen from 2 to 4 ppm which is a change by a factor of 2, the rate of transformation increases by a factor of 2.7. This becomes easy to understand if one considers the degrees of freedom regarding the path of the inclusion composition the important effects relate to the position of point A in Figure 5-4. This point is constrained to sit on the liquidus line which runs approximately parallel to the $Al_2O_3 - MgO$ binary, hence one would expect the relative

fluxes of Al, Mg and oxygen to have a greater effect on the position of this point than the flux of Calcium. The changes in these fluxes will be affected by changes in the concentrations of the relevant elements. The finding, that changes in calcium concentration had a negligible effect on the composition path relative to changes in the other elements, is entirely consistent with this expectation. It is worth noting that calcium concentration does affect the rate of transformation.

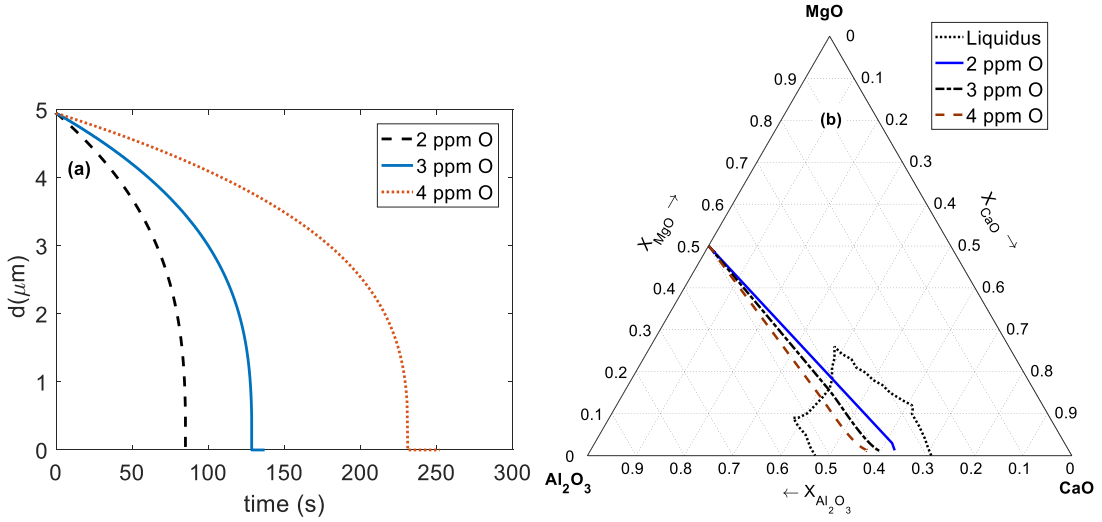

Figure 5-11. Effect of dissolved O on transformation rate [Ca] = 0.2 ppm, [Mg] = 0.3 ppm, [Al] = 300 ppm (a) Change of diameter with time and (b) path of modification in phase diagram

Changing dissolved aluminum from 200 to 400 ppm decreases transformation time by a factor of 1.7. Increasing aluminum content of the steel shifts composition of liquid magnesium calcium aluminate in equilibrium with the spinel toward higher Al_2O_3 as it is seen in Figure 5-12(b).

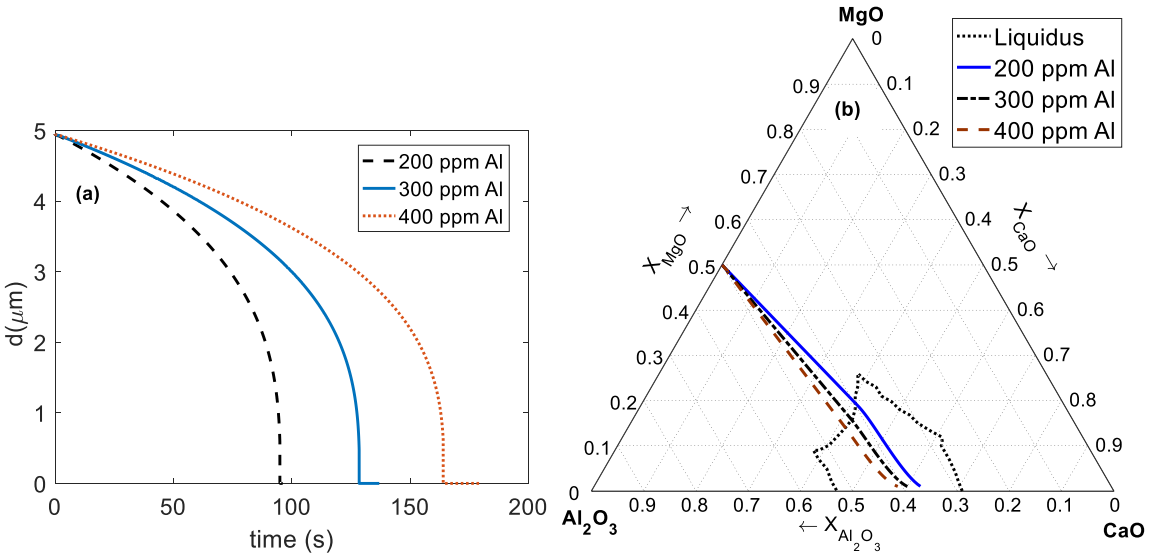

Figure 5-12. Effect of dissolved Al on transformation rate. [Ca] = 0.2 ppm, [Mg] = 0.3 ppm, [O] = 3 ppm (a) Change of diameter with time and (b) path of modification in phase diagram

It should be noted that in reality these concentrations cannot be changed independently as they are determined by equilibrium of steel and inclusions and a change in any species is followed by changes of other species to reach equilibrium. These calculations are done only for the sake of determining significance of different transport steps.

In summary, these sensitivity analyses show that the transformation rate is in a regime of mixed control among rate of supply of calcium and removal of magnesium and transfer through the boundary layer. These steps are coupled by a mass balance and equilibrium at the inclusion interface, resulting in non-linear dependencies of the rate on these solute concentrations.

5.3.3 Comparison with alumina

A multi-layer kinetic model has been developed by the authors [15] for transformation of alumina inclusions. It was concluded that the model can be simplified with little loss in

accuracy by considering only liquid calcium aluminate as the product layer. So, in this work, transformation of one-layer model for alumina is compared with spinel transformation.

Figure 5-13 shows transformation rate of alumina and spinel. Complete transformation of alumina happens 4.3 times faster than for the spinel.

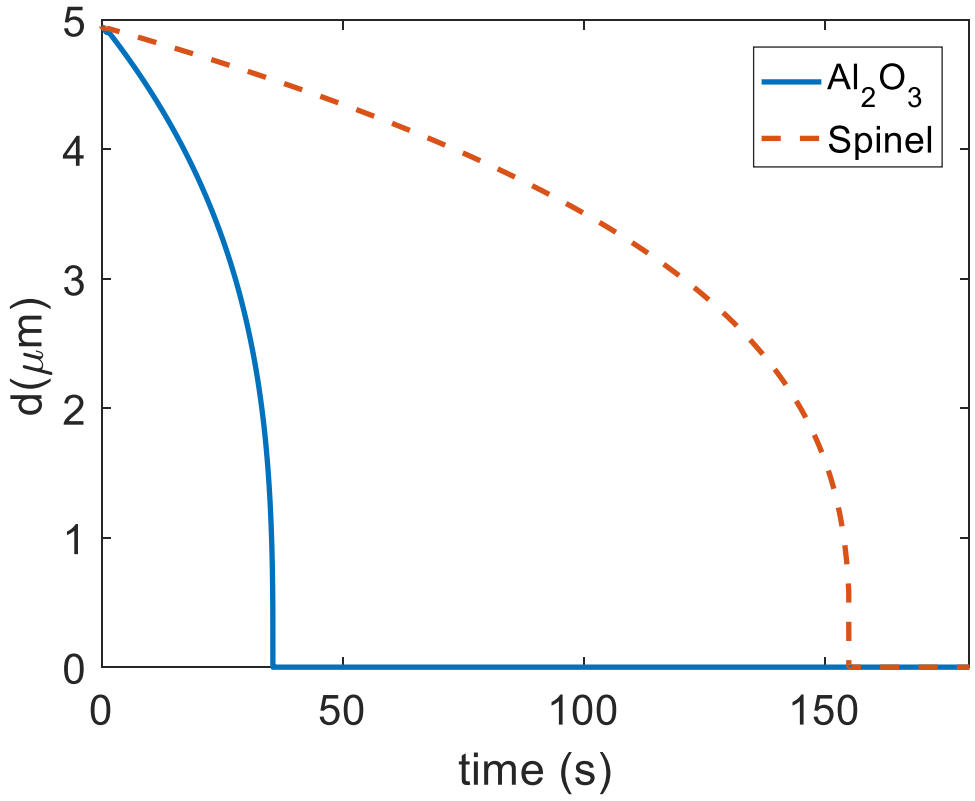

Figure 5-13. Comparison of modification of alumina and spinel, 0.2 ppm [Ca], 300 ppm [Al], 0.5 ppm [Mg], 3 ppm [O]

Modification of alumina occurs by partial reduction of alumina, but in the case of spinel it proceeds by reduction of MgO. As the ratio of O in Al_2O_3 to CaO is more than one, modification of alumina by CaO results in rejection of oxygen to the melt. However, there

is not significant oxygen exchange in the modification of spinel. On the other hand, lower dissolved Mg increases the transformation rate of spinel. Therefore, lower magnesium concentrations in the metal the transformation rate of the spinel is higher.

5.3.4 Compositional trajectory of inclusions during industrial-scale ladle process

In the present work of the authors [16] a multicomponent steel-slag kinetic model developed by Graham and Irons [2] coupled with a steel-inclusion kinetic model was used to calculate the change of composition of steel, slag and alumina inclusions during ladle processing. In addition an a model of calcium dissolution and reaction developed by Lu et al. [12] was used to calculate dissolution rate of calcium to the melt during calcium treatment. The model also considers the stirring effect, the effect of ladle furnace power on temperature and change of composition due to alloying addition.

From the result of previous section it is found that diffusion within inclusions is so fast that it happens almost instantly. This is an important finding as it allows a simplification of the model by considering homogeneous inclusions in which the exchange of magnesium and calcium within the inclusions is calculated. Here, homogeneous means that diffusion within the inclusion is assumed to be fast and the composition of inclusion is determined by flux of solutes to the inclusion-steel interface. A schematic diagram of such inclusion and corresponding concentration gradient is shown in Figure 5-14.

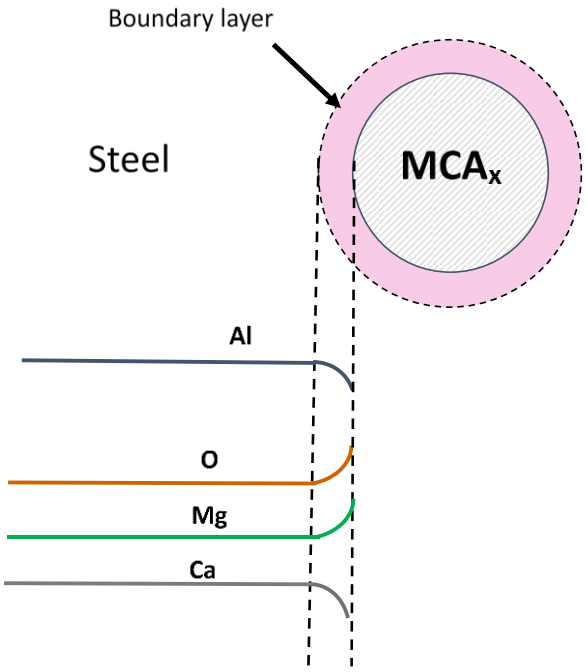

Figure 5-14. Schematic diagram of assumed homogeneous inclusions and concentration gradient at the inclusion-steel interface

The change of composition of an alumina inclusion during ladle process is shown in Figure 5-15. Ladle conditions for the calculations are the same as in previous work [16] as listed in Table 5-2 and Table 5-3.

Table 5-2. Initial steel composition (Wt %)

C	Mn	P	S	Si	Al	N	Ca	O
0.0501	1.03	<0.016	0.0123	0.063	0.0268	0.0045	0.00019	<0.001

Table 5-3. Ladle processing conditions for calculations

Initial steel temperature (K)	1867
Steel mass (tonne)	164.5

Slag mass (tonne)	2.58
Ladle diameter (m)	3.2
Ar flow rate ($Nm^3/h/plug$)	4 at low stirring regime and 25 at high stirring regime

As expected due to reaction of steel and slag Mg is reduced from the slag which in turn causes the inclusions to transform to magnesium aluminate inclusions. Later, during Ca injection these inclusions are modified to magnesium calcium aluminates and eventually low magnesium calcium aluminate. The model successfully predicts the evolution path of alumina inclusions as sown in Figure 5-15. The plant data is shown in this figure as average composition of inclusions at different stages of the ladle process.

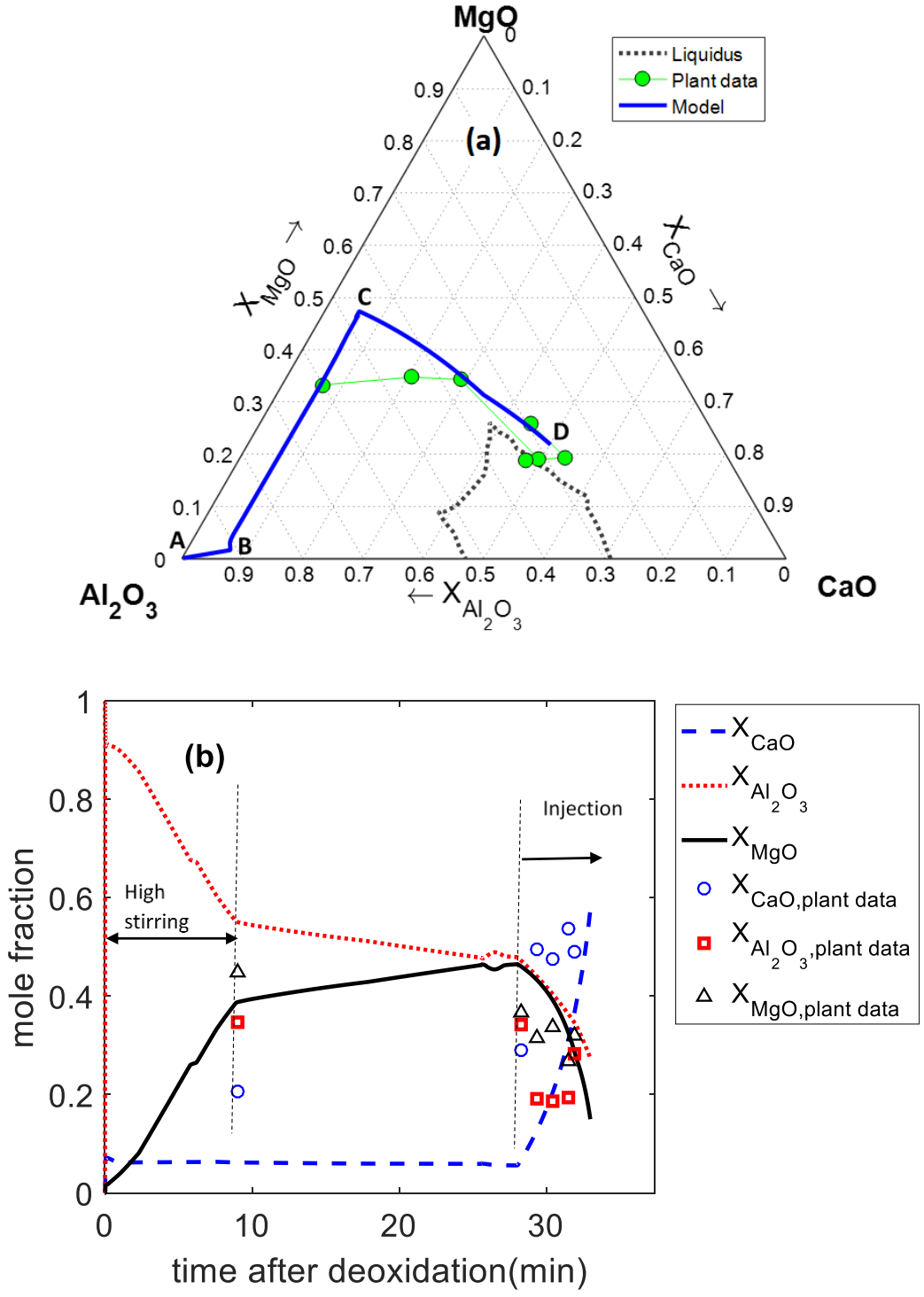

Figure 5-15. (a) Evolution path of oxide inclusions (b) change of composition of oxide inclusions with time during ladle process

According to plant measurements there is approximately 2 ppm Ca in the melt before injection. This is total calcium which is summation of calcium in inclusions and dissolved calcium in steel. The jump at the beginning of the process (AB in Figure 5-15) is due to reaction of alumina inclusions and the calcium already present in the melt. During high stirring period which promotes reduction of MgO in the slag by aluminum in the steel, concentration of magnesium increases in the molten steel. The alumina inclusions react with dissolved magnesium and are transformed to magnesium aluminate spinel (BC in Figure 5-15). The model underestimated mole fraction of CaO before injection. This can be due to introduction of some calcium to the molten steel by alloying addition such as FeSi which is not considered in the model as the exact chemical composition of alloying addition was not available. Eventually by calcium treatment of steel, spinel inclusions absorbs dissolved calcium and are modified to liquid MCA_x (CD in Figure 5-15). It should be noted that although the composition of inclusions at the end of injection lies outside of the liquidus region, in reality because the inclusions contain small amount of other elements such as silicon, the liquidus is larger than calculated for the ternary system of $CaO - Al_2O_3 - MgO$ presented in this work.

5.4 Discussion

In the literature, although there exists some research regarding the thermodynamics of spinel modification, there are few studies concerning the rate controlling step of spinel inclusion transformation by calcium [10].

Previous work by the authors on alumina transformation to liquid calcium aluminate [15,16] showed that in the case of alumina transformation, the rate of supply of calcium to

the melt is the rate controlling step. Galindo et al. [18] arrived at a similar conclusion in a study on the transformation of single particles of alumina inclusions to magnesium aluminate spinel. The same conclusion is reached in this work regarding modification of spinel inclusions to liquid magnesium calcium aluminate. Diffusion within the product layer is so fast that if there is high activity of calcium and low activity of magnesium in the molten steel; the modification of the spinel is completed in a very short time. This result does not agree with work by Yang et al. [10] in which it was claimed that diffusion of Mg in the product layer is the rate controlling step. However, they assumed a solid product layer in which the diffusivity of Mg was much lower than Ca. The present authors believe that the product layer is liquid in which Ca, Al and Mg have similar diffusivities. The existence of this liquid product layer is reported in the literature [7,8]. Also, it was shown that the mechanism of modification is reduction of MgO by calcium which is consistent with the observations of Pretorius et al. [8].

Figure 5-9-Figure 5-12 shows that rate of modification of spinel increases with lower dissolved magnesium in the steel, higher calcium, lower oxygen and lower aluminum due to a higher driving force. Also, changing the concentration of dissolved species in the melt changes the composition of liquid MCA_xin equilibrium with spinel; lower Mg or higher Al contents of the steel leads to production of lower MgO, higher Al_3O_3 in the magnesium calcium aluminate. However, reduction of magnesium from spinel inclusions increases the magnesium content of the steel melt until it reaches close to the equilibrium value with magnesium calcium aluminate inclusions. Thus, the rate of transformation of spinel should be lower than that of alumina. This seems to be in contradiction with some other studies

[8,29,30], which suggested that modification of the spinel may be faster that of alumina, because in the case of alumina solid CA_6 is the first phase to form, whereas for spinel a liquid phase forms first and diffusion through the liquid layer is faster. However, the model presented in the current work, and that previously published for modification of alumina, showed that the transformation was controlled by supply of calcium and that complete modification of spinel takes longer than alumina under ladle metallurgy conditions.

The trajectory seen for modification of spinel shown in Figure 5-15(a) is slightly different from those predicted in Figure 5-9-Figure 5-12. This is because in reality oxygen content of the steel is not constant and is consumed by inclusions and it drops to a very low level and magnesium concentration in the steel increases as it is dissolved into the steel from inclusions. At lower oxygen and higher magnesium concentration composition of liquid MCA_x shift toward higher MgO content.

Even though complete modification of spinel takes longer, it is not necessary to have fully liquid inclusion since it is suggested that good castability of steel can be achieved even with just partially liquid inclusions [31].

5.5 Conclusions

In the current work, a mathematical model is proposed to quantitatively describe the kinetics of calcium treatment of $MgAl_20_4$ spinel inclusion in the ladle furnace. This multi component diffusion model considers transfer of Ca, Al, Mg and O through the boundary layer and within product layer coupled with thermodynamic equilibrium at the interfaces. This is the first model describing the multi component kinetics for $MgAl_20_4$.

1. The rate control for spinel modification by calcium treatment is mixed between mass transport of magnesium and calcium through the steel inclusion boundary and rate of supply of solutes to the bulk steel. This is slightly different from the case of alumina modification where the control is dominated by calcium supply to the bulk steel.

2. A small concentration of calcium, less than 1 ppm, is sufficient to modify spinel inclusions to liquid magnesium calcium aluminate.

3. The current model suggests that if calcium is dissolved in the steel and reaches a spinel inclusion, the transformation will be rapid.

4. The multicomponent transformation model has excellent agreement with plant data predicting the evolution path in the following order: $Al_2O_3 -> MgAl_2O_4 -> MCA_x(liquid)$

5.6 Acknowledgement

The Authors are grateful for the support of the members of the McMaster Steel Research Centre, the Natural Sciences and Engineering Research Council of Canada and ArcelorMittal Dofasco.

5.7 References

[1] A. Ghosh: Secondary Steelmaking: Principles and Applications, 1st Ed., CRC Press, London, 2001, , pp. 203–17.

[2] K. J. Graham and G. A. Irons: in Int. Symp. Highly Innov. Nov. Oper. "Future Steelmak. Metall., 2010, pp. 65–74.

[3] E.B. Pretorius, H.G. Oltmann, and B.T. Schart: AISTech 2013 Proc., 2013, pp. 993–1026.

[4] Jh. Park and H. Todoroki: ISIJ Int., 2010, vol. 50, pp. 1333–46.

[5] Sh. Yang, Q. Wang, L. Zhang, J. Li, and K. Peaslee: Metall. Mater. Trans. B, 2012, vol. 43, pp. 731–50.

[6] G. J. W Kor: in Steelmak. Conf. Proc., 1989, pp. 39–44.

[7] N. Verma, P. C. Pistorius, R. J. Fruehan, and R. J. Lee: in Mater. Sci. Technol. Conf. Exhib. 2009, MS T'09, Pittsburgh, PA, 2009, pp. 1042–53.

[8] E. B. Pretorius, H.G. Oltmann, and T. Cash: Iron Steel Technol., 2010, vol. 7, pp. 31–44.

[9] Y. Kang, F. Li, K. Morita, and D. Sichen: Steel Res. Int., 2006, vol. 77, pp. 785–92.

[10] Sh. Yang, Ji. Li, X. Gao, and Y. Ma: Metall. Min. Ind., 2014, pp. 66–71.

[11] F. Wells: Structural Inorganic Chemistry, 5th Ed., 1984, pp. 312–18.

[12] D. Lu, G. A. Irons, and W. Lu: Ironmak. Steelmak., 1994, vol. 21, pp. 362–72.

[13] Y. Ito, M. Suda, Y. Kato, H. Nakato, and K. Sorimachi: ISIJ Int., 1996, vol. 36, pp. S148–50.

[14] Y. Higuchi, M. Numata, Sh. Fukagawa, and K. Shinme: ISIJ Int., 1996, vol. 36, pp. 151–54.

[15] Y. Tabatabaei, K. S. Coley, G. A. Irons, and S. Sun: Metall. Mater. Trans. B, 2017, vol. 49, pp. 375–87.

[16] Y. Tabatabaei, K. S. Coley, G. A. Irons, and S. Sun: Metall. Mater. Trans. B, 2018, Volume 49, pp 2022–37.

[17] O. Levenspiel: Chemical Reaction Engineering, 2nd Ed., John Wiley & Sons, New York, 1999, pp. 570–77.

[18] A. Galindo, G. A. Irons, K. S. Coley, and S. Sun: in Challenges Transform. Solut. to Sustain. Steelmak. Cast. Environ. Metall. Innov. CTSSC-EMI Symp. 2015, Tokyo, Japan, 2015.

[19] A.H. Aza, J. E Iglesias, P. Pena, and S. Aza: J. Am. Ceram. Soc., 2000, vol. 83, pp. 919–27.

[20] J. Szekely and N. J. Themelis: Rate Phenomena in Process Metallurgy, 1st Ed., Wiley-Interscience, New York, 1971, pp. 609–17.

[21] F. Oeters: Metallurgy of Steelmaking, 1st Ed., Düsseldorf: Verlag Stahleisen, 1994, pp. 316–35.

[22] M. L. Kapoor and M. G. Frohberg: in Chem. Metall. Iron Steel, 1971, pp. 17–22.

[23] H. Gaye and J. Welfringer: in Second Int. Symp. Metall. Slags Fluxes, 1984, pp. 357–75.

[24] K J Graham and G a Irons: in AISTech - Iron Steel Technol. Conf. Proc., Pittsburgh, PA, 2008, pp. 5–13.

[25] M. Hino and K. Ito: Thermodynamic Data for Steelmaking, 1st Ed., Tohoku University Press, Tokyo, 2010, pp. 16–17.

[26] H. Fujiwara, A. Hattori, and E. Ichise: Tetsu-To-Hagane/Journal Iron Steel Inst. Japan, 1999, vol. 85, pp. 201–7.

[27] J-D. Seo and S-H. Kim: Steel Res., 2000, vol. 71, pp. 101–6.

[28] A. Gilat and V. Sabramaniam: Numerical Methods for Engineers and Scientists, 3rd Editio, Wiley, 2013, p. 99−165.

[29] S. F. Yang, J. Sh. Li, Z. F. Wang, J. Li, and L. Lin: Int. J. Miner. Metall. Mater., 2011, vol. 18, pp. 18–23.

[30] N. Verma, P. C. Pistorius, R.J. Fruehan, M.S. Potter, H.G. Oltmann, and E.B. Pretorius: Metall. Mater. Trans. B, 2012, vol. 43, pp. 830–40.

[31] C. Pistorius, P. Presoly, and K. Tshilombo: in Int. Sohn Symp. TMS, 2006, pp. 373–78.

[32] T. Saito and K. Maruya: Diffusion of Calcium in Liquid Slags, 1958.

[33] Y. Oishi, M. Namba, and J.A. Pask: J. Am. Ceram. Soc., 1982, vol. 65, p. 247−253.

[34] G. A. Irons, C. W. Chang, R. I L Guthrie, and J. Szekely: Metall. Trans. B, 1978, vol. 9, pp. 151–54.

Chapter 6

Tracking Inclusions During Ladle Refining Using a Kinetic Model for the Compositions of Metal, Slag and Inclusions

The structure of Chapter 6 was proposed by Dr. Kenneth S. Coley and Dr. Gordon A. Irons. Data analysis and modeling were carried out by me. Dr. Kenneth S. Coley provided very helpful discussion during model results analysis. The first draft was prepared by me and edited to the final version by Dr. Kenneth S.Coley, Dr. Gordon A. Irons and Dr. Stanley Sun. This chapter will be submitted as a two part paper shortly.

Abstract

A kinetic model to track the reactions in a ladle furnace was presented in a recent paper by the authors, in which following chemical processes were considered: (1) rate of slag-steel reaction, (2) rate of supply of calcium during calcium treatment, (3) rate of steel-inclusion reactions including oxides and sulfides. In this work the model is further validated by comparing predicted and measured composition of inclusions and dissolved species in the steel for additional plant heats. Also, sensitivity analysis has been carried out to investigate effect of different parameters including sulphur content of steel, total oxygen, slag composition and reoxidation of steel on composition of inclusions during ladle process. The developed model offers potential for control and optimization of the operation of a ladle furnace.

6.1 Introduction

In production of aluminum killed steels, aluminum is added to deoxidize the steel. The alumina inclusions tend to float out of the steel to the slag during argon stirring. However, many of these inclusions are too small to rise rapidly and remain in the steel. To achieve high cleanliness, the steel must be monitored and controlled precisely [1] The term "clean steel" is commonly associated with low non-metallic inclusion content in the steel. It is well known that these smaller alumina inclusions can transform to magnesium aluminate spinel inclusions $MgAl_2O_4$ by reaction with dissolved magnesium from top slag or ladle refractories or from magnesium contamination of ferroalloy additions [2-6]. Calcium treatment is an effective approach to modify solid alumina and spinel inclusions which are not eliminated from the melt to less harmful liquid calcium aluminates or magnesium calcium aluminate inclusions [7-10]. Ca addition decreases the volume fraction of oxide and sulphide inclusions and controls the composition, morphology, and distribution of those remaining inclusions. Moreover, Ca treatment may modify the shape of MnS stringer inclusions to less elongated $MnS-CaS$ inclusions [11]. However, excessive calcium treatment may cause formation of solid CaS inclusions leading to nozzle clogging in ladle or tundish [12]. So it is important to have a precise control over Ca addition.

Establishing a model to describe the evolution of these inclusions in the ladle furnace is indeed a challenge as reactions at the interface between top slag and steel and other process parameters, such as alloying elements, steel flow and inclusion separation can affect the composition of inclusions. Many studies have been done on modeling and understanding

the mechanism of inclusion evolution during ladle treatment [8,10,13-15]. A detailed review of these models is presented in the authors' previous work [16].

A kinetic model was previously developed by authors [16] that was used to predict the changes in the composition of calcium aluminate inclusions, as well as slag and steel and formation of oxide and sulphide inclusions during ladle refining. The predictions were in good agreement with a limited number of plant results from ArcelorMittal Dofasco. It was found that rate of transformation of alumina inclusions is determined by rate of supply of Ca to the melt from Ca bubbles. Also, it was found that CaS inclusions mainly form at the injection plume. In further study by the authors [17] a model for modification of spinel inclusions was proposed and validated using plant data.

The present work aims to explore a wider range of ladle conditions using the previously developed kinetic model and to validate the resulting predictions against available plant data from ArcelorMittal Dofasco. Parameters investigated include dissolved sulphur, total oxygen content, stirring intensity, and slag composition. Sensitivity analysis is also performed to investigate effect of these factors on the composition of the inclusions during ladle refining.

6.2 Outline of the model

A model developed by Lu et al. [1] was adopted for the dissolution rate of calcium into the steel in the present work. According to this model, calcium dissolving from a calcium bubble through the boundary layer reacts with diffusing oxygen and sulfur at the reaction plane to form CaO and CaS, causing the calcium concentrations to drop to sub-ppm levels

in the bulk of the steel. This low level of dissolved calcium modifies the alumina and magnesium aluminate spinel particles to calcium aluminate. All of these inclusions compete for the available calcium. Inclusion-steel interfacial concentrations were calculated by considering elemental mass balances and local thermodynamic equilibria at the various inclusion interfaces. Control of the reactions was mixed between supply of reactants (Ca from the bubbles and Mg from the slag) and mass transfer to the inclusions [18-19].

A multicomponent kinetic model developed by Graham and Irons [6] was used to calculate the effect of steel - slag reactions during ladle processing. The model is based on a mixed coupled reaction model proposed by Ohguchi et al. [20] and developed to describe dephosphorization and deoxidation. The kinetic model assumes that the rates are controlled by multicomponent transport in both metal and slag. Moreover, it was assumed that chemical reactions are sufficiently fast such that there exists local equilibrium at the slag-metal interface. The model also takes into account the stirring effect, the effect of ladle furnace power on temperature, and change of composition due to alloying addition. A schematic diagram of calculations is shown in Figure 6-1. The details of the model; assumptions, concentrations at the inclusion-steel and steel-slag interfaces, mass transfer coefficients and a flow chart of calculations are described in detail in the authors' previous publication [16] and are presented in section 4.2 of this thesis.

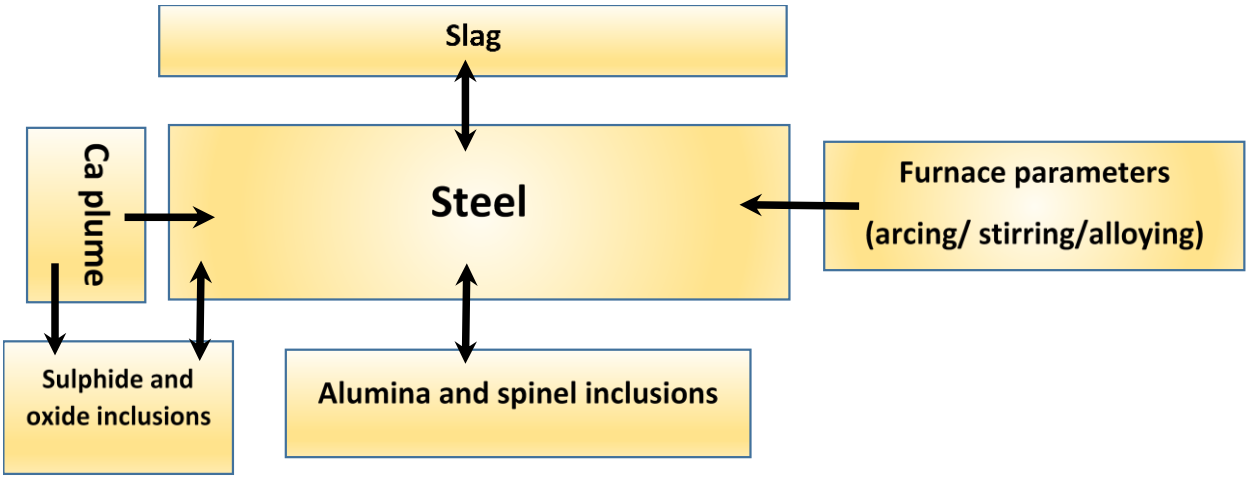

Figure 6-1. Schematic diagram of the coupled steel-slag-inclusion kinetic model

6.3 Results and discussion

In this section, the prediction of inclusions compositions by the current model is validated for number of heats. Also, the ladle conditions regarding steel chemistry, total oxygen, slag chemistry and calcium injection are varied and the kinetic model is employed to predict effect of each parameter on inclusion evolution path during the ladle process.

6.3.1 Comparison of model with industrial data

6.3.1.1 Ladle conditions

The typical chemical compositions of the steel and the slag used in a ladle are listed in Table 6-1 and Table 6-2 respectively and the operational conditions are shown in Table 6-3.

Table 6-1. Steel composition at the beginning of ladle process (Wt. %)

C	Mn	P	S	Si	Al	Ca	Fe and other
0.03-0.08	0.8-1.5	<0.015	<0.015	<0.06	0.025-0.05	< 5	Balance

Table 6-2. Slag composition at the beginning of ladle process (Wt. %)

P_2O_5	TiO_2	CaS	FeO	CaO	MnO	SiO_2	MgO	Al_2O_3	Other
<0.02	<0.5	0.5-1.5	0.5-1.5	40-55	< 1.5	5-15	5-15	25-30	balance

Table 6-3. Ladle processing conditions for calculations

Initial steel temperature (K)	1873
Steel mass (tonne)	164.5
Slag mass (tonne)	2.58
Ladle diameter (m)	3.2
Ar flow rate (Nm^3/h/plug)	2 plugs,~5 at low stirring regime and ~25 at high stirring regime

The average size and number of alumina inclusions per unit volume of steel were estimated from automated SEM data using the Schwartz-Saltykov method [21]. This data was used to define the initial total oxygen for the model.

The coupled model (Figure 6-1) was used to predict evolution of alumina inclusions during the ladle process for several heats listed in Table 6-4.

Table 6-4. S, Al and Ca content (ppm) in the steel

	Before Ca injection						After Ca injection
	[S] before de-S	[S] after de-S	**$\Delta[S]_{de\text{-}S}$**	$[Al]_s$	$[Al]_{tot}$	**$\Delta[Al]$**	$[Ca]_{tot}$
Heat 1	122	37	**85**	305	319	**14**	44
Heat 2	122	17	**105**	354	373	**19**	33
Heat 5	113	58	**55**	404	416	**12**	47
Heat 6	185	50	**135**	333	345	**12**	59
Heat 8	78	31	**47**	503	520	**17**	69
Heat 9	84	23	**61**	374	393	**19**	40
Heat 10	32	13	**19**	403	413	**10**	51

In the previous work [16] to develop and validate model particular attention was given to the inclusions. The detection threshold for inclusions diameter for automated SEM analysis was set to 0.5 microns and it was found that a considerable number of inclusions were less than 2 microns. However, for most ArcelorMittal Dofasco heats, such as the ones listed in Table 6-4, the threshold for analysis is set to 2 micron. The number of inclusions was estimated using difference between total and soluble aluminum in a procedure developed at ArcelorMittal Dofasco [22]. For estimation of number of inclusions it was assumed that the average diameter of alumina inclusions is 1.5 micron (which was the case for Heat 1) and with the knowledge of ppm of Al associated with inclusions, total mass of Al_2O_3 inclusions and consequently number of inclusions were calculated. The total number of alumina inclusions calculated at the start of process for each heat was kept constant

throughout the process. Also, as the stirring data was not available for heat 3 – 10, the extent of stirring was estimated using the desulfurization data from the heats, since they are directly related. Figure 6-2 shows the change of composition of oxide inclusions during ladle process predicted by the model and plant data.

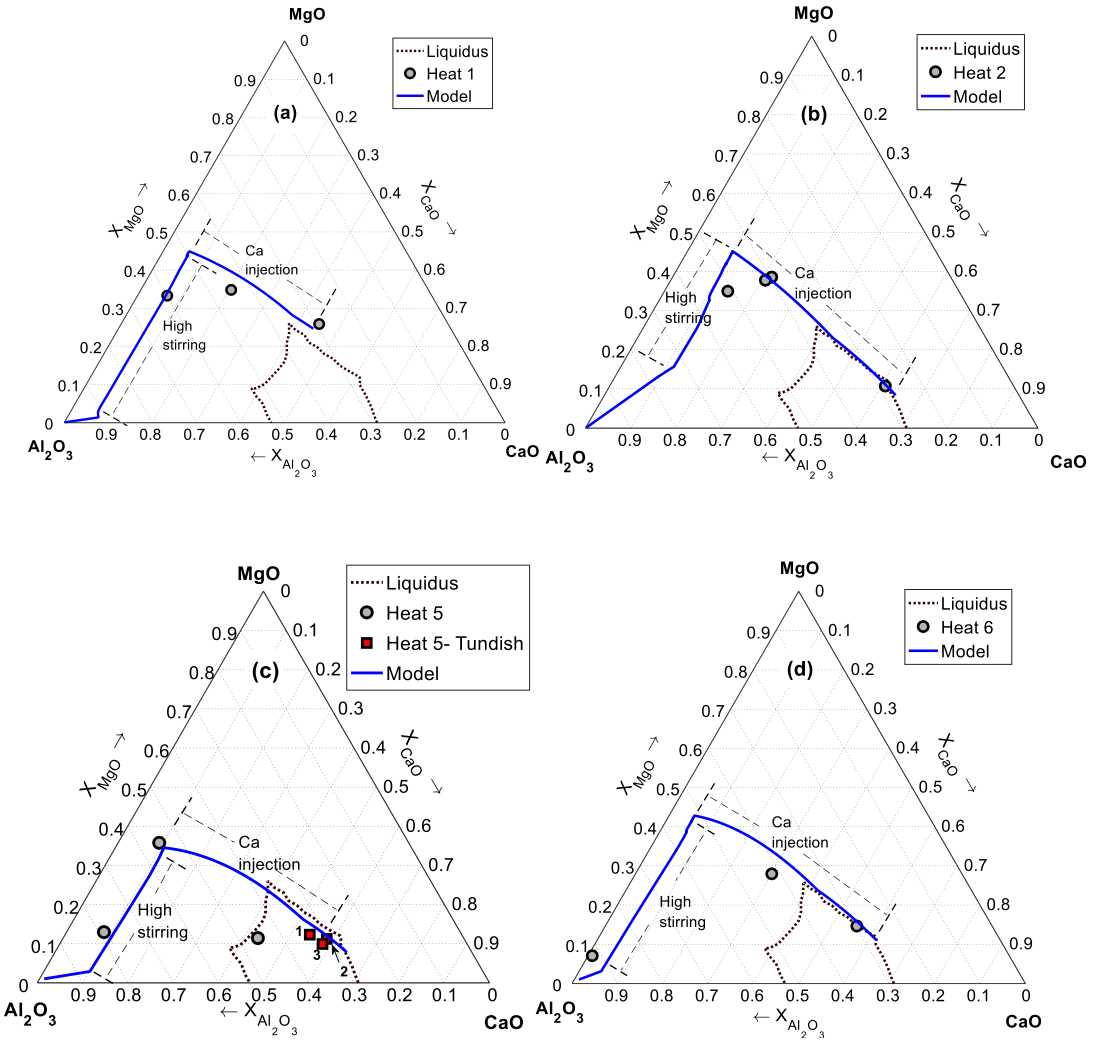

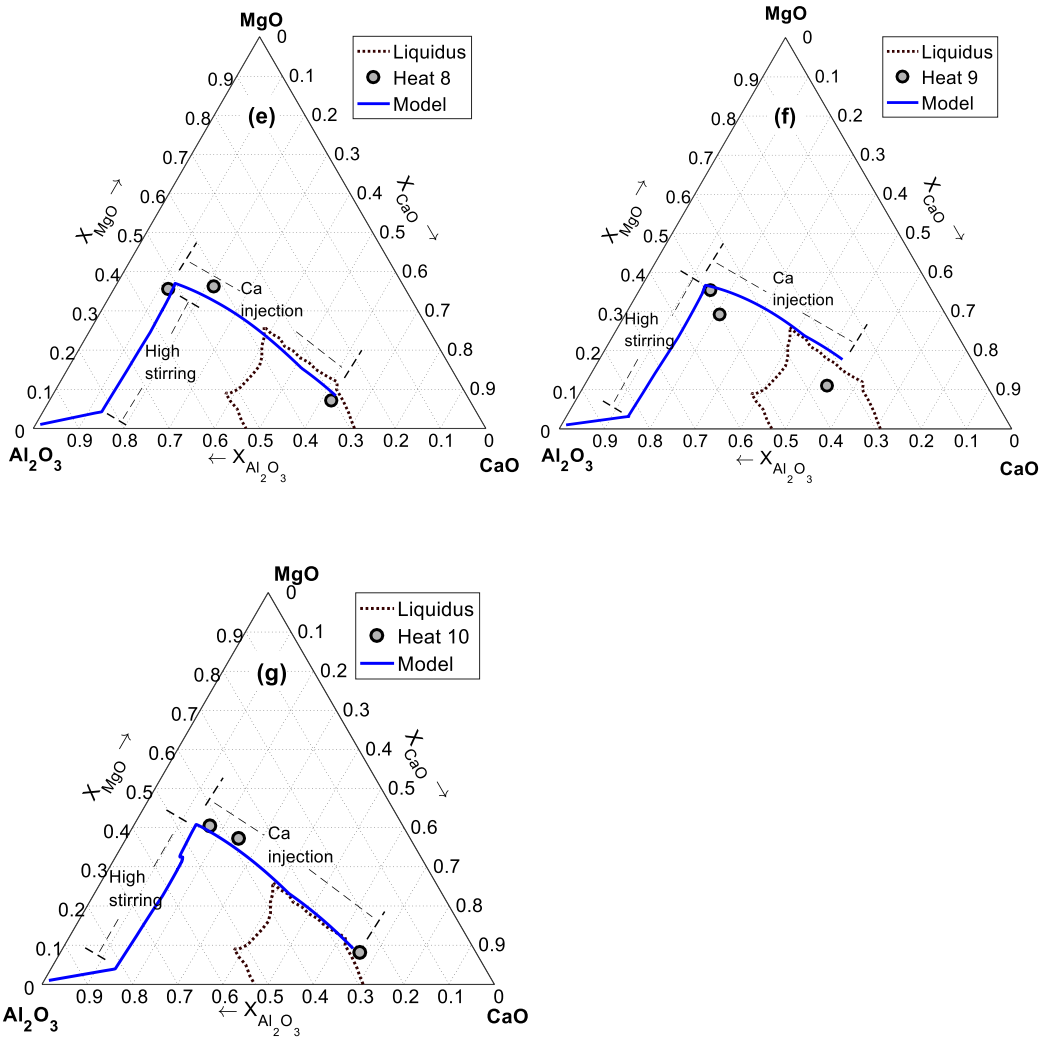

Figure 6-2. Prediction of change of composition of oxide inclusions during ladle process for the heats listed in Table 6-4

Figure 6-2 shows the results of the model are in good agreement with plant data. Only for Heat 5 the predicted average composition for inclusions was different from the measured average composition of inclusions after Ca injection. In this sample surprisingly there was much higher number of pure alumina incluions after Ca injection compared to other heats. One reason for that could be reoxidation of sample. Unfortunately that was the only available sample from ladle. But, three samples were available from tundish, one at

the beginning of casting, one in the middle and one at the end of casting. Those sample were analyzed and are presented in Figure 6-2 (c). The average composition of oxide inclusions in tundish samples is similar and agrees with model prediction. For all heats at the beginning of the process, there is a jump in CaO and MgO content of inclusions because of reaction of alumina inclusions and the calcium and magnesium already present in the melt. During the high stirring period dissolved Mg increases in the steel due to reduction of MgO from the slag. This magnesium reacts with the alumina inclusions to form magnesium aluminate spinel. Finally, during Ca injection the composition of inclusions moves to higher CaO lower MgO content in the liquid area.

Figure 6-3 compares the predicted and calculated concentrations of dissolved species in the steel. There is good agreement between the model calculations and the measured values for dissolved Sulphur, aluminum and silicon for all of the heats presented. At the beginning of process some aluminum is added followed by high stirring to kill the steel and slag, and to promote desulphurization. Dissolved [Al] also reacts with the slag to reduce [Si] and [Mg] from the slag. The observed increase in Mg in the inclusions and the transformation from alumina to spinel shown in Figure 6-2 is associated with this high stirring period. Ca injection was carried out during the last few minutes of the process. The last sample in all heats was taken after calcium injection. In previous work was found that Ca treatment can enhance mass transfer in the steel since Ca bubbles form during Ca treatment and these bubbles induce stirring much in the same way as injected argon gas. Not including the calcium contribution to stirring in the model may well be the source of the observed over -prediction of [Al] and associated under-prediction of silicon in some heats (Heat 1,2 and

6). The rate of injection of calcium is approximately 7 kg/min. if we assume 25 % recovery of Ca injected, 75% of the injected Ca form bubbles which is 5.25 kg/min which would give 173Nm^3 /h which is just under 3.5 times the gas injection rate for argon during high stirring periods.

$$5.25\ \frac{kg}{min} = \frac{5.25}{0.0408}\ \frac{gmol}{min} = 134.8\ \frac{mol}{min} = 2.88\frac{(Nm^3)}{min} = 172.95\frac{(Nm^3)}{h} \qquad \textbf{(6-1)}$$

However, Ca bubbles stirring is not as efficient as Ar since the bubbles size and distribution is not controlled. Besides that, there might be disruption of the slag/metal interface during injection. Therefore, the effect of calcium bubble stirring on enhancement of mass transfer is different than that of argon. Further analysis is required to quantify effect of Ca bubbles on mass transfer in the metal phase.

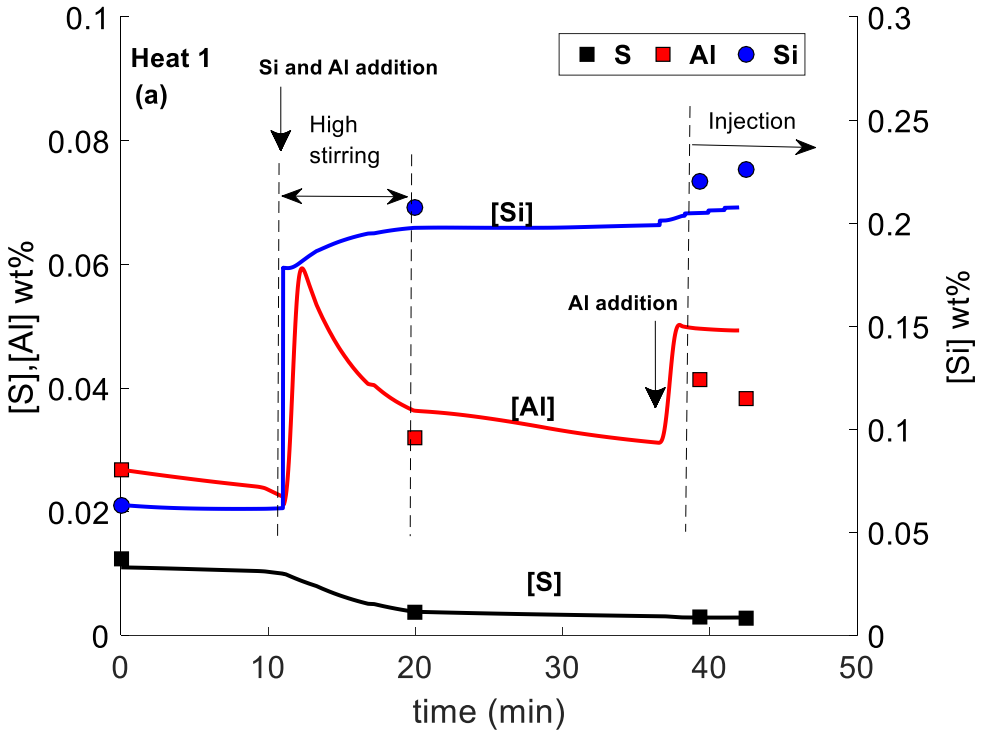

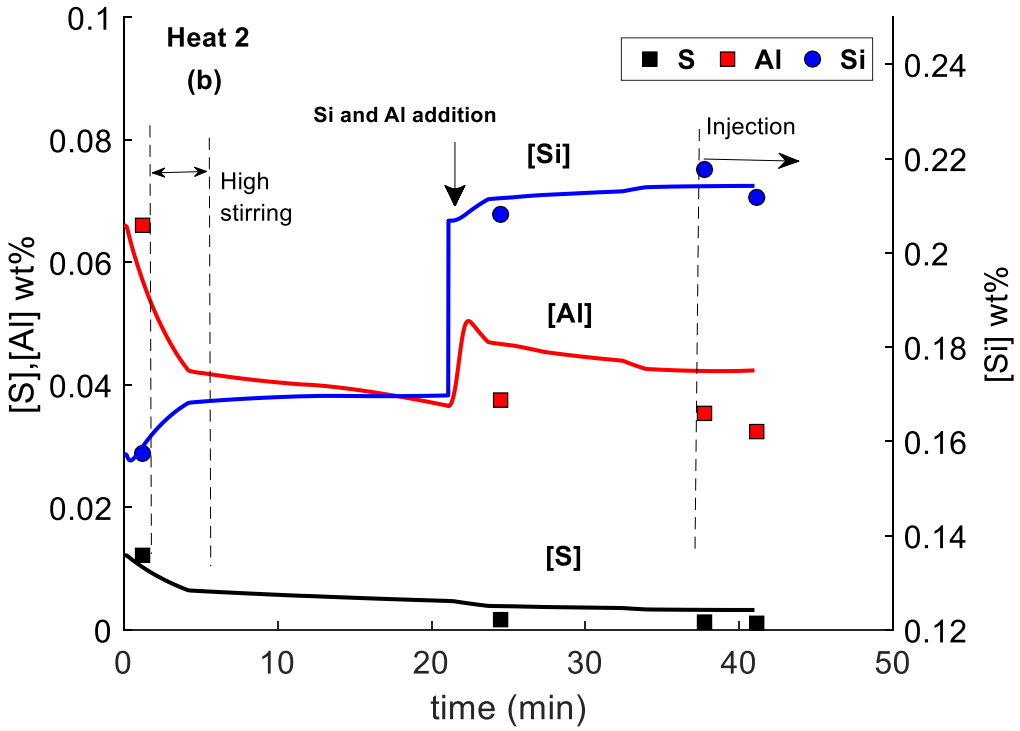
Heat 2
(b)
S
Al
Si
Si and Al addition
Injection
High
stirring
[Si]
[Al]
[S]
[S],[Al] wt%
[Si] wt%
time (min)
0.1
0.08
0.06
0.04
0.02
0
0.24
0.22
0.2
0.18
0.16
0.14
0.12
0
10
20
30
40
50

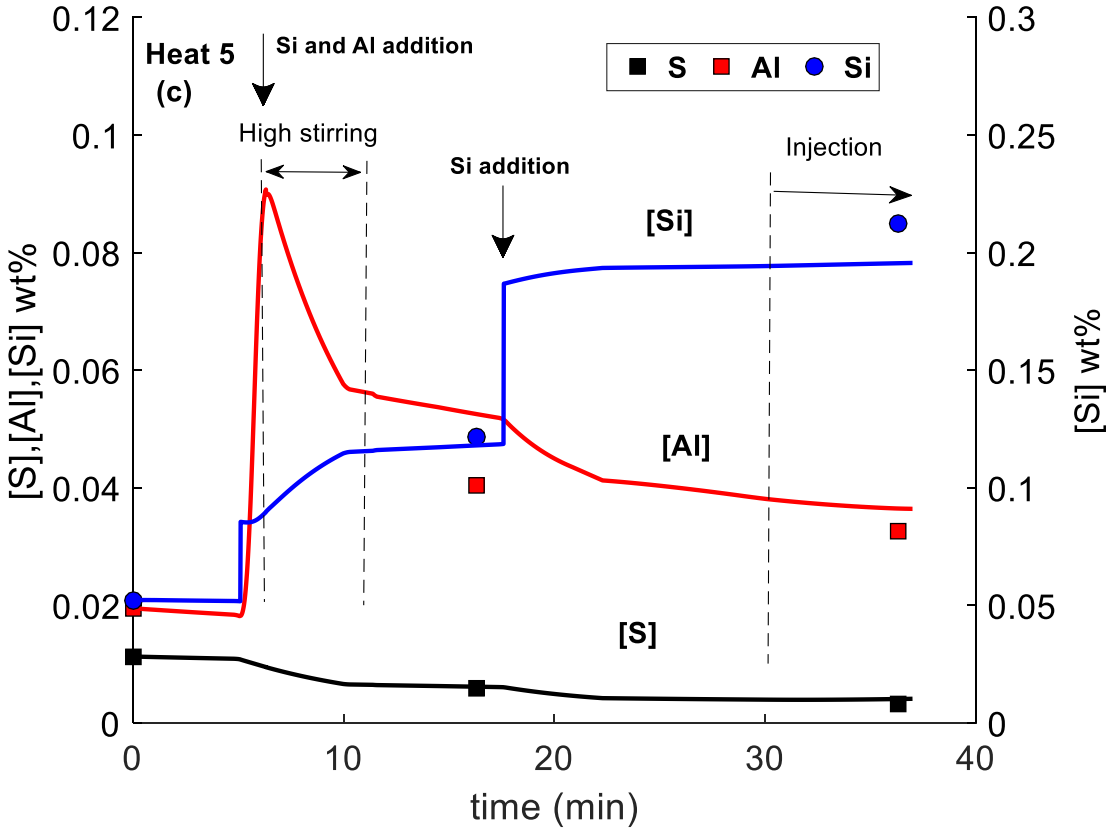
Heat 5
(c)
Si and Al addition
High stirring
Si addition
Injection
S
Al
Si
[Si]
[Al]
[S]
[S],[Al],[Si] wt%
[Si] wt%
time (min)
0.12
0.1
0.08
0.06
0.04
0.02
0
0.3
0.25
0.2
0.15
0.1
0.05
0
0
10
20
30
40

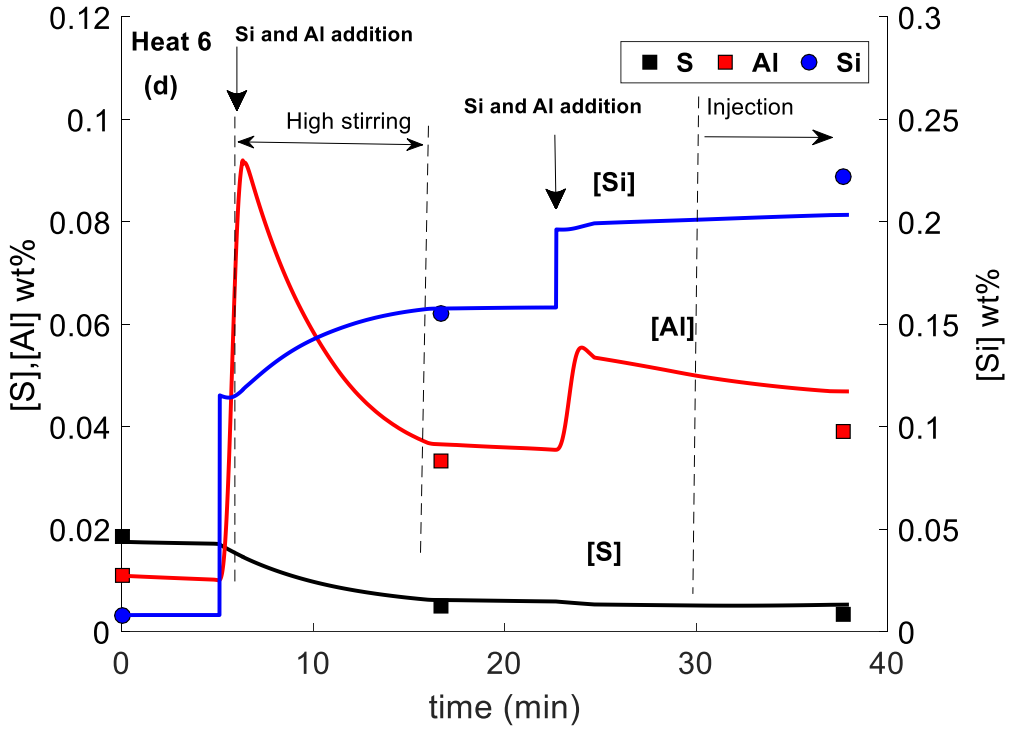
Heat 6
(d)
Si and Al addition
High stirring
Si and Al addition
Injection
S
Al
Si
[Si]
[Al]
[S]
[S],[Al] wt%
[Si] wt%
time (min)
0.12
0.1
0.08
0.06
0.04
0.02
0
0.3
0.25
0.2
0.15
0.1
0.05
0
0
10
20
30
40

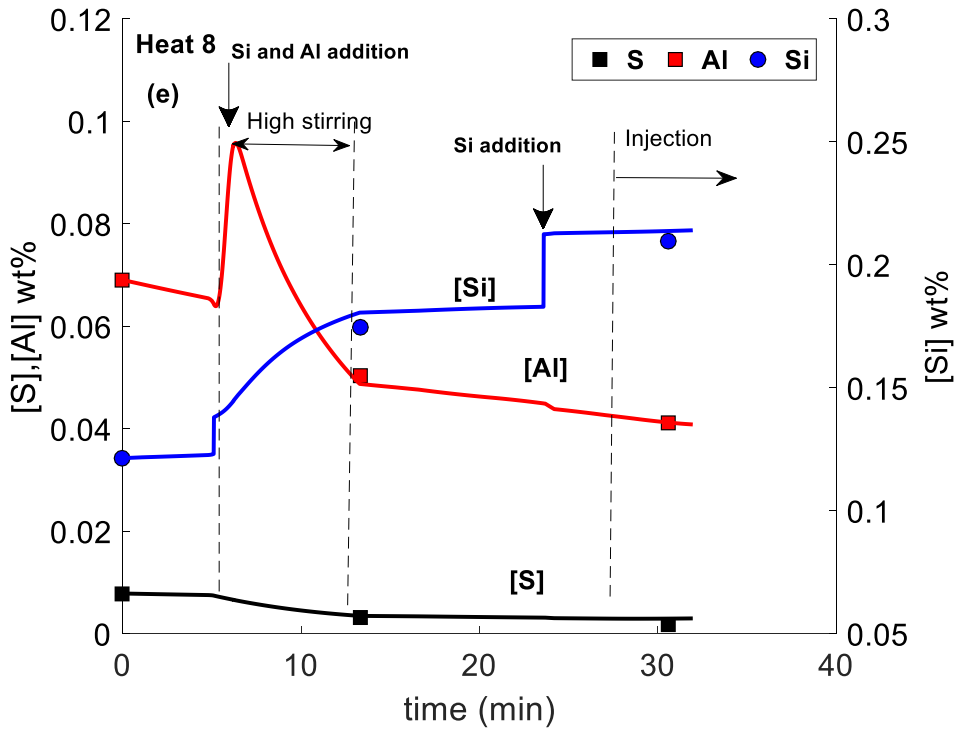
Heat 8
(e)
Si and Al addition
High stirring
Si addition
Injection
S
Al
Si
[Si]
[Al]
[S]
[S],[Al] wt%
[Si] wt%
time (min)
0.12
0.1
0.08
0.06
0.04
0.02
0
0.3
0.25
0.2
0.15
0.1
0.05
0
10
20
30
40

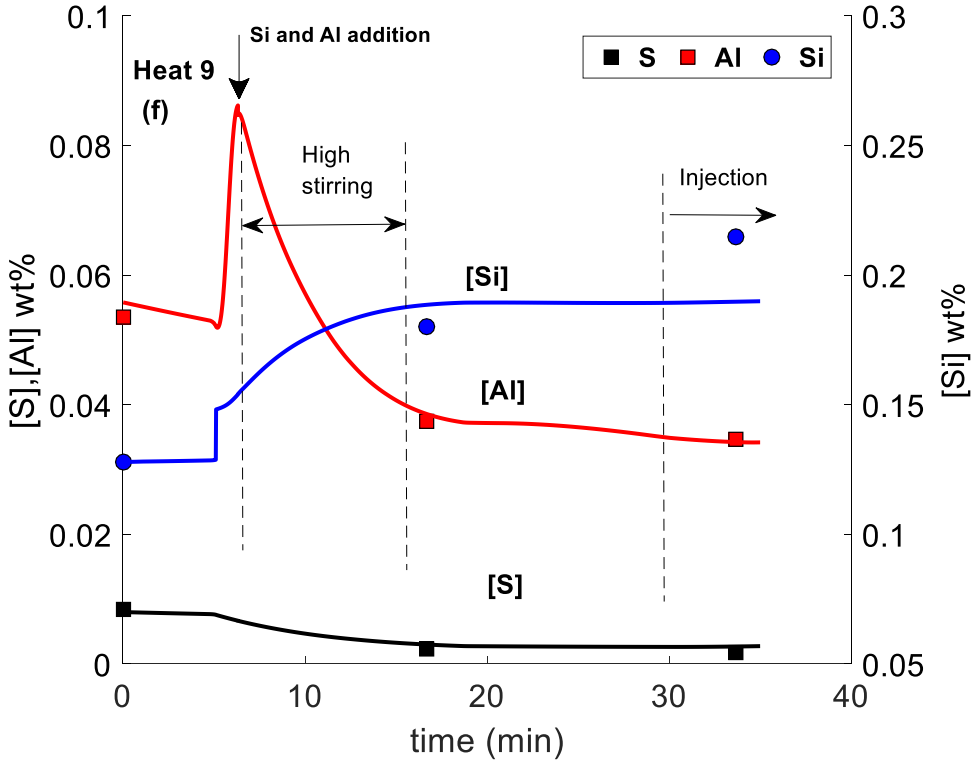
Heat 9
(f)
Si and Al addition
S
Al
Si
High
stirring
Injection
[Si]
[Al]
[S]
[S],[Al] wt%
[Si] wt%
time (min)
0.1
0.08
0.06
0.04
0.02
0
0.3
0.25
0.2
0.15
0.1
0.05
0
10
20
30
40

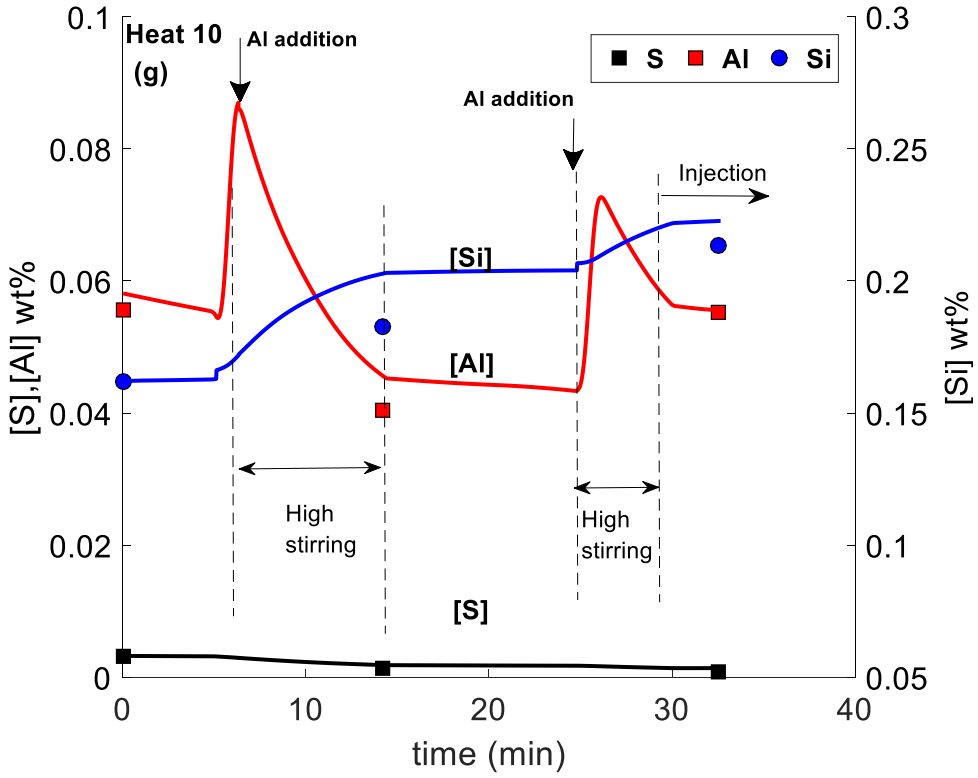
Heat 10
(g)
Al addition
S
Al
Si
Al addition
Injection
[Si]
[Al]
[S]
High
stirring
High
stirring
[S],[Al] wt%
[Si] wt%
time (min)
0.1
0.08
0.06
0.04
0.02
0
0.3
0.25
0.2
0.15
0.1
0.05
0
10
20
30
40

Figure 6-3. Measured and calculated bulk concentrations in the steel phase

Figure 6-4 shows change of bulk concentration of components in the slag phase for Heat 1. Since the measurements for slag chemistry were not available for other heats, the slag chemistry is shown for only this heat, though all heats follow the same trend.

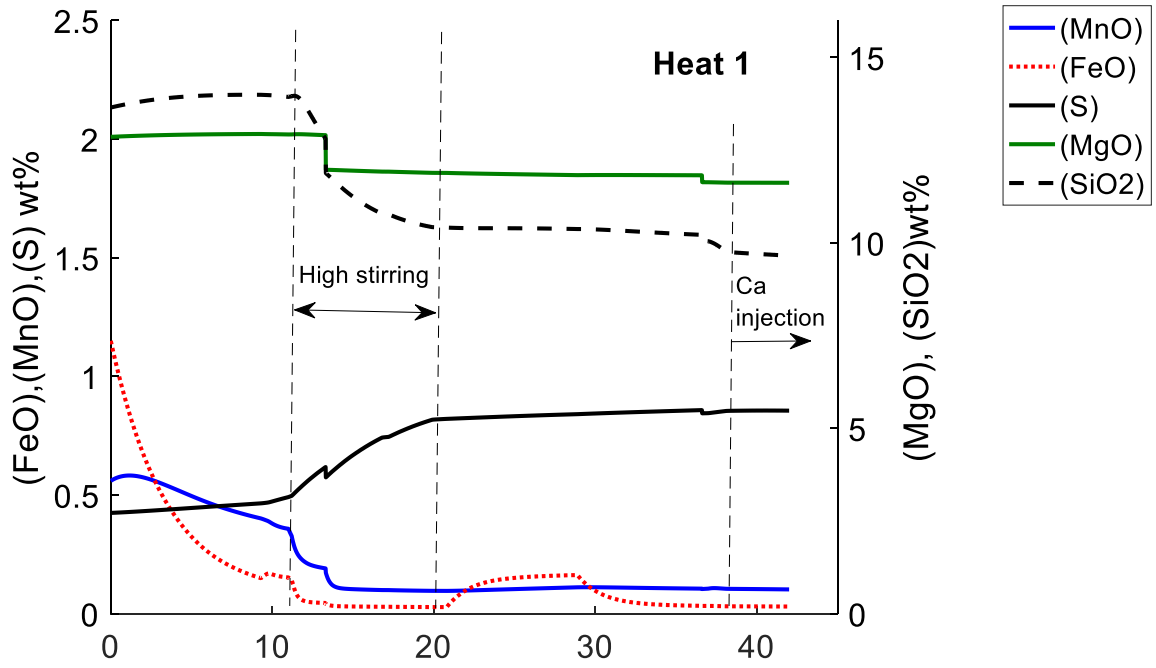

Figure 6-4. Calculated bulk concentrations in the slag phase

From the beginning of the ladle process FeO and MnO content start to decrease because of steel-slag reaction, although the rate is lower before high stirring period. During high stirring the mass transfer in the steel increases which in turn increases reaction at the steel-slag interface and FeO, MnO reduction increases and they finally reach equilibrium. High stirring also promotes desulphurization and reduction of SiO_2 in the slag as it is seen in

Figure 6-4. The sharp drop in the concentration of components in the slag in the middle of high stirring period corresponds to dilution by CaO addition to the slag.

6.3.2 Parametric Study

6.3.2.1 Sulfur content

It is well known that steel with higher sulphur content has a tendency to form solid CaS inclusions. Holappa et al. [23] defined a "liquid window" over a range of temperature inside which liquid calcium aluminate inclusions are stable. At low calcium content, desired low melting temperature calcium aluminates do not form, whereas CaS is formed at high calcium levels.

Lu et al. [8], from their laboratory experiments concluded that higher initial sulphur activity to oxygen activity ratio in the melt favors sulphide inclusion formation, whereas a lower ratio favors oxide formation. But, it should be noted that in their experiments dissolved oxygen content was up to 60 pmm whereas in industrial condition the oxygen concentration is not more than 5 ppm before Ca injection as the steel is aluminum killed. In this circumstance formation of CaS is much more favourable than CaO and amount of CaO produced in negligible. In our previous work [16] it was concluded that most of sulphide inclusions form at the reaction plane. Higher sulphur in the molten steel results in a larger amount of sulphide inclusions which in turn decreases the rate of calcium dissolution in the melt. On the other hand the fundamental kinetic model for alumina transformation [24] showed that rate of modification of alumina inclusions is controlled by rate of supply of calcium to the inclusions. Hence, increasing sulphur content

of the steel adversely affects the modification of inclusions since the injected calcium will be consumed by sulphur rather than alumina.

Figure 6-5 shows the effect of varying sulphur on the rate of transformation of alumina inclusions to calcium aluminate as calculated by the current model. The term $t_{tansformation}$ shows the time required for complete transformation of the alumina core to liquid calcium aluminate when a shrinking core model is assumed. Increasing dissolved sulphur, increases the time required for completion of the transformation as expected.

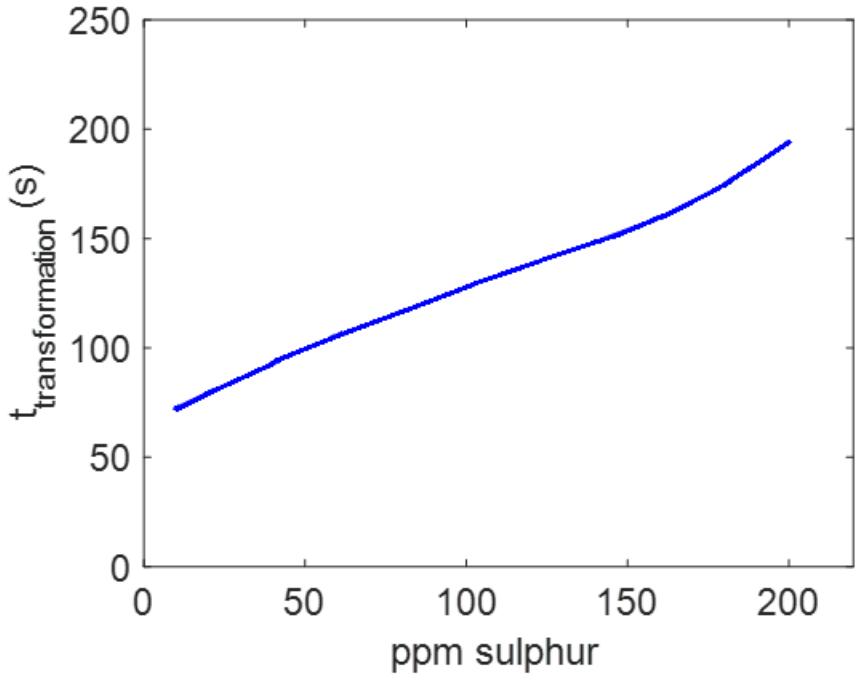

Figure 6-5. Effect of sulfur content of the steel on the modification of alumina inclusions to calcium aluminate (composition of steel and slag are taken from Heat 1)

Figure 6-6 shows inclusion composition from heat 10 and heat 6 which had different sulphur contents before Ca injection. Heat 10 and heat 6 were chosen for this comparison because they have similar Δ[Al], which is the difference between the total aluminum and

dissolved aluminum. Δ[Al] is considered a reasonable estimate of the total oxygen in the steel (mass of inclusion) [8], which might otherwise affect the extent of modification. The extent of modification of inclusions for Heat 10 (with a sulphur content of 13 ppm) is higher compared to Heat 6 (which has a higher sulphur content of 50 ppm) even though 59 ppm total calcium is injected for heat 6 in comparison to 51 ppm for heat 10.

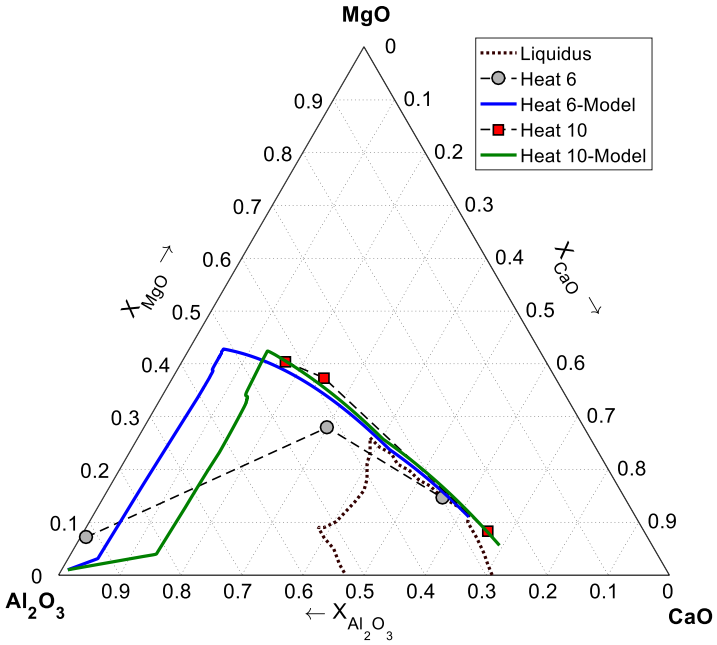

Figure 6-6. Composition of inclusions before and after Ca injection for two heats with different sulphur content before injection

As the heats considered in this study follow very similar operating conditions in terms of oxidation, slag composition and stirring, it is difficult to use the data to investigate the effect of these parameters on inclusion evolution. Hence, in the rest of this paper a parametric analysis of conditions assumed for the steel and slag is presented. The base case for the initial composition of the steel and top slag is presented in Table 6-5 and Table 6-6,

respectively. Unless otherwise stated, 10 min of high stirring is assumed during the ladle process for desulphurization.

Table 6-5. Base composition for steel at the beginning of ladle process (Wt. %)

C	Mn	P	S	Si	Al	N	Fe
0.05	1	0.01	0.01	0.06	0.04	0.005	balance

Table 6-6. Base composition for top slag (Wt. %)

P_2O_5	TiO_2	CaS	FeO	CaO	MnO	SiO_2	MgO	Al_2O_3	Other
0.01	0.3	0.5	2	50	1	8	8	30	0.19

6.3.2.2 **Amount of inclusions**

The initial total oxygen is related to the total amount of the Al_2O_3 inclusions in Al-killed steels as this value consists of the ppm of dissolved oxygen in steel $[O]$ and ppm of oxygen bonded to the oxide inclusions.

Higher total oxygen implies a larger amount of inclusions. Therefore, at constant a Ca injection rate, dissolved calcium is distributed between larger numbers of inclusions which implies a lower transformation rate since the rate of modification is controlled by rate of Ca supply which is determined by mass transfer coefficient of calcium from bubbles through boundary layer and interfacial area of bubbles. $k_{Ca,L} \times A_{B,L}$ was determined to be $0.37 \times 10^{-4}\ S^{-1}$ in previous work [16]. The effect of total oxygen on the trajectory of inclusion composition during ladle processing is presented in Figure 6-7. As the number of particles decreases due to the lower total oxygen assumed it implies that a similar amount of Mg provided by the slag is distributed among the fewer inclusions in the system.

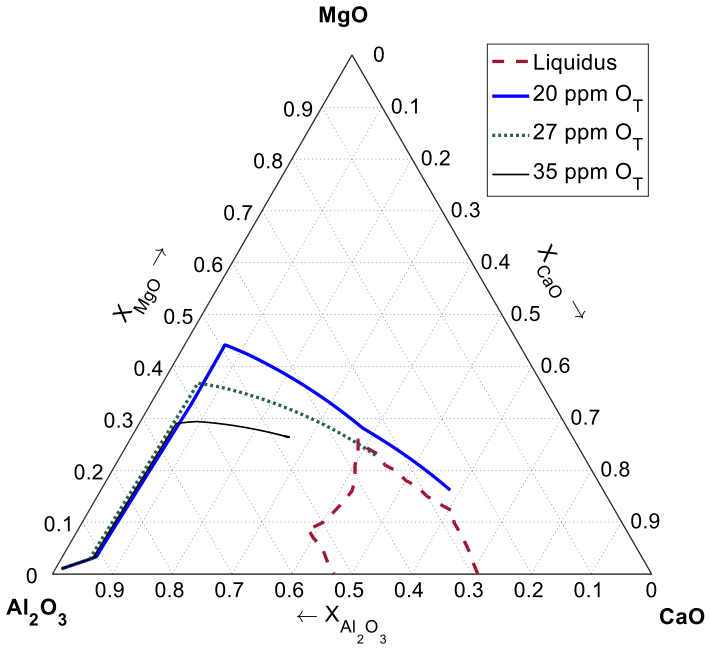

Figure 6-7. Effect of total oxygen on trajectory of inclusion modification during ladle process

With the same stirring intensity, the Mg pick up from the slag is the same. Therefore, steel with a smaller mass of oxide inclusions induces a higher amount of Mg pick up and spinel formation in the inclusions as [Mg] released from the slag is distributed among fewer particles. Also, with the same amount of Ca injected, having higher amount of inclusions lowered the calcium content of inclusions. Thus, to reach the liquid region, a higher amount of Ca is required. In a study by Sun et al. [8] a "Ca treatment index" was developed which is the ratio of total calcium in the melt to the difference between the total aluminum content and soluble aluminum in the steel. It was found that Ca treatment index was a reasonable predictor of the calcium requirement for modification of inclusions in each heat. The foregoing observations are consistent with the findings of Sun et al. [22].

6.3.2.3 Size of inclusions

Most of the indigenous inclusions detected by automated SEM analysis were in the range of 1 to 5 microns diameter. Given this situation, the size of alumina inclusions was varied in the model from 2 to 5 microns to analyze effect of size on the inclusion modification rate.

The effect of size of alumina inclusions on the rate of alumina transformation is shown in Figure 6-8. For this calculation, the total oxygen is kept constant, i.e. the number of inclusions is changed so that the total mass of alumina inclusions is the same.

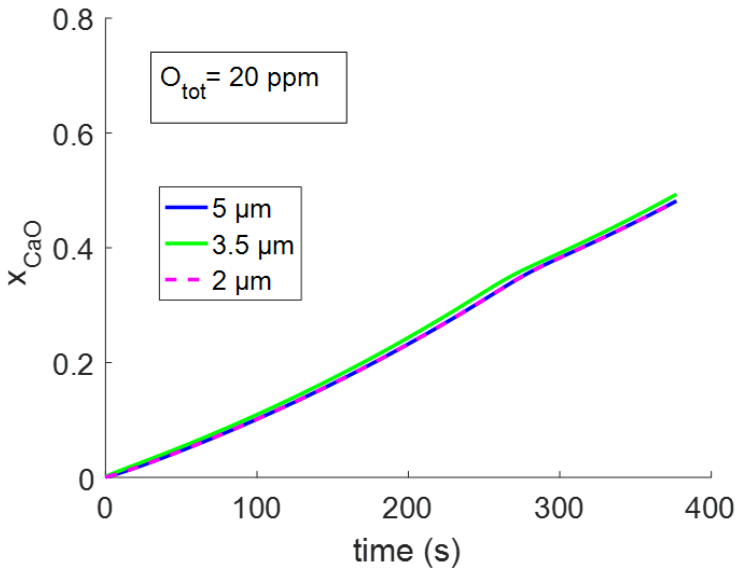

Figure 6-8. Effect of size of alumina inclusions on the rate of modification of alumina by calcium

As is seen in Figure 6-8, changing the size of inclusions while the total mass is constant, does not change the rate of transformation. This result is consistent with previous findings by the authors [24] that the rate of modification of alumina inclusions is controlled by rate of supply of calcium to the inclusions. Hence, when the calcium injected into the steel

reaches the inclusions the reaction is effectively instantaneous. This observation has a beneficial practical use for modeling that it is not necessary to know the exact size distribution of the inclusions to predict the modification rate. If the total mass of inclusions is known, the rate of transformation can be estimated. However previous work by the authors (see Figure 5-3, in Chapter 5 of this thesis), it is clear that all inclusions do not transform at the same rate because at any given time there is a wide range of inclusion compositions. One explaination of this observation that is consistent with the modelling results is that some of these inclusions are formed by minor reoxidation event which means they would not be present a throughout calcium injection and would only be modified by residual calcium. The earlier inclusions formed the more time and calcium would have been available for modification.

6.3.2.4 **Stirring**

In this analysis the stirring intensity is varied while keeping all other parameters constant at base case conditions i.e. Table 6-5 and Table 6-6. The results for the variation of oxide inclusion evolution is shown in Figure 6-9. 'High stirring' in Figure 6-9 refers to the base case with 10 min of high stirring (25 Nm^3/h/plug), whereas 'low stirring' refers to the case in which the stirring was assumed to be 5 Nm^3/h/plug throughout process.

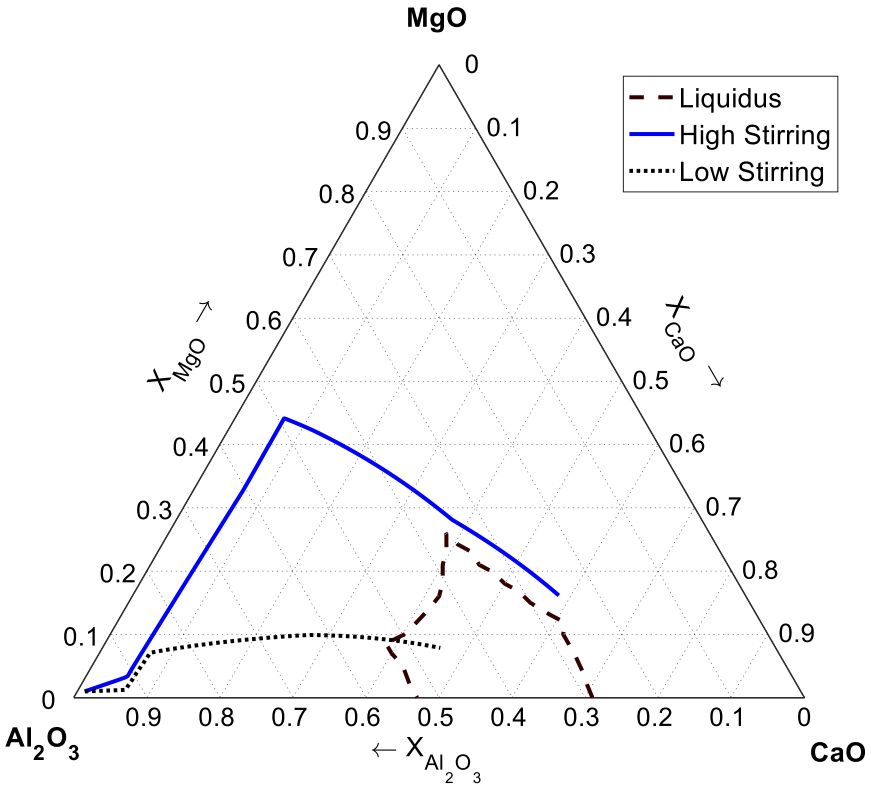

Figure 6-9. Effect of stirring on the modification path

The inclusions under low stirring remain mainly as alumina with a very small amount of magnesium (approximately 0.1 mole fraction) before Ca injection, while with a high stirring the transformation to spinel in the particles is much closer to completion. This is expected as high stirring enhances mass transfer of species in the molten steel which in turn increases the reduction of species in the slag such as MgO. On the other hand the reversion of Si is more pronounced in the high stirring regime as it is seen in Figure 6-10. These results are consistent with the industrial evidence that the pickup of [Si] is linked to an increase in the formation of spinel [5]. Under low stirring, desulfurization is slow leading to a higher sulfur content of the steel before calcium injection as shown in

Figure 6-10. Thus, the modification of inclusions is very sensitive to stirring rate. Higher sulphur content in the steel causes formation of larger amount of sulphides during injection which delays modification of inclusions as discussed in section 6.3.2.1. Figure 6-11 demonstrates total calclum and Ca in form of sulphides in the steel for low and high stirring cases. As it is seen in Figure 6-11 to reach the 100% liquid area 90 ppm Ca is required for heats employing low stirring, whereas for heats involving 10 minutes of high stirring only 50 ppm is sufficient. The amount of CaS formed is also almost twice in the case of low stirring compared to high stirring heats. It is worth noting that the total calcium pickup is higher for low stirring heats because the higher sulphur concentration in these heats will lead to an enhanced rate of calcium pick-up but not to more efficient calcium use. In summary, stirring intensity has multiple simultaneous effects on Si reversion, desulphurization and inclusion modification all of which have to be taken into account in optimizing the process.

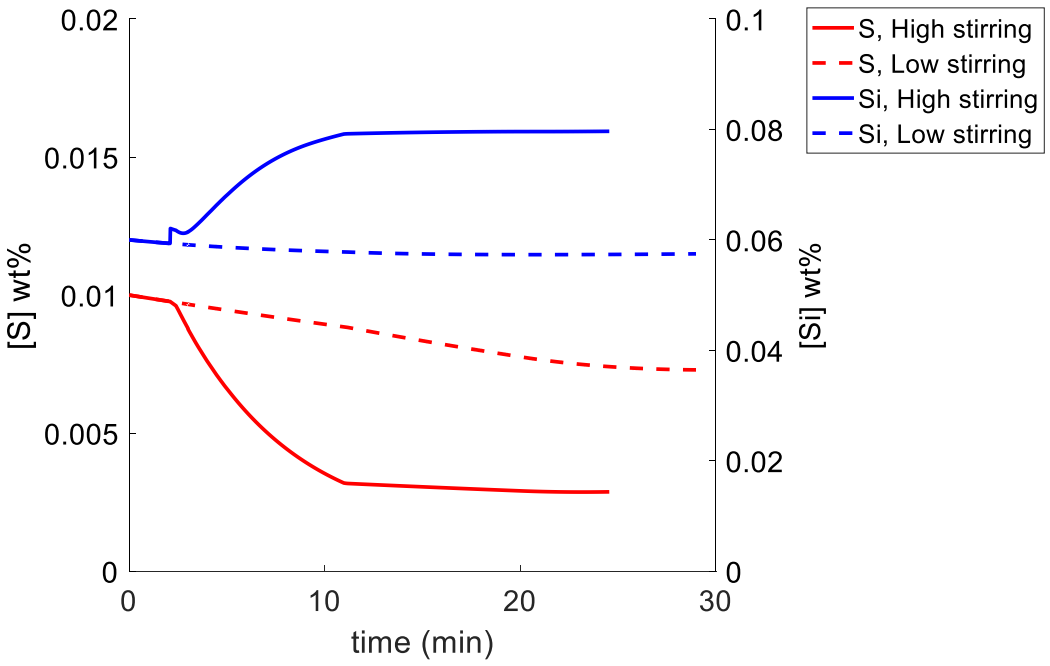

Figure 6-10. Sulfur and silicon content during ladle process for low and high stirring

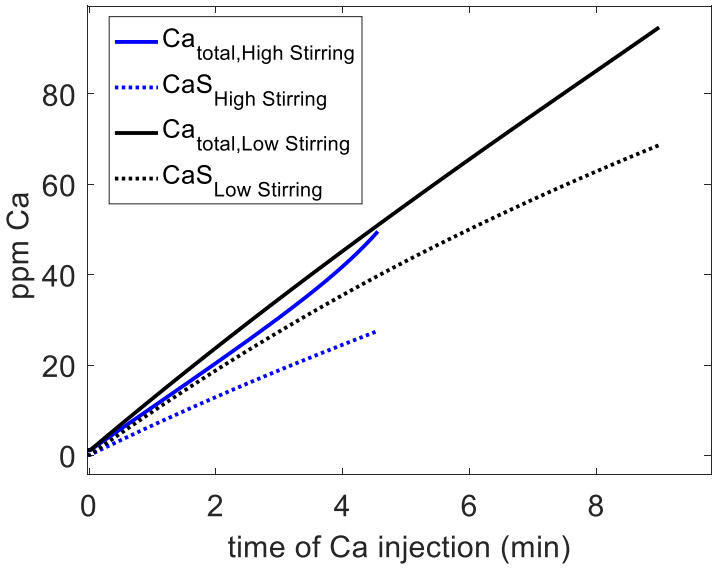

Figure 6-11. Total Ca and Ca in form of sulphides for low and high stirring heats

6.3.2.5 Slag composition

6.3.2.5.1 FeO and MnO

To analyze oxidation potential of the slag on the evolution path of inclusions, the initial slag composition was modified from the base case as listed in Table 6-7 with different $FeO + MnO$ contents. The compositions were chosen to maintain an initial ratio of $\frac{FeO}{MnO} \approx 2$.

Table 6-7. Initial slag composition in wt. % with different oxidation potential

	P_2O_5	TiO_2	CaS	FeO	CaO	MnO	SiO_2	MgO	Al_2O_3	Other	$(FeO + MnO)$
A	0.01	0.3	0.5	1	51	0.5	8	8	30.5	0.19	**1.5**
B	0.01	0.3	0.5	2	50	1	8	8	30	0.19	**3**
C	0.01	0.3	0.5	4	48	2	8	8	29	0.19	**6**

The effect of oxidation level of the slag on evolution of inclusions is shown in Figure 6-12.

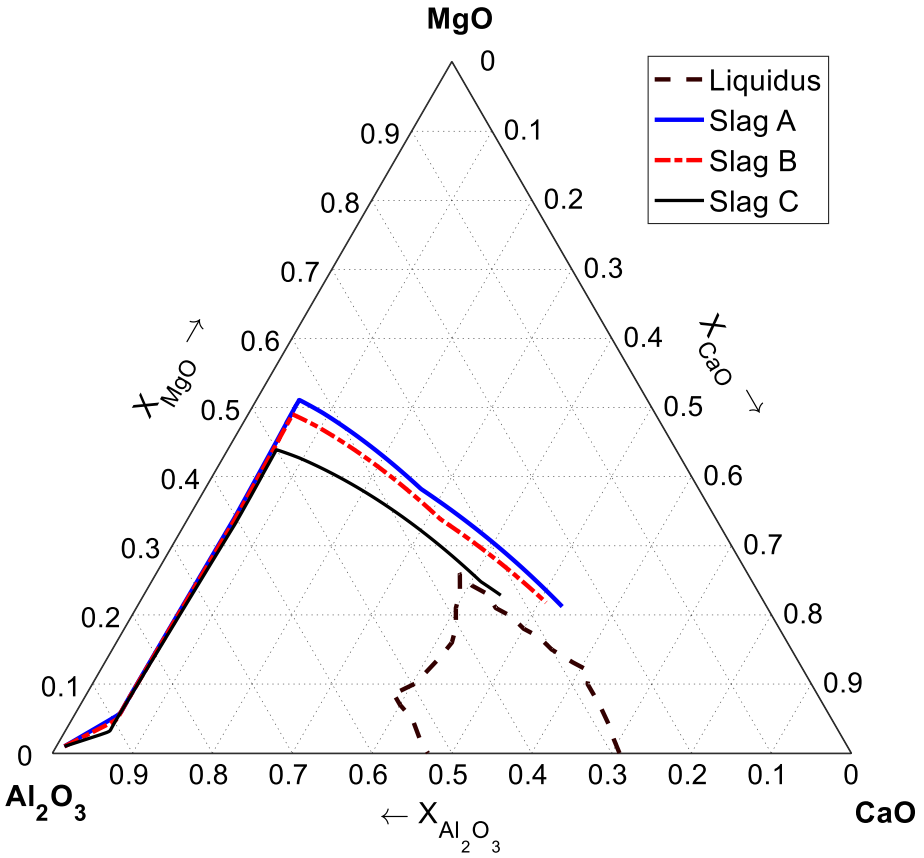

Figure 6-12. Effect of oxidation level of the slag on the evolution of inclusions

With decreasing initial oxidation potential of the slag, the Mg content of the spinel is slightly higher, although the effect is not significant. The respective slag reduction progress is presented in Figure 6-13. At higher oxidizing conditions in the slag, the aluminum reacts with the FeO and MnO instead of MgO which delays release of Mg into the steel. It also results in higher total oxide contents which will take longer to modify. Lower dissolved magnesium in the steel makes alumina inclusions more stable than spinel. However, having high stirring intensity and giving enough time, concentration of FeO and MnO eventually

reach equilibrium as shown in Figure 6-13. Increase in FeO content of the slag at 9 min and 21 min corresponds to arcing which leads to oxidation of Fe and formation of FeO.

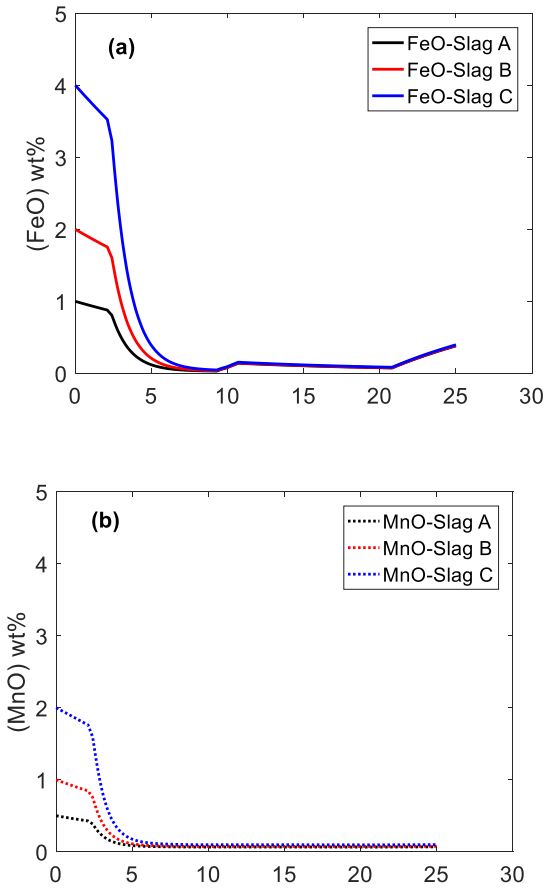

Figure 6-13. Slag deoxidation progress (a) FeO (b) MnO

6.3.2.5.2 MgO

As mentioned earlier, reduction of magnesia in the slag by aluminum in the steel is the primary source of magnesium in the steel. Hence, a higher concentration of MgO in the slag leads to more dissolved magnesium in the steel which in turn transforms alumina inclusions to magnesium aluminate spinel. Figure 6-14 shows the predicted trajectory of inclusion modification for three slags with different initial MgO content as described in.

Table 6-8. Initial slag composition in wt. % with different MgO content

	P_2O_5	TiO_2	CaS	FeO	CaO	MnO	SiO_2	MgO	Al_2O_3	Other
D	0.01	0.3	0.5	1	50	0.5	8	**8**	30	0.19
E	0.01	0.3	0.5	4	51.5	2	8	**5**	30.5	0.19
F	0.01	0.3	0.5	4	53	2	8	**2**	33	0.19

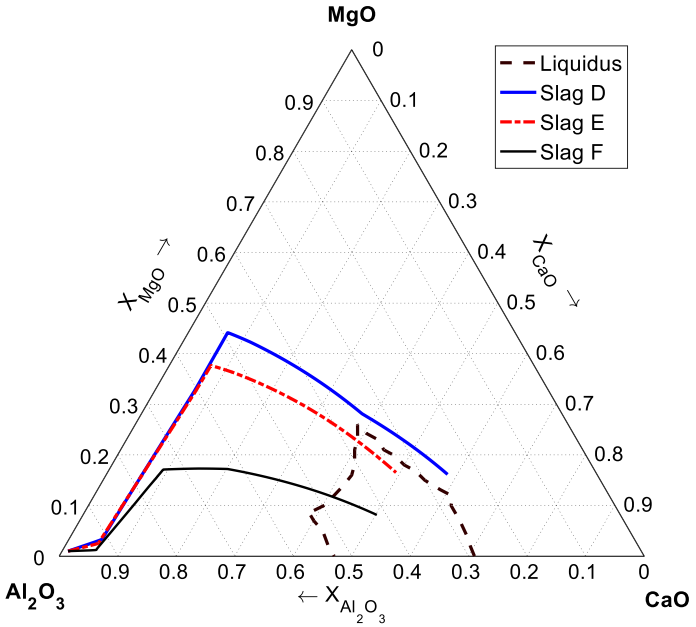

Figure 6-14. Effect of MgO in the slag on modification of alumina inclusions

The results indicate a decrease in the amount of spinel with decreasing initial MgO in the slag as expected. Change of slag MgO is unlikely to have a drastic effect on the

desulphurization process suggesting that control over the MgO content of the slag can help to reduce spinel formation. Harada, et al. [14] came to similar conclusions.

6.3.2.6 **Reoxidation**

Figure 6-15 shows the effect of reoxidation of molten steel on the composition of inclusions after calcium treatment. For this calculation, it was assumed that dissolved oxygen in the steel is increased up to approximately 5 ppm. It is seen that with increasing dissolved oxygen in the steel, oxygen reacts with dissolved aluminum and magnesium which in turn increases alumina mole fraction in the inclusions. The change of the total number moles of components in the $CaO - Al_2O_3\_MgO$ inclusions is presented in Figure 6-16.

Pretorius et. al. [25] stated that any increase in the oxygen potential of the steel due to reoxidation after Ca injection could lead to secondary spinel formation. The present work shows that reoxidation can also change the composition of primary liquid magnesium calcium aluminate inclusions to form spinel.

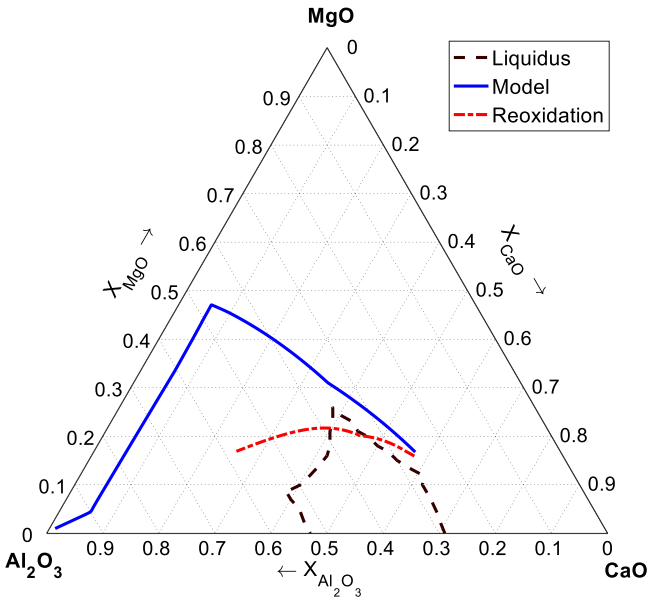

Figure 6-15. Effect of reoxidation on composition of oxide inclusions after calcium treatment

In another study by Pretorius et al. [5] the reoxidation of steel by thermodynamic calculations was investigated using FactSage. They showed that by increasing amounts of oxygen in the steel bulk composition of inclusions changes toward higher alumina and magnesia similar to the finding of the current study.

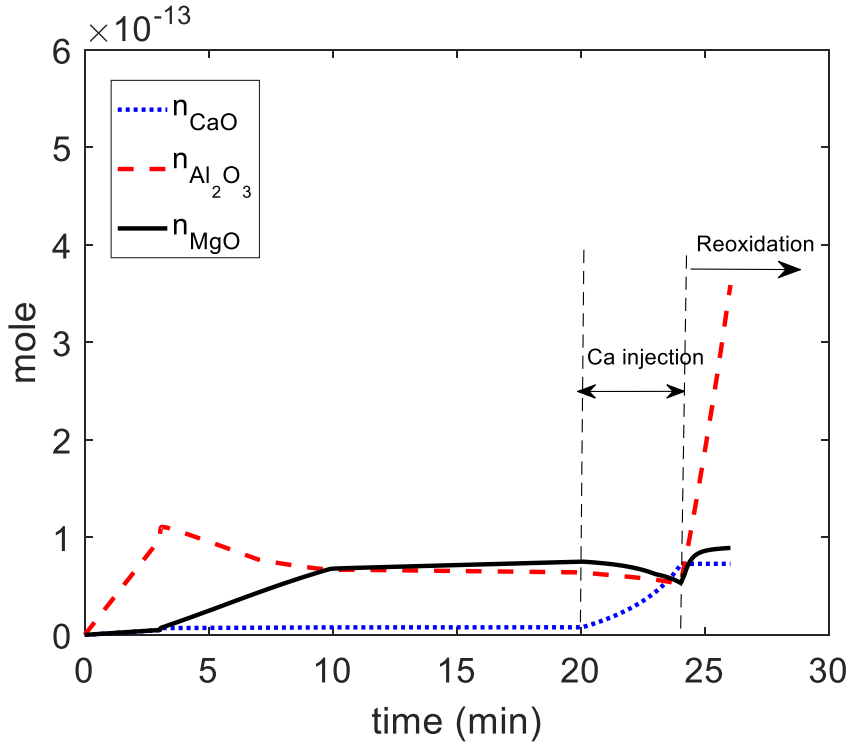

Figure 6-16. Change of components in the oxide inclusions during Ca injection and reoxidation

6.4 Conclusions

A kinetic model to simulate the reactions among slag, steel and inclusions in a ladle furnace was developed. In the present work, the influence of different parameters on modification of inclusions before and during calcium treatment was studied to offer better control of inclusions in the ladle furnace. The following conclusions are derived:

1. Higher sulphur content of the steel before calcium injection suppresses the modification of alumina inclusions as the calcium will be consumed by sulfur rather than alumina inclusions.

2. With increasing total oxygen which reflects the total amount of alumina inclusions, at the same injection conditions, rate of transformation of inclusions decreases.

3. Changing the size of inclusions while the total amount of inclusion is kept constant, does not affect the rate of transformation.

4. Higher stirring enhances reduction of MgO in the slag which in turn provides more dissolved Mg for the inclusions and increase the Mg content of spinel inclusions.

5. Higher oxidation potential of the slag leads to formation of spinel with higher alumina content.

6. Higher MgO content of the slag promotes formation of spinel with higher Mg content

7. Reoxidation of steel which increases dissolved oxygen in the steel can cause change of composition of inclusions towards higher alumina content.

6.5 References

[1] S. Abdelaziz, G. Megahed, I. El-Mahallawi, and H. Ahmed: Ironmak. Steelmak., 2009, vol. 36, pp. 432–41.

[2] T. Nishi and Kaoru Shinme: Tetsu-to-Hagane(Journal Iron Steel Inst. Japan), 1998, vol. 84, pp. 837–43.

[3] G. Okuyama, Koji Yamaguchi, Syuji Takeuchi, and Ken-ichi Sorimachi: 2000, vol. 40, pp. 121–28.

[4] K. Mizuno, H Todoroki, M. Noda, and T. Tohge: Iron Steelmak., 2001, vol. 28, pp. 93–101.

[5] E.B. Pretorius, H.G. Oltmann, and B.T. Schart: AISTech 2013 Proc., 2013, pp. 993–1026.

[6] K. J. Graham and G. A. Irons: in Int. Symp. Highly Innov. Nov. Oper. "Future Steelmak. Metall., 2010, pp. 65–74.

[7] G. J. W Kor: in Steelmak. Conf. Proc., 1989, pp. 39–44.

[8] D. Lu, G. A. Irons, and W. Lu: Ironmak. Steelmak., 1994, vol. 21, pp. 362–72.

[9] Z. Han, L. Liua, M. Lind, and L. Holappa: Acta Metall. Sin., 2006, vol. 19, pp. 1–8.

[10] Y. Higuchi, M. Numata, Sh. Fukagawa, and K. Shinme: ISIJ Int., 1996, vol. 36, pp. 151–54.

[11] T. Lis: METALURGIJA, 2009, vol. 48, pp. 95–98.

[12] S. K. Choudhary and A. Ghosh: ISIJ Int., 2008, vol. 48, pp. 1552–59.

[13] H. Visser, R. Boom, and M. Biglari: ATS Int. Steelmak. Conf., 2008, pp. 172–80.

[14] A. Harada, N. Maruoka, H. Shibata, and Sh. Kitamura: ISIJ Int., 2013, vol. 53, pp. 2110–17.

[15] M. A. Van Ende and In Ho Jung: Metall. Mater. Trans. B Process Metall. Mater. Process. Sci., 2016, vol. 48, pp. 1–9.

[16] Y. Tabatabaei, K. S. Coley, G. A. Irons, and S. Sun: Metall. Mater. Trans. B, 2018, Volume 49, pp 2022–37.

[17] Y. Tabatabaei, K.S. Coley, G. A. Irons, and S. Sun, 2018, https://doi.org/10.1007/s11663-018-1354-0.

[18] J. Szekely and N. J. Themelis: Rate Phenomena in Process Metallurgy, 1st Ed., Wiley-Interscience, New York, 1971.

[19] F. Oeters: Metallurgy of Steelmaking, 1st Ed., Düsseldorf: Verlag Stahleisen, 1994.

[20] S. Ohguchi, D.G.C. Robertson, B. Deo, P. Grieveson, and J.H.E Jeffes: Ironmak. Steelmak., 1986, vol. 11, pp. 202–13.

[21] F. Schamber: Introduction to Automated Particle Analysis by Focused Electron Beam, 2009.

[22] S. Sun, S. Waterfall, N. Strobl, D. Liao, and D. Holdridge: in 8th Int. Symp. High-Temperature Metall. Process., 2017, pp. 347–57.

[23] L. Holappa, M. Hämäläinen, M. Liukkonen, and M. Lind: Ironmak. Steelmak., 2003, vol. 30, pp. 111–15.

[24] Y. Tabatabaei, K. S. Coley, G. A. Irons, and S. Sun: Metall. Mater. Trans. B, 2017, vol. 49, pp. 375–87.

[25] E. B. Pretorius, H.G. Oltmann, and T. Cash: Iron Steel Technol., 2010, vol. 7, pp. 31–44.

[26] M. L. Kapoor and M. G. Frohberg: in Chem. Metall. Iron Steel, 1971, pp. 17–22.

[27] H. Gaye and J. Welfringer: in Second Int. Symp. Metall. Slags Fluxes, 1984, pp. 357–75.

[28] K. J. Graham and G. A. Irons: in AISTech - Iron Steel Technol. Conf. Proc., Pittsburgh, PA, 2008, pp. 5–13.

[29] K. Graham: Ph.D thesis, McMaster University, 2008.

[30] D. G. C. Robertson, B. Deo, and S. Ohguchi: Ironmak. Steelmak., 1984, vol. 11, pp. 41–55.

Chapter 7

Summary and conclusions

7.1 Summary and contributions

The main objectives of this project were to understand modification of inclusions during ladle process. A kinetic model for inclusion evolution before and during calcium treatment in the Ladle Metallurgy Furnace was developed. By coupling of the 'inclusion model' to previous kinetic models for the slag-steel reactions and injection of calcium, a comprehensive model for ladle furnace was developed, which allowed prediction of trajectory of average inclusion composition as well as steel and slag during ladle process. These objectives were achieved as demonstrated in Chapter 3, Chapter 4 and Chapter 5. The important outcomes of this work are:

In Chapter 3, a fundamental multi-layer kinetic model was developed for predicting modification of alumina inclusions to calcium aluminate in the liquid steel. This model considers mass transfer in the steel and diffusion through a multi-phase product layer. A sensitivity analysis of this model examining the effect of a two order of magnitude change in, diffusion in the solid product layers, diffusion in the liquid calcium aluminate and mass transport in the liquid steel as well as a change in calcium concentration in the steel, demonstrated that the only significant factors in controlling the rate of transformation were mass transport in the liquid steel and concentration of calcium in the steel. These observations, which are consistent with the fact that experimental studies of calcium treatment did not find multiple product layers on the surface of partially transformed

inclusions, justified the use of a simplified inclusion transformation model for use in combination with the steel/slag kinetic model and the calcium injection model (Chapter 4). It is also worth noting that in none of the cases tested, was the time for transformation as long as that found in calcium treatment of steel and that the effect of calcium concentration was greater than any of the other parameters tested. The last two findings suggested that the rate determining step for calcium treatment of alumina, is most likely to be controlled by calcium supply to the steel, rather than transport within the inclusion or in the boundary layer in the steel surrounding the inclusion. This particular hypothesis is consistent with previous work in the author's laboratory and was explored in more detail in Chapter 4.

Chapter 4 presents details of the coupled kinetic model for slag-steel-inclusion reactions. The kinetic model developed in Chapter 3 was coupled with a model for calcium injection from Lu et al. [1] which allowed simultaneous calculation of rate of transformation of alumina inclusions and formation of calcium sulphide and calcium oxide inclusions. The kinetic model for inclusions and calcium injection was also combined with the model developed for slag-steel reactions by Graham and Irons [41]. The only parameter fitted to the current data, was the $k_{Ca,L} \times A_{B,L}$ for calcium in the bubble plume. The comprehensive coupled model successfully predicted the rate of alumina modification, sulphide inclusion formation and steel composition change before and during Ca treatment showing excellent agreement with data from plant trials. The results showed that due to the huge interface of inclusions and fast reaction of inclusions with dissolved calcium shown in Chapter 3, any calcium supplied to the steel from calcium bubbles instantly reacts with alumina inclusions to form calcium aluminates. Hence, the dissolved calcium in the steel

reaches a very low concentration in equilibrium with inclusions. The model also showed that due to the high affinity of calcium for sulphur and oxygen, most of the calcium diffusing from the Ca bubbles to the steel reacts with dissolved sulphur and oxygen at the calcium injection plume to form sulphide and oxide inclusions and only a small fraction dissolves to the steel. Typically, because the dissolved oxygen is extremely low in Al-killed steel, the amount of oxide inclusions formed at the plume is very limited. The model matched the reduction of calcium from slag during strong stirring period which is sufficient for partial modification of alumina inclusions to calcium aluminate as observed in ArcelorMittal Dofasco plant data and by other researchers [46,49]. The distribution of sulphide and oxide inclusions as well as total calcium were also calculated by the model which showed good agreement with plant data. One interesting observation was that after 2 min of Ca injection calcium aluminate inclusions reached saturation with respect to CaO (which was considered in the model) and further calcium injection led to calcium sulphide formation. As the current model runs fast enough and due to similarity of worldwide operations, with only fine adjustment to local conditions, it can be used in wide range industrial plants for process control.

It should be noted that in real industrial conditions pure alumina inclusions are rarely observed immediately before calcium treatment. Alumina inclusions always react with dissolved magnesium provided by reduction of MgO in the slag or other sources such as refractories, to form magnesium spinel inclusions. These inclusions may also transform by reaction with calcium to form liquid magnesium calcium aluminates.

Chapter 5 addresses the evolution of oxide inclusions from the first formation of alumina, to spinel formation by reaction between the alumina inclusions and magnesium reduced from the slag, to final modification of the spinel by calcium injection. The model includes the slag metal kinetic model and the calcium injection model discussed in Chapter 4 which are combined with an inclusion transformation model. The inclusion transformation model includes formation of spinel from alumina and modification of the spinel by calcium. Both spinel formation and transformation to calcium aluminate are reversible and in competition with each other. A shrinking core model was assumed considering mass transfer of solute (Mg, Ca, Al and O) through the liquid steel boundary layer to and from the inclusion and diffusion within the product layer formed on the surface of the inclusion. The mechanism of calcium modification of spinel was found to be reduction of MgO in the inclusions by dissolved Ca in the steel. A sensitivity analysis was also carried out to examine the importance of diffusion in liquid product layer, mass transfer through the boundary layer and concentration of dissolved solutes in the steel on the rate of modification. Change of diffusion coefficient by an order of magnitude in the boundary layer changes the rate approximately by the same order of magnitude, whereas varying of diffusion coefficient in product layer by two orders of magnitude did not change the rate of transformation. Thus, the conclusion with respect to rate controlling step was similar to finding in Chapter 3, that rate of spinel modification was controlled partially by calcium supply to the steel and partially by Mg and Ca exchange by transport through the boundary layer between the steel and the inclusion. This conclusion is consistent with finding by Galindo [42] for formation of spinel inclusions from reaction of alumina with

dissolved magnesium. The sensitivity analysis in the present work demonstrated that the rate of transformation of spinel is controlled by mass transfer through boundary layer and rate of supply of calcium and removal of magnesium. Therefore, modification of spinel inclusions with calcium was found to be more difficult than that of alumina since dissolved magnesium in the steel reaches equilibrium with inclusion and makes it more difficult to reduce MgO from spinel inclusions. It was also found that the composition of the product layer varies with relative flux of Al, Mg, Ca and O from the steel through the boundary layer. Higher dissolved magnesium in the steel resists the flux of magnesium through the boundary layer decreasing the rate of calcium modification and increasing the concentration of MgO in the liquid product. This is also the case for aluminum. However, effect of calcium on transformation is different. According to the $CaO - Al_2O_3\_MgO$ phase diagram, the composition of the liquid product layer in equilibrium with spinel lies on a line approximately parallel to the $Al_2O_3 - MgO$ side of the diagram, which means changing calcium concentration in the melt has a little influence on the trajectory of the inclusion composition, although it changes the rate of transformation.

The overall inclusion-steel- slag coupled model developed in Chapter 5 was verified against one heat from ArcelorMittal Dofasco. In Chapter 6 the comparison with industrial data was extended to several additional heats with a range of characteristics. The average composition of inclusions during ladle processing as well as change of concentration of dissolved species and rate of desulphurization was predicted with excellent agreement. A sensitivity analysis of the coupled kinetic model for the slag, steel and inclusions was performed to compare the effect of the different processing conditions in the ladle furnace

on evolution of inclusions. The results confirm the finding from Chapter 4 with regards to effect of ratio of amount of alumina inclusions to rate of supply of both magnesium and calcium on transformation of inclusions. It was found that higher sulphur content in the steel can delay modification of inclusions which is also suggested by other authors as described in Chapter 2. The analysis revealed the significance of stirring intensity on the evolution of inclusion composition. The model demonstrated that the stirring has influence on composition of inclusions in two different ways: a) changing the rate of slag-steel reaction which in consequence changes the rate of supply of Mg from the slag to the steel affecting formation of spinel inclusions and b) rate of desulphurization that leads to different sulphur concentration in the steel at the start of Ca treatment. The effect of composition of slag in terms of oxidation level and MgO content on evolution of inclusions composition was examined. The results showed that change of composition of slag directly affects composition of inclusions in the steel which again confirms the close link among slag, steel and inclusions in the ladle furnace. Higher oxidation levels of slag hinder reduction of MgO by aluminum in the steel which in consequence decreases the Mg content of the inclusions. Also, reducing MgO content of the slag directly leads to decrease in the Mg fraction in the inclusions. Reoxidation of steel can change the composition of inclusions as it increase dissolved oxygen in the steel. Due to high dissolved content of the steel, dissolved oxygen in the reacts with aluminum to increase alumina in the inclusions.

7.2 Specific Findings

Theoretical analysis based on a model of the ladle furnace combining slag metal reactions, with calcium injection and inclusion transformation has been combined with

analysis of industrial data to elucidate the kinetics of modification of oxide inclusions and formation of sulphide inclusions in the ladle furnace. The project objectives proposed in section 1.2 were achieved. The key conclusions from this research project are:

1. A fundamental model developed for alumina transformation to calcuium aluminate in Chapter 3 showed that for a single alumina inclusion in a steel mass transport through the steel inclusion boundary layer and concentrations of dissolved species have a significant effect on the rate control for the aluminate transformation and the influence of diffusion within the inclusion is negligible. It was also found that the control through the boundary layer is mixed between oxygen, aluminum and calcium transport, and complicated by the imposed equilibria amongst CaO and $Al_2 0_3$ in the phase at the surface and dissolved Ca, Al and O.

2. Based on the multi-layer kinetic model and using the accepted literature values for the transport properties, modification of alumina to liquid calcium aluminate is extremely fast and the reactions of the inclusion is complete within a few seconds. This suggests that:

    a) Due to a large number of inclusions with enormous interfacial area in the steel, the bulk steel composition will closely follow equilibrium with inclusions.

    b) If calcium is sufficiently available, an alumina inclusion will transform rapidly to generate as much liquid calcium aluminate as possible.

c) The multi-layer model could be replaced by simple one-layer model of growth of the liquid calcium aluminate layer with little loss of accuracy.

3. The coupled slag-steel-inclusion model presented in Chapter 4 showed that modification of alumina inclusions is controlled by the rate of supply of calcium to the melt. Hence, the inclusions consume the injected calcium so rapidly that the dissolved calcium reaches a fairly constant low value approximately 0.1-0.2 ppm during calcium treatment.

4. Comparing results of modeling with plant data in Chapter 4 demonstrated that:

   a) Calcium transferred from the slag especially during high stirring period could be sufficient to partially modify alumina inclusions to calcium aluminate.

   b) The rate of steel slag reactions during calcium injection is increased due to the contribution of Ca injection to stirring in addition to that of argon.

   c) By assuming that formation of CaS inclusions occurs only at the injection plume, the model offers remarkable prediction sulfide formation determined using plant data, hence it can be concluded that most CaS is formed at the plume.

5. In Chapter 5 a shrinking core kinetic model was developed for modification of spinel by calcium. The model showed that:

a) The rate control for spinel modification by calcium treatment is mixed between mass transport of magnesium and calcium through the steel inclusion boundary and rate of supply of solutes to the bulk steel.

b) A small concentration of calcium, less than 1 ppm, is sufficient to modify spinel inclusions to liquid magnesium calcium aluminate.

c) The composition of magnesium calcium aluminate produced by reaction of Ca with spinel as well as rate of transformation is influenced by concentration of dissolved Ca, Mg, Al and O in the steel, although the magnitude of the effect of each species is different. Higher concentrations of dissolved Mg and Al in the steel induces liquid magnesium calcium aluminate with higher content of magnesium and aluminum respectively. Whereas changes to the Ca concentration only slightly changes the composition of liquid product.

6. Sensitivity analysis for the variation of the process parameters in the ladle furnace Chapter 6 concluded that:

a) Higher sulphur content of the steel before injection induces higher consumption of calcium by sulfur rather than alumina inclusions which delays the modification of alumina inclusions.

b) The rate of Ca supply in relation to the mass of inclusions determines rate of modification. So, under the same injection conditions, increasing the total mass of alumina inclusions reduces rate of transformation of

the inclusions, while changing the size of inclusions for the same total mass of inclusions, does not affect the rate of transformation.

c) The rate of supply of Mg from the slag to the steel controls the Mg content of inclusions prior to injection. For example, higher stirring enhances reduction of MgO in the slag which in turn provides more dissolved Mg for the inclusions and increase Mg content of inclusions. Higher oxygen potential of the slag leads to formation of inclusions with higher alumina content as the FeO and MnO are reduced by reaction of steel and slag instead of MgO. Also, higher MgO concentration in the slag promotes formation of inclusions with higher Mg content as expected.

d) Reoxidation of steel which increases its dissolved oxygen can cause change of composition of inclusions towards higher alumina content since the dissolved oxygen reacts with dissolved aluminum to increase alumina content of inclusions.

References

[1] D. Lu, G. A. Irons, and W. Lu: *Ironmak. Steelmak.*, 1994, vol. 21, pp. 362–72.

[2] Worldsteel Association: *Overview of the Steelmaking Process*, 2013.

[3] A. Ghosh and A. Chatterjee: *Iron Making and Steelmaking: Theory and Practice*, 2008.

[4] K. Wünnenberg: *Rev. Métallurgie*, 2005, vol. 102, pp. 687–692.

[5] R. Dekkers, B. Blanpain, P. Wollants, F. Haers, C. Vercruyssen, and B. Gommers: *Ironmak. Steelmak.*, 2002, vol. 29, pp. 437–44.

[6] G. M. Faulring, J.W. Farrell, and D. C Hilty: in *Electr. Furn. Conf. Proc.*, 1980, pp. 219–29.

[7] S. W. Robinson, I. W. Martin, and F. B. Pickering: *Met. Technol.*, 1979, vol. 6, pp. 157–69.

[8] L. Zhang and B. G. Thomas: in *XXIV Natl. Steelmak. Symp.*, Morelia, Mich, Mexico, 2003, pp. 138–83.

[9] K. Graham: Ph.D thesis, McMaster University, 2008.

[10] D. G. C. Robertson, B. Deo, and S. Ohguchi: *Ironmak. Steelmak.*, 1984, vol. 11, pp. 41–55.

[11] M. L. Kapoor and M. G. Frohberg: in *Chem. Metall. Iron Steel*, 1971, pp. 17–22.

[12] H. Gaye and J. Welfringer: in *Second Int. Symp. Metall. Slags Fluxes*, 1984, pp. 357–75.

[13] A. Ghosh: *Secondary Steelmaking: Principles and Applications*, 1st Ed., CRC Press, London, 2001.

[14] S. Seetharaman: in *Treatise Process Metall.*, L. Holappaa and O. Wijkb, eds., United Kingdom, 2014, pp. 347–74.

[15] Li Feng Zhang and Brian G Thomas: *ISIJ Int.*, 2003, vol. 43, pp. 271–91.

[16] P. Kaushik, J. Lehmann, and M. Nadif: *Metall. Mater. Trans. B Process Metall. Mater. Process. Sci.*, 2012, vol. 43, pp. 710–25.

[17] R Kiessling and N Lange: *Non-Metallic Inclusions in Steel*, Metals Society, 1978.

[18] K. Sasai and Y.Mizukami: *ISIJ Int.*, 1996, vol. 36, pp. 45–51.

[19] T J Baker, F P L Kavishe, and J Wilson: *Mater. Sci. Technol.*, 1986, vol. 2, pp. 576–82.

[20] N. Bannenberg: in *Steelmak. Conf. Proceedings.*, 1995, pp. 457–63.

[21] E. B. Pretorius, H.G. Oltmann, and T. Cash: *Iron Steel Technol.*, 2010, vol. 7, pp. 31–44.

[22] N. Verma, P. C. Pistorius, R.J. Fruehan, M.S. Potter, H.G. Oltmann, and E.B. Pretorius: *Metall. Mater. Trans. B*, 2012, vol. 43, pp. 830–40.

[23] P. Vasilij, K. Blaženko, and H. W.: *Steel Res.*, n.d., vol. 62, pp. 289–95.

[24] G .J. W. Kor and P. C. Glaws: in *Making, Shap. Treat. Steel*, 1998, pp. 661–713.

[25] K. Larsen and R.J. Fruehan: *ISS Trans.*, 1991, pp. 125–32.

[26] G. Ye, P. Jonsson, and T. Lund: *ISIJ Int.*, 1996, vol. 36, pp. S105–8.

[27] L. Holappa and H. Ylönen: in *Fifth Int. Iron Steel Congr. Steelmak. Proceedings, Vol. 69*, Washington D.C, 1986, pp. 277–83.

[28] L. Holappa, M. Hämäläinen, M. Liukkonen, and M. Lind: *Ironmak. Steelmak.*, 2003, vol. 30, pp. 111–15.

[29] G. Eriksson and K. Hack: *Metall. Trans. B*, 1990, vol. 21, pp. 1013–23.

[30] H. Visser, R. Boom, and M. Biglari: *ATS Int. Steelmak. Conf.*, 2008, pp. 172–80.

[31] Y. Ito, M. Suda, Y. Kato, H. Nakato, and K. Sorimachi: *ISIJ Int.*, 1996, vol. 36, pp. S148–50.

[32] Y. Higuchi, M. Numata, Sh. Fukagawa, and K. Shinme: *ISIJ Int.*, 1996, vol. 36, pp. 151–54.

[33] Z. Han, L. Liua, M. Lind, and L. Holappa: *Acta Metall. Sin.*, 2006, vol. 19, pp. 1–8.

[34] O. Levenspiel: *Chemical Reaction Engineering*, 2nd Ed., John Wiley & Sons, New York, 1999.

[35] K.C Ahlborg: in *Fifth Int. Conf. Clean Steel*, Budapest, 1997, pp. 151–56.

[36] N. Verma, P. C. Pistorius, R.J. Fruehan, M. S. Potter, H.G. Oltmann, and E. B. Pretorius: *Metall. Mater. Trans. B*, 2012, vol. 43, pp. 830–40.

[37] S. F. Yang, J. Sh. Li, Z. F. Wang, J. Li, and L. Lin: *Int. J. Miner. Metall. Mater.*, 2011, vol. 18, pp. 18–23.

[38] Sh. Yang, Q. Wang, L. Zhang, J. Li, and K. Peaslee: *Metall. Mater. Trans. B*, 2012, vol. 43, pp. 731–50.

[39] Sh. Yang, J. Li, X. Gao, and Y. Ma: *Metall. Min. Ind.*, 2014, pp. 66–71.

[40] J. Peter, K. D. Peaslee, D. G. C. Robertson, M. Hall, and B.G Thomas: in *AISTech - Iron Steel Technol. Conf. Proc.*, 2005, pp. 959–73.

[41] K. J. Graham and G. A. Irons: in *Int. Symp. Highly Innov. Nov. Oper. "Future Steelmak. Metall.*, 2010, pp. 65–74.

[42] A. Galindo, G. A. Irons, K. S. Coley, and S. Sun: in *Challenges Transform. Solut. to Sustain. Steelmak. Cast. Environ. Metall. Innov. CTSSC-EMI Symp. 2015*, Tokyo, Japan, 2015.

[43] A. Harada, N. Maruoka, H. Shibata, and Sh. Kitamura: *ISIJ Int.*, 2013, vol. 53, pp. 2110–17.

[44] A. Harada, N. Maruoka, H. Shibata, M. Zeze, and N. Asahara: *ISIJ Int.*, 2014, vol. 54, pp. 2569–77.

[45] D. Kumar: Ph.D thesis, Carnegie Mellon University, 2018.

[46] D. Kumar and P. C. Pistorius: in *Proc. 10th Int. Conf. Molten Slags, Fluxes Salts*, John Wiley & Sons, Hoboken, NJ, USA, 2016, pp. 145–53.

[47] M. A. Van Ende and In Ho Jung: *Metall. Mater. Trans. B Process Metall. Mater. Process. Sci.*, 2016, vol. 48, pp. 1–9.

[48] K. J. Graham and G. A. Irons: in *AISTech - Iron Steel Technol. Conf. Proc.*, Pittsburgh, PA, 2008, pp. 5–13.

[49] J. H. Shin, Y. Chung, and J. H. Park: *Metall. Mater. Trans. B*, 2017, vol. 48, pp. 46–59.

[50] P. R. Scheller and Q. Shu: *Steel Res. Int.*, 2014, vol. 85, pp. 1310–16.

[51] D. A. Jerebtsov and G. G. Mikhailov: *Ceram. Int.*, 2001, vol. 27, pp. 25–28.

[52] D-Z. Lu: Ph.D thesis, McMaster University, 1992.

The end